The development of lipid nanoparticle formulations *via* flash nanoprecipitation

Cameron Hogarth

June 2023

Thesis submitted in accordance with the requirements of the University of Liverpool for the degree of Doctor in Philosophy

Abstract

Therapeutic nanomedicine, the use of nanoscale drug delivery vehicles such as lipid nanoparticles, is a powerful tool that has been employed to aid in the formulation and delivery of drugs due to issues such as: poor aqueous solubility, poor permeability and poor stability, poor pharmacokinetics. Throughout this thesis, efforts were made to provide greater understanding around the fundamentals of drug lipid nanoparticle formulation identifying key parameters which provide greater control over lipid nanoparticle formulation *via* flash nanoprecipitation.

Firstly, the properties of materials found within the core of lipid nanoparticles, such as drugs and/or lipids, were assessed with a specific focus on LogP. A series of carbonate and carbamate-based prodrugs of the hydrophilic drug lamivudine were synthesised with varying the alkyl chain length conjugated to the drug in order to systematically target various LogP. Formulations of a prodrug consisting of conjugated dodecyl alkyl chains with a LogP of 11.44 resulted in solid prodrug nanoparticle formulations with greater control over nanoparticle size and size distribution. This behaviour could be explained by the LaMer model whereby a higher degree of supersaturation was achieved with prodrug of higher LogP resulting in greater nucleation and a controlled growth phase. This high LogP formulation also showed long-term dispersion stability of 28 days due to the poor solubility of the prodrug minimising Ostwald ripening. Furthermore, demonstrated how formulations of dodecyl prodrug could enable high drug loading within the core as less host material i.e. solid lipid was required. Formulations with a core composed of 100 % dodecyl prodrug translated to a 14 wt % loading of prodrug relative to overall solid mass (inclusive of surfactant) and an active drug loading of 4.48 %. Meanwhile, blending with a complex mixture of lipids demonstrated how the crystallinity of the core could be controlled.

The properties of the surfactants used for lipid nanoparticle formulation were then investigated and found a blend of both pegylated and unpegylated lipid surfactants could achieve a higher wt % of core material with respect to the surfactant due to the properties of the unpegylated surfactant resulting in nucleation alongside the lipid and/or prodrug. As a result, formulations with an elevated prodrug loading of 30 wt % of solid mass (surfactant and lipid and prodrug) translating to 9.6 % active drug loading were prepared and found to be stable up to 28 days.

The properties of lipid nanoparticle formulations with regards to ratio of pegylated lipid surfactant to unpegylated lipid surfactant, wt % of core material and concentration of cryoprotectant/lyoprotectant were investigated in order to achieve a formulation of high drug loading which could be successfully freeze dried and redispersed. This knowledge was then applied to redisperse a formulation into physiological buffer solution and investigate prodrug activation with and without porcine liver esterase. It was deemed the dodecyl prodrug could only be activated to release drug from the nanoparticle in the presence of enzyme achieving a release of ~ 37 % after 9 weeks in the presence of a single batch of enzyme.

Finally, fundamentals of nanoparticle formulation and stability were applied to develop a formulation containing ionizable cationic lipid for the potential delivery of mRNA. A fluorescent dye was incorporated within formulations which varied in PEG chain length of the pegylated lipid surfactant to determine effects on particle formation and stability as well as cellular uptake. The role of the positive charge of the ionisable lipid was found to be instrumental for achieving intracellular accumulation with samples stabilised by Brij S20 and Brij S100 recording significant fluorescence and IL-8 response. Meanwhile, samples containing the neutral lipid failed to accumulated intracellularly. In addition, samples stabilised by the negatively charged pegylated lipid also failed to accumulate.

Preface

Publications

Evaluating the impact of systematic hydrophobic modifications of model drugs on the control, stability and loading of lipid-based nanoparticles. **C. Hogarth**, K. Arnold, A. McLauchlin, S. P. Rannard, M. Siccardi and T. O. McDonald, *J. Mater. Chem. B*, 2021, **9**, 9874–9884. doi:10.1039/d1tb02297k.

High drug loading solid lipid nanoparticles, nanostructured lipid carriers and nanoemulsions for the dual drug delivery of the HIV drugs darunavir and ritonavir. H. Elkateb, H. Cauldbeck, E. Niezabitowska, **C. Hogarth**, K. Arnold, S. Rannard and T.O. McDonald, Journal of Colloid and Interface Science Open, 2023, 11. doi:10.1016/j.jciso.2023.100087.

Manuscripts in preparation

Navigating the Challenges of Lipid Nanoparticle Formulation: The Role of Unpegylated Lipid Surfactants in Enhancing Drug Loading and Stability. **C. Hogarth**, K. Arnold, S. Wright, S. P. Rannard and T. O. McDonald,

Conferences Attended and Posters presented

1. ACS Spring Meeting and Expo (Bonding Through Chemistry), San Diego, USA, March 20-24th 2022 (Poster)
2. Annual meeting 2022 of the British Society of Nanomedicine, Swansea, UK, August 22nd-23rd 2022 (Talk)
3. Early Career Researcher Summer Virtual Meeting, June 16-17th 2021 (Talk)

Acknowledgments

Firstly, I would like to express a sincere thank you to Dr. Tom McDonald for giving me the opportunity to carry out the work presented in this thesis. Tom's ongoing support and guidance throughout my PhD has enabled me to improve my research, presentation and writing skills, develop my own knowledge and research, have the opportunity to present my findings at the ACS Meeting Spring 2022 and above all prove myself as a scientist

In addition, I offer my gratitude to my colleagues especially those part of the McDonald group; including previous members of the group: Jess Taylor, Steph Edwards, Heba Elkateb, Dominic Gray, Edyta Niezabitowska. I would like to acknowledge the Functional Materials Team for their constant encouragement and support during this time especially Prof. Steve Rannard, Dr Helen Cauldbeck and Dr Marco Giardiello for their support as well as their role in the meetings and Seminar Days.

Additionally, I would like to recognise Keith Arnold for his role in the CryoSEM analysis, Amy Lunt for performing PXRD analysis, Andy McLauchlin and Steve Wright for their support with DSC analysis and Neill Liptrott from the Department of Pharmacology for his input and guidance along with Chris David for performing the cell work in my thesis.

Special thanks to IOC Oleochemical and Lipoid for their generosity in donating materials which enabled me to perform various studies within this thesis.

Finally, I would like to thank my family for their support throughout the years as well as a special thanks to my fiancé Poppy.

List of Abbreviations

3TC lamivudine

ALC-0159 2-((polyethylene glycol)-2000)-N,Nditetradecylacetamide

ALC-0315 (4-hydroxybutyl)azanediyl)bis(2-hexyldecanoate)

Brij S20 polyoxyethylene 20 stearyl ether

CHNS elemental analysis

CLogP calculated *n*-octanol/water partition coefficient

Cryo-SEM cryogenic scanning electron microscopy

Da Daltons

DiI 1,1'-didoctadecyl-3,3,3',3'-tetremethylindocarbocyanine perchlorate

DLS dynamic light scattering

DMG-MPEG-2K 1,2-dimyristoyl-rac-glycero-3-methoxypolyethylene glycol-2000

DOPE 1,2-dioleoyl-sn-glycero-3-phosphoethanolamine

DOTAP-Cl 1,2-dioleoyl-3-trimethylammonium-propane chloride salt

DSC differential scanning calorimetry

DSPC distearoylphosphatidylcholine

DSPE-MPEG-2K *N*-(carbonyl-methoxypolyethylene glycol-2000)-1,2-diastearoyl-*sn*-glycero-3-phosphoethanolamine sodium salt

ESI electrospray ionisation mass spectrometry

FTIR Fourier transform infra-red spectroscopy

HLB hydrophilic-lipophilic balance

HPLC high-performance liquid chromatography

IL-8 Interleukin 8

LogP *n*-octanol/water partition coefficient

mRNA messenger ribonucleic acid

NLCs nano structured lipid carrier

NMR nuclear magnetic resonance

PBS phosphate buffered saline

PDI polydispersity index

PEG polyethylene glycol

pKa acid dissociation constant

PXRD powder x-ray diffraction

SEM scanning electron microscopy

SLNs solid lipid nanoparticles

SM-102 8-((2-hydroxyethyl)(6-oxo-6-(undecyloxy)hexyl)amino)octanoic acid,1-octylnonyl ester

SPN solid prodrug nanoparticle

TEM transmission electron microscopy

THF tetrahydrofuran

Tm phase transition temperature

TRIS tris(hydroyxlmethyl)aminomethane

Wt% weigh percentage

Table of contents

CHAPTER 1

Introduction

Chapter 1 - Introduction

1.0. Nanomedicine

Nanomedicine is a field of research that employs materials operating on the nanometre scale (1-1000 nm)[1] for use in diagnosis, monitoring, prevention, and treatment of disease. In particular, nanomedicine drug delivery systems have been designed to address problems related to physiochemical properties of drugs. For some year, reports have suggested that ≥40% of drugs within clinical use are hydrophobic,[2] and ≥90% of new drug candidates within the developing pipeline may be described as either Class II (high permeability, low solubility) or Class IV (low permeability, low solubility) categories using the biopharmaceutics classification system.[3] Although the pharmaceutical industry considers drug hydrophobicity as a negative physical property, new therapy development is increasingly reliant on poorly water soluble compounds. Drug delivery systems have therefore become more important and target the enhancement of administration to ensure the therapeutic behaviour of poorly soluble drugs. Nanomedicine has also been reported to address key pharmacological challenges for drug delivery such as; rapid metabolism and excretion of drug, and untargeted drug distribution resulting in undesired side effects/toxicity. For example, in 1995 the liposomal formulation of the anticancer drug doxorubicin otherwise known as DOXIL became the first FDA approved cancer nanomedicine.[4] DOXIL demonstrated how containment of doxorubicin within a liposome decorated in polyethylene glycol (PEG) improved drug bioavailability due to reduced drug metabolism, while also avoiding the reticuloendothelial system resulting in prolonged circulation and a greater accumulation at the target site.[5] Containment of the drug also drastically limits the toxicity the encapsulated drug doxorubicin, which previously resulted in severe side effects with conventional therapy.[5] Furthermore, it is now conceivable for systems to target a specific site by modifying the surface of nanoparticles to express active targeting ligands.[6] Since DOXIL, nanomedicine has progressed especially in the area of lipid nanoparticles. The more recent example are the COVID-19 vaccines whereby lipid nanoparticles enabled the delivery of messenger ribonucleic acid (mRNA).[7] Overall, this significant step demonstrates how far nanomedicine has come and how it may continue to be employed to overcome challenges faced within the area of medicine.

1.1. Lipid nanoparticles

Lipid nanoparticles are particular group of nanoparticles composed of lipids and/or lipid-based materials such as lipophilic surfactants. Lipid molecules are already widespread within nature, as an energy source or a key components of cell membranes. For this reason, lipid molecules are often biocompatible, and this aids in the application of transporting membranes around the body, while also preventing unwanted accumulation.[8]

The success of the liposomal DOXIL formulation has contributed to worldwide interest in nanotechnology and specifically lipid nanoparticles. Since then, various drug delivery vehicle derivatives of the lipid bilayer of liposomes have been devised by utilising a wide range of lipids such as nanoemulsions, solid lipid nanoparticles (SLNs) and nanostructured lipid carriers (NLCs), Fig. 1.1. Generally, the structure of a lipid nanoparticle can be broken down into two components, a core which is typically composed of lipid(s), and a surfactant layer that encapsulates the core and provides stabilisation.

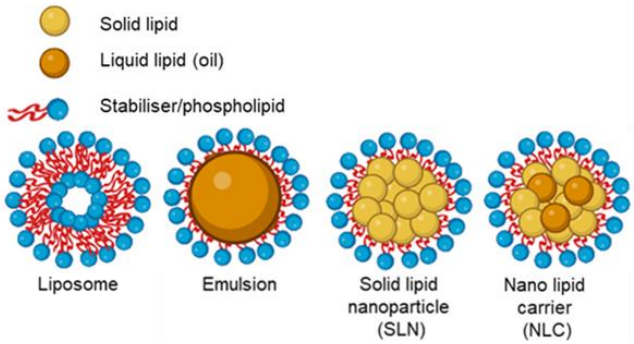

Figure 1.1- Illustrations of various lipid nanoparticle drug delivery systems.

1.1.1. Core lipids

The role of lipids found in the core of lipid nanoparticles is typically to host a drug and/or prodrug within the nanoparticle. The wide interest in lipid nanoparticles has resulted in a library of lipid materials that have been trialled for lipid nanoparticle formulation. Consequently, the different properties of lipid molecules possess has generated various lipid nanoparticle structures. For example, lipid nanoparticles composed of lipids which exist as a liquid oil at room temperature result in the formulation of Nanoemulsions, while those that are solid at room temperature and form a solid core resulting in solid lipid nanoparticles (SLNs). Finally, blends of solid and liquid lipids have been trialled resulting in the development of the NLC. These different types of lipid nanoparticles offer differing advantages and disadvantages. For example, the benefits to the inclusion of the liquid lipid are potentially higher drug loading depending on drug solubility within this oil.[9] However, nanoemulsions (composed entirely of liquid lipids) typically display rapid diffusion of drugs out from the lipid core resulting in burst release. This behaviour is due to the low viscosity of the oil core.[10] Meanwhile, the completely solid core of the SLN has been reported to prevent/slow coalescence and thus are of greater stability compared to emulsions.[11] However, the highly crystalline nature of the lipid core has been shown to result in polymorphic transitions leading to burst expulsion of drug and poor drug loading.[12] Meanwhile, NLCs which consist of a blend solid and liquid lipids in an attempt to achieve high drug loading yet preserve stability by preventing maintaining the structural integrity provided by the solid lipid yet disrupting the crystallinity to slow/prevent polymorphic transitions.[13,14] As a result,

the choice of lipids for the core of lipid nanoparticles appears to be crucial in determining formulation stability.

1.1.2. Lipid surfactants

Surfactants are molecules with both hydrophilic and hydrophobic elements thus making them amphiphilic. Surfactants are commonly found at interfaces due to their ability to reduce the interfacial tension between hydrophilic and hydrophobic phases. As a result, surfactants have been widely explored for use in colloidal dispersions to reduce the interfacial tension while also providing repulsive forces which are greater than the Van der Waals forces of attraction between particles that cause flocculation. Vast amounts of research has been undertaken investigating a broad range surfactants for application in lipid nanoparticles each differing in aspects such as chemistry, architecture and physical charge.[15] There are various categories regarding surfactant charge for example anionic (negatively charged), cationic (positively charged), zwitterionic and non-ionic surfactants. Non-ionic surfactants may be used to stabilise dispersions by employing steric repulsion, meanwhile ionic surfactants stabilise dispersions by means of electrostatic stabilisation and/or electrosteric.[16] Although a common challenge faced is finding a surfactant composition that may produce a colloidal formulaiton with the desired properties for its application. In some cases, large scale screening experiments are used to investigate various types, combinations and amounts of surfactant,[17] however such an approach can be time consuming and inefficient. Furthermore, not only the type of surfactant but the concentration has detrimental impact of the stability of a colloidal dispersion. Depletion flocculation occurs when too much polymer is added and the non-adsorbed polymer becomes too highly concentrated in the bulk rather than between two closely spaced particles.[18] The result is an osmotic pressure difference and solvent moves from low concentration between particles to high concentration in the bulk thus causing particles to aggregate. Meanwhile bridging flocculation may also occur whereby a high molecular weight polymer at low concentration adsorbs to the surface of more than once particle bringing the particle together, Fig.1.2.[18–20] As a result, there is a clear requirement for greater understanding of surfactants starting with stucture property relationships.

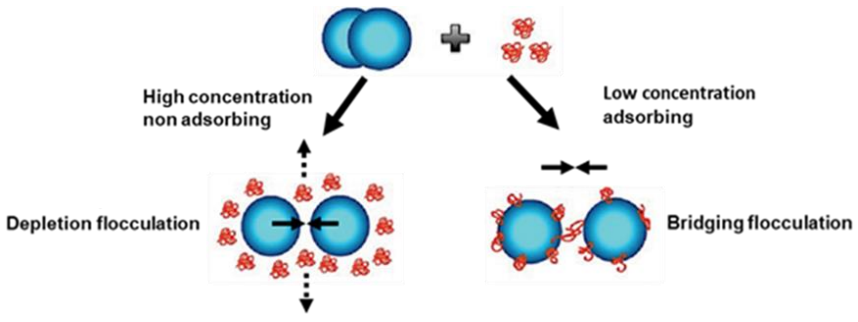

Figure 1.2- Schematic diagram illustrating potential mechanisms for depletion and bridging flocculation. Adapted from Pouralhosseini *et al*.[18]

1.1.3. Steric stabilisation

One way in which dispersants may provide repulsive forces is by steric stabilisation. Steric stabilisation is a term given to a dispersant which stabilises particles without the means of ionic interactions.[21] Typically, a particle will be covered by a polymeric tail which will be soluble in the continuous phase of the formulation. For example, lipid surfactants consisting of polyethylene glycol chains are employed in the formulation of lipid nanoparticles. The PEG chains become solvated and extend out into aqueous solution. As particles approach one another the concentration of the soluble tails increases between particles which is unfavourable due to an increase in osmotic pressure and the system reacts by diluting the tails i.e. solvent molecules force themselves between the particles resulting in separation. In addition, upon particles approaching one another polymeric chains intermingle resulting in a loss of degree of freedom and thus a decrease in entropy which is unfavourable due to an increase in Gibb's free energy, therefore particles then separate. It is thought that the combination of these two effects is what provides steric stabilisation, Fig.1.3.[22,23] As a result, key parameters surrounding surfactants that provide steric stabilisation such as molecular weight should be thoroughly explored.

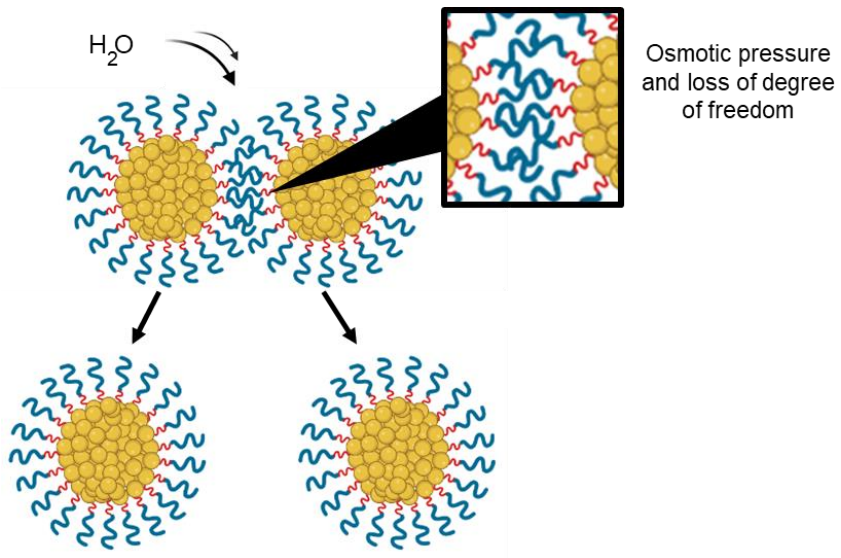

Figure 1.3- Illustration of steric stabilisation by means of osmotic pressure and loss of degree of freedom upon intermingling of steric stabilising chains

1.1.4. Electrostatic stabilisation

Electrostatic stabilisation is another method of providing stability to colloidal dispersions and is explained by the electrical double layer. It may form when components of the nanoparticle possess charge for example ionic stabilisers or even the ionizable cationic lipids found in mRNA lipid nanoparticles.[7] Essentially, charged particles attract counter ions from aqueous solution which develops cloud of ions around the particle. As two particles approach each other the two clouds of ions overlay and like charges repel resulting in the separation of particles, Fig.1.4. On the other hand, electrostatic stabilisation may be lost as the concentration of salt in the continuous phase increases resulting in a screening of charge.[24] As a result, electrostatic stabilisation is often combined with steric stabilisation for colloidal systems in what is known as electrosteric stabilisation. The employment of electro-steric is commonly found with colloidal formulations in the application of nanomedicine due to the various types and concentrations of salts found at within the body. Although, Goodman *et al*. have reported cationic gold nanoparticles to be toxic, whereas anionic equivalents were found to be non-toxic.[25] As a result, considerations surrounding the type and extent of electrostatic stabilisation must be carefully considered.

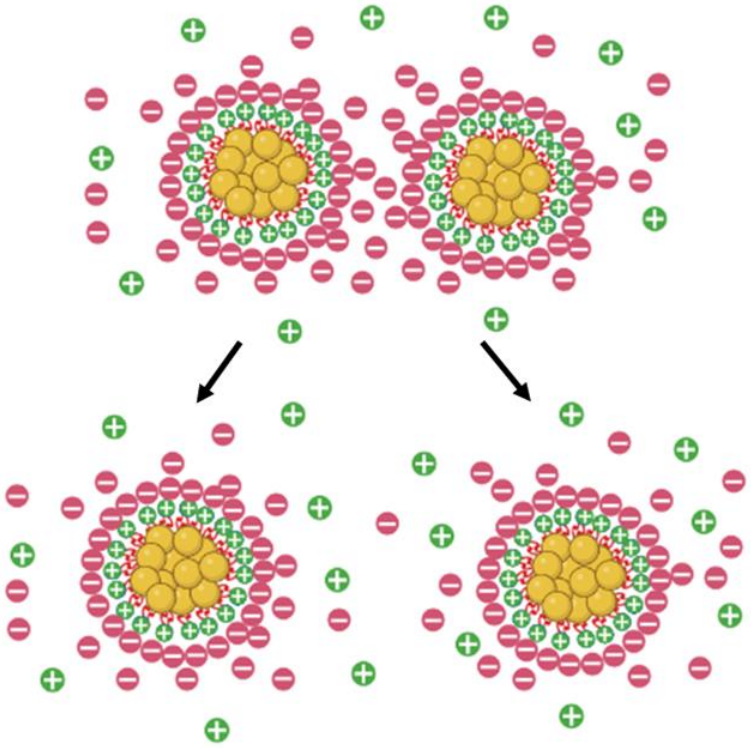

Figure 1.4- Illustration of the stern double layer of electrostatically stabilised nanoparticles and how overlapping clouds of ions results in repulsion and particle stabilisation.

1.1.5. Hydrophilic-lipophilic balance (HLB)

Attempts to streamline the surfactant selection process have involved identifying the design rules for nanoparticle production, one way this has been done is by characterising surfactants by their various properties for example the Hydrophilic-lipophilic balane (HLB) scale.The HLB scale was developed in 1949 by William Griffin to aid in surfactant selection in order to meet the 'required HLB' for a specific application to result in good performance. The HLB scale, defines non-ionic surfactants by their ratio of molecular weight of hydrophilic and hydrophobic components by dividng the atomic mass of the hydrophilic portion by the molecular weight of the entire molecule times by 20.[26] For example the various HLB ranges have been categorised to offer the following uses; 4-6, water in oil emulsifiers; 7-9, wetting agents; 8-18, oil in water emulsifiers; 13-15, detergents; and 10-18 are solubilisers.[26] Furthermore, the required HLB value of the surfactant tends to provide the lowest degree of interfacial tension between the two phases.[26] Unfortunately, ionic surfactants such as cationic, anionic and zwitterionic cannot be assigned a true HLB as the weight percentage calculation is skewed by presence of charge which enhances the hydrophilic component of the surfactant making it more hydrophilic. In addition the alternative Davies' method for HLB which calculates based on chemical groups is very limited.[27] Nevertheless, approximate values for HLB may be determined experimentally by the ionic surfactant's solubility or dispersibility in water; no dispersibility in water HLB 1-4, poor dispersion HLB 3-6, milky dispersion after vigorous agitation HLB 6-8, stable milky dispersion HLB 8-10, translucent to clear dispersion HLB 10-13 and a clear solution HLB 13+.[26] As a result, HLB appears to be a useful tool in categorising surfactants based on their desired role in application.

1.1.6. Challenges faced by Lipid nanoparticles

Unfortunately, the development of lipid nanoparticles has suffered from poor drug loading largely due to poor encapsulation of drug leading to the composition of formulations being dominated by surfactants.[28] Furthermore, lipid nanoparticles commonly suffer from poor stability primarily due to aggregation, Ostwald ripening or polymorphic transitions of the lipid core. As a result, the progression of research surrounding lipid nanoparticles has been hindered.

1.1.6.1. Ostwald ripening

Ostwald ripening is another phenomenon that is often also responsible for colloidal instabilities in lipid nanoparticles. It is a thermodynamically driven process whereby smaller particles undergo dissolution into the continuous phase and deposit in the larger particles.[29] The larger particles are favoured over smaller particles due to their lower chemical potential. Therefore, Ostwald ripening results in an increase in the overall particle size of the formulation.[30] The effect of Ostwald ripening in palladium nanocrystals has been successfully visualised by Zhang *et al*. and shown by Fig.1.5 whereby

transmission electron microscopy (TEM) images taken after 6 (a), 24 (b), 48 (c) and 72 hours (d) show how smaller particles were consumed by larger particles.[31]

Some advances have been made to slow/prevent Ostwald ripening by employing various surfactant stabilisers to enhance steric and electrostatic stabilisation, however screening a diverse range of surfactants tends to be a lengthy process which lacks efficiency. Another key factor determining the rate of Ostwald ripening is the solubility of the hydrophobic material (*e.g.* the lipids) in the continuous phase. Early investigations by Wooster *et al.* have highlighted how the aqueous solubility of an oil had a major impact on the stability of nano-emulsions. Specifically, compounds with very low aqueous solubilities such as triglyceride oils possessed a profound resistance to Ostwald ripening due to their severe insolubility in water.[32,33] As a result, it is likely that the solubility of components within SLNs are key factors in controlling Ostwald ripening.

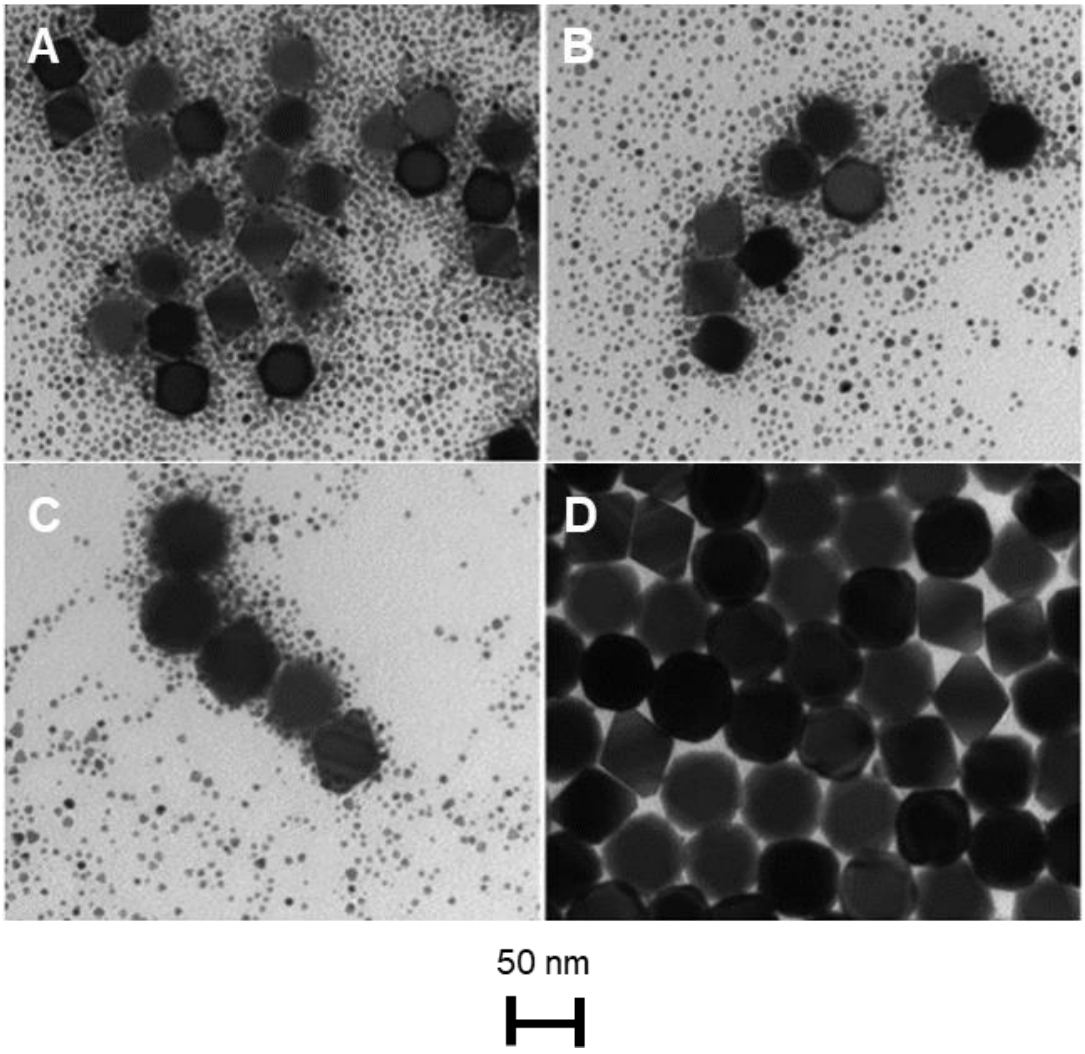

Figure 1.5- TEM images of palladium nanocrystals displaying Ostwald ripening over (A) 6, (B) 24, (C) 48 and (D) 72 hours. Adapted from Zhang *et al*. with permission from the Royal Society of Chemistry.[31]

1.1.6.2. Polymorphism

Polymorphic transitions are linked to highly crystalline materials whereby materials may change in crystal form from e.g. from the α to the more stable and favoured β form.[11] Helgason *et al.*, have previously shown that polymorphic transitions of SLNs lipid core can induce changes in nanoparticle morphology from spherical to a needle-like form depicted by Fig.1.6, which can result in drug expulsion.[34] The cause of such transitions is that upon initial formulation the solid lipid of lipid nanoparticles such as SLNs tend to not adopt the most thermodynamically stable and favoured crystal form and overtime may experience a change from e.g. alpha to beta form.

As an approach to address polymorphic transitions in SLNs Jenning *et al.* demonstrated that blending liquid and solid lipids can disrupt the crystal structure of the solid lipid, therefore delaying recrystallisation and improve physical stability, as shown by Fig.1.7.[13,35] It was found that increasing the concentration of oil in lipid carrier nanoparticles resulted in the depression and broadening of the solid lipid melting peak measured by differential scanning calorimetry (DSC), thus indicating a reduction in crystal order.[35] This development led to what is now known as a nano lipid carrier (NLC) which was deemed the 2nd generation solid lipid nanoparticle. Additionally, similar strategies were employed and applied to solid lipid nanoparticles by Bunjes *et al.* who demonstrated how blends of various solid lipids at different ratios can cause imperfections and disrupt the crystal structure of lipid nanoparticles. They showed that the greatest imperfections to the crystal structure of a lipid nanoparticle may be achieved using a complex mixture of lipids. The results highlighted how different ratios of lipids can change the melting temperature, enthalpy and rate of recrystallisation.[34] An investigation by Salminen *et al.* highlighted how high melting lecithin facilitated physically stable SLNs, while low melting lecithin resulting in nanoparticle growth.[36] Therefore, strategies that can be used to disrupt the ability of lipids and drug to crystallise are very useful in developing lipid-based nanocarriers of higher stability.

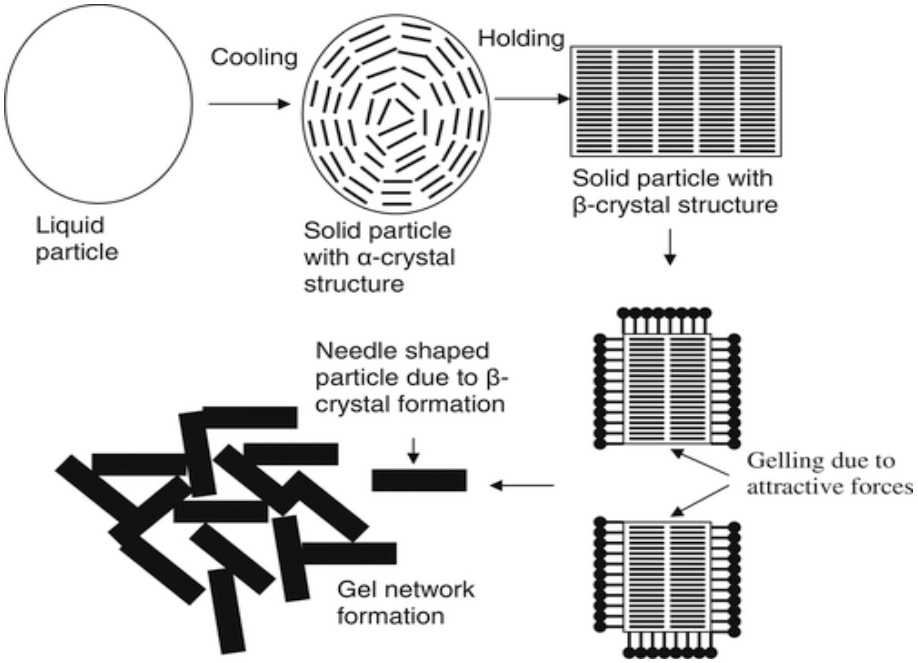

Figure 1.6- Proposed model of polymorphism of tripalmitate SLNs by Helgasen *et al*. with permission from John Wiley and Sons.[12]

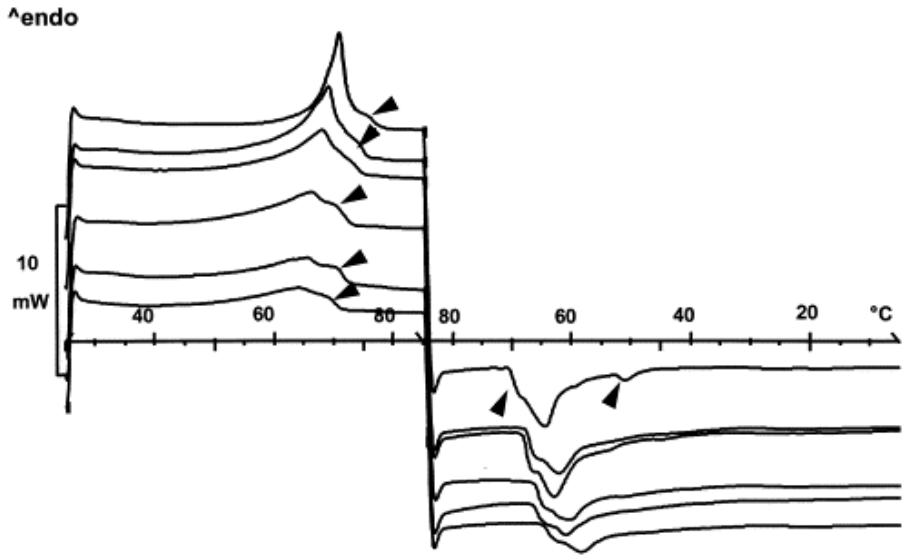

Figure 1.7- DSC scans of SLN dispersions containing various loadings of Miglyol oil (from top 0, 8, 16, 28, 33 and 38 %). Samples were subjected to a heating ramp from 25 to 85 before a cooling ramp from 85 to 5 at a rate of 5 K/min. Overall displays suppression of Compritol melting peak with increasing content of Miglyol. Dark triangles point out presence of other polymorphs. Adapted from Jenning *et al*. with permission from Elsevier[35]

1.2. Flash Nanoprecipitation

Lipid nanoparticles may be produced by a range of methods including high shear homogenisation, hot or cold homogenisation, ultrasonication and microfluidics. Flash nanoprecipitation is a particularly interesting route for lipid nanoparticle production due to its simplicity and fast process speed which also offers potential for scale up *via* continuous processing.[37,38] Indeed, this process has already been realised in the formulation of nanolipomers (polymer nanoparticle/liposome hybrid) with the use of microfluidics.[39] Furthermore, the advancement of microfluidics has resulted in the development of various mixer geometries which create micromixing conditions needed for high local supersaturation enabling greater control over mixing.[40,41] Nevertheless, the principle occurring in flash nanoprecipitation and microfluidic nanoprecipitation is the same; the lipid(s) and drug(s) are dissolved in a water-miscible organic solvent, which is later mixed with a solution of aqueous surfactant. The organic solvent diffuses through the aqueous medium meanwhile the lipid and drug precipitate and are stabilised by the surfactant due to their poor aqueous solubility, Fig.1.8.[38]

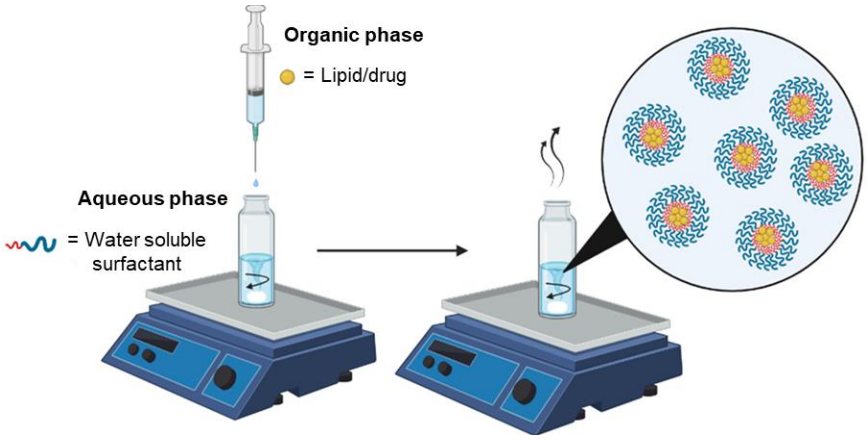

Figure 1.8- Simplified illustration of a lab scale flash nanoprecipitation.

1.2.1. LaMer model

Many materials used to form lipid nanoparticles have higher degrees of crystallinity, therefore the formation of lipid nanoparticles can be followed by the LaMer model of crystal nucleation and growth.[42] This applies to nanoparticles formed by a bottom up method such as flash nanoprecipitation.[43] The LaMer model states that upon mixing the injected solute exists as a monomer (Fig.1.9 A), until the solute becomes supersaturated, thereby triggering nucleation, Fig.1.9 B. Nucleation and growth then proceed in a simultaneous fashion competing for the consumption of supersaturated solute, until the solute concentration falls below the critical nucleation threshold whereby new nucleation events can no longer occur, Fig.1.9C. Meanwhile, nanoparticles may continue to grow by; diffusion of solute, aggregation and Ostwald ripening.[40,42,44] The degree of growth may be

prevented/limited in the presence of a surfactant which provides stability to the growing nuclei clusters/particles.[45]

Growth by diffusion occurs as the precipitating material operates by a stepwise molecular growth of solute on the particle/nuclei surface, Fig.1.10 A. Although, this may be limited by increasing the degree of nucleation and increasing the formation of nucleic, therefore there is less material available to diffuse onto the nuclei/particle surface. Growth by aggregation is where two or more nucleic come together to form a larger aggregate- Fig.1.10 B, this process may be limited by the presence of a surfactant to produce small and mono disperse nanoparticles.[40] Although, this is highly dependent on how efficient the surfactant is at stabilising the system as failure to stabilise the nucleic efficiently will result in aggregation. The third type of particle growth is Ostwald ripening (which has been described in section 1.1.6.1.) results in the overall growth of the average particle size of the formulation, Fig.1.10C.

Dalvi and Dave suggested that according to the LaMer model, small nanoparticles with a narrow distribution (low polydispersity) can be produced if a high rate of nucleation can be achieved while also limiting any growth phase. On the other hand, a slower rate of nucleation results in a dominant growth phase and a formulation of large particle size and broad distribution (high polydispersity).[46] Dalvi *et al*. linked a higher rate of nucleation to a higher degree of supersaturation and demonstrated strategies to increase the degree of supersaturation. These strategies were; variation of solute concentration; variation of temperature; and the selection and ratio of solvents and anti-solvents.[46] Furthermore, Liu *et al*. found that by changing the ratio of good solvent tetrahydrofuran (THF) to antisolvent (water) from 1/4 to 1/20 (THF/water, vol%) resulted in a change in corresponding average size decrease from 120 to 70 nm due to greater antisolvent leading to greater supersaturation and a potentially shorter period of growth.[47] As a result, it appears the solubility of a compound plays a critical role in controlling the size and polydispersity of the nanoparticles that are formed by flash nanoprecipitation.

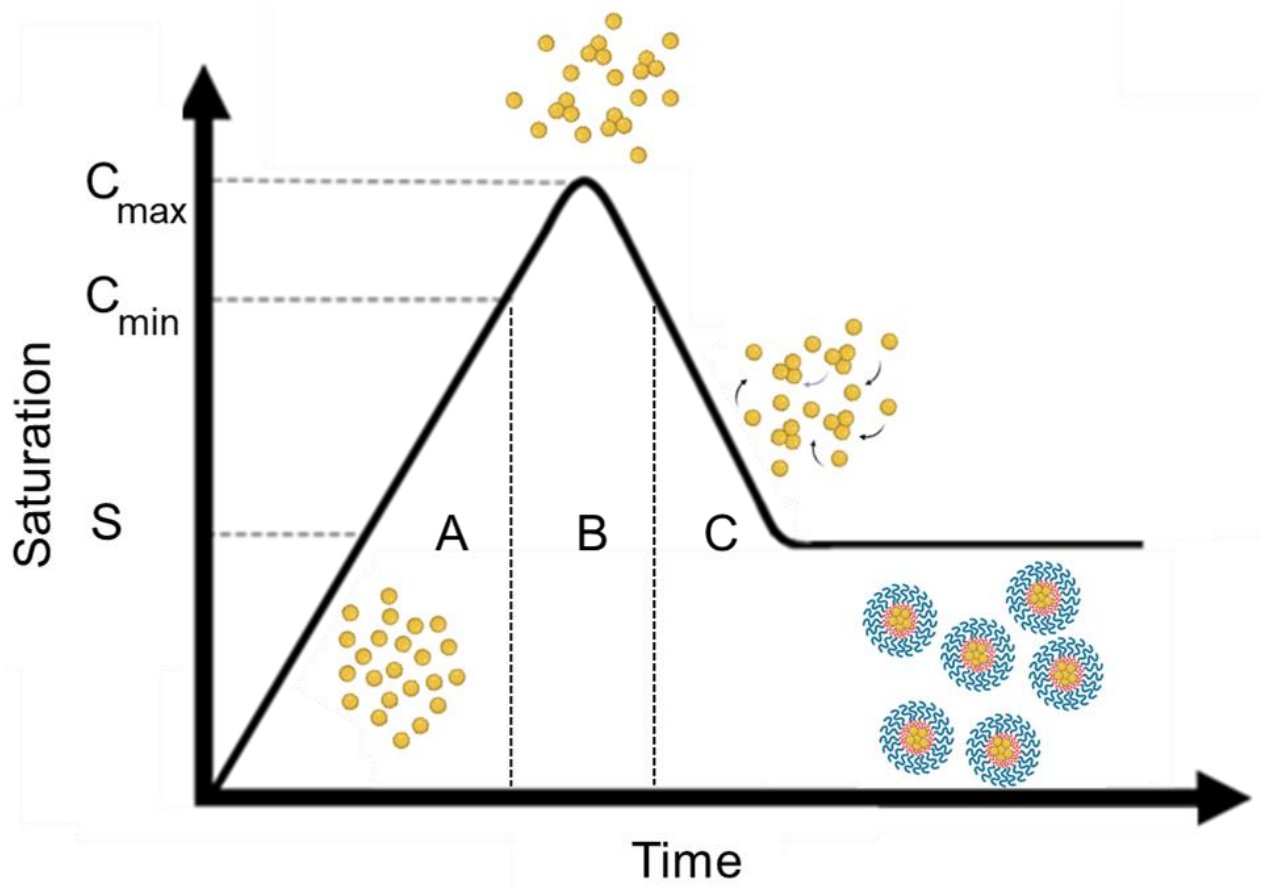

Figure 1.9- Plot of LaMer model whereby (S) is the solubility of the monomer, (C_{min}) is the hypothetical minimum supersaturation required for nucleation, and (C_{max}) is the hypothetical limiting supersaturation. A) Material injected by flash nanoprecipitation. B) Material become supersaturated resulting in nucleation. C) Solute concentration dips below minimum for nucleation resulting in a growth only phase until stabilised by surfactants forming particles.

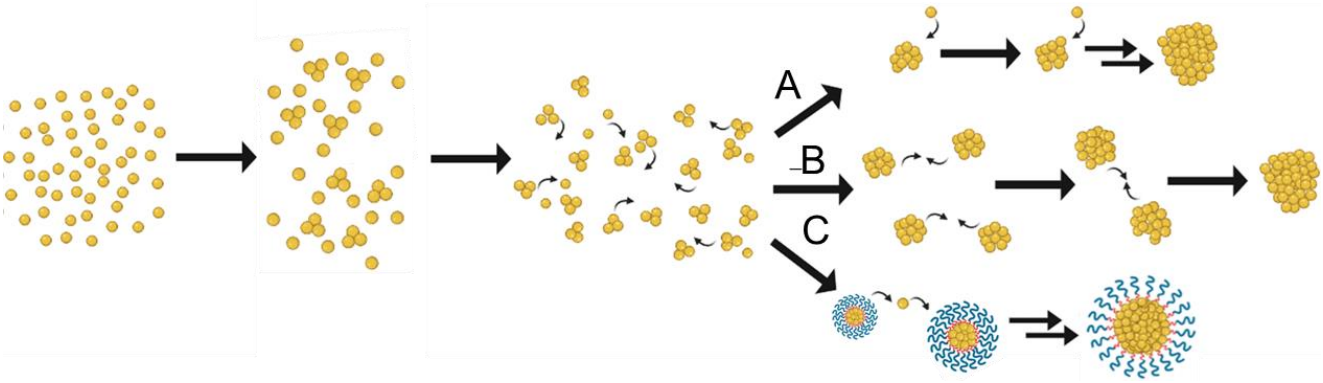

Figure 1.10- Illustration of the LaMer model of nucleation and growth. Illustration depicting the three methods of particle growth; A) Growth by diffusion, B) Growth by aggregation and C) Growth by Ostwald ripening.

1.3. *n*-octanol/water partition coefficient (LogP)

The *n*-octanol/ water partition coefficient is known as Log P is a measure of a molecule's lipophilicity, by means of a balance between a molecules hydrophobic and hydrophilic features. It may be calculated experimentally by investigating the proportion of material dissolved in either phase of an *n*-octanol/water mixture or by using a mathematical model. Therefore, molecules of high lipophilicity can be correlated with extreme hydrophobicity. Additionally, the aqueous solubility of a compound is closely linked to Log P; molecules with higher Log P values are generally less water soluble. Calculated values for lipophilicity can be determined by a wide range of calculation descriptors, which typically are robust predictors of experimental Log P values.[48] Research by Zhu investigated the correlation between Log P and stability of drug nanoparticles formulated by flash nanoprecipitation. The study investigated various hydrophobic drug molecules each ranging in value of Log P calculated by the ACDLog P algorithm. They showed that nanoparticles made up of molecules with a Log P > ~12 showed good stability. Meanwhile, any nanoparticles formed from compounds with Log P values between approximately 2 and 9 showed signs of fast Ostwald ripening and recrystallisation. Finally, compounds with a Log P lower than 2 were generally unable to form nanoparticles due to their high solubility in water.[33] Furthermore, the conditions surrounding Log P and stability set by Zhu have been supported by further studies by Pustulka using the miLog P algorithm.[45] This suggested that nanoparticles could be produced using compounds with a log P greater than ~6.[45] Although, slight differences have been found between various algorithm models.[49] It is also likely that the higher Log P compounds also possessed lower aqueous solubilities which hindered any likelihood of Ostwald ripening. This work firstly supports how Log P has potential to be used as a predictive tool with regards to nanoparticle stability, while there is a clear need for further research focused on the relationship between Log P and nanoparticle stability. Therefore, it is likely that the solubility of a compound not only influences the stability of the nanoparticles but also the size and the polydispersity of the nanoparticles that are formed.

1.4. Prodrugs

A challenge faced by modern day medicine is how the physical properties of drugs may hinder or prevent their potential therapeutic effect. Many barriers to drug development arise during drug formulation due to pharmacokinetics issues with the drug molecule. Reasons for pharmacokinetics vary from; poor aqueous solubility, poor absorption as well as rapid clearance/metabolism and toxicity.[50] As a result, research has developed the strategy of synthesising prodrugs. A prodrug is a derivative of the parent drug molecule which upon undertaking an enzymatic or chemical

transformation *in vivo* will revert back to the original drug molecule. The reasoning behind the development of prodrugs vary from improving physiochemical or pharmacokinetic properties of pharmacological agents.[50,51] The design step of a prodrug is imperative to its function as properties of prodrugs may influence physical properties as well as alter *in vivo* aspects such as biodistribution, efficacy and toxicity.[4] Furthermore, during prodrug design one must not only consider the prodrug itself but also consider the potential degradation products. Nevertheless, it is common that materials used to conjugate to drugs are biocompatible. An example being lipid drug conjugates whereby drugs are conjugated to lipid derivatives commonly found in nature.[52] For example, upon activation esters are known to degrade to release the parent alcohol and fatty acid. Meanwhile, carbamate esters are known to degrade releasing the parent alcohol drug along with carbamic acid which then rapidly degrades releasing the corresponding amine and carbon dioxide.[53] Similarly carbonate esters degrade to release two parent alcohols and carbon dioxide.

1.4.1. Types and methods of preparing prodrugs

Overtime a wide variety of different functional groups have been employed in efforts to establish a covalent bond between the drug and the pendant moiety to synthesise a prodrug. Examples of the various functional groups involved in prodrug synthesis are summarised by Fig.1.11. With respect to lipid nanoparticle formulation a specific strategy of prodrugs are lipid drug conjugates. Lipid drug conjugates essentially involve the therapeutic drug to be covalently bonded to a lipid molecule such as; fatty acids, fatty alcohols, glycerides, phospholipids and steroids.[54,55] In doing so the physical properties such as hydrophobicity and lipophilicity can be drastically changed. This has been demonstrated by Olbrich *et al*, whereby high drug loading ~33 % of the water soluble diminazene diaceturate within a solid lipid nanoparticle was achieved by conjugating the drug to fatty acids.[55] Furthermore, Shi *et al*. successfully conjugated the topoisomerase inhibitor SN38 to cholesterol *via* an ester linkage. The resultant prodrug was then formulated and integrated within the scaffold of a liposome. Findings displayed improved encapsulation of the prodrug compared to the drug while also improving drug tolerability, extended blood circulation and increased preferential accumulation. An example of how properties such as LogP can be dramatically changed during the conjugation of a lipid derivative is the reaction of emtricitabine with various chain lengths of n-alkyl chloroformates to produce prodrugs for semi solid prodrug nanoparticle formulation by Hobson *et al*.[17] The schematic overview of the strategy employed from prodrug synthesis to prodrug screening and particle formulation and prodrug release and activation is depicted by Fig.1.12-A. Furthermore, the library of prodrug was characterised by their corresponding calculated LogP (cLogP) against the number of 'hits' whereby that specific prodrug successfully produced a particle formulation during the screening process, relationship is depicted by Fig.1.12-B. An observable trend was how the number of hits

increased with increasing cLogP of prodrug. [54] Despite the clear advantages of lipid drug conjugates challenges such as bond stability exist as lipid drug conjugates are commonly conjugated by ester bonds, which may also be easily hydrolysed resulting in premature release of drug. Due to the vast variety in prodrug structures a classification of prodrug type has been developed which categorises prodrugs according to the site of conversion and location of activation, Table 1.[56] Overall, due to the wide range potential for prodrug synthesis avenues it appears a promising strategy for the future of drug formulation.

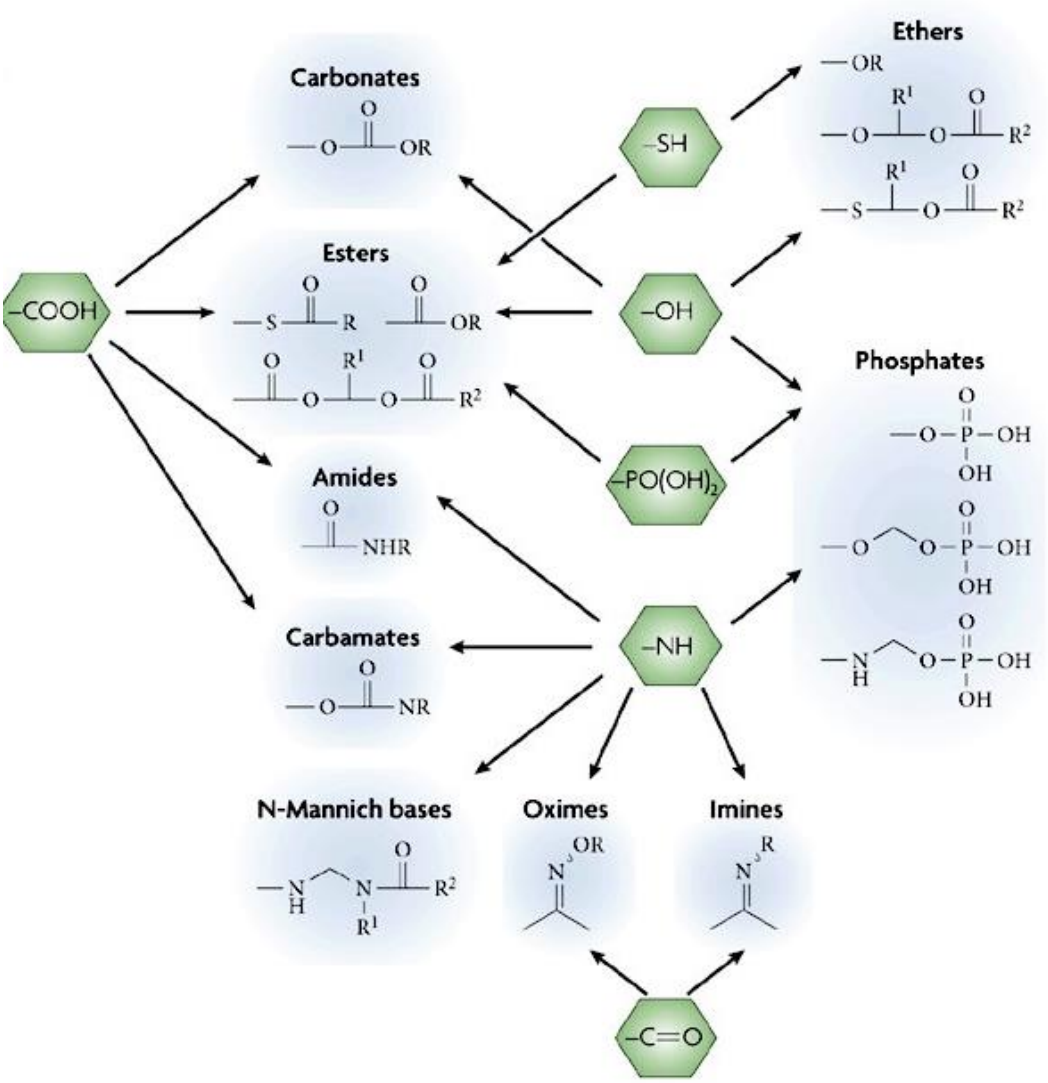

Figure 1.11- Illustration mapping out the various functional groups involved to form common linkers found in prodrug synthesis. Figure by Rautio *et al.* reproduced with permission from Springer Nature.[50]

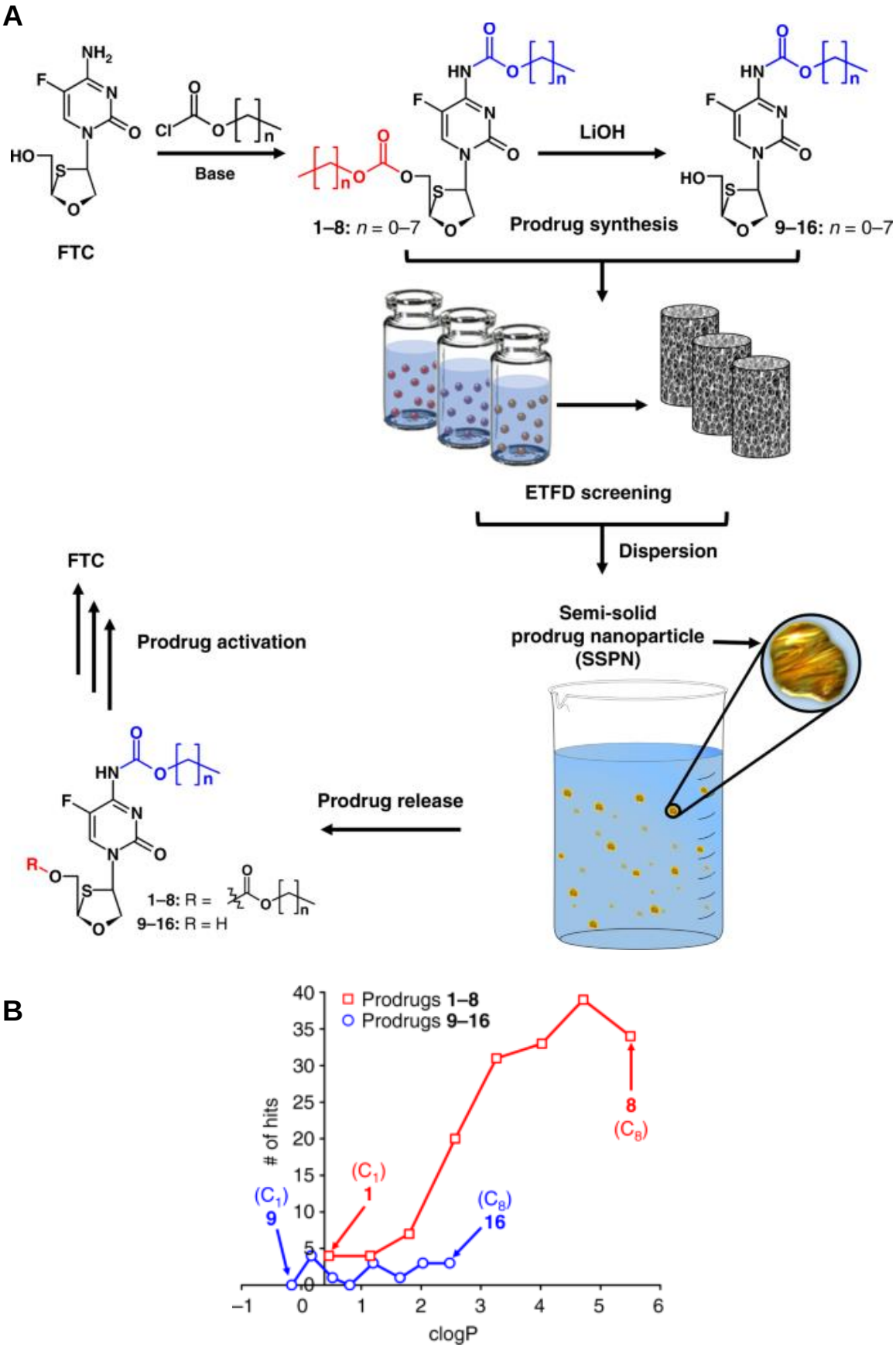

Figure 1.12- A) Schematic overview of strategy employed by Hobson *et al*. B) Relationship between cLogP and the number of hits identified for each prodrug candidate. Figure by Hobson *et al.* reproduced with permission from Springer Nature.[17]

Table 1.1- Table of prodrug classification adapted from Wu et al.[56]

Prodrug types	Site of Conversion	Subtypes	Tissue Location of Conversion	Examples
Type I	Intracellular	A	Therapeutic Target Tissues/Cells	Acyclovir, 5-Flurouracil, Zidovudine
		B	Metabolic Tissues (liver, GI mucosal cell, lung, etc.)	Primidone, Heroin, Phenacetin
Type II	Extracellular	A	GI Fluids	Oxyphenisatin, Sulfrasalazine
		B	Systematic Circulation and Other Extracellular Fluid Compartments	Acetylsalicylate, Bambuterol, Fosphenytoin
		C	Therapeutic Target Tissues/Cells	ADEPs, GDEPs, VDEPs

1.4.2. Prodrug activation

Once a prodrug has been successfully designed and formulated it is common for a series of prodrug activation experiments to be performed. These experiments investigate whether the prodrug may revert back to the drug under physiological conditions and, while also determining the rate of release. Rates of release may vary depending on the formulation i.e. is the prodrug free or encapsulated within a particle, while the type of linker used to synthesise the prodrug may also impact the rate of release. For example, ester bonds are subject to hydrolysis and may result in release of drug.[54] Although, reports by Huang *et al*. suggest esters and ester derivatives vary in rates of hydrolysis.[57] Due to the potential for prodrug hydrolysis it is common for prodrug activation/drug release experiments to consist of a control whereby the release of drug is assessed in the absence of enzyme as well as in the presence of enzyme.[54] Both experiments are commonly performed under physiological conditions such as in phosphate buffered saline (PBS) at pH ~7.4 with a maintained temperature of 37 °C while maintain sink conditions. Typical experimental set up may be by dialysis whereby the enzyme and

particles containing prodrug are encapsulated within a dialysis chamber while the membrane allows permeability of degradation products such as the drug to migrate into the dialysate. Aliquots are usually taken of the dialysate over periods of time and may be analysed by high-performance liquid chromatography (HPLC) with a UV detector to quantify drug release over time.[17] Alternatively, a one pot set up may be employed as long as sink conditions are maintained. Samples may simply be quenched with methanol and centrifuged prior to HPLC analysis.[17] As long as the drug is UV active the release may be quantified by comparing the UV signal detected at the given retention time to that of a predeveloped calibration graph of various concentrations of drug and their corresponding UV signal.[17] Fig.1.13-A displays a HPLC stack plot highlighting the increase in peak intensity of the drug over time, meanwhile Fig.1.13-B displays the standard calibration standard curve which is a linear plot indicated by the R^2 =0.99, which is used to determine the concentration of drug at various time points. Finally, Fig.1.13-C displays the corresponding structures of prodrug and the drug released emtricitabine. Furthermore, in their work, Hobson *et al*. linked the *in vitro* data to *in vivo via* modelling, this predicted sustained release of emtricitabine, giving rise to potential application as a long acting injectable.[17]

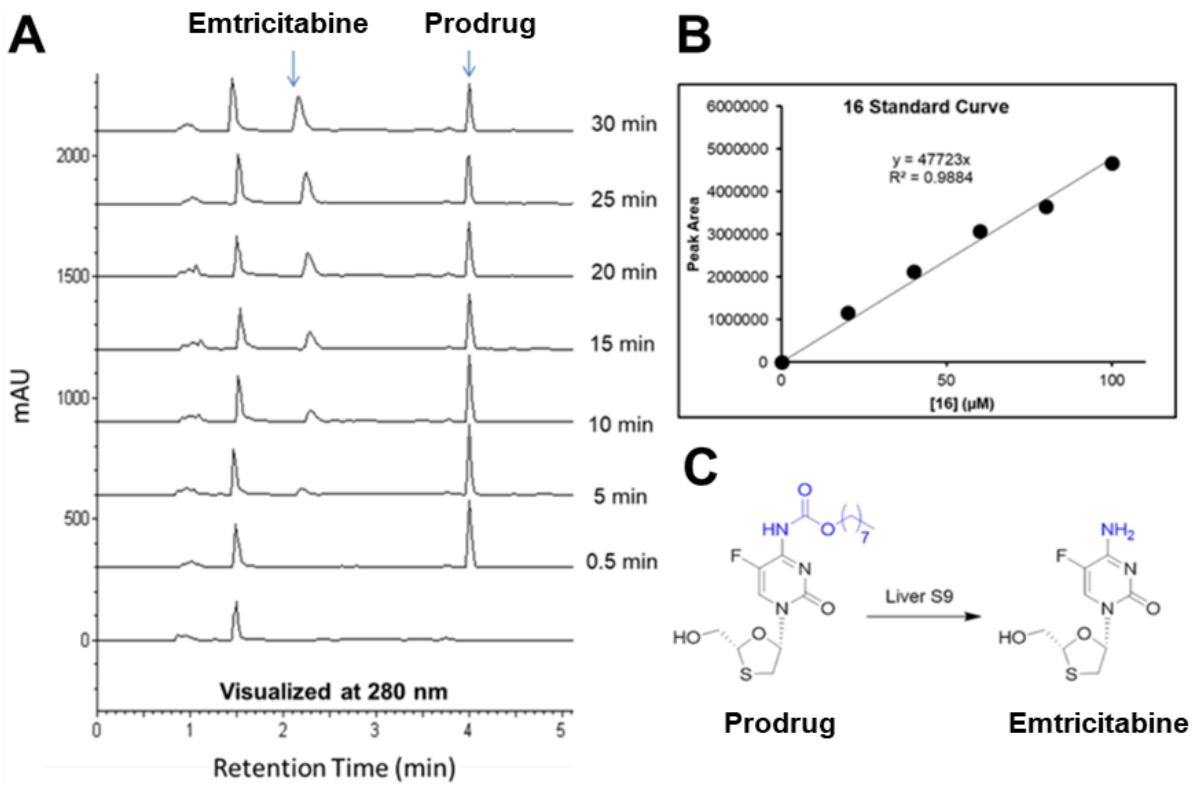

Figure 1.13- A) HPLC Stack plot measured at 280 nm, B) standard linear calibration plot and C) structures of the corresponding prodrug and drug. Figure by Hobson *et al.* reproduced with permission from Springer Nature .[17]

In addition to the wide variety of linkers used a range of enzymes may be trialled and various types of esterase enzymes are commercially available. Nevertheless, a common esterase found in activation studies of ester-based prodrugs is porcine liver esterase.[54] The drug release over time data of an *in vitro* drug release from a prodrug liposomal formulation carried out by Shi *et al* is shown by Fig.1.14. This particular study investigated the release in the presence and the absence of porcine liver esterase to cleave an ester linker. The release data shows rapid release to ~ 50 % within 12 hours and > 70 % after 5 days while in the presence of 50 U/mL enzyme. The experiment also reveals a much slower release is achieved in the absence of enzyme. Thus, proving the prodrug was successfully activated to release the drug in the presence of enzyme while also possessing some instability at physiological conditions in the absence of enzyme. Overall, suggesting the strategy of prodrugs may be used to tune drugs to more desirable physical properties which enable formulation within a nanoparticle and may provide avenue to achieve sustained release of active material.

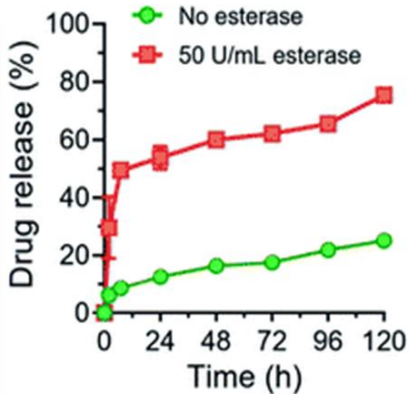

Figure 1.14- *In vitro* drug release profiles from ester-based prodrug incorporated within a liposomal formulation. Release was performed at physiological conditions in absence and in the presence of 50 U/mL enzyme. Reproduced from Shi *et al.* with permission from the Royal Society of Chemistry.[54]

1.5. Cryopreservation of lipid nanoparticles

Lipid nanoparticles may suffer from poor colloidal stable over a prolonged period of time. Furthermore, active ingredients that may be encapsulated within a colloidal dispersion such as mRNA are commonly prone to degradation by hydrolysis.[7] As a result, research has looked towards methods to preserve formulations for long term storage to enhance feasibility of colloidal pharmaceutical formulation by allowing time for storage and shipment. Cryopreservation is a strategy commonly employed to enable the long-term stability of nanoparticle formulations to enable storage while being readily available upon request. More recently cryopreservation has received vast attention due to

being explored as a solution for gene therapy lipid nanoparticle vaccines.[58–61] The two key methods of cryopreservation are freeze thaw and freeze drying otherwise known as lyophilisation.[58]

1.5.1. Freeze thaw

Freeze thaw is a process whereby nanoparticle formulations are frozen and stored in their frozen state to lock in the nanoparticles within ice, until needed whereby the formulation is allowed to thaw out and release the nanoparticles to return to a colloidal formulation. The process of freeze thaw is therefore relatively simple and has been employed as a method to preserve the stability of the mRNA COVID-19 BioNTech/Pfizer and Moderna vaccines. In this process, the formulations are frozen at temperatures as low as -70 °C before thawing out prior to use,[62,63] Fig.1.15-A. Nevertheless, despite the potential benefits of freeze thaw, the process induces stress on formulations. Upon freezing, the water in aqueous formulations nucleates to produce ice crystals which grow until the entirety of the water within the sample becomes solid ice, Fig.1.15-B.

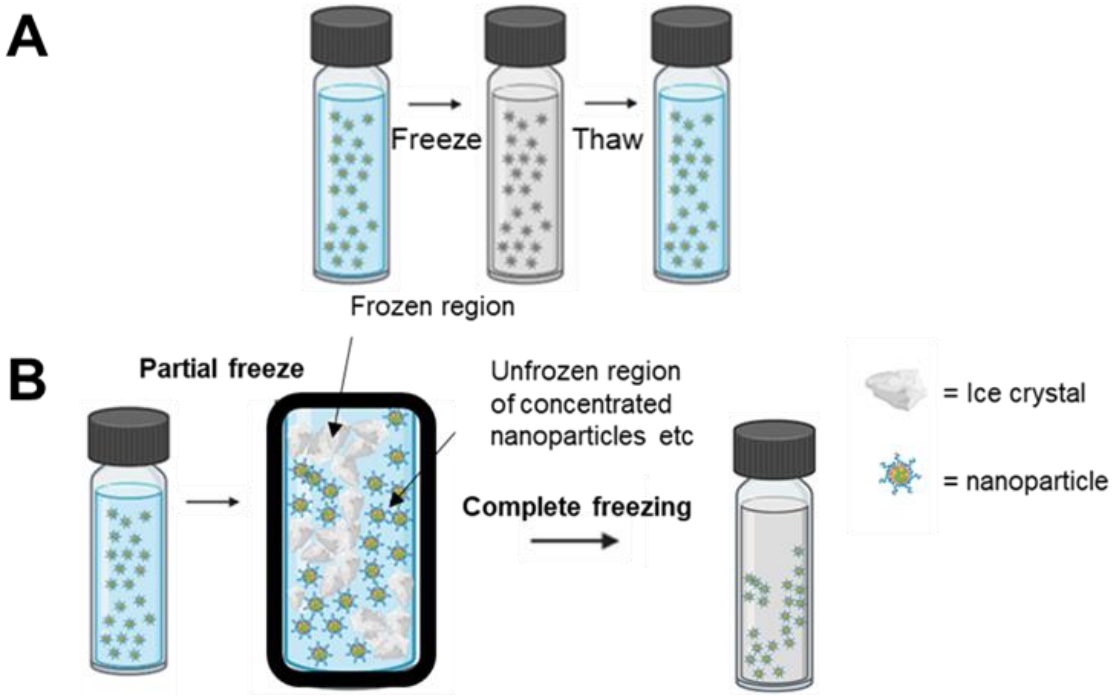

Figure 1.15- Illustration summarising the steps of freeze thaw. B) Illustration depicting the concentration of nanoparticles during ice crystal formation

Unfortunately, during the growth of the ice crystals the nanoparticles may be concentrated in areas of unfrozen solution along with any buffers, non-encapsulated materials or additives such as cryoprotectants.[64] This induces stress upon colloidal stability causing close contact between nanoparticles facilitating particle-particle attractive interactions and potentially particle

aggregation.[65] This theory is supported by the sucrose-water phase diagram which shows how a dilute sucrose concentration increases in concentration during freezing until the temperature reaches the glass transition temperature of the maximally cryo-concentrated solution, shown as T'g on Fig.1.16. The glass transition temperature is defined by the temperature at which a material transitions from a rigid to flexible state.[66]

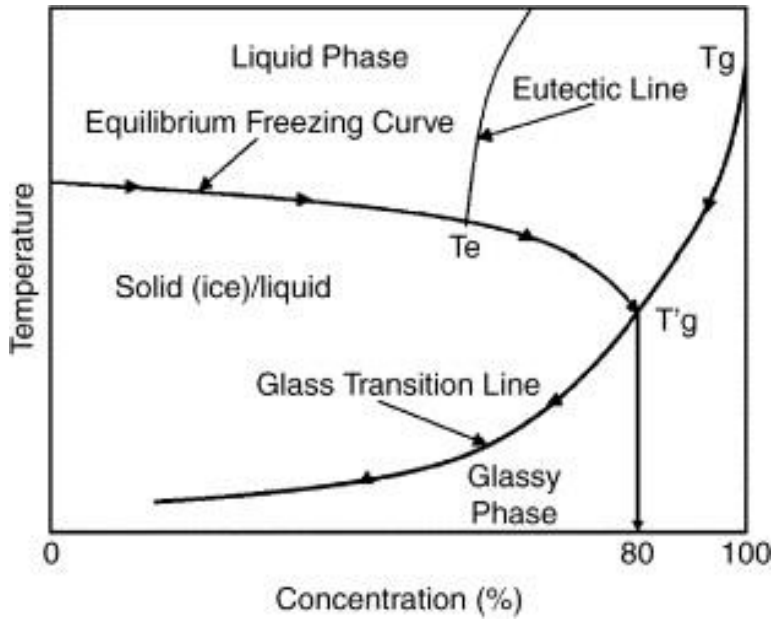

Figure 1.16- Phase diagram for sucrose-water mixtures showing relationship of concentration, temperature and Tg'. Reproduced from Abdelwahed et al. with permission from the Elsevier.[66]

As a result, the rate of freezing is a parameter that has previously been investigated due to the influence on ice crystal nucleation and growth. A study by Schwarz *et al*. investigated the rate of freezing by freezing samples at – 25 °C in a freezer (slow) vs freezing in liquid nitrogen at – 196 °C (fast). Samples frozen in liquid nitrogen showed smaller diameters in the largest 10 % of particles in the size distribution, Fig.1.17. The results suggested rapid freezing in liquid nitrogen resulted in greater stability of the formulation during cryopreservation.[67] It is hypothesised that a faster rate of freezing resulted in more rapid, smaller and uniform crystal formation which resulted in a more homogenous distribution of nanoparticles within the ice and less and therefore less concentrated nanoparticles.[67,68] Although, it has been argued the stability of a formulation may vary depending on the chosen stabiliser in the nanoparticle formulation as one stabiliser may favour fast freezing while another favours slow freezing.[69] Due to the implications of freeze thaw many researchers are now using it as a method to screen formulation properties to be later trialled for freeze drying.[70]

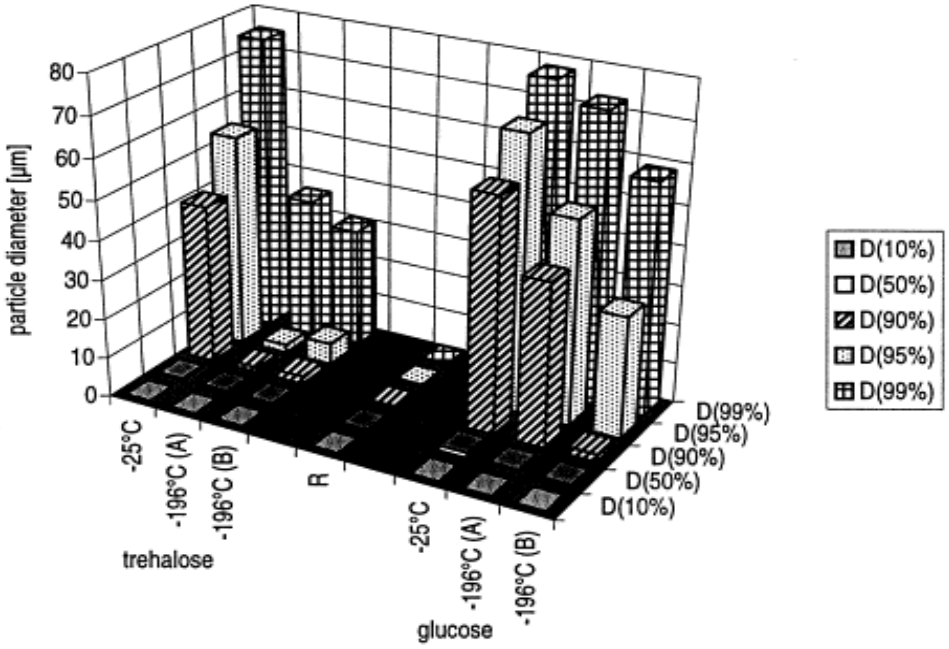

Figure 1.17- Graph displaying differences in particle diameter data obtained by DLS of reconstituted lyophilised particle formulations depending on the freezing rate. Freezing methods; slow freezing at -25 °C, rapid freezing by addition of formulation to liquid nitrogen (- 196 °C (A)) or by dipping the whole vial into liquid nitrogen (- 196 °C (B)). Reproduced from Schwarz *et al*. with permission from the Elsevier.[67]

1.5.2. Freeze drying/Lyophilisation

Freeze drying/lyophilisation is a multistep process whereby the formulation is frozen before being dried using a freeze dryer by a primary drying step *via* sublimation, followed by a secondary drying step of desorption of resident moisture to leave a solid monolith described as a 'cake' or 'scaffold'.[71,72] The freeze dried 'cake' may then be stored until required whereby the cake may be rehydrated resulting in reconstitution to redisperse the nanoparticles and return to a colloidal formulation.[67] The multistep process of freeze-drying is depicted by Fig.1.18. Alternatively, the freeze-dried material may also be incorporated within tablets for oral administration.

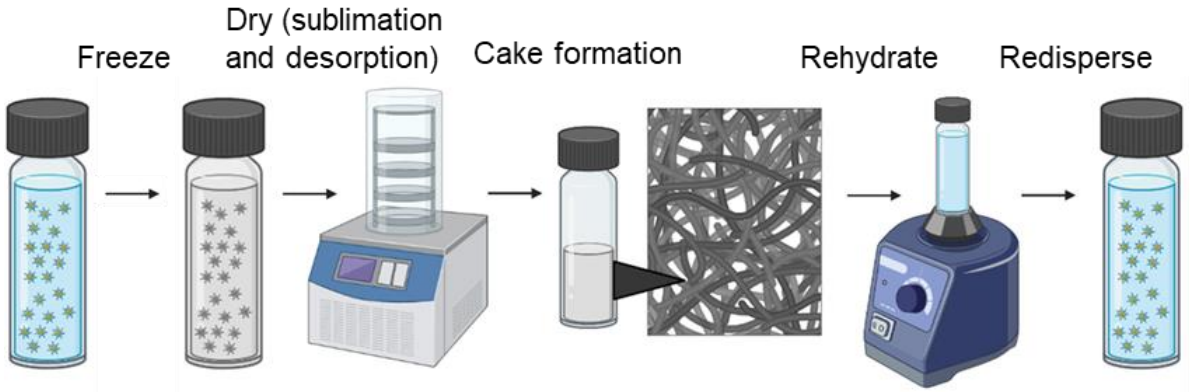

Figure 1.18- Illustration summarising the steps of freeze-drying/lyophilisation

Sublimation of ice operates *via* the sublimation principle whereby water is transformed from the solid state (ice) to the gaseous state (water vapour) bypassing the liquid state (water), represented by A on Fig.1.19. Sublimation occurs at temperature and pressure below that of the triple point (0.001 °C and 0.006 kPa for water). As a result, the formulation must be first frozen before placing under vacuum. Once under vacuum and maintained below the vapour pressure of water, sublimation occurs and is driven by the pressure differential between the product and the condenser. As a result, a condenser is required at a temperature lower than that of the product in order to cool the temperature of the solvent to decrease pressure.[73]

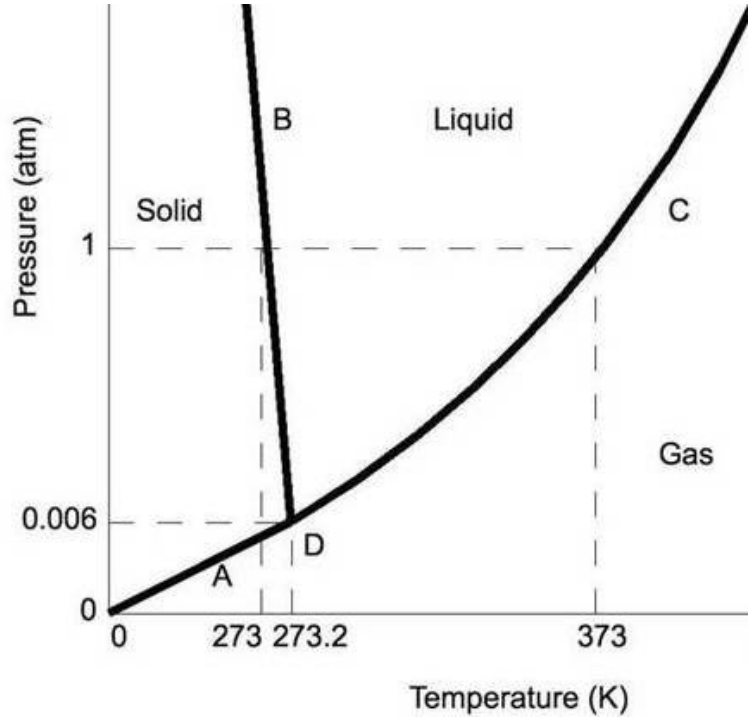

Figure 1.19- Phase diagram of water under pressure highlighting the triple point adapted from www.chem.libretexts.org.[74] A) Sublimation line; B) Melting line; C) Boiling line; D) Solid Liquid Vapour triple point.

Fig.1.20 displays scanning electron microscopy (SEM) images taken of a polymer scaffold produced by freeze-drying indomethacin nanoparticles stabilised by a PEG-based polymer. The authors showed that the formation did not display aggregation of nanoparticles and could be reconstituted in water to reform the aqueous nanoparticle dispersion. The porous structure of the cake/scaffold was the result solutes being spatially arranged during freezing as ice crystals form which was then exposed during the of sublimation of ice.[72]

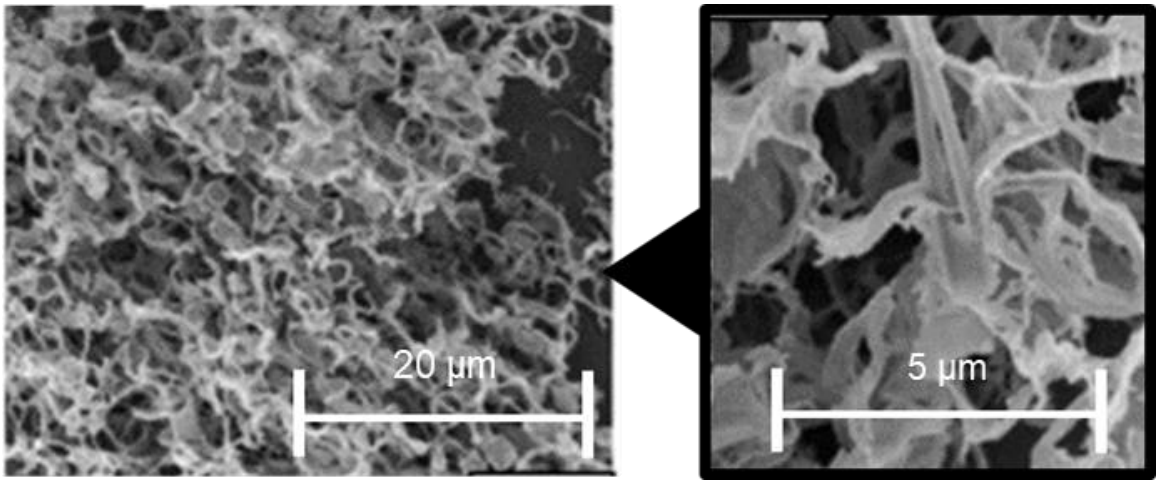

Figure 1.20- SEM images of polymer scaffolds with indomethacin nanoparticles. Adapted from Zhang *et al*. with permission from the Elsevier. [71]

Unfortunately, the added steps of freeze-drying subject the formulation to further stress. During freeze drying/lyophilisation as the ice is sublimed there is no longer any ice to maintain separation of nanoparticles which can potentially causes nanoparticle aggregation. In some cases, aggregation is irreversible and the sample cannot be redispersed. Furthermore, a freeze-dried cake/scaffold may have a vastly expanded surface area and may not be capable of maintaining its structural integrity leading to cake collapse as shown by Fig.1.21. In addition, cakes are commonly sensitive to air and moisture which may result in cake collapse and often poor redispersion.[75] For that reason, studies have been performed to investigate cake stability at various storage conditions such as temperature and humidity.[76] Although, it has been suggested that moisture content is not always a deciding factor in whether cakes collapse or not, thus suggesting it may be down to the material or amount used as a cryoprotectant/lyoprotectant.[77]

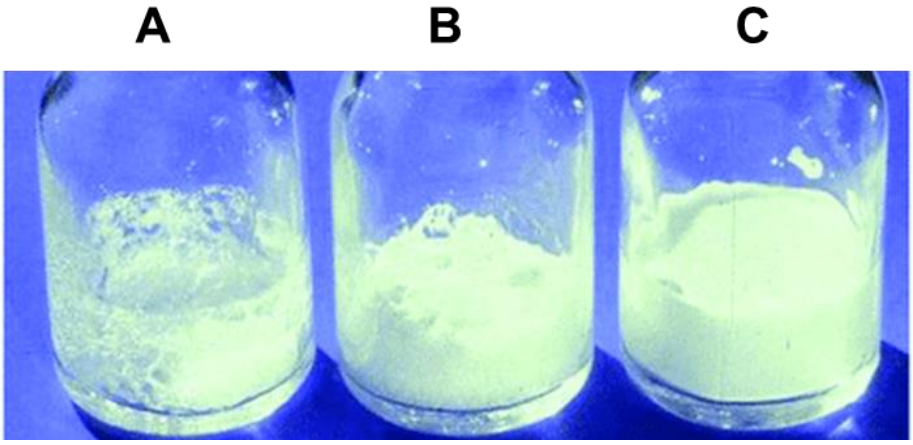

Figure 1.21- Photos taken of freeze-dried materials to display differences in cake stability. A) Complete collapse, B) Partial collapse and C) No evidence of collapse. Adapted from Patel *et al*. with permission from Elsevier.[78]

Much research has gone into investigating cake appearance and product quality, with links made between the mechanism of ice nucleation and crystal growth with the solute distribution within a frozen matrix. It is believed that a controlled ice nucleation may result in a reduced primary drying time and thus a more homogenous cake appearance.[79] Although, other researchers have suggested that a non-uniform cake may have no impact on the product quality.[78] Nevertheless, Fig.1.22 clearly shows the differences of internal structure between; two different sugars sucrose and trehalose (Fig.1.22 A and B) with both forming amorphous porous matrices. Sucrose formed a less porous matrix; the differences between with and without a cryoprotectant/lyoprotectant as in the absence of an additive presented a poorly porous structure which included large holes suggesting cake collapse (Fig.1.22 A and C or B and C). In addition if the ratio of additive to nanoparticle is not high enough a cake may show signs of cake collapse similar to that in the absence of any additive (Fig.1.22 B and D).[80]

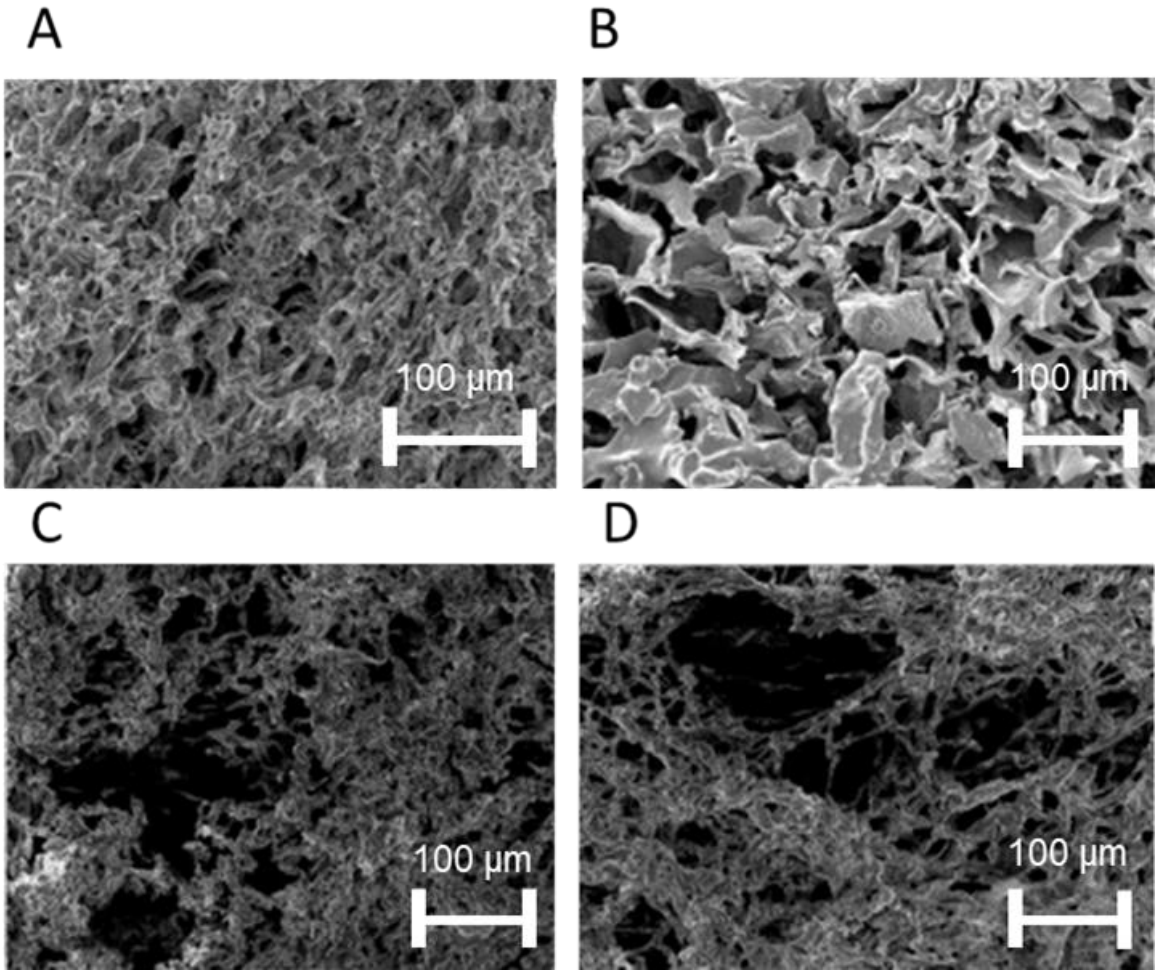

Figure 1.22- SEM images of freeze dried liposome formulations; A) in the presence of sucrose (sugar to lipid, S:L) = 5:1, B) in the presence of trehalose S:L = 5:1, C) in the absence of cryoprotectant/lyoprotectant and D) in the presence of trehalose S:L = 3:1. Adapted from Sylvester *et al*. with permission from the Elsevier [80]

In the development of lipid nanoparticle formulations many routes incorporate the use of organic solvents which should be removed from pharmaceutical formulations, therefore another advantage to freeze drying is the ability to remove residue organic solvents from formulations.[81] However, the inclusion of more than one solvent does make understanding the process more complex; there have also been reports of how freeze drying co-solvent systems can decrease instances of cake collapse depending on cosolvent and the ratio of cosolvent and solvent. For example, DeLuca *et al*. studied how accelerated freeze-drying rates of aqueous solutions may be achieved upon addition of 5 and 10 % *tert*-butanol. They suggested that by introducing *t*-butanol then the drying times could be shortened. They proposed this was due to the sublimation of *t*-butanol during primary drying which left cakes which were highly porous structures and therefore, facilitated an accelerated of water vapour.[82] Although, the organic solvent must freeze under the conditions employed during lyophilisation otherwise will result in cake collapse.[82,83]

Another parameter commonly explored is the method of redispersion. Upon rehydration some cakes may rapidly dissolve with the aid of manual shaking while others require some assistance. Additionally, the variability between manual shaking has led to the development of various redispersion methods. Sonication is an efficient method of redispersion, however proves difficult in a real-life clinical setting.[67] As there is also variation in the degree of redispersion it is common in literature for formulations to be graded on their ability to redisperse for example Amis *et al*. employ the grading system of; 1- fully redispersed, 2- redispersed but signs of slight aggregation or particle size increase, 3- poorly redispersed.[75] Other studies by Schwarz highlighted how the inclusion of drug within a solid lipid nanoparticle may impair the reconstitution quality, although an explanation as to why was not provided.[67]

Overall, there appears to be several variables that may influence the redispersiblity of a formulation, although the common link between all is the structural integrity of the cake formed upon freeze-drying. With any signs of cake collapse massively damaging the quality of the formulation post redispersion. Furthermore, it is desirable for any cake formed to easily dissolve without the need of sonication while also not be impacted by the inclusion of drug.

1.5.3. Cryoprotectants and Lyoprotectants

Nanoparticle formulations typically often cannot withstand the stresses of cryopreservation alone. As a result, additive agents such as cryoprotectants may be added to formulations to help maintain colloidal stability during the stressful events of freezing. Similarly, lyoprotectants may be used to maintain separation and stability of nanoparticles during the sublimation step of lyophilisation.

Materials act as cryoprotectants by three different mechanisms. Firstly, by establishing a protective layer around particles by hydrogen bonding between the cryoprotectant and the polar functional groups at the surface of the particle.[84] Secondly, by forming glass matrices when frozen bellow their glass transition temperature which prevents aggregation.[85] Finally, particle isolation hypothesis whereby materials maintain separation of particles during freezing due to an increase in viscosity of the unfrozen phase caused by concentration of the cryoprotectant.[85] As a result, many materials that act as cryoprotectants also act as lyoprotectants. In essence, cryoprotectants/lyoprotectants work by replacing water molecules and preventing aggregation of nanoparticles,[75] as shown by Fig.1.23. Furthermore, materials proven as efficient cryo/lyoprotectants are various sugars such as sucrose, trehalose, glucose and mannitol as well as some polymers such as PEG based polymers.[66,75,86] Although some sugars appear to be more efficient and are more commonly used in literature such as sucrose.[66,67] Consequently, cryoprotectants and lyoprotectants are commonly investigated over a range of various concentrations for example common concentrations are 1, 5 and 10 % w/v.[75] Overall, cryoprotectants and lyoprotectants have potential to massively improve the stability of lipid nanoparticle formulations against the stresses of freezing and drying although variables such as type and concentration of cryoprotectants/lyoprotectants requires further research.

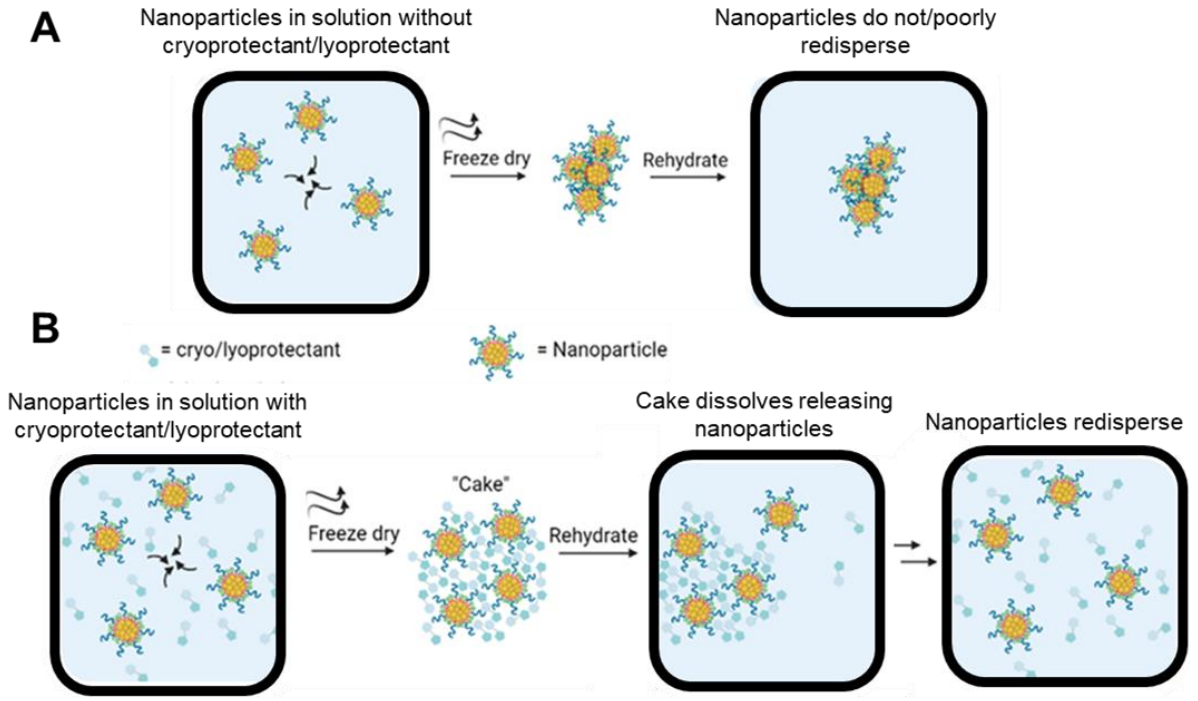

Figure 1.23- A) Illustrates how aggregation may occur in the absence of a cryoprotectant or lyoprotectant during freeze drying. B) Illustrates how the water replacement theory works during lyophilisation to maintain colloidal stability.

1.6. Lipid nanoparticles for nucleic acid delivery

Nucleic acids polymers such as mRNA are a single stranded molecule of RNA that has recently been investigated to revolutionise a new age of medicine known as genetic therapy.[87] Essentially mRNA is a genetic sequence which acts as the instructions for a cell to synthesise a protein. Therefore, the delivery of mRNA has potential in a medical setting by providing the body with the essential instructions to synthesise essential molecules such as spike proteins or antibodies which are necessary in encounters with viruses such as COVID-19. Since the successful application of mRNA vaccines against COVID-19 much more attention has been drawn to the technology of mRNA. Experts believe potential application could stretch wider than combating viruses and could be used in the treatment of cancer and neurological diseases such as multiple-sclerosis and Parkinson's,[88–90] consequently the application of nucleic acid-based therapy appears to be endless. Nevertheless, mRNA if introduced to the body without the aid of a delivery vehicle will result in degradation as well as lack the ability to cross cellular membranes resulting in poor immunogenicity.[91] As a result, research has led to the investigation of various delivery vehicles that not only protect the mRNA but aid in the delivery of mRNA to cells.

1.6.1. Development of LNPs for nucleic acid delivery

Various structures have been trialled for mRNA delivery such as the adeno-associated viral vector. Adeno-associated viral vectors were employed during the COVID-19 pandemic in the Oxford/Astra Zeneca vaccine,[92] although the BioNTech/Pfizer and Moderna vaccines at achieved the highest efficacy at 95 %.[93,94] Which has led to Wei *et al*. suggest how the lipid nanoparticle vehicle is the most advanced vector and most favoured going forward.[91] The development of lipid nanoparticles for the encapsulation and delivery of nucleic acids started with attempts to encapsulate nucleic acids within traditional liposomes. However after poor encapsulation efficiencies liposomal formulations were modified to include cationic lipids such as 1,2-dioleoyl-3-trimethylammonium-propane chloride salt (DOTAP-Cl).[95] The result was the formation of a lipoplex. Lipoplexes share similarities to the lipid nanoparticles used today as both still employ the strategy of using a cationic lipid to complex with the anionic backbone of nucleic acids. On the other hand, lipoplexes were found to contain much of the cationic phospholipid on the exterior membrane of the nanoparticle resulting in mRNA complexing to the exterior of lipoplexes rather than being encapsulated and thus less protection of the mRNA.[95] Further modifications have thus led to the development of the lipid nanoparticle structure known today. Despite still sharing similarities with its earlier counterparts the structure of the lipid nanoparticle known today is distinctly different. Molecular modelling by Leung *et al*. suggested the nucleic acid containing lipid nanoparticles contain random cavities of water surrounded by lipid

monolayers. Whereby, the nucleic acids are bound to the monolayers which has been depicted by Fig.1.24. The model predicted a ratio of ionizable cationic lipid/helper lipid/cholesterol/pegylated lipid of (4:1:4:1; mol/mol and a nucleic acid to lipid ratio of ~0.05 wt/wt).[96] Leung *et al* supported their model with data from studies investigating the stability of nucleic acid against bovine pancreatic RNase A which suggests encapsulation of nucleic acid due to resistance to degradation compared to free nucleic acid, Fig.1.25. Furthermore, Leung *et al*. also performed ^{31}P nuclear magnetic resonance (NMR) which revealed when formulated within a lipid nanoparticle the signal from free nucleic acid was lost Fig.1.26-B. This suggested that the mRNA was immobilized within the core compared to free mRNA (Fig.1.26-A) and once the lipid nanoparticle had become solubilised then the mRNA was releasedFig.1.26-C.[96] This study has been further supported by Evers *et al*. who performed also cryo-TEM analysis of some nucleic acid containing lipid nanoparticles and found distinct difference compared to a traditional liposome. Fig.1.27-A Displays the proposed structure of an nuclei acid containing lipid nanoparticle while Fig.1.27-B displays a cryo-TEM image displaying an electron rich core due to electron diffraction from the ionizable cationinc lipid and nucleic acid within the particle. Meanwhile, Fig.1.27-C) displays the structure of a traditional liposome and Fig.1.27-D a cryo-TEM image of a traditional liposome formualtion which distinctly displays an aqueous core due to electron densities consistent with the exterior of the liposome.[97] These key differences were imperative in determining the structure of the new class of lipid nanoparticles.

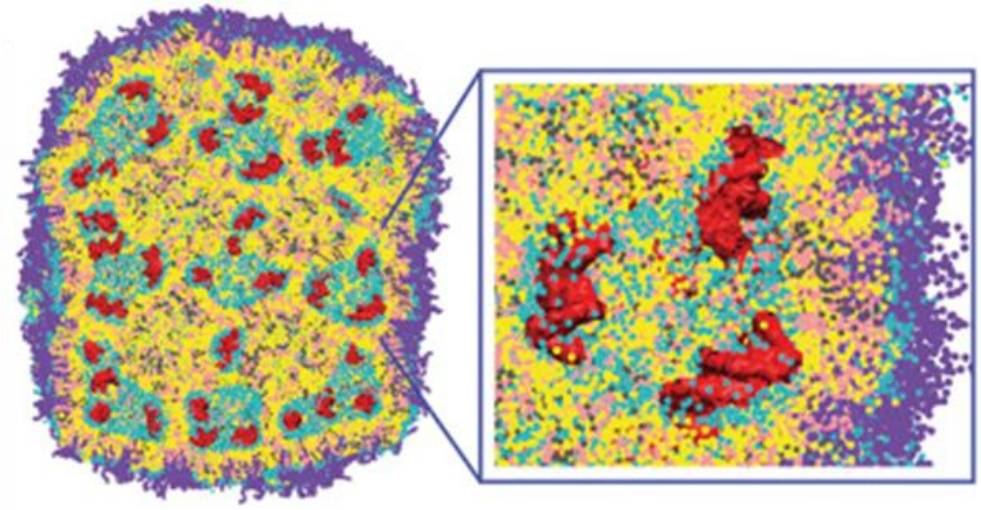

Figure 1.24- Molecular modelling image of the structure of a nucleic acid containing lipid nanoparticle. Colour coding represent distinct components of the lipid nanoparticle; yellow, ionizable cationic lipid; pink, cholesterol; grey, helper lipid; purple, pegylated lipid; red, nucleic acid. Note the author did not display water in this image for clarity. Reproduced from Leung et al. with permission from The American Chemical Society.[96]

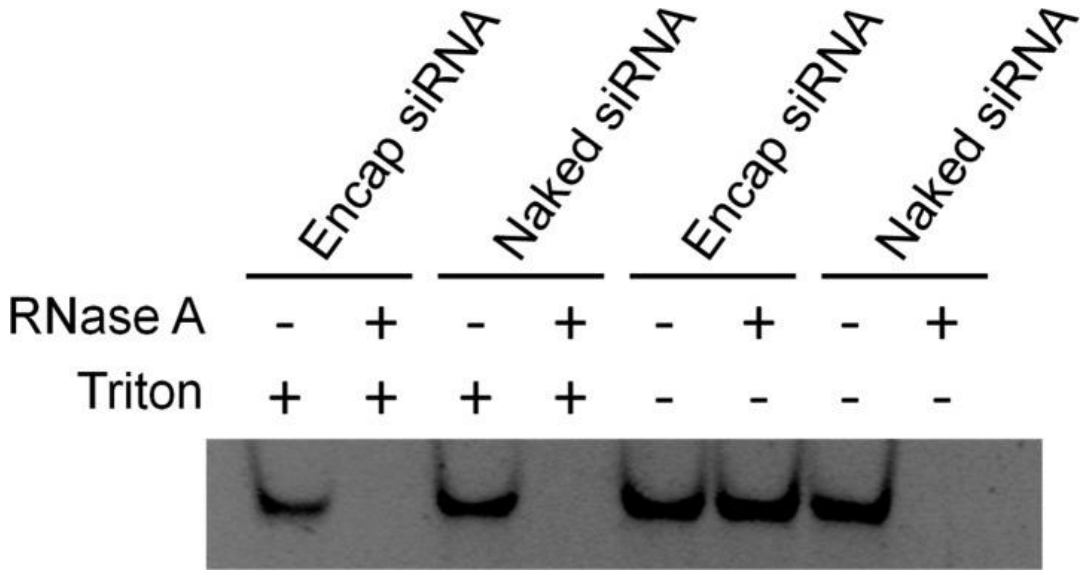

Figure 1.25- Study by Leung *et al*. supporting the theory of nucleic acid encapsulation within a lipid nanoparticle due to protection against external RNase. Tests show how nucleic acid when free is degraded by the RNase while protected when encapsulation. Triton used to solubilise lipid nanoparticle and thus prove presence of nucleic acid for used as a control. Reproduced from Leung et al. with permission from The American Chemical Society [96]

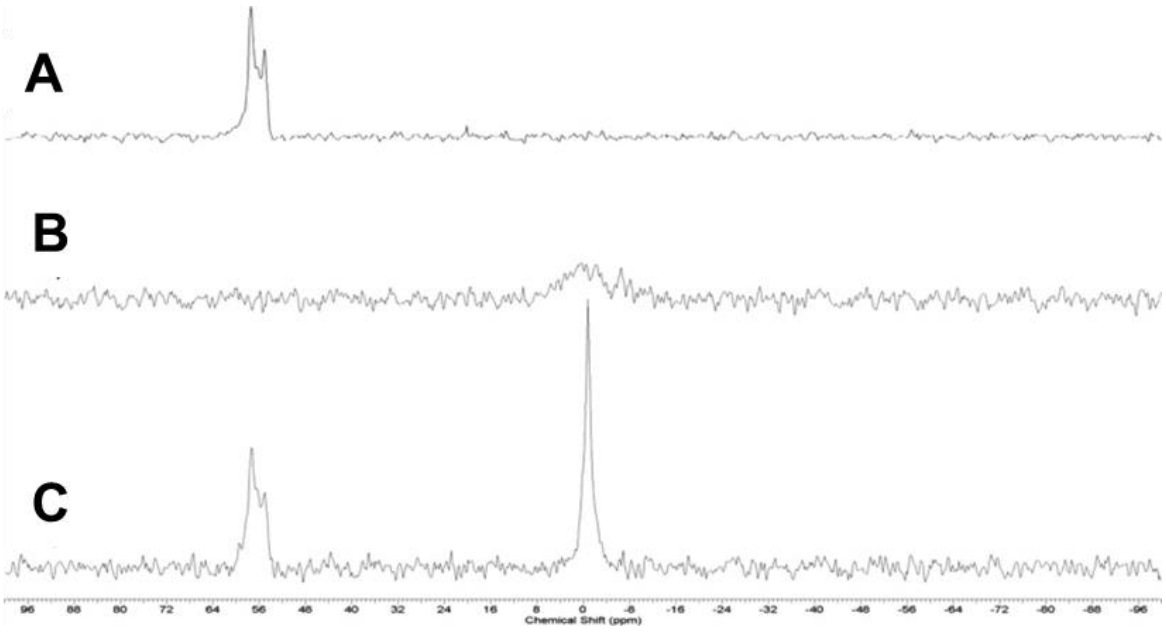

Figure 1.26- Study by Leung *et al*. further supporting theory of nucleic acid encapsulation within a lipid nanoparticle due to disappearance of peak on ^{31}P spectrum (B) for nucleic acid when formulated within a lipid nanoparticle thus suggesting encapsulation. Spectrum (A) displays the appearance of peak on ^{31}P spectrum for free nucleic acid. Spectrum (C) displays appearance of peak on ^{31}P spectrum for nucleic acid once the lipid nanoparticle has been solubilised to free the encapsulated nucleic acid. Reproduced from Leug et al. with permission from the American Chemical Society.[96]

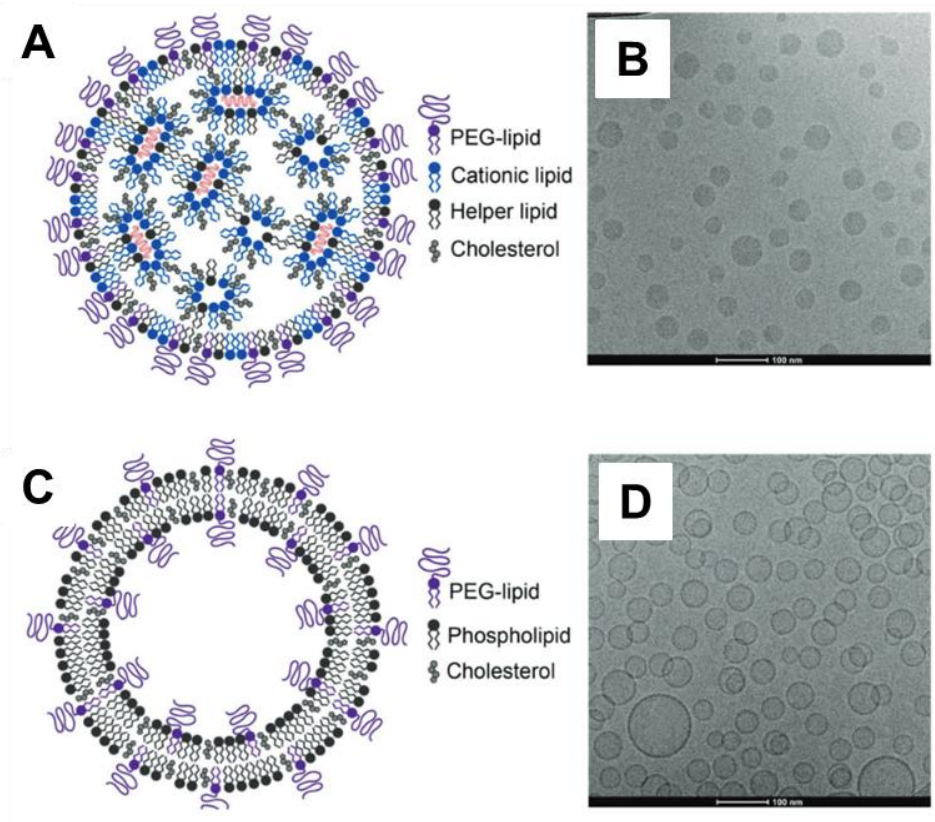

Figure 1.27- Compilation of images showing structural differences between that of a mRNA lipid nanoparticle and that of a traditional liposome. A) Structure of an nuclei acid containing lipid nanoparticle. B) Corresponding cryo-TEM image displaying an electron rich core due to electron diffraction from the ionizable cationinc lipid and nucleic acid within the particle. C) The structure of a traditional liposome. D) Corresponding cryo-TEM image displaying an aqueous core due to electron densities consistent with the exterior of the liposome. Reproduced from Evers *et al*. with permission from John Wiley and Sons. [97]

1.6.2. Components of LNPs for nucleic acid delivery

Other than mRNA itself, lipid nanoparticles for the delivery of mRNA contain four other key structural components; neutral phospholipid, cholesterol, pegylated lipid and an ionizable cationic lipid. Each of which are depicted schematically in Fig.1.28-A. Each of these components plays a role in achieving the goal of delivering the nucleic acid to the site of action i.e. cytoplasm of target cell. Production is commonly performed by microfluidics applying the principles of nanoprecipitation, whereby an aqueous phase is mixed under continuous and controlled conditions to produce lipid nanoparticles with diameter < 100 nm.[98,99] The aqueous phase typically consisting of buffer and nucleic acid i.e. mRNA. Meanwhile, the organic phase usually employs ethanol as an organic solvent and containing solutes such as the ionizable cationic lipid, helper lipid, pegylated lipid and cholesterol. Upon mixing, the solvent polarity increases and the components dissolved in the organic phase become supersaturated and nucleate. As well as nucleation, the ionizable cationic lipid also becomes protonated in the presence of the buffer such as citrate buffer pH 3-4 to ensure protonation.[100]

Consequentially, complexes between the ionized cationic lipid and the mRNA form due to electrostatic attractions between the positive charges of the cationic lipid and the negative charges of the nucleic acid backbone. The result is the generation of micelles whereby the nucleic acid is encapsulated by the cationic lipid.[96,101] These micelle complexes of ionized cationic lipid and nuclei acid then aggregate and are encapsulated by the helper lipid and pegylated lipid and cholesterol, Fig.1.28-B.[98] The pH of formulations is typically then increased to physiological conditions by dialysis against a secondary buffer such as tris(hydroyxlmethyl)aminomethane (TRIS).[7] In addition, cryoprotectants such as sucrose may be also be added to formulations to aid stability during cryopreservation. The blend and ratio of materials used in the nucleic acid lipid nanoparticles has been extensively investigated to examine the importance of each components roles in not only the encapsulation of nucleic acid but the efficacy of formulations once administered.[102] Table 2 lists the composition of the BioNTech/Pfizer and Moderna COVID-19 vaccines.

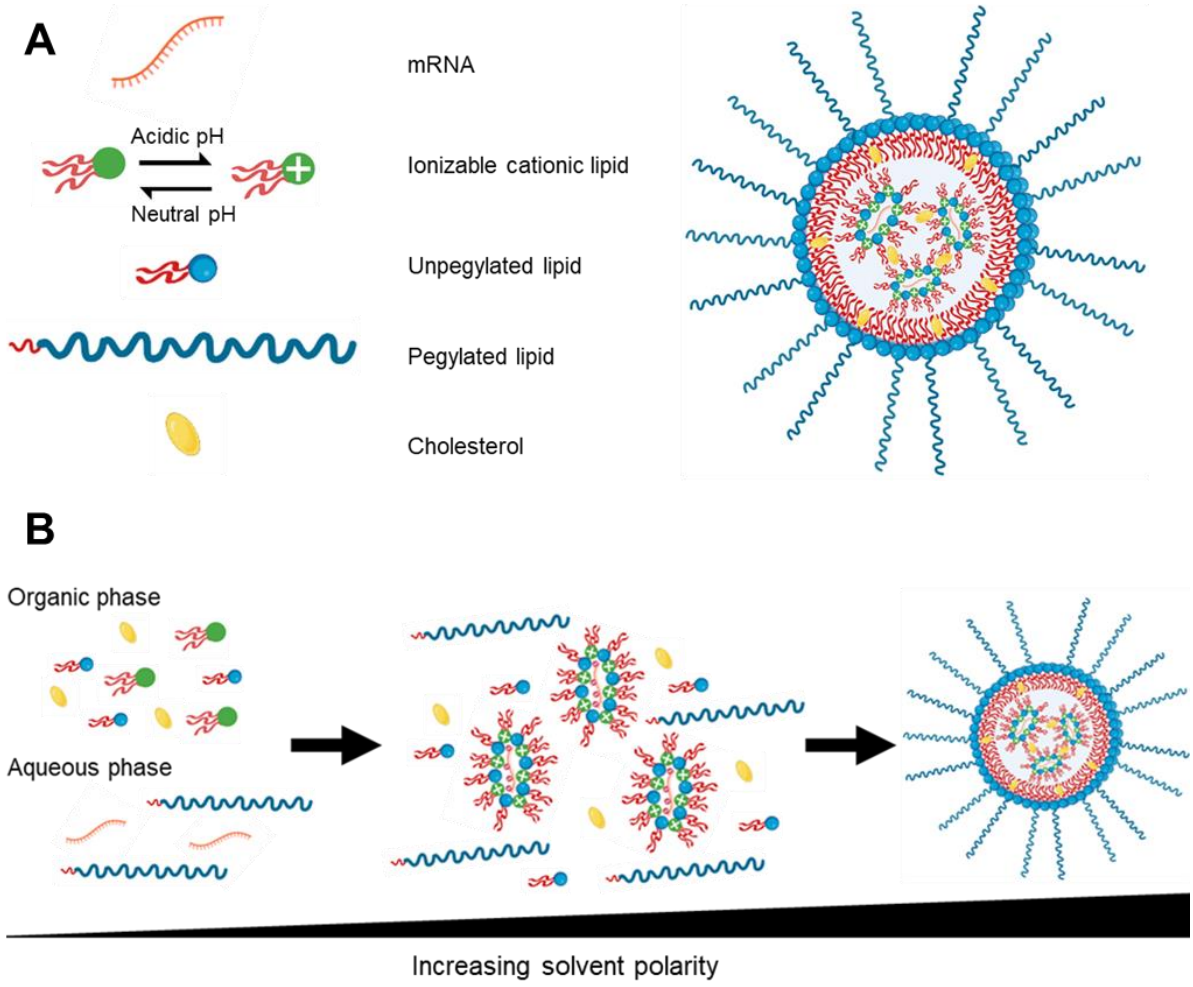

Figure 1.28- A) Illustration of lipid nanoparticle structure and individual components. B) Illustration of the how the lipid nanoparticles assemble during formulation.

Table 1.2- Composition of BioNTech/Pfizer and Moderna COVID-19 mNRA vaccines, adapted from Schoenmaker et al.[7]

	BioNTech/Pfizer mRNA vaccine	**Moderna mRNA vaccine**
Mrna dose	30 µg	100 µg
Lipid nanoparticle components (Ionizable cationic lipid, pegylated lipid, helper lipid, cholesterol)	**(ALC-0315)** [(4-hydroxybutyl)azanediyl)bis(2-hexyldecanoate)], (**ALC-0159)** (2-((polyethylene glycol)-2000)-N,Nditetradecylacetamide), (**DSPC**) distearoylphosphatidylcholine **Cholesterol**	**(SM-102)** (8-((2-hydroxyethyl)(6-oxo-6-(undecyloxy)hexyl)amino)octanoic acid,1-octylnonyl ester), (**DMG-MPEG-2K)** (1,2-dimyristoyl-rac-glycero-3-methoxypolyethylene glycol-2000) (**DSPC**) distearoylphosphatidylcholine **Cholesterol**
Molar lipid ratio (%) Ionizabe cationic lipid: helper lipid: cholesterol: Pegylated lipid	46.3 : 9.4 : 42.7 : 1.6	50 : 10 : 38.5 : 1.5
Molar ratios (N/P) Ionizable cationic lipid's nitrogen: nucleotide's phosphate	6	6
Buffer	0.01 mg potassium dihydrogen phosphate, 0.07 mg disodium hydrogen phosphate dihydrate pH 7-8	Tris pH 7-8
Other excipients	0.01 mg potassium chloride, 0.36 mg sodium chloride, 6 mg sucrose and water	Sodium acetate, sucrose and water

1.6.2.1. Ionisable cationic lipid

The ionizable cationic lipid is typically a tertiary amine that is ionically neutral at pH 7, and becomes cationic due protonation of the amine under acidic conditions below the acid dissociation constant (pK_a) of the lipid. Evers *et al*. have suggested that the most potent ionizable lipids for transfection have an pK_a 6.2-6.5.[97] The test for pK_a typically consists of a binding assay such as 2-(p-toluidino)-6-napthalene sulfonic acid which fluoresces upon binding.[101]

The specific cationic lipid used in the Moderna and BioNTech/Pfizer vaccine varies, although the role during formulation is the same; the ionizable lipid facilitates mRNA encapsulation due to forming a complex with the slightly negatively charged mRNA backbone. Although the positive charge has been suggested to play a role in the biodistribution of lipid nanoparticles within the body. Despite the blood being near neutral pH it is believed approximately 10 % of the ionizable lipid still carries a positive charge,[101] and data suggests that this positive charge and not only lipid particle size has an influence on the degree and composition of protein corona formation around the lipid nanoparticle and thus adsorption and distribution.[103] Furthermore, upon forming a complex, ionizable cationic lipids are known to form multilamellar vesicles within a core lipid nanoparticle (as shown by Fig.1.24 and 1.28-A), due to the cone geometry of the ionizable cationic lipid which favours hexagonal H_{II} formation.[104] It is believed upon entering cells by endocytosis the pH environment starts to decrease as the endosome matures.[105,106] Thus, the ionizable cationic lipids within the lipid nanoparticle play a role in mediating endosomal membrane disruption by forming electrostatic interactions with the anionic membrane of the endosome to enable mRNA release into the cytosol. [97,101,106] Nonetheless, it has been estimated approximately less than 5 % of nucleic acid polymers actually escape from endosomes into the cytoplasm due to the process of endosomal recycling performed within the cell.[107] As a result, optimising the ionizable cationic lipid for endosomal escape is an area of focus.

Ionizable cationic lipids have also been reported to trigger unwanted immune responses against lipid nanoparticles. A study by Hasset *et al*. investigated 30 different lipid nanoparticle formulations and the data proposed the degree of immunogenicity was highly dependent on the structure of the ionizable cationic lipid by specifying an optimum pK_a of between 6.6-6.9.[108] Another complication involving ionizable cationic lipids is the toxicity related to positive charge of the head group.[109,110] Accordingly, efforts have been made to develop biodegradable ionizable cationic lipids by incorporating ester bonds within the structure of the head group. Results showed an increase in biodegradability due to rapid elimination and clearance which lead to an overall increase in tolerability.[108] Another side effect of employing some ionizable cationic lipids is the formation of lipid-mRNA adducts which hinder mRNA activity in lipid nanoparticle systems.[111]

Due to ionizable cationic lipids playing an essential role in nucleic acid delivery vast amounts of research has been performed to investigate structure property relationships in order to optimise formulation efficacy and limit toxicity and preserve nucleic acid activity.[97,106,108,111,112] For instance, during the development of lipid nanoparticles for nucleic acid delivery a team from Moderna developed 30 ionizable cationic lipids before determining SM-102 which had a pK_a of 6.68 was the best for their COVID-19 vaccine. SM-102 was described as possessing desirable properties such as good biodegradability, tolerability, protein expression as well as immunogenicity.[113,114] The structures of SM-102 and BioNTech/Pfizer's ALC-0315 are shown by Fig.1.29.[108] Hence, it is clear pK_a of the ionizable lipid has been identified as a key parameter, although there is a definitive requirement to optimise this factor and efforts have been made to identify other defining parameters. For example, a study by Hashiba *et al*. identified symmetry and carbon number as two key defining parameters to describe changes in ionizable lipid structure to correlate structure property function.[112]

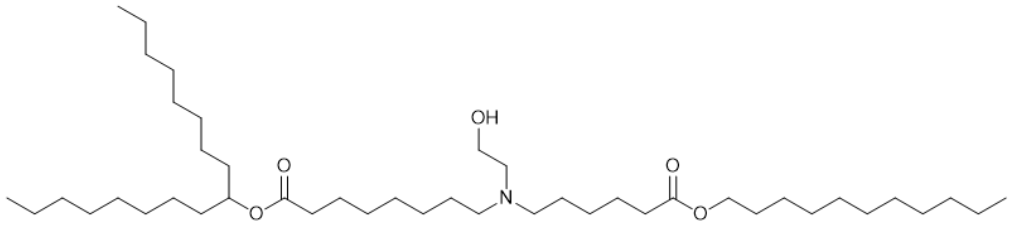

SM-102

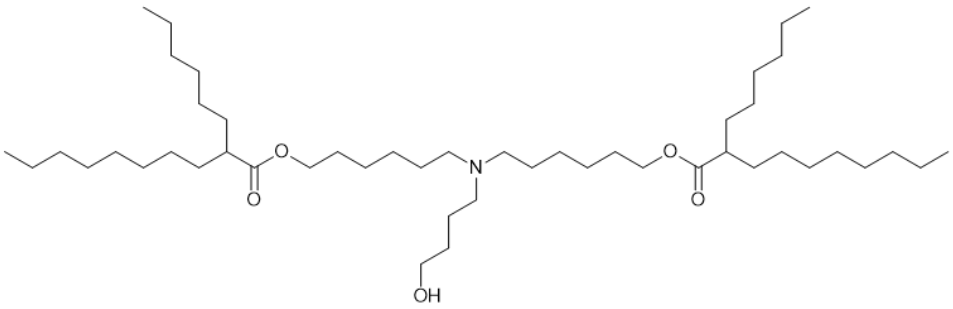

ALC-0315

Figure 1.29- Structures of the ionizable cationic lipids SM-102 and ALC-0315 used in the BioNTech/Pfizer and Moderna COVID-19 vaccines.

1.6.2.2. Helper lipid

Neutral phospholipids also known as 'helper lipids' aid in the formation of lipid nanoparticles while have also been reported to aid in the ability of a lipid nanoparticle to fuse with the cell membrane for internalisation.[97] An example of a neutral phospholipid used in lipid nanoparticles are phosphatidylcholines such as DSPC, Fig.1.30-A. DSPC is a natural component of cell membranes and therefore has a high biocompatibility. It is believed the cylindrical geometry of DSPC is what favours bilayer formation thus leading to the formation of a liposome characteristics shown by nucleic acid lipid nanoparticles. Other than DSPC, another phospholipid known in the formation of nucleic acid lipid carriers is 1,2-dioleoyl-sn-glycero-3-phosphoethanolamine (DOPE), Fig.1.30- A. Unlike DSPC, DOPE has unsaturated acyl chains and therefore favours conical shape rather than cylindrical. As a result, studies have shown DOPE has been referred to as a fusogenic lipid due to its ability to form the inverted hexagonal H_{II} which has been reported to promote membrane fusion.[104] Interestingly, when DSPC has been replaced by DOPE then the formulation efficacy reduced.[102] Thus, calling for greater research and understanding surrounding structure property relationships and their role in nanoparticle formulation and delivery. Other phosphatidylcholines with variations in chain length such as DPPC have also been used as helper lipids in the formulation of lipid nanoparticles. The structures of DPPC, DSPC and DOPE are shown by Fig.1.30-A. Meanwhile, the difference in phospholipid shape and their favoured membrane formation are shown by Fig. 1.30-B and C.

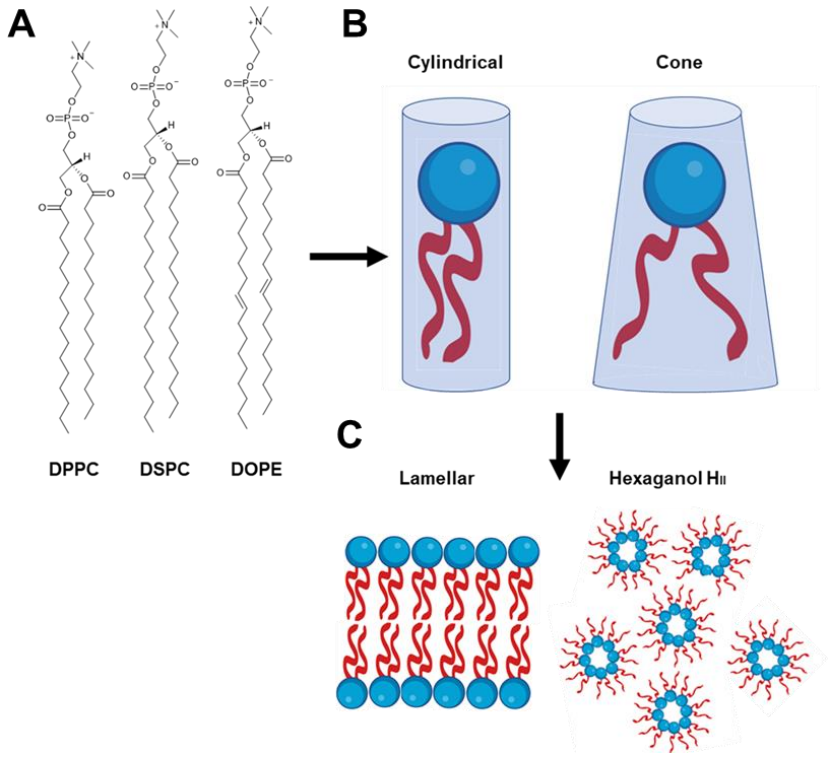

Figure 1.30- A) Structure of various helper lipids used in the formulation of lipid nanoparticles. B) The differences in cylindrical and cone structures. C) The different membranes formed dependant on phospholipid shape.

1.6.2.3. Cholesterol

Cholesterol is another neutral lipid commonly found in the cell membranes of biological systems, the structure displayed in Fig.1.31-A. Its incorporation into lipid nanoparticle formulations has been attributed to intercalate into bilayers and influence the packing of lipids specifically membrane fluidity and permeability. As a result, cholesterol has been found to be evenly distributed within lipid nanoparticles. Furthermore, cholesterol has been found to reduce permeability of lipid nanoparticles consisting of helper lipids with a low liquid-gel phase transition temperature (T_m). This behaviour is due to inducing tighter packing and greater order in what is described as the "condensation effect" displayed by Fig.1.31-B.[115] On the other hand, upon mixing of cholesterol with lipids with a high liquid-gel transition temperature, it is thought the opposite effect can occur resulting in an overall increase in membrane fluidity.[115] In either condition, the addition of cholesterol pulls the membrane towards a liquid ordered phase, and therefore the extent of change in lipid system was found to be dependent on the lipid formulation as well as temperature, T.[116] For example, DPPC and DSPC have high liquid-gel transition temperatures of 41 °C and 55 °C, while DOPE has a liquid-gel transition temperature of – 16 °C and is in the liquid state at physiological temperatures.[117] In addition, loading of cholesterol at ~ 30 mol % has also been found to increase circulation time of phosphatidylcholine based liposomal formulations due to significantly reducing the extent of blood proteins binding to DSPC liposomes.[118] Interestingly, claims have also been made over cholesterols ability to promote fusion with the membrane of endosomes thus improving intracellular release into the cytoplasm and overall efficacy.[119] As a result, cholesterol also plays a crucial role in the formation, stability and application of lipid nanoparticles.

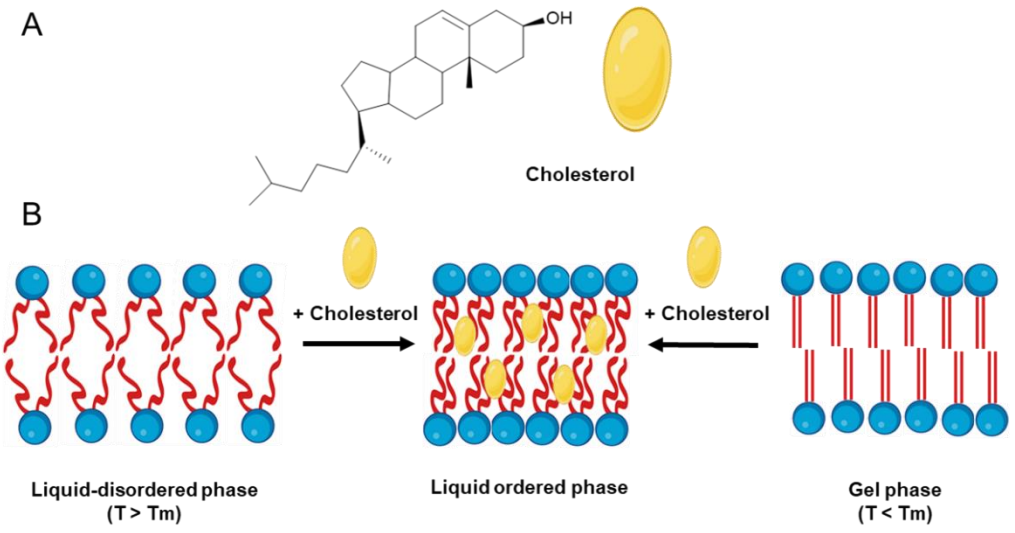

Figure 1.31- A) Structure of cholesterol. B) Illustration depicting the effect of addition of cholesterol on lipid membranes and three different phases of lipid membranes; liquid disordered, liquid ordered and gel phase.

1.6.2.4. Pegylated lipid

Pegylated lipids are lipid surfactants whereby a polyethylene glycol polymer is conjugated to a lipid unit which typically consists of lipid tails/chains attached to a central linker. The lipid unit typically is embedded within the membrane, meanwhile the peg chain extends out into the aqueous solution. Pegylated lipids are relatively low in mol % composition of lipid nanoparticle formulations, however, they play a crucial role in the lipid nanoparticle. First of all, the pegylated lipid plays a role in controlling the population size and dispersity during formulation, while also providing the necessary steric stability to the colloidal formulation by preventing aggregation upon storage.[120] The stability provided by pegylated lipid surfactants is often monitored by DLS and zeta potential over a period of time and reveal no/minimal variation in size or zeta potential. In the absence of PEG, formulations have shown to be highly unstable while also varying broadly in size.[121] It is hypothesised the reason behind controlling formulation size is due to pegylated lipid surfactants only being found on the exterior of the nanoparticle formulation, thus increasing the mol % of pegylated lipids will result in a decrease in particle size.[122]

Another role of pegylated lipid surfactants such as DSPE-MPEG-2K is to prevent rapid clearance and achieve prolonged circulation time once in the body.[123] PEG coated nanoparticle were believed to have limited cellular interactions and achieve stealth bypassing body's immune system. Although, the degree of which PEG provides 'stealth' to avoid the body's immune system has been challenged with the accelerated blood clearance phenomenon, which is an immunogenic response to foreign entities such as lipid nanoparticles resulting in the rapid clearance of pegylated vehicles.[124,125] Furthermore, there have been reported cases of anaphylaxis in recipients of the BioNTech/Pfizer or Moderna COVID-19 vaccine due to an allergy to PEG.[126,127] Nevertheless, the beneficial effects of coating liposomal formulations with pegylated lipids was well documented during the development of the anti-cancer drug formulation of doxorubicin called Doxil which employed the pegylated lipid DSPE-MPEG-2K. Another complication surrounding the use of PEG is that formulations with a high surface coverage of pegylated lipids have shown to suffer from poor cellular uptake and endosomal escape. This is likely due to limiting the interaction between the ionizable cationic lipid and the cell membranes, thus creating a trade-off.[128,129]

The development of pegylated lipids has produced a variety of structures as shown by Fig.1.32. ALC-0159 and DMG-MPEG-2K are the pegylated lipids used in the COVID-19 vaccines.[7] While, mPEG2000-DSG and DSPE-MPEG-2K are two other examples of pegylated lipids which possess longer lipid chains. It is clear from Fig.1.32 that key interest of variation appears to be the chain length of the lipid tails within the lipid unit as well as the head of the lipid unit which is used to connect the lipid chains to the PEG chain. One effect observed from varying the chain length is the tendency of the pegylated

lipid to remain attached to the lipid nanoparticle. It has been found with shorter lipid tails tend to desorb from the lipid nanoparticles in and effect known as 'PEG shedding'. The result of this suggested shorter circulation times with pegylated lipids possessing shorter lipid tail lengths.[123,128]

The favouritism of a PEG chain length corresponding to a molecular weight of 2000 Daltons (Da) is likely due to studies by Suk *et al*. which revealed particularly short circulation times of pegylated lipids with very short PEG chain lengths < 1000 Da. Whereas, pegylated lipids with long peg i.e. > 5000 Da led to a clear increase in circulation time. Alternatively, when the molecular weight of PEG was between 350 -2000 Da the differences in circulation time were negligible.[130] Similar effects were also observed with increased PEG density on the nanoparticle surface. Interestingly, the effect of PEG molecular weight on cellular uptake and/or endosomal escape of lipid nanoparticle has not been thoroughly investigated.

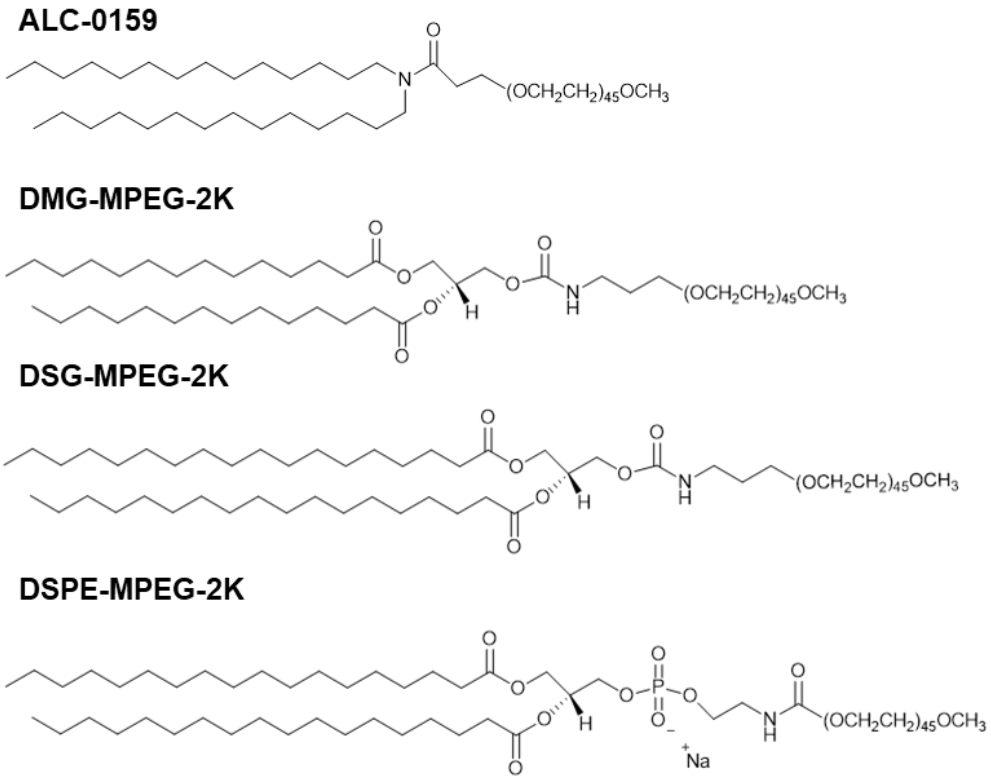

Figure 1.32- Structures of various pegylated lipids commonly used in the formulation of lipid nanoparticles for the delivery of nucleic acids

1.7. Methods of investigating lipid nanoparticle performance *in vitro*

In order for a lipid nanoparticle formulation to be successful, it must succeed in passing various physical and biological barriers. Upon formulation there are physical barriers such as colloidal stability and preventing nucleic acid degradation/ drug metabolism. On the other hand, once administered in a patient there are various biological barriers such as rapid clearance, poor circulation time, poor membrane permeability/cellular internalisation, poor ability to escape from an endosome etc.[107] Consequently, various methods have been developed to assess the performance of a lipid formulation at delivering the nucleic acid to the cytoplasm within a cell where it can for fill its therapeutic effect. Fig.1.33-A. illustrates the various stages upon reaching the cell target and releasing the mRNA. A common method used to assess particle accumulation/internalisation is by incorporating a lipophilic dye which acts as a tracer.[54,131] A study by Kim *et al*. successfully employed the lipophilic dye 1,1'-didoctadecyl-3,3,3',3'-tetremethylindocarbocyanine perchlorate (DiI) which was loaded into the core of various lipid-based nanoparticle formulations to assess cellular accumulation and/or uptake.[131] Fig.1.33-B. displays confocal microscopy images of SKOV3 cells treated with various lipid-based formulations, in this study the nuclei were stained blue and the red fluorescence of DiI suggests potential accumulation/uptake of the nanoparticles. This study investigated and showed how lipid-based carriers with PEG stabilisers which may be cleaved based on pH resulted in greater levels of cell internalisation *via* endocytosis due to much greater fluorescence of DiI at slightly acidic pH. Furthermore, nucleic acid delivery has also been imaged by means of fluorescent proteins. An example being mRNA molecules tethered or tagged with fluorescent proteins.[132] The degree of fluorescence may also be quantified by flow cytometry a technique commonly employed to attempt to quantify cell membrane permeation by nanoparticle drug carrier systems.[133] Another method of investigating the ability of nanoparticle formulations to permeate through cell membranes is by performing multiplex analysis of the cell culture supernatant. Multiplex analysis uses various analytes such as cytokines or Interleukin 8 (IL-8) which is a chemokine secreted by cells as a way of cell communication and is associated with inflammation.[134] The release of cytokine and chemokines has been closely correlated with nanoparticle uptake.[133]

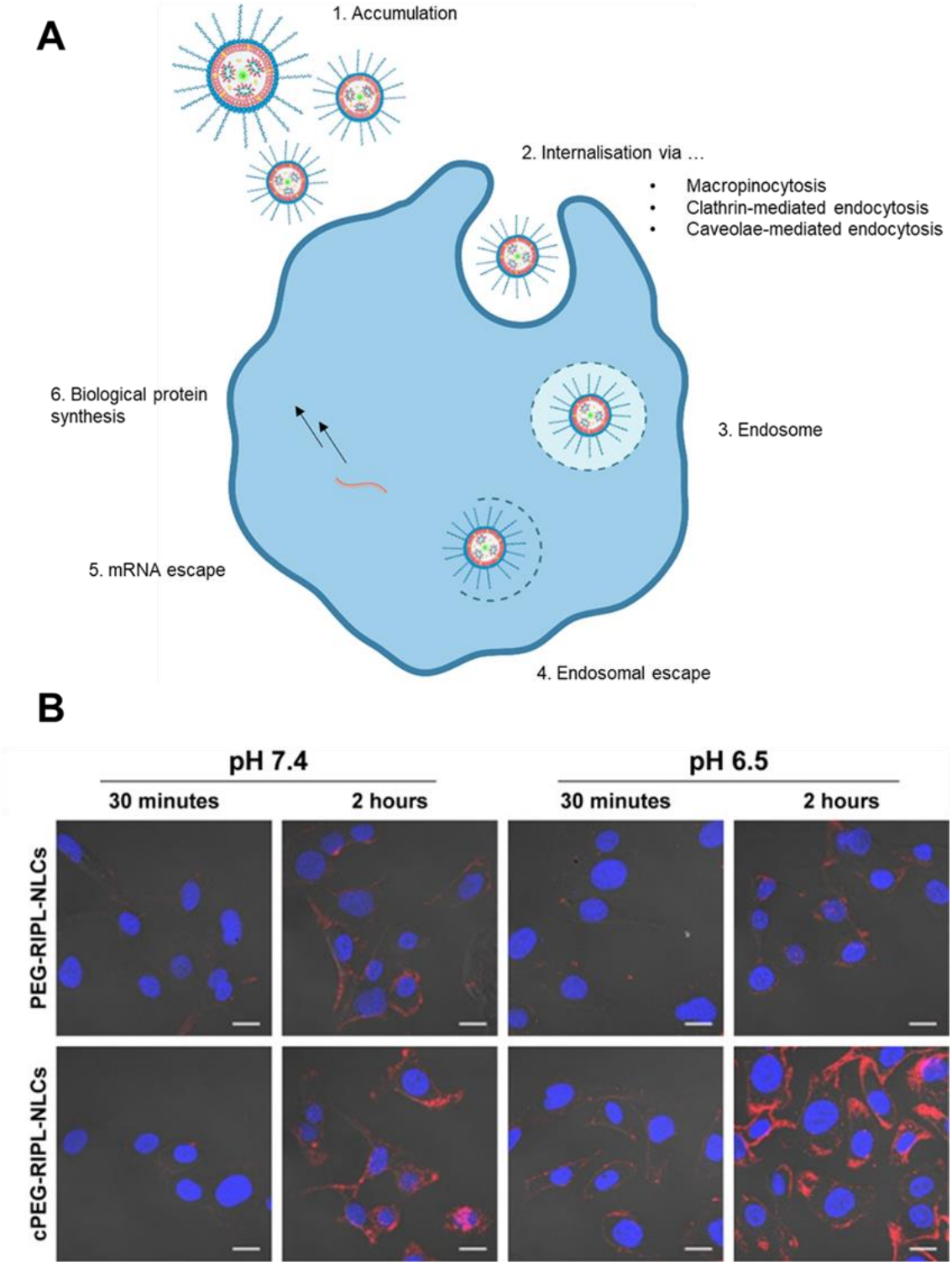

Figure 1.33- A) Illustration depicting the various stages of nucleic acid delivery from accumulation to nucleic acid release into the cytoplasm. B) Confocal microscopy images of SKOV3 cells incubated with lipid-based formulations containing 100 ng/mL DiI. Overall displays cell accumulation/internalisation. International Journal of Nanomedicine 2022: 17 1309-1322, originally published by and used with permission from Dove Medical Press Ltd.[131]

1.8. Thesis outlines and aims

The aim of the research within this thesis was to develop and implement a strategy to improve lipid nanoparticle formulation of hydrophilic and hydrophobic drugs, while considering and addressing the challenges faced by lipid nanoparticles. In doing so, the fundamentals of lipid nanoparticle formulation and stability were investigated and applied over the following chapters. The thesis is composed of five experimental chapters, each chapter includes a brief introduction containing the underlying literature which provided support and guidance for the consequent research.

Chapter 2 explores the route of prodrug synthesis from a model drug in order to investigate LogP as a model towards particle stability within a formulation as the formulation resists Ostwald ripening. Furthermore, the most promising prodrug will be taken forward and blended with a complex mixture of lipids in an attempt to control the crystallinity of the core as a way of preventing/slowing polymorphism. The use of dynamic light scattering (DLS), cryogenic scanning electron microscopy (Cryo-SEM), optical microscopy, differential scanning calorimetry (DSC) and powder X-ray diffraction (PXRD) were implemented in determining formulation stability and investigating the physical interactions within the core of the lipid nanoparticle formulations. The overall, results enabled a hydrophilic model drug to be chemically modified and blended with a complex mixture of lipids within lipid nanoparticle resulting in a formulation with signs of reduced core crystallinity and improved stability in aqueous solution.

Chapter 3 explores the relationship between structure and property of lipid surfactants specifically between pegylated and unpegylated lipid surfactants. In doing so, were able to provide greater understanding of how the properties of surfactants such as HLB and molecular weight result in different behaviour during lipid nanoparticle formulation. The research probes the reasoning for unpegylated lipid surfactants being given the name helper lipids based on their properties. It was hypothesised due to the hydrophobic nature of unpegylated lipid surfactants they would nucleate alongside core lipids. Thus, resulting in greater control over nanoparticle formulations of core materials at extremely high LogP and elevated weight percentage (wt %) of core lipids compared to during production compared to pegylated lipid surfactants. Furthermore, blends of pegylated and unpegylated lipid surfactants were trialled leading to the successful development of a formulation at 40 wt % of tricaprin and the dodecyl prodrug synthesised in Chapter 2, thus resulting in elevated drug loading. The stability of formulations was monitored by DLS, cryo-SEM, optical microscopy and signs of clear changes in physical appearance.

Chapter 4 investigates cryopreservation with regards to lipid nanoparticle formulation. Cryopreservation is a potential avenue to long term storage of lipid nanoparticle formulations,

although cryopreservation inflicts a considerable degree of stress on colloidal stability. As a result, various parameter of the formulation such as the ratio of pegylated lipid surfactant to unpegylated lipid surfactant and the wt % or core material to surfactants were examined to investigate how the degree of steric stabilisation may impact formulation stability. Furthermore, parameters such as concentration of the cryoprotectant/ lyoprotectant sucrose were also examined to establish conditions in which formulations could withstand the stresses of freezing and drying during freeze thaw and/or freeze drying. The ability to freeze dry and redisperse formulation containing dodecyl prodrug synthesised in Chapter 2 at elevated wt % were examined.

Chapter 5 applies the knowledge developed from Chapters 2,3 and 4 in order to freeze dry and redisperse a formulation containing dodecyl prodrug at elevated drug loading due to an elevated wt % of core material before examining the drug release at physiological conditions both in the presence and absence of porcine liver esterase enzyme. As a result, the stability of the formulation was examined for triggered release upon; elevated temperature and presence of salt as well as presence of enzyme. Results revealed no detectable drug release in the absence of enzyme, although in the presence of enzyme 37 % release was achieved after 9 weeks.

Finally, Chapter 6 employs some of the fundamental knowledge gained from previous chapters in the formulation of lipid nanoparticles for the application of mRNA delivery. Parameters such as particle size and charge as well as type and molecular weight of pegylated lipid surfactant were examined for their effect on cellular uptake. Formulations were examined by incorporating a fluorescent dye as a tracer to indicate signs of accumulation as well as measuring levels of Interleukin-8 released from cells.

CHAPTER 2

Evaluating the impact of systematic hydrophobic modification of model drugs on the control, stability and loading of lipid-based nanoparticles

This work has been published as C. Hogarth, K. Arnold, A. McLauchlin, S. P. Rannard, M. Siccardi and T. O. McDonald, *J. Mater. Chem. B*, 2021, **9**, 9874–9884. The paper was written by Cameron Hogarth with edits made by other coauthors. All work contained in the paper was carried out by Cameron with the exception of Cryo-SEM which was performed by Keith Arnold. This chapter is an expanded and adapted version of the content in the paper

Chapter 2 -Evaluating the impact of systematic hydrophobic modification of model drugs on the control, stability and loading of lipid-based nanoparticles

2.1. Introduction

Lipid nanoparticle stability remains a challenge that hinders the progression of many therapeutic treatments. Instability of lipid nanoparticles typically stems from Ostwald ripening and polymorphic transitions.[12,33,45] Studies by Jennings *et al* and Bunjes *et al*. have demonstrated how a blend of various lipids may be employed to disrupt the crystallinity of the core of lipid nanoparticles which has shown improved stability.[13,34] Jennings *et al*. specifically blended an increasing amount of oil into the core of solid lipid and used DSC analysis to determine the decrease in core crystallinity which was characterised by a broadening and suppression of peak intensity during lipid melt. Thus, this work suggested that the inclusion of oil into lipid nanoparticles was a potential route to prevent/delay polymorphic transitions of the crystalline core of lipid nanoparticles. Furthermore, research by Zhu *et al*. investigated correlation between LogP of drug molecules and nanoparticle stability when formulated using flash nanoprecipitation. Their findings suggested that formulations composed of drug with a LogP greater than approximately 12 experience little to no instability caused by Ostwald ripening.[33] The systematic modification of a drug molecule to alter its LogP would allow for a more detailed investigation into the factors controlling lipid nanoparticle formation and growth. Dalvi *et al*. have reported by applying LaMer model can be used to model lipid nanoparticle formation. They showed a higher degree of supersaturation translates to a higher rate of nucleation potentially resulting in a formulation of smaller average nanoparticle size and a narrower size distribution, all achieved by decreasing the solubility of the drug.[42,46] A suitable approach for this modification has previously been demonstrated by Hobson *et al*. where reversible chemical modification of the hydrophilic drug emtricitabine was conducted to increase its LogP and enable formulation as drug nanoparticles which could be used as a long-acting injectable.[17] Lamivudine (Fig. 1) is a very similar molecule to emtricitabine, however is structurally less complex due to the absence of fluorine. It has a LogP < 2 (too hydrophilic to formulate efficiently within a hydrophobic nanoparticle) and possesses amine and alcohol groups to allow modification with various hydrophobic alkyl chloroformates to form stable prodrugs with reversible carbonate and carbamate bonds. Overall, a strategy has been outlined in order to improve lipid nanoparticle stability, although further research and investigation is required.

2.2. Chapter Aims

In this chapter the aim was to systematically investigate how LogP of a set of prodrugs controls nanoparticle formation and stability as a lipid nanoparticle, Fig. 2.1. We hypothesised that the same synthesis employed by Hobson *et al*. could be applied for lamivudine, with the alkyl chloroformates carefully selected based on LogP values predicted for prodrugs. The approach also examines potential for solid prodrug nanoparticles formed with a core loading of 100% prodrug which have loadings much higher than the majority of SLNs reported in the literature. In order to investigate a broad range in LogP, three prodrugs were synthesised from the hydrophilic drug lamivudine. We also investigated the effect of crystallinity of the prodrugs in various blends, while also documented the effect on drug loading, particle size, polydispersity and stability.

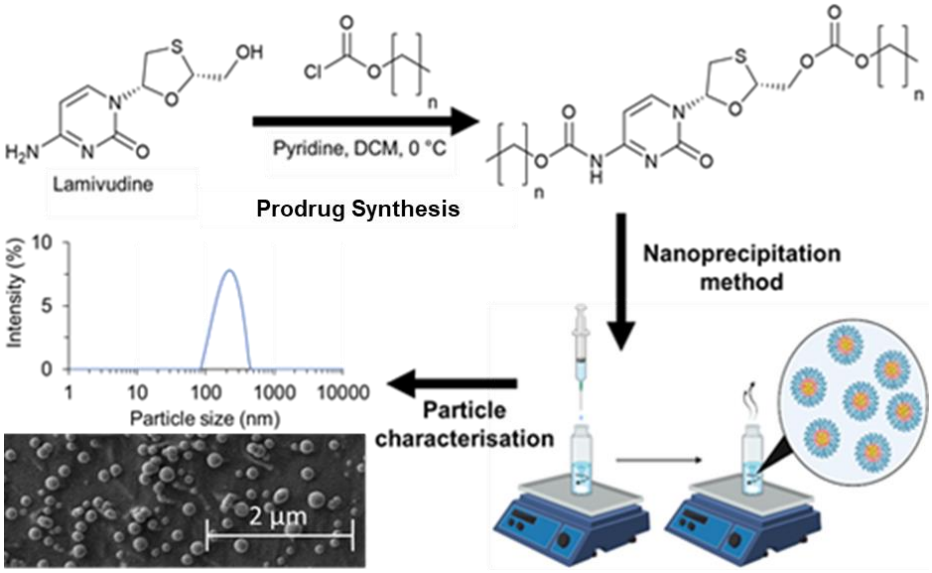

Figure 2.1. - Schematic overview of a strategy to investigate the relationship between LogP and nanoparticle characteristics such as particle size, polydispersity and morphology of lipid-based nanoparticles. Three prodrugs of lamivudine were synthesised by reacting with various length alkyl chloroformates to produce carbonate and carbamate bonds. The prodrugs were then nanoprecipitated into an aqueous solution of Brij S20 to achieve prodrug nanoparticles for characterisation

2.3. Results and Discussion

2.3.1. Synthesis of hydrophobic prodrugs of lamivudine

Three prodrugs modified conjugating alkyl chains with the aid of carbamate and carbonate ester linkers were produced using the strategy previously demonstrated by Hobson *et al.* The reactions occurred at the 5'-hydroxyl and amino groups of lamivudine. To better understand the relationship between LogP and nanoparticle stability, the alkyl chloroformates used were of specific chain lengths based on the calculated LogP to produce prodrugs of lamivudine. The alkyl chloroformates were n-butyl, n-octyl and n-dodecyl chloroformates, while the corresponding calculated LogP of the target prodrugs were 2.98, 7.21 and 11.44 respectively- LogP were calculated using a mathematical model employed as part of ChemDraw. Prodrugs targeted for synthesis are displayed in Fig.2.2.

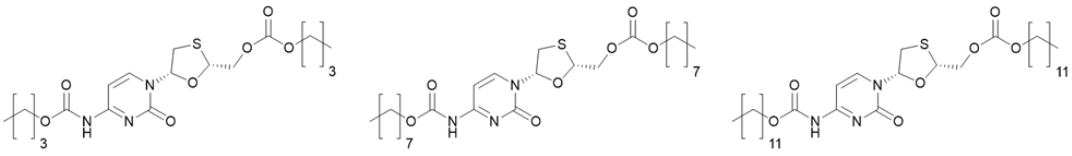

Figure 2.2- Structures of prodrug synthesised; butyl, octyl and dodecyl prodrugs.

2.3.2. Carbamate and carbonate esterification

Lamivudine (3TC) prodrugs modified at the 5-hydroxyl and amino groups were synthesised in a rapid reaction between the alkyl chloroformate at both the alcohol and amine functional groups. The reaction mixture was performed in anhydrous dichloromethane and left for 48 hours in order to obtain a high yield of product. The crude materials were washed with 1 M hydrochloric acid aqueous solution, water and brine wash before further purification by flash column chromatography. The purified prodrugs were all white solid materials. Due to the presence of basic pyridine the reaction mechanism likely follows a pathway whereby the alkyl chloroformates suffer nucleophilic attack by the nitrogen in pyridine due to the lone pair of electrons on the nitrogen unable to delocalise around the ring.[135] Thus, resulting in a chloride ion as a leaving group.[136] Before the oxygen of the alcohol and the nitrogen of the amine of 3TC functioning as a base replacing the chlorine to synthesise both a carbonate and carbamate ester groups at the corresponding alcohol and amine groups of 3TC, Fig.2.3. Meanwhile, the reaction also forms pyridine hydrochloride as a biproduct. With regards to the rate of bond formation it is reasonable to assume the carbamate ester bond would be favoured over the carbonate ester due to amines being stronger nucleophiles.[137]

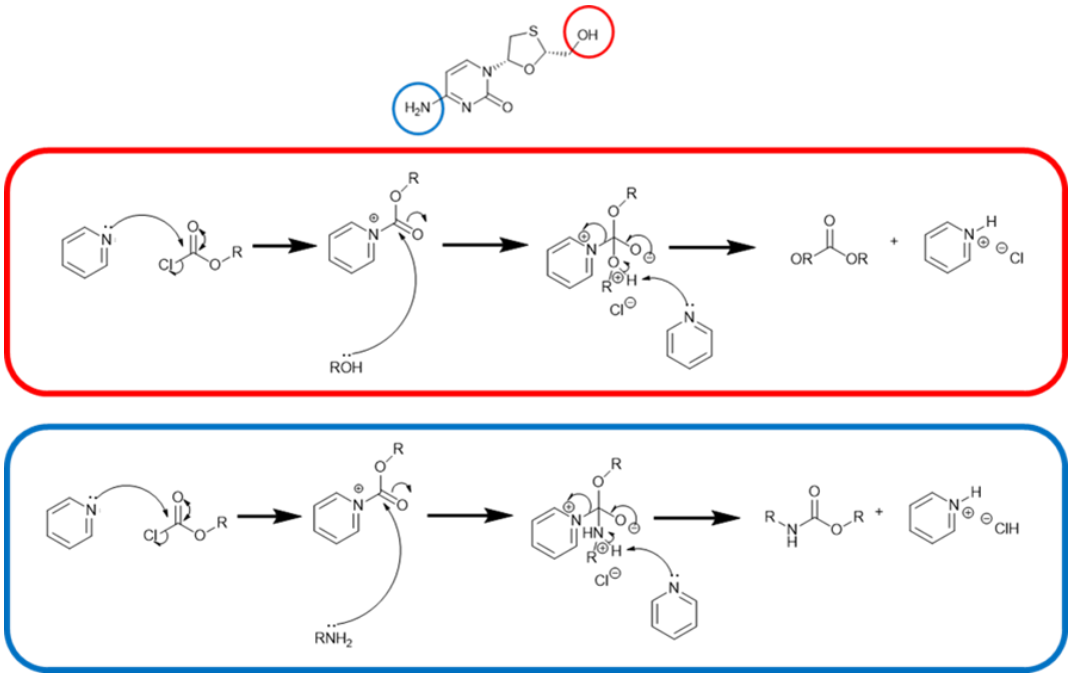

Figure 2.3- Proposed reaction mechanism at both alcohol and amine of lamivudine.

2.3.3. Characterisation of hydrophobic prodrugs of lamivudine

Each prodrug was characterised with the following proton and carbon NMR, Fourier transform Infra-red spectroscopy (FTIR), electrospray mass spectrometry and elemental analysis (CHNS). The ^{1}H NMR spectrum of the purified butyl prodrug is presented by Fig. 2.4. The presence of additional peaks labelled a + o, b + n, c + m and e + l further suggests formation of carbonate and carbamate bonds. Di-conjugation was confirmed when the integration ratios of hydrogens agreed with the expected ratios of hydrogens between the additional peaks from the alkyl chains and a single hydrogen form the original 3TC. Another indication of conjugation to the amine is the integration of the peak j which is ~1 indicating only one proton is attached to the nitrogen atom and the other has been displaced to form the carbamate bond. The ^{13}C NMR displayed an increase in the number of environments to include those of the conjugated alkyl chain as expected and are shown below by Fig 2.5. The ^{1}H and ^{13}C NMR spectrums for the other prodrugs may be found in the Appendix, Fig. 2.1-2.4. From the series of FTIR spectra Fig. 2.6, neither of the drug prodrug synthesised possess a broad -OH absorption (~3200 cm^{-1}) which is present in spectra A of 3TC. This suggests that conjugation has occurred at the 5' hydroxy group to form a carbonate ester. Furthermore, compared to 3TC each of the drug prodrug possess two additional absorption bands at ~1740 and 1671 cm^{-1} indicating the presence of two additional C=O groups. This further suggests conjugation at the alcohol but also at the amine to produce a carbonate and a carbamate ester. There is also a noticeable increase of intensity of the C-H absorption bands at ~2900 cm^{-1} between spectra B, C and D due to the increase in alkyl chain length conjugated to the 3TC.

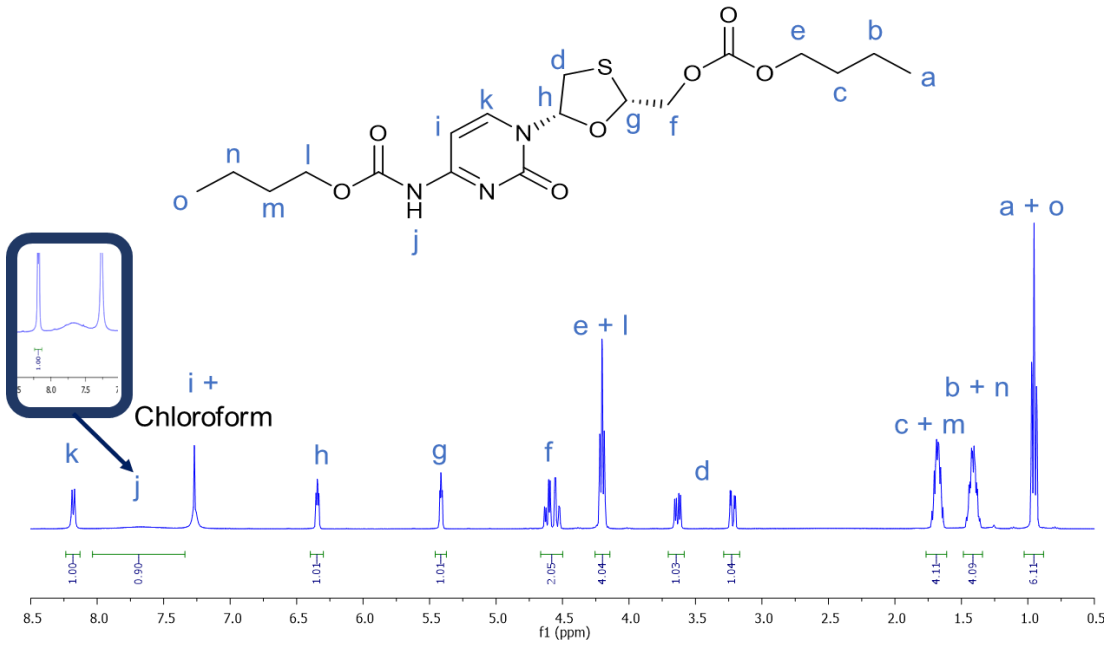

Figure 2.4-^{1}H NMR (400 MHz) spectra of butyl drug analogue in $CDCl_3$

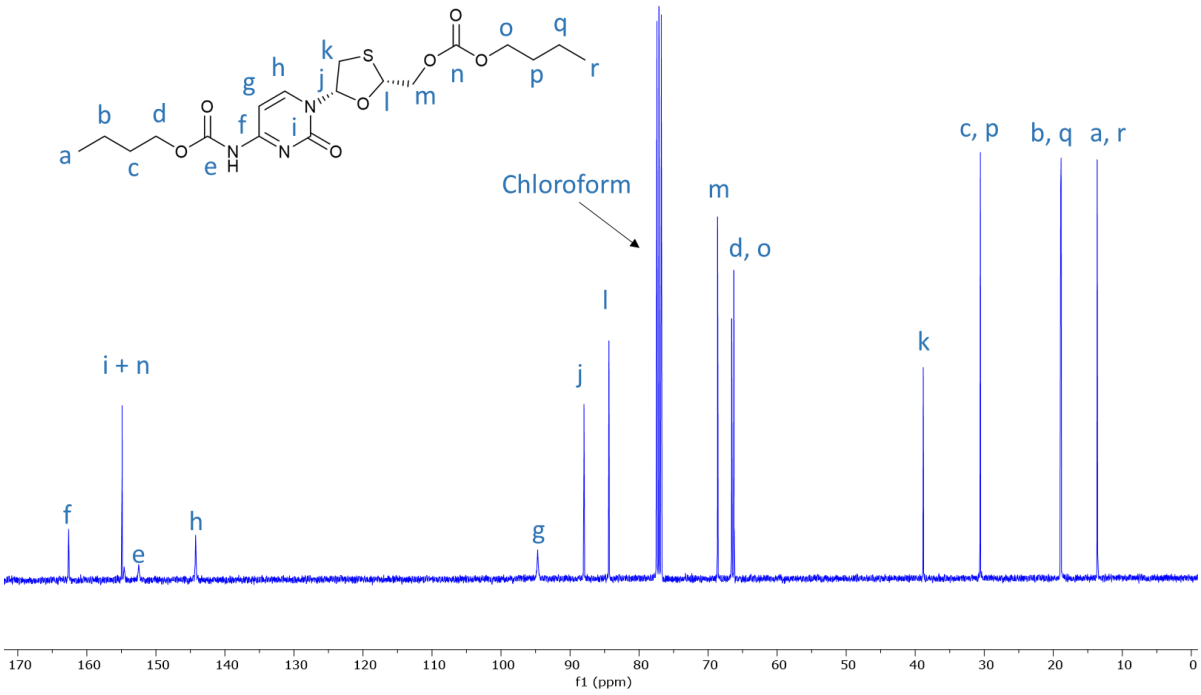

Figure 2.5-^{13}C NMR (400 MHz) spectra of butyl drug analogue in $CDCl_3$

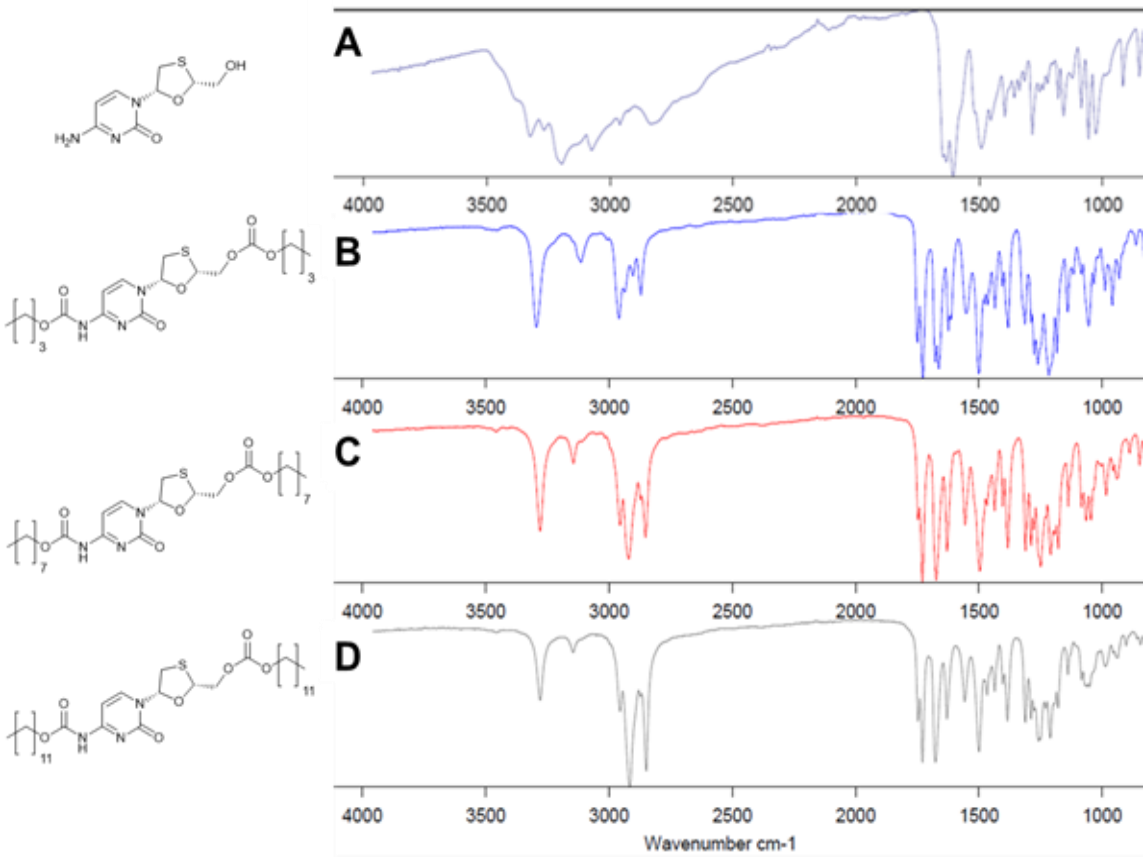

Figure 2.6- FTIR data of A) Lamivudine and drug analogues; B) Butyl C) Octyl D) Dodecyl

Each of the prodrugs were also characterised by both elemental CHNS analysis and by mass spectrometry. The data in the tables below further supports the NMR data as calculated and measured values for CHNS (Table 2.1) and the molecular ion peak (Table 2.2) were very similar and thus in agreement with the desired products. In conclusion, the characterisation data presented suggests that the three hydrophobically modified prodrugs were successfully prepared; butyl prodrug, octyl prodrug and dodecyl prodrug.

Table 2.1- CHNS elemental analysis data for butyl, octyl, dodecyl drug analogues

		Calculated				**Measured**			
Sample	**Empirical formula**	% C	% H	% N	% S	% C	% H	% N	% S
Butyl prodrug	$C_{18}H_{27}N_3O_7S$	50.34	6.34	9.78	7.46	50.36	6.35	9.9	7.22
Octyl prodrug	$C_{26}H_{43}N_3O_7S$	57.65	8.00	7.76	5.92	57.74	8.04	7.94	5.97
Dodecyl prodrug	$C_{34}H_{59}N_3O_7S$	62.45	9.09	6.43	4.90	62.37	8.98	6.26	5.00

Table 2.2- Electron spray mass spectrometry data for butyl, octyl and dodecyl drug analogue

	Calculated (m/z)		**Measured (m/z)**	
Sample	**(M+H)+**	**(M+Na)+**	**(M+H)+**	**(M+Na)+**
Butyl prodrug	430.1642	452.1462	430.1634 (-0.0008)	452.1463 (+0.0001)
Octyl prodrug	542.2894	564.2714	542.2890 (-0.0004)	564.2709 (-0.0005)
Dodecyl prodrug	654.4146	676.3966	654.4142 (-0.0004)	676.3962 (-0.0004)

2.3.4. Formulation of prodrug nanoparticles

The range of LogP of prodrugs enabled us to investigate some of the key boundaries in LogP previously reported by Zhu *et al*. The length of the alkyl chain on the prodrugs resulted in a decrease of active drug in molar wt % of the overall molecule and thus potentially the core of the nanoparticle (not including mass of surfactant), Fig.2.7. However, for this work, the prodrugs were used as model active, as such the drug loading was not a key focus at this stage.

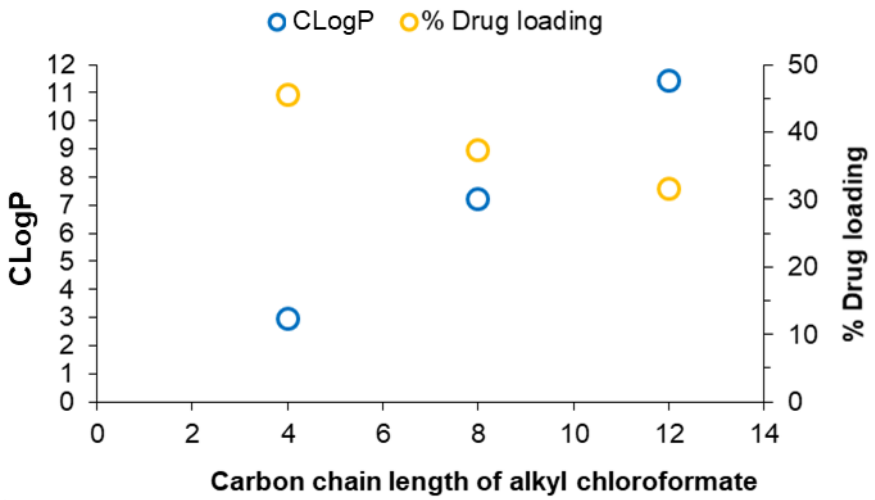

Figure 2.7- Graph displaying the trend of decreasing active drug loading with increasing alkyl chain length of the chloroformate conjugated to the model drug

Each of the prodrugs were nanoprecipitated into a fixed volume of the surfactant Brij S20 (polyoxyethylene 20 stearyl ether). Brij S20 is a pegylated lipid derived from stearic acid molecules conjugated to a polyethylene glycol (PEG) 1000 $gmol^{-1}$ chain. PEG has been widely used to provide a steric stabilisation for lipid nanoparticles.[138]

Upon addition of the octyl and dodecyl prodrug solutions in THF to the aqueous antisolvent resulted in the formation of a weakly turbid nanoparticle formulation as the nanoparticles were formed, Meanwhile, upon addition of the butyl prodrug solution the formulation remained clear (Fig. 2.8), thus indicating potential solubility of the butyl prodrug within the continuous phase and hindering nanoparticle formation.

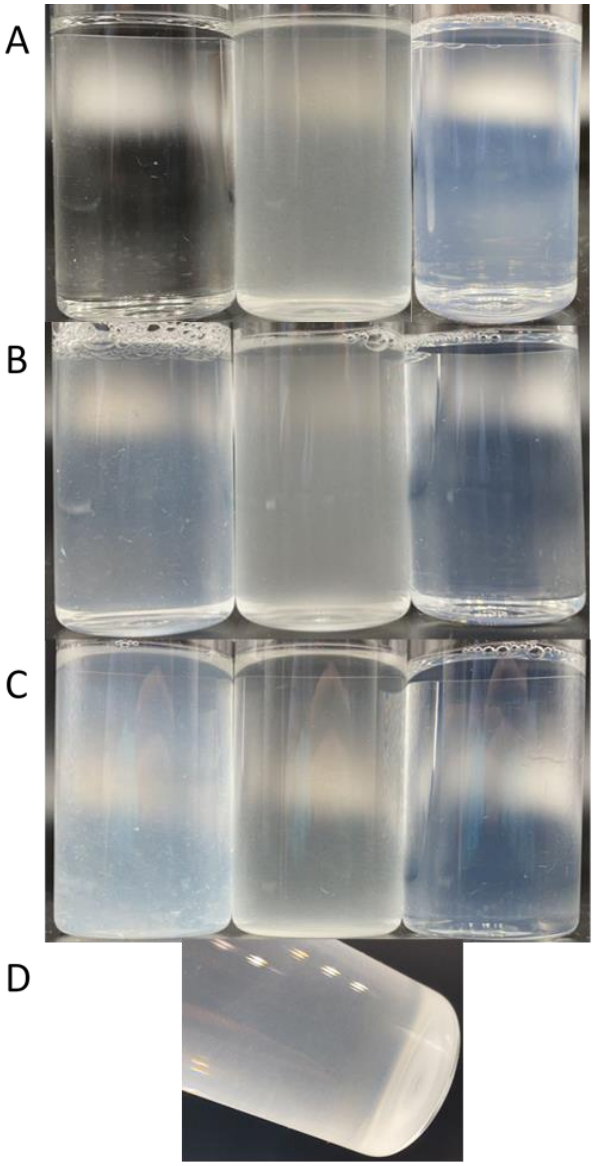

Figure 2.8-From left to right photos of butyl, octyl and dodecyl drug analogue formulations A) Day 0 after 1 hour, B) Day 2 after removal of THF, C) Day 6 short term storage at 4 °C . Overtime butyl drug analogue formulation completely crystallised upon removal of THF resulting in the formation of visible needles on day 2 which grow and are highly noticeable on day 6; octyl drug analogue formulation is turbid after one hour with a notable glittery effect, until day 6 where crystals sediment. Dodecyl drug analogue formulation virtually clear. And remains unchanged over time. D) Octyl drug analogue formulation day 6 alternative angle showing sedimented material

The formulations were analysed by DLS 1 hour after formulation- while THF still present, the dodecyl solid prodrug nanoparticle (SPN) formulation was on average 151 nm in diameter and 0.14 polydispesitry index (PDI). DLS measurements of the butyl SPN formulations revealed a hydrodynamic diameter of 30 nm with a derived count rate approximately 1% of that of the dodecyl SPN formulations, thus further suggesting solubility of the butyl prodrug due to an extremely low concentration of nanoparticles of butyl prodrug/micelles of Brij S20. Herein was concluded the butyl prodrug was too soluble in the continuous phase mixture of both water and THF which was likely due

it's low LogP of 2.98 which in turn drastically hindered nanoparticle formation. The DLS data for the octyl prodrug formulation was bimodal containing micron sized aggregates and therefore was deemed not suitable for DLS due to impacting the accuracy of the measurements. Soon after DLS measurements the octyl prodrug formulation possessed a shimmering appearance that is associated with anisotropic crystals scattering light at multiple angles, thus suggesting rapid particle size growth and crystallisation of the prodrug likely due to Ostwald ripening.[139] The presence of anisotropic crystals within the octyl SPN formulation was later confirmed by optical microscopy Fig. 2.9.

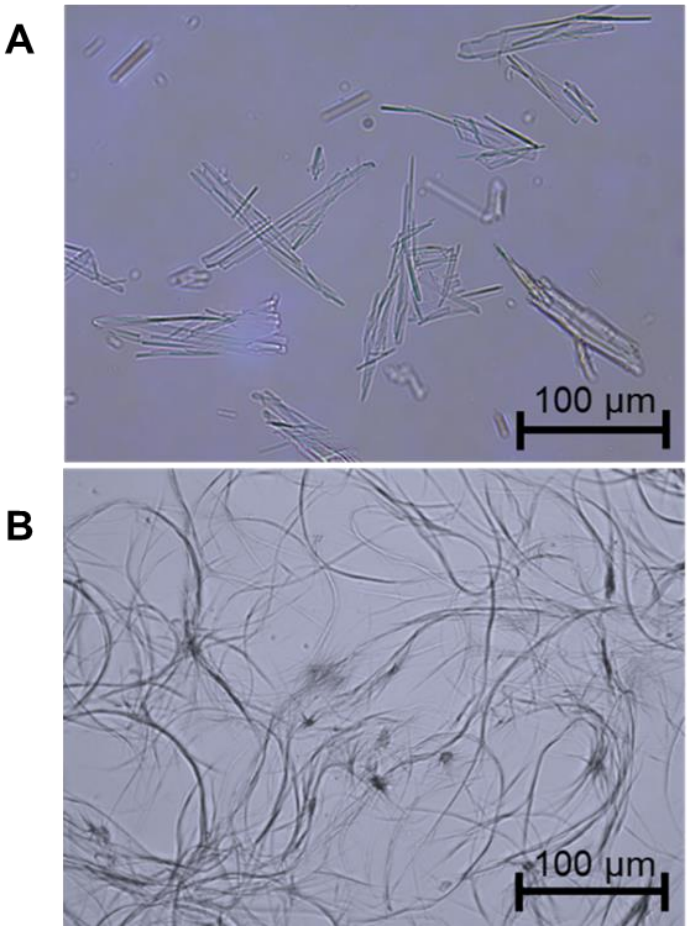

Figure 2.9- Optical Microscopy images of the prodrug formulations A) Confirming the presence of anisotropic crystals of octyl drug analogue indicating poor stability due to Ostwald ripening DAY 6. B) Butyl drug analogue formulation DAY 6.

After 2 days the THF had evaporated and the dependence of stability on LogP became highly noticeable as the butyl prodrug formulation increased in turbidity. The butyl prodrug formulation also contained visible aggregates which became even more visible on day 6 (Fig. 2.8-C), which likely formed due to loss of solubility within the continuous phase resulting in saturation of the butyl prodrug as the THF evaporated. As a result, instigated the rapid and extensive growth of nanoparticles. Meanwhile, the octyl prodrug formulation still possessed the shimmering appearance until day 6 where the

formulation had sedimented (Fig.2.8-D). The dodecyl SPN formulation appeared unchanged (Fig.2.8-A, B and C), however a slight increase in particle size and PDI was observed by DLS, Fig 2.10. This was attributed to a small degree of Ostwald ripening during solvent evaporation. Nevertheless, the dodecyl SPN formulations appeared to remain stable upon storage at 4 °C, as there was no further notable change on day 6 or 28, Fig 2.10, likely due to steric stabilisation provided by Brij S20. In addition, the data from Fig. 2.10 also highlights the large degree of reproducibility between dodecyl prodrug formulations – the relative standard deviation of particle size between three replicate samples was 7, 18, 23 and 9 for day 0, 2, 6 and 28 measurements. Measurement of zeta potential confirmed that the dodecyl nanoparticles were stabilised solely by steric stabilisation due to an average net charge of -1.9 mV.

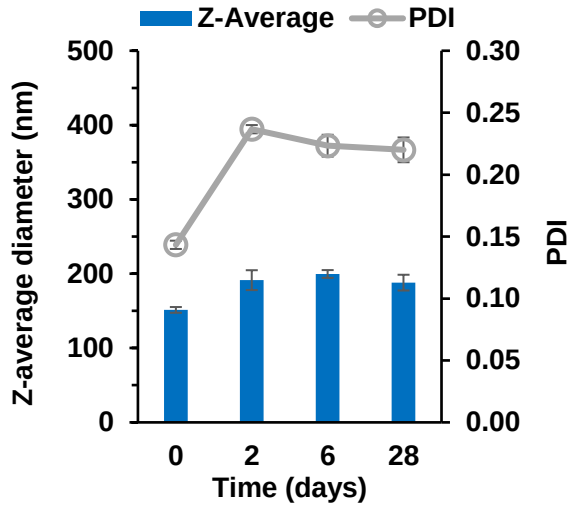

Figure 2.10- Data collected measuring both particle size and polydispersity of dodecyl SDAN formulations over 28 days. Samples prepared in triplicate and error bars calculated on standard deviation between measurements. Samples were stored at 4 °C after day 2 measurement.

Attempts were made to characterise each of the SPN formulations using cryo-SEM two days after formulation. Cryo-SEM was used in order to allow the visualisation of the particles without any significant drying effects that can occur in conventional scanning electron microscopy. Unfortunately, it was not possible to conclusively image either the butyl or octyl prodrug formulations, however it was deemed with the dodecyl SPN formulation, spherical nanoparticles were observed (Fig 2.11-A) these morphologies differed considerably from the elongated objects that were seen for the cryoSEM images of a control of Brij S20 alone Fig. 2.12. The measurement of 200 particles from the cryo-SEM images revealed an average particle diameter of 136 nm with and a standard deviation of 44, thus in agreement with data obtained by DLS – after factoring in the solvent sphere on the surface of nanoparticles that is included in the DLS measurement. The diameter distribution graph based on the cryo-SEM data can be seen in Fig 2.11-B. Fig.2.11-C also displays an overlay comparing the data

obtained from the cryo-SEM image which has been normalised for comparison with the size distribution data obtained by DLS which shows both cryo-SEM and DLS were in agreement.

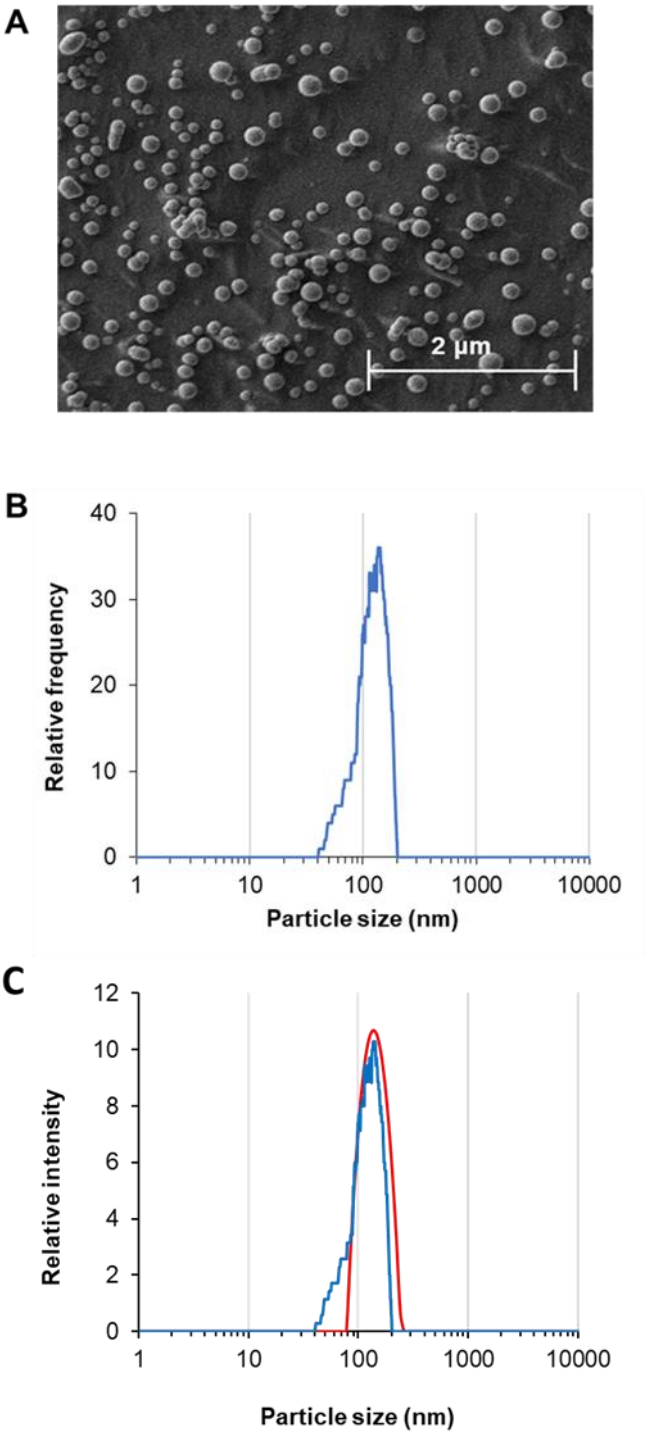

Figure 2.11- Further characterisation data using Cryo-SEM A) Cryo-SEM image of the dodecyl drug analogue formulation, B) Size distribution graph using data calculated by ImageJ based on cryo-SEM image of dodecyl drug analogue formulation. A sample size of 200 particles and a bin size of 1 was used. C) An overlay of a normalised size distribution of the data obtained from the cryo-SEM image with the size distribution obtained by DLS.

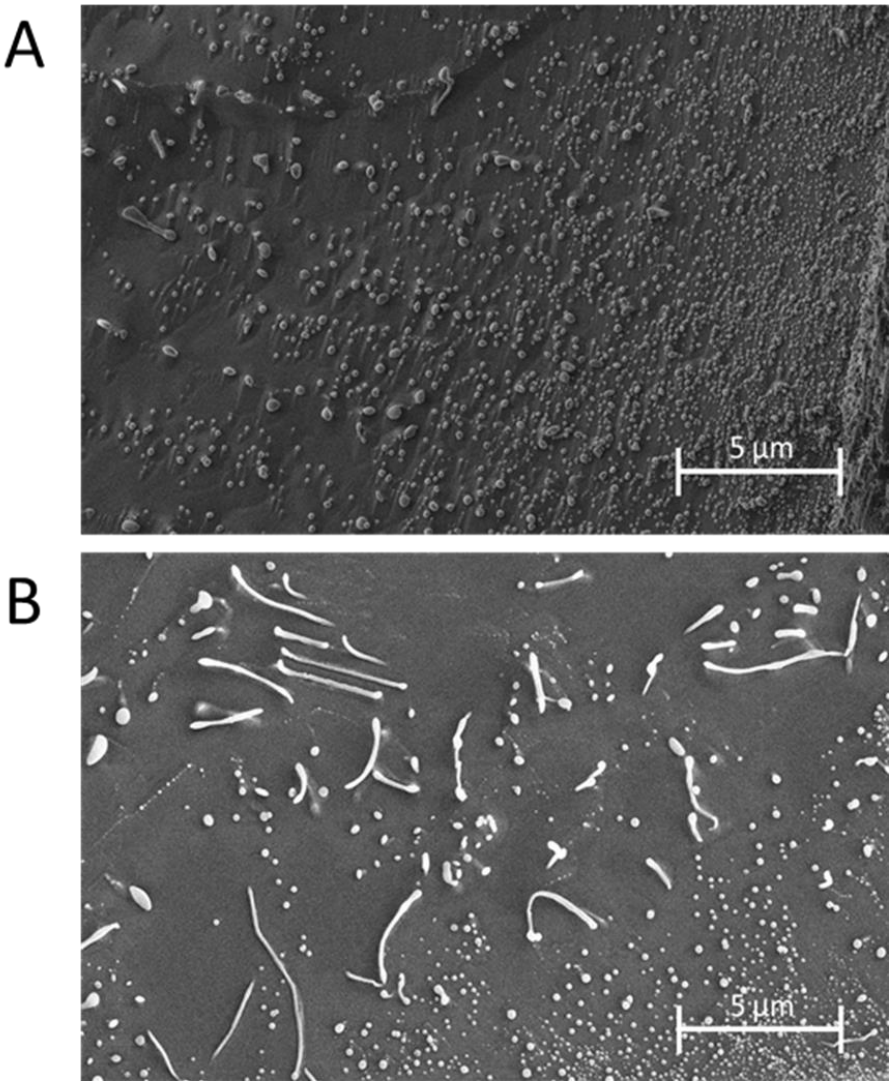

Figure 2.12- Cryo SEM images of A) dodecyl SPN formulation displaying a large number of spherical shaped objects deemed to be nanoparticles B) Brij S20 solution control displaying evidence of large string like and some small spherical artefacts created by the Brij S20 surfactant.

The data from various microscopy techniques alongside DLS and photographic data fitted to the LaMer model of nanoparticle formation, whereby prodrugs of higher LogP have a higher degree of supersaturation and thus nucleate at a faster rate which competes with the growth phase producing nanoparticles of smaller and uniform size. On the other hand, a low LogP results in a lower degree of supersaturation therefore slow nucleation was resulting in a longer period of nucleation events, thus upon growth a broader particle distribution was established, as shown schematically in Fig. 2.13.

In essence, the nanoparticle formulation properties were heavily dependent on the LogP of the prodrug and display evidence for the ability to tune these properties accordingly by applying LaMer model. Furthermore, the high LogP of the dodecyl SPN formulation appeared to resist Ostwald ripening over the analysis duration we have investigated. Conversely, nanoparticles made of prodrugs

with lower LogP showed greater Ostwald ripening, due to their greater solubility in the continuous phase. This solubility enabled faster mass transport from the smaller nanoparticles to the larger nanoparticles/growing crystal. This data agrees with Zhu suggesting drugs with a LogP between 9 and 12 are potentially stable. Given the favoured properties of the dodecyl prodrug nanoparticles, further studies were carried out on this prodrug.

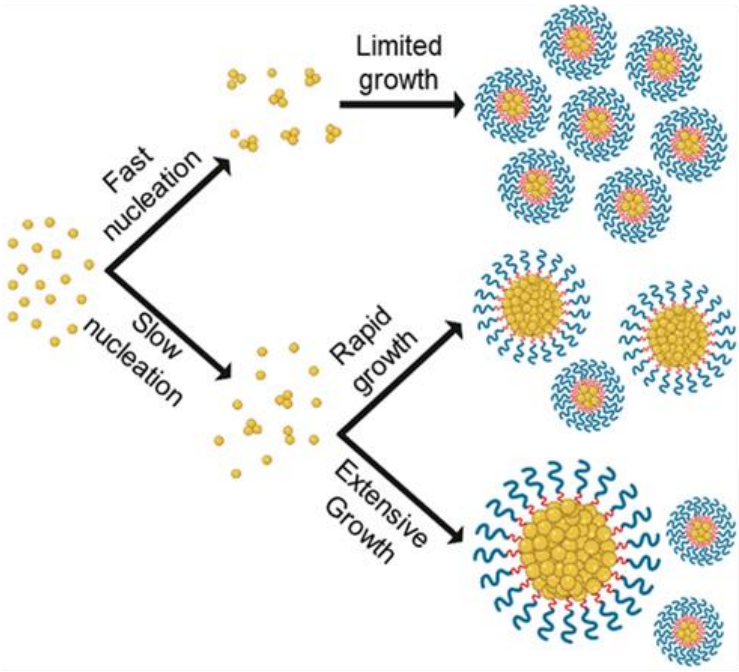

Figure 2.13- Illustrates how the difference in rate of nucleation as a result of differences in LogP may affect particle size and size distribution of formulations according to LaMer model

2.3.5. Formulation of prodrug blends

A conclusion from earlier data was the octyl prodrug was slower to nucleate than the dodecyl drug prodrug due to differences in LogP, therefore a hypothesis was proposed that a blend may result in the dodecyl prodrug aiding nanoparticle formation by providing nuclei from which the octyl prodrug could grow. Another advantage of the blending approach is the potential to achieve higher drug loadings due to a higher proportion of the octyl prodrug is made up of the model active lamivudine. Fig. 2.14 shows data obtained by DLS for various blends of dodecyl and octyl prodrug. For each blend, particles were detected and measured by DLS, all of which were of comparable average particle size to that of 100% dodecyl prodrug formulation. Thus, the dodecyl prodrug had indeed aided in nanoparticle formation. Furthermore, as the % of octyl prodrug was increased in the blends the PDI generally increased along with broader margins for error thus suggesting a loss of control over nanoparticle formation. However, shortly after the DLS measurement the blend of 25% dodecyl/75% octyl prodrug displayed signs of instability by means of a shimmering effect again suggesting the

presence of anisotropic crystals (as was seen for the 100 % octyl prodrug formulation). On the other hand, the blends of 75% dodecyl/25% octyl prodrug and 50% dodecyl/50% octyl prodrug appeared stable on day 0 due to no notable changes in appearance. Nevertheless, during the 2-day period of removal of THF by evaporation, the blends of dodecyl and octyl prodrug quickly increased in particle size as the 75% dodecyl/ 25% octyl formulation grew on average by 4300 nm after 2 days. While the 50% dodecyl/50% octyl prodrug formulation also possessed a shimmering effect again suggesting a large degree of crystal particle growth to form anisotropic crystals and was no longer suitable for particle size measurement by DLS. This suggests despite aiding particle formation the continuous phase of water/THF was still too soluble for the octyl prodrug thus enabling Ostwald ripening.

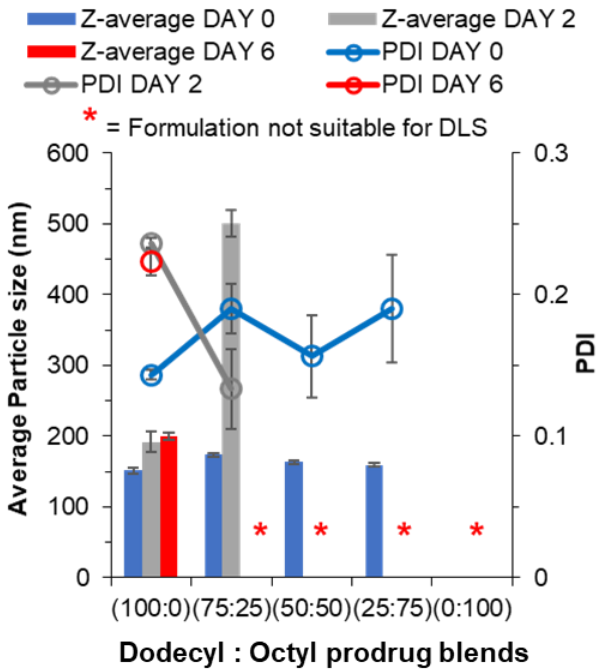

Figure 2.14- Particle size and size distribution data for blends of dodecyl and octyl drug analogue formulations obtained by DLS.

2.3.6. Formulation of lipid/prodrug blends

The dodecyl prodrug was employed further to investigate the effect of blending a prodrug with a complex mixture of lipids in the form of Imwitor 900k, a mixture of mono-, di- and triglycerides of both palmitic and stearic acid. An important consideration in terms of blending the prodrug with lipid is that it will in turn reduce the active drug loading. Fig. 2.15 displays the relationship between the drug loading in the formulation and the composition of the formulation. It is clear that formulations composed of 100% prodrug offer excellent active drug loadings (32% w/w) in the core of the nanoparticles. Furthermore, Fig. 2.15 also shows how a good level of drug loading is maintained as the dodecyl prodrug is blended with Imwitor 900k at various ratios.

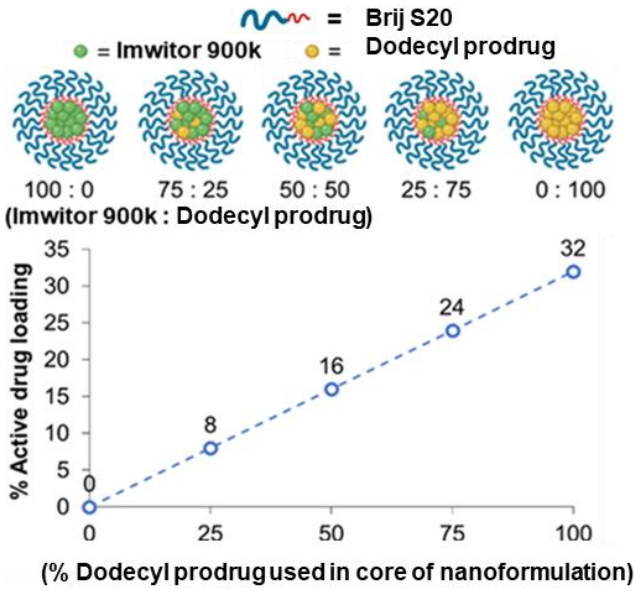

Figure 2.15- The relationship between drug analogue loading and active drug loading within the core for each of the various lipid/drug analogue blend formulations

Lipid-based nanoparticles were then formed using blends of prodrug with Imwitor 900k to investigate the effect of composition on particle size, distribution and stability. Fig. 2.16 displays particle size and polydispersity data obtained for each of the lipid/prodrug blends over a 4-week period. The measurement on day 0 reflects particle properties immediately after preparation, day 2 provides a timepoint for when no more THF remained in the continuous phase due to the disappearance of peaks at 1.85 and 3.7 ppm on a 1 H NMR spectrum, Appendix Fig. 2.5.[140] While, day 6 reflected on short term stability upon storage at 4 °C and day 28 provides a measure of the longer-term dispersion stability at 4 °C. On Day 0, the effect of increasing the prodrug concentration in the nanoparticles resulted in a slight decrease in the average particle size for each of the blends. Additionally, there was a more pronounced decrease in polydispersity with increasing prodrug concentration in the blend suggesting the size distribution had become much narrower. A possible explanation for the decrease in dispersity and particle size is the differences in LogP. Imwitor 900k consists of 40–55% monoglycerides,[141] both glyceryl monostearate and glyceryl monopalmitate have a moderate LogP of 6.3 and 7.4. LogP values in this range will result in an overall decrease in rate of nucleation as the percentage of Imwitor 900k was increased. Furthermore, low LogP may also offer an explanation as to why the 100% Imwitor nanoparticles suffer from growth between day 6 and day 28 resulting in a shimmering effect similar to that seen with the octyl prodrug, Appendix Fig 2.6. Despite this, the 100% Imwitor 900k nanoparticles appear to be stable and resist Ostwald's ripening up to a point between day 2 and 6, which was likely due to the high LogP of the remaining di- and triglycerides of Imwitor 900k following a fast degree of nucleation. All the lipid/prodrug blend formulations showed very little change in

particle properties at the time points, any changes were likely within error. This finding suggests that each of the blend formulations of lipid and dodecyl prodrug were stable for up to 4 weeks.

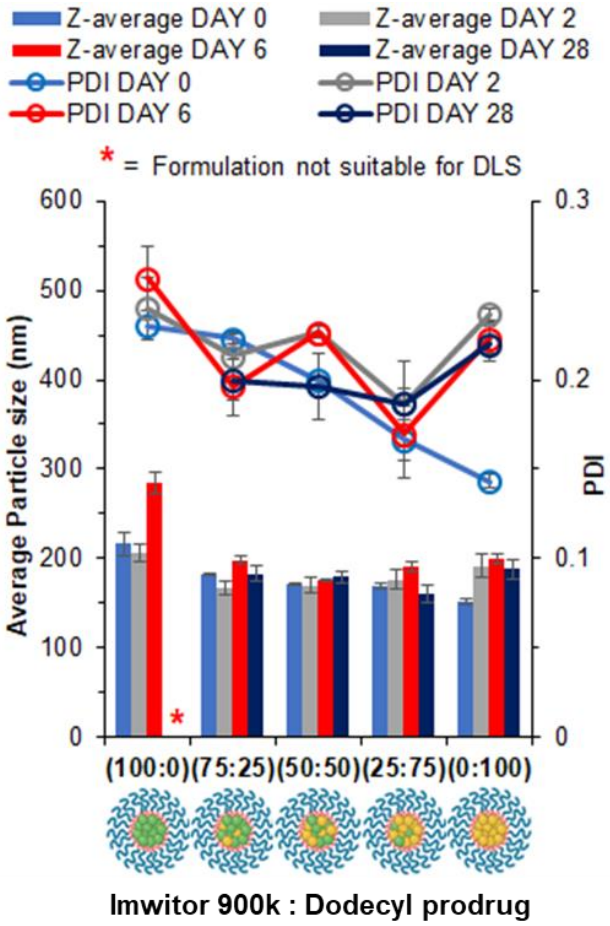

Figure 2.16- Particle size and size distribution data for each of the lipid/dodecyl drug analogue blends obtained by DLS over a 28-day period. Samples prepared in triplicate and error bars calculated on standard deviation between measurements. Samples were stored at 4 °C after day 2 measurement.

In order to better understand the effect of blending on the crystallinity of both the lipid and dodecyl prodrug DSC experiments were carried out. Firstly, the starting materials for the nanoparticle formulations were investigated individually, (Fig. 2.17). Brij S20 showed crystalline behaviour with a melting peak at approximately 40 °C. Imwitor 900k showed a broad melting endotherm with a melting temperature of approximately 60 °C. The slightly broader melting behaviour was likely due to Imwitor 900k being composed of a mixture of lipids rather than a single pure molecule. The endotherm for the dodecyl prodrug was sharp, with a peak at high temperature at approximately 89 °C. In order to assess the compatibility of the lipid and the prodrug, a 50:50 binary mixture of dodecyl prodrug and Imwitor 900k was prepared by melting the two compounds together allowing to solidify followed by thermo-analysis by DSC. The thermogram for this binary mixture possessed an intense peak at a lower temperature than that of both Imwitor 900k and dodecyl prodrug which suggests the presence

of a eutectic mixture.[142] On the other hand, an additional weaker transition was also observed in the range of 55-62 °C which may indicate the co-existence of a small amount of crystalline Imwitor 900k suggesting the dodecyl prodrug may have instead solubilised within Imwitor 900k (Fig. 2.17). Nevertheless, the absence of a dodecyl prodrug transition indicates the dodecyl prodrug is of good compatibility with Imwitor 900k, meanwhile introduced a degree disorder of the Imwitor 900k crystal structure.[143] The onset temperatures and peak temperatures for each of the samples is summarised in Table 2.3.

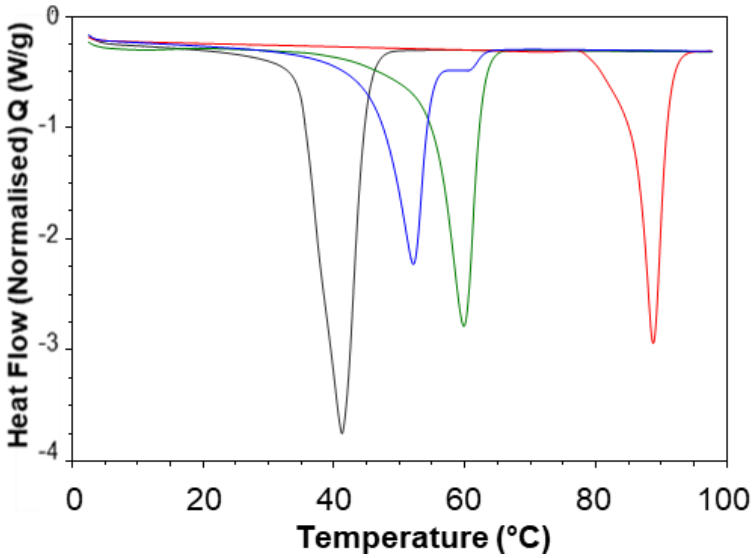

Figure 2.17- Overlay of 2nd heat DSC thermograms for each bulk material nanoparticle component as non-formulated materials; Brij S20 (grey), Imwitor 900k (green), dodecyl drug analogue (red). Overlay includes a 50:50 binary mixture between Imwitor 900k and the dodecyl drug analogue (blue).

Table 2.3- Numerical data corresponding to each of the DSC analysis of the non-formulated components used in Fig 2.17

	Onset Temperature (°C)	**Peak temperature (°C)**
Brij S20	32.9	39.7
Imwitor 900k	54.6	59.9
Dodecyl prodrug	85.6	88.8
Binary mixture (Imwitor 900k/Dodecyl prodrug at 50:50)	46.2	52.1

The thermal properties of the lipid-based nanoparticle blends were then investigated. Fig. 2.18 displays an overlay of thermograms for each of the nanoparticle formulations. The most pronounced melting transition that was observed for all formulations was Brij S20 peak at approximately 35-45 °C, this was due to Brij S20 comprising 86 % of the total mass of each sample while the core comprised 14 %. The endotherms ocurring in the region 45-65 °C corresponded to the nanoparticle core

crystallinity, with endotherms in the range ~45-55 °C for the Imwitor 900k and ~55-75 °C for the dodecyl prodrug. For the formulation of 100 % Imwitor 900k the average peak temperature for Imwitor 900k was 51.1 °C. It was clear that the ratio of Imwitor 900k and dodecyl prodrug determined the crystallinity of the two compounds. Firstly, as expected for 100% Imwitor 900k nanoparticles only one peak was present in this region (see Fig. 2.18 inset). As the percentage of dodecyl prodrug was increased to 25 % the magnitude of the Imwitor 900k endotherm decreased, whilst also shifting left to a lower melting temperature. This change in peak behaviour was described by Jenning *et al*. as peak depressions.[13] No endotherm for the prodrug was observed in the region of 60-75 °C. The presence of a single peak at this ratio suggested the Imwitor 900k and dodecyl prodrug exists as a solid solution with the dodecyl prodrug completely solvated within the solid lipid core of the nanoparticles. This behaviour in the nanoparticles was that same as seen for the binary mixture of only lipid and prodrug shown in Fig. 2.17. As the ratio of dodecyl prodrug was increased further to ratio of 50:50 the Imwitor 900k endotherm again experienced peak depression, however an additional peak was also present at a higher temperature of approximately 54 °C, thus indicating the presence of two different crystalline forms.[34] As the amount of prodrug in the composition was further increased to a ratio of 25:75 the endotherm corresponding to the prodrug became more pronounced and shifted to higher temperatures of approximately 60 °C and 65 °C as the ratio of dodecyl prodrug was increased to 75 and then 100 %. Additionally, the peak for Imwitor 900k completely disappeared at 75 % prodrug. Consequently, we hypothesise that at 75 % prodrug, the core existed as Imwitor 900k solubilised within the prodrug. Comparison between the unformulated material and nanoparticle formulations showed peak broadening and a shift of endotherms to lower melting temperature for both the core nanoparticle materials i.e. Imwitor 900k or dodecyl prodrug (see Table 2.4) compared to the corresponding bulk material (Table 2.3). Similar findings have been reported by Siekmann and Westesen.[144] This suggests a decrease in crystal perfection which can be attributed to small size of the nanoparticles and an interaction between the surfactant and the core.

Table 2.4 - Numerical data corresponding to each of the DSC analysis of the formulated components for 100 % dodecyl drug analogue nanoparticles

	Average onset Temperature (°C)	**Difference (+/-) to unformulated onset temperature (°C)**	**Average peak temperature (°C)**	**Difference (+/-) to unformulated peak temperature (°C)**
Imwitor 900k	55.2	+ 0.6	58.9	- 1.0
Dodecyl prodrug	53.1	- 32.5	64.9	- 23.9

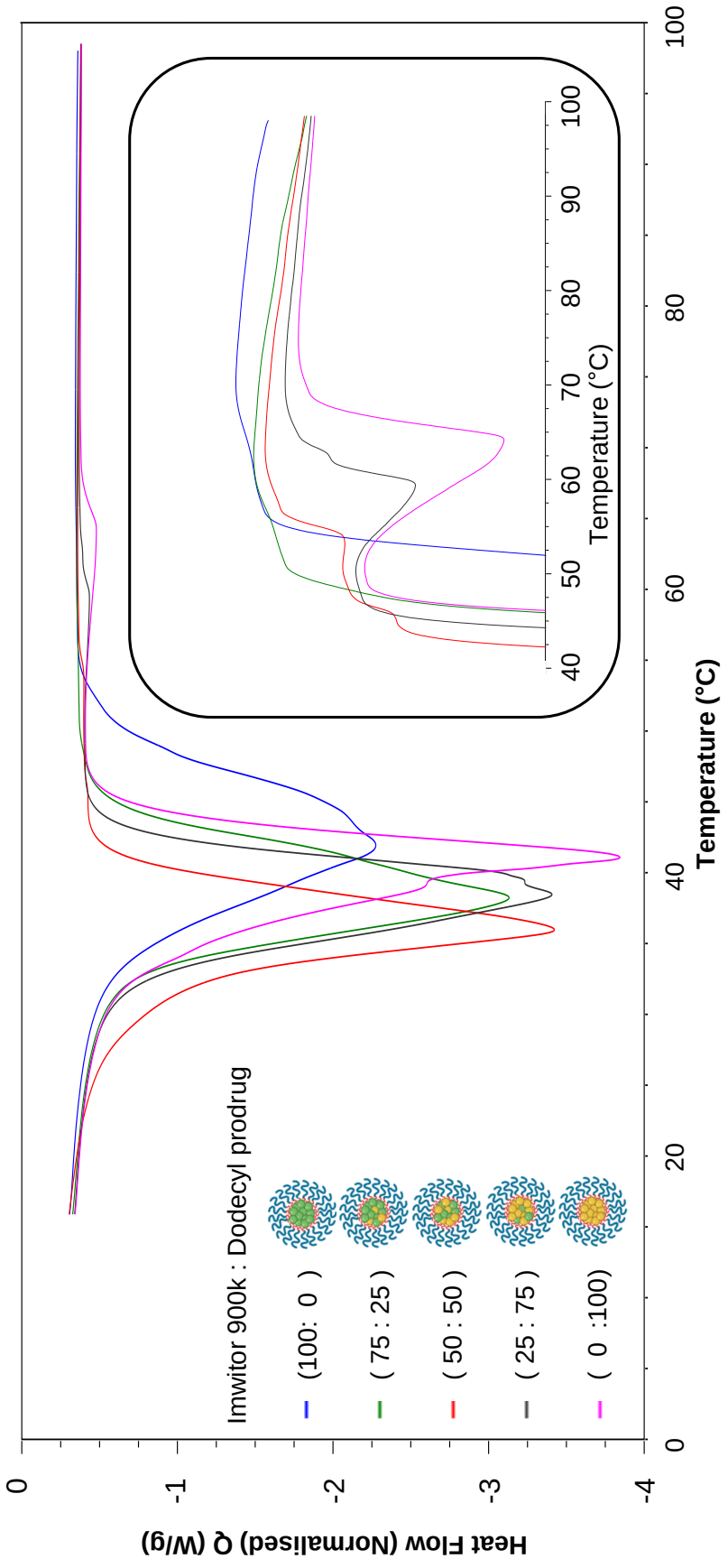

Figure 2.18-Overlay of DSC traces for each of the nanoparticle formulations. The insert shows the region 40-100 which indicates the effect of core composition on the crystallinity of the lipid and drug analogue within the core of nanoparticles

In addition, a notable trend between formulation ratio of Imwitor 900k to prodrug and shifts in the melting temperatures and enthalpies for both the dodecyl prodrug and Imwitor 900k. For the prodrug, the melting temperature and crystallinity decreased as the percentage of Imwitor increased in the formulation (Fig.2.18). Indeed, the prodrug was entirely amorphous when the prodrug represented 25 % of the core mass formulation. It was not possible to carry out a similar analysis for the Imwitor 900k due to some overlap of the melting enthalpies with those from Brij S20, however it was clear that the melting temperature decreased and the enthalpy for the melted also decreased with increasing prodrug concentration. Furthermore, lack of core crystallinity was further supported by PXRD analysis shown Fig. 2.19. The graphs display an overlay of PXRD analysis of the various components within the formulation at 25 % dodecyl prodrug 75 % Imwitor 900k compared to the formulation itself. It is clear that no peaks for the dodecyl prodrug are present in the analysis performed on the formulation further supporting the DSC analysis and the belief that the dodecyl prodrug is indeed amorphous at 25 % of the core mass, Fig.2.20-A. Two peaks do exist at ~19.5 and 23.5 2θ which potentially overlay with either Imwitor 900k or the Brij S20 (Fig.2.20-B and C), however due to the intensity of the Brij S20 peak on DSC analysis relative to that of Imwitor 900k it was plausible to assume the peaks visible for the formulation on PXRD analysis were likely that of Brij S20. These results provide strong evidence of the Imwitor and the dodecyl prodrug were contained in the same particles (rather than separate nanoparticle populations), additionally the blending reduced the crystallinity of both compounds relative to that of the bulk material. This work demonstrates how the crystallinity of a nanoparticle core can be tuned by blending with various components.

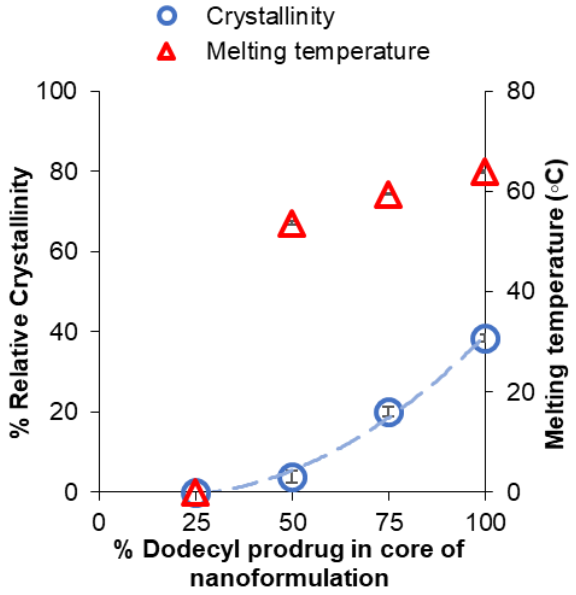

Figure 2.19- Graph showing the relationship between percentage of dodecyl drug analogue within the core and the crystallinity od dodecyl drug analogue relative to that of the bulk.

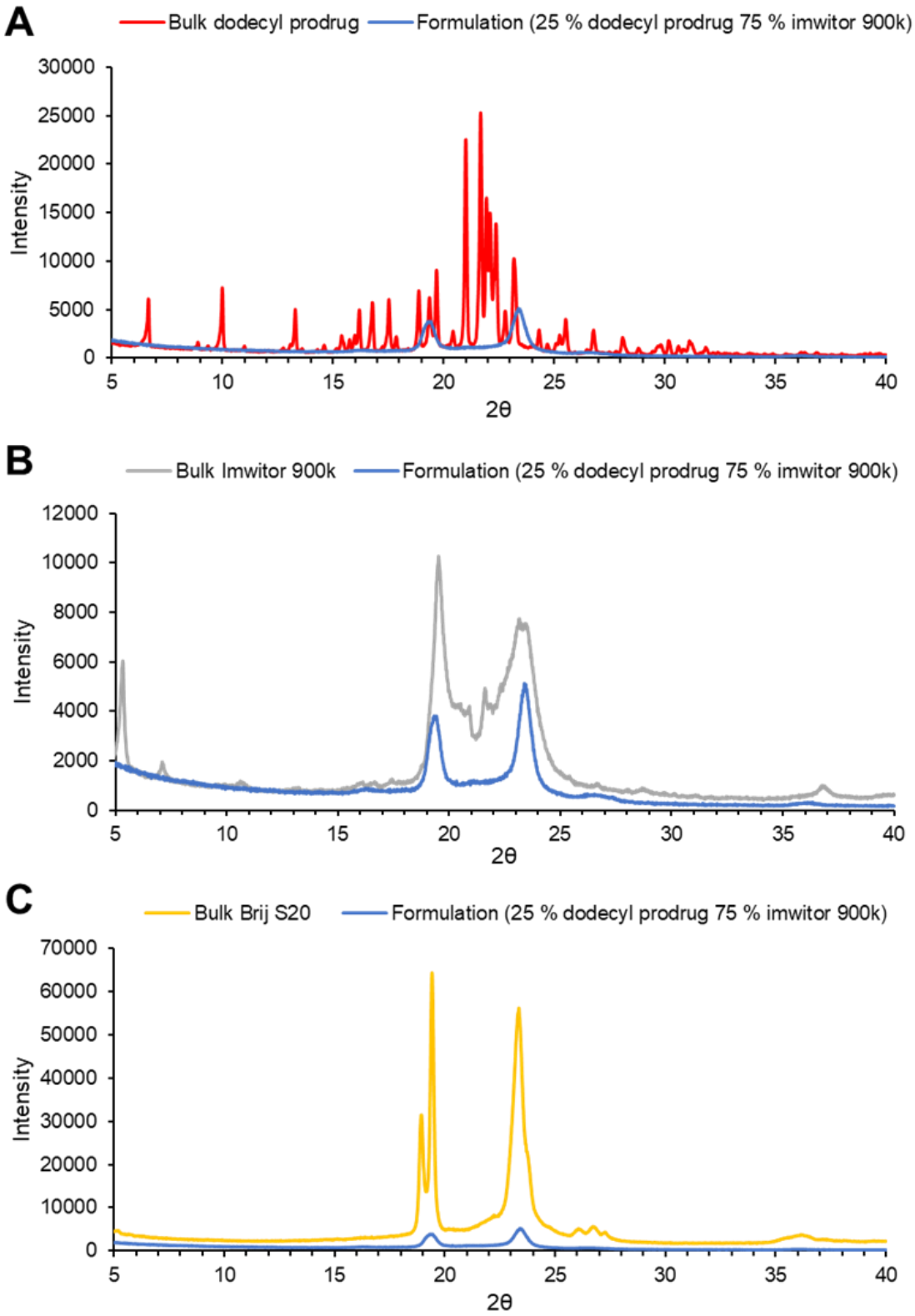

Figure 2.20- PXRD analysis of individual components of formulation as bulk materials vs analysis of dodecyl prodrug Imwitor 900k blend formulation (25 %/75 %). A) Dodecyl prodrug, B) Imwitor 900k, and C) Brij S20.

2.4. Conclusions

In this study the effects of LogP of carbamate and carbonate-based prodrug on the formation and stability of SLN and SPN were investigated. As per the LaMer model, with increasing LogP (and the likely higher degree of supersaturation and faster rate of nucleation) smaller nanoparticles with a narrow size distribution were produced. Furthermore, the prodrug with the highest LogP (11.44) resulted in highly stable formulations which maintained size and dispersity for up to at least 4 weeks. Meanwhile prodrugs of lower LogP experienced considerable growth resulting in micron sized aggregates as a result of Ostwald ripening. This work agrees with Zhu et al. that molecules with a LogP in the range 9-12 produce potentially stable nanoparticles by nanoprecipitation. While demonstrates a more systematic approach and in depth understanding that molecules with an elevated LogP may be formulated to form stable particles of a small size and narrow size distribution.[33] As a result, demonstrates how LogP can be used as a tool to tune and optimise nanoparticle formulations in the future. Additionally, this work demonstrates how poorly water-soluble drugs may be formulated with or without the need of prodrug synthesis to achieve high drug loading formulations. This work also opens the door to potential combination nanoparticles with both hydrophilic and hydrophobic drugs. Meanwhile, this work builds on that of Jennings *et al*.,[13] and Bunjes *et al*.,[34] by demonstrating how blending drug/prodrug with a lipid such as Imwitor 900k tackles issues such as high crystallinity of the nanoparticle core, thus potentially providing a solution to prolong nanoparticle stability against any polymorphic transitions.

2.5. Future work

It would be useful to do further studies while employing other model drugs to strengthen the hypothesis. In doing so, other chemistries may be explored of both the drug and the linker bond to investigate whether LogP may be used as a universal indicator for stable nanoparticle formulation with regards to prodrugs.

2.6. Experimental

Materials

Brij S20, tetrahydrofuran, anhydrous materials (pyridine, dichloromethane) and deuterated solvents ($CDCl_3$) were all purchased from Sigma Aldrich. Each were used as received apart from $CDCl_3$ where 0.1% tetramethylsilane was added. All other solvents were reagent grade and purchased from Fischer Scientific and used as received. Alkyl chloroformates were purchased from Tokyo chemical industry and used as received. Magnesium sulphate ($MgSO_4$) and concentrated hydrochloric acid (HCl) were also purchased from Fischer Scientific. HCl was diluted down to a 1M solution, meanwhile $MgSO_4$ was

used as received. Imwitor® 900K (glyceryl monostearate) was kindly gifted from IOI Oleochemical, Hamburg. Lamivudine was purchased from Top Well Medipharma Group.

Methods

General synthesis of prodrugs using n-alkyl chloroformates

In an oven dried 100 ml round-bottom flask, cooled under dry nitrogen, 3TC (2.98 g, 1.0 eq., 0.013 mol) was suspended in anhydrous DCM (150 mL). Anhydrous pyridine (3.08 g, 3.0 eq., 0.039 mol) was also charged to the round bottom flask before the reaction mixture was purged with dry nitrogen for approximately 30 minutes and cooled to 0 °C using an ice bath. The reaction was initiated by the dropwise addition of *n*-alkyl chloroformate (2.2 eq., 0.029 mol). The reaction mixture was allowed to warm to room temperature and left stirring for 22 hours. The product was washed three times with 1 M HCl aqueous solution, and the organic phase was washed with brine, dried with $MgSO_4$ and filtered before removing volatiles from the reaction mixture *via* reduced pressure. The resulting residue was purified *via* silica chromatography (hexane 50 : 50 ethyl acetate) to obtain a white powder which was dried in a vacuum oven at 20 °C.

Characterisation data of prodrugs

Butyl drug analogue (butyl(1-((2*R*,5*S*)-2-((((butyloxy)carbonyl)oxy)methyl)-1,3-oxathiolan-5-yl)-2-oxo-1,2-dihydropyrimidin-4-yl)carbamate): yield 0.7 g (37%); m.p. 82–84 °C; elemental analysis (calcd for $C_{18}H_{27}N_3O_7S$: C, 50.34; H, 6.34; N, 9.78; S, 7.46; found: C, 50.36; H, 6.35; N, 9.9; S, 7.22%); V_{max}/cm^{-1} 3455w (NH), 3295s, 3114w, 2960s, 2936w and 2903w (CH); 1750s, 1727s and 1677s (CO), 1501s (CC), 1260s (CO); ^{1}H NMR (400 MHz, $CDCl_3$) δ ppm; 0.9 (6H, t, CH_3), 1.3–1.4 (4H, m, CH_2), 1.6–1.75 (4H, m, CH_2), 3.4 (2H, dd, CH_2), 4.2 (4H, t, CH_2), 4.6 (2H, m, CH_2), 5.4 (1H, s, CH), 6.3 (1H, s, CH), 7.25 (1H, d, CH), 7.4–8.1 (1H, broad s, NH), 8.2 (1H, d, CH); ^{13}C NMR NMR (100 MHz, $CDCl_3$) δ ppm; 13.60 (s, 1C), 13.63 (s, 1C), 18.86 (s, 1C), 18.92 (s, 1C), 30.56 (s, 1C), 30.59 (s, 1C), 38.83 (s, 1C), 66.25 (s, 1C), 66.58 (s, 1C), 68.62 (s, 1C), 84.37 (s, 1C), 87.98 (s, 1C), 94.68 (s, 1C), 144.24 (s, 1C), 152.49 (s, 1C), 154.60 (s, 1C), 154.89 (s, 1C), 162.65 (s, 1C); HRMS (ESI) *m/z*: calcd for $C_{18}H_{27}N_3O_7S$, 430.16 $[M + H]^+$, 452.15 $[M + Na]^+$, found 430.16, 452.15.

Octyl drug analogue (octyl(1-((2*R*,5*S*)-2-((((octyloxy)carbonyl)oxy)methyl)-1,3-oxathiolan-5-yl)-2-oxo-1,2-dihydropyrimidin-4-yl)carbamate): yield 0.88 g (37%); m.p. 72–74 °C; elemental analysis (calcd for $C_{26}H_{43}N_3O_7S$: C, 57.65; H, 8.00; N, 7.76; S, 5.92; found: C, 57.74; H, 8.04; N, 7.94; S, 5.97%); V_{max}/cm^{-1} 3457w (NH), 3295s, 3114w, 2955s, 2920w and 2852w (CH); 1747s, 1729s and 1673s (CO), 1501s (CC), 1278s (CO); ^{1}H NMR (400 MHz, $CDCl_3$) δ ppm; 0.9 (6H, t, CH_3), 1.3–1.4 (20H, m, CH_2), 1.6–1.75 (4H, m, CH_2), 3.4 (2H, dd, CH_2), 4.2 (4H, t, CH_2), 4.6 (2H, m, CH_2), 5.4 (1H, s, CH), 6.3 (1H, s,

CH), 7.25 (1H, d, CH), 7.4–8.1 (1H, broad s, NH), 8.2 (1H, d, CH); ^{13}C NMR NMR (100 MHz, $CDCl_3$) δ ppm; 14.06 (s, 2C), 22.60 (s, 2C), 25.62 (s, 1C), 25.69 (s, 1C), 28.59 (s, 1C), 29.11 (s, 1C), 29.12 (s, 2C), 29.14 (s, 1C), 31.73 (s, 1C), 31.75 (s, 1C), 38.85 (s, 1C), 66.58 (s, 2C), 68.94 (s, 1C), 84.39 (s, 1C), 88.00 (s, 1C), 94.64 (s, 1C), 144.28 (s, 1C), 152.42 (s, 1C), 154.61 (s, 1C), 154.90 (s, 1C), 162.60 (s, 1C); HRMS (ESI) *m*/*z*: calcd for $C_{26}H_{43}N_3O_7S$, 542.29 $[M + H]^+$, 564.27 $[M + Na]^+$, found 542.29, 564.27.

Dodecyl drug analogue (dodecyl (1-((2*R*,5*S*)-2-((((dodecyloxy)carbonyl)oxy)methyl)-1,3-oxathiolan-5-yl)-2-oxo-1,2-dihydropyrimidin-4-yl) carbamate): yield 0.75 g (26%); m.p. 78–80 °C; elemental analysis (calcd for $C_{34}H_{59}N_3O_7S$: C, 62.45; H, 9.09; N, 6.43; S, 4.90; found: C, 62.37; H, 8.98; N, 6.26; S, 5.00%); V_{max}/cm^{-1} 3459w (NH), 3279s, 3146w, 2955s, 2916w and 2849w (CH); 1747s, 1728s and 1676s (CO), 1500s (CC), 1276s (CO); ^{1}H NMR (400 MHz, $CDCl_3$) δ ppm; 0.9 (6H, t, CH_3), 1.3–1.4 (32H, m, CH_2), 1.6–1.75 (8H, m, CH_2), 3.4 (2H, dd, CH_2), 4.2 (4H, t, CH_2), 4.6 (2H, m, CH_2), 5.4 (1H, s, CH), 6.3 (1H, s, CH), 7.25 (1H, d, CH), 7.4–8.1 (1H, broad s, NH), 8.2 (1H, d, CH); ^{13}C NMR NMR (100 MHz, $CDCl_3$) δ ppm; 14.10 (s, 2C), 22.67 (s, 2C), 25.63 (s, 1C), 25.70 (s, 1C), 28.60 (s, 1C), 28.68 (s, 1C), 28.88 (s, 2C), 29.19 (s, 1C), 29.22 (s, 1C), 29.33 (s, 2C), 29.48 (s, 2C), 29.54 (s, 1C), 29.57 (s, 1C), 29.60 (s, 1C), 29.63 (s, 1C), 31.90 (s, 1C), 32.65 (s, 1C), 38.87 (s, 1C), 66.55 (s, 1C), 66.62 (s, 1C), 68.96 (s, 1C), 84.44 (s, 1C), 88.01 (s, 1C), 94.68 (s, 1C), 144.31 (s, 1C), 152.41 (s, 1C), 154.89 (s, 1C), 155.43 (s, 1C), 162.55 (s, 1C); HRMS (ESI) *m*/*z*: calcd for $C_{34}H_{59}N_3O_7S$, 654.41 $[M + H]^+$, 676.40 $[M + Na]^+$, found 654.41, 676.40.

General nanoparticle preparation

Method adopted for SPN and SLN formulation was nanoprecipitation. For the aqueous phase, the surfactant Brij S20 was dissolved to prepare a 500 ml stock solution in distilled water (1 mg mL^{-1}) and left overnight at 21 degrees Celsius under mechanical stirring (300 rpm). Regardless of the composition a stock solution of the lipid/drug analogue phase (2 mg mL^{-1}) was prepared in tetrahydrofuran which was sealed and left at room temperature under mechanical stirring (300 rpm) for 30 minutes. Portions of the stock solution(s) were then taken for injection (2 mg mL^{-1}, 2 mL)- see table 2.5. The 2 mL lipid/drug analogue solution was charged dropwise into the vortex of Brij S20 aqueous solution (24 mL) in a 40 ml vial while mechanically stirring (800 rpm). To ensure consistency in time of injection the shot was charged by removing the plunger of a clamped syringe resulting in a steady flow through the hypodermic needle. The combined mixture was left stirring to allow evaporation of tetrahydrofuran over 2 days at a room temperature (∼21 °C) in a fume cupboard with an average air velocity of 0.35 m s^{-1}. Samples were then stored at 4 °C.

Table 2.5- Organic phase composition depending on blends of Imwitor 900k and dodecyl prodrug

Core composition	Volume tricaprin stock solution (mL)	Volume prodrug stock solution (mL)	Total volume organic phase injectable shot (mL)
100 % Imwitor 900k	2	0	2
75 % Imwitor 900k 25 % dodecyl prodrug	1.5	0.5	2
50 % Imwitor 900k 50 % dodecyl prodrug	1	1	2
25 % Imwitor 900k 75 % dodecyl prodrug	0.5	1.5	2
100 % dodecyl prodrug	0	2	2

Analytical techniques

LogP/CLogP

Calculated using the mathematical model employed by ChemDraw software.

Nuclear magnetic resonance (NMR)

^{1}H NMR and ^{13}C spectra were recorded using a Bruker DPX-400 spectrometer operating at 400 and 100 MHz respectively. Solvents used for NMR spectroscopy were $CDCl_3$ and D_2O. Chemical shifts (δ) are reported in parts per million (ppm).

Fourier Transform Infrared Spectroscopy (FTIR)

Fourier-transform infrared spectroscopy (FT-IR) was performed using a Thermo NICOLET IR200, between 400 cm^{-1} to 4000 cm^{-1}. Samples were loaded either neat, using an attenuated total reflectance accessory.

Elemental analysis (CHNS)

Elemental analyses were obtained from a Thermo FlashEA 1112 series CHNSO elemental analyser.

Electrospray mass spectrometry

Electrospray ionisation mass spectrometry (ESI) data were recorded in the Mass Spectrometry Laboratory at the University of Liverpool using a MicroMass LCT mass spectrometer using electron ionisation and direct infusion syringe pump sampling. All materials were diluted with methanol. Dilution concentration was dependent on the molecular weight of the entity.

Dynamic light scattering (DLS) and Zeta potential

Samples were analysed by DLS using The Anton Parr Litesizer™ 500 to obtain a *Z*-average and size distribution (PDI) and zeta potential of nanoparticle dispersion. 2 ml of each sample with a concentration between 1.14–1.33 mg ml^{-1} (total solids *i.e.* surfactant, lipid and/or drug analogue) was measured in standard 3 ml fluorimeter cuvettes with a pathlength of 10 mm. All measurements were carried out at 25 °C with a fixed backscattering angle of 175° using automated setting of a maximum of 60 runs at 10 seconds per run (*i.e.* time of run approximately 6 minutes). Samples were done in triplicate. Zeta potential was also measured using Anton Parr Litesizer™ 500. Samples were diluted using 0.01 M NaCl solution at a ratio of 1 : 1 and measured in a Malvern zetasizer nano series disposable folded capillary cell. All measurements were carried out at 25 °C using automated setting of a maximum of 1000 processed run.

Differential scanning calorimetry (DSC)

Nanoparticle formulations were freeze dried down in a glass vial before weighing out into Aluminium pans. Performed by a TA DSC25. The freeze-dried nanoparticle formulations were equilibrated at 10 °C before heating to 100 °C at a rate of 10 °C per minute. The bulk samples were heated to 100 °C at a rate of 10 °C per minute before being cooled back down to 0 °C at a rate of 5 °C per minute and again heating back up to 100 °C at a rate of 10 °C per minute. Measurements were carried out in triplicate.

Cryogenic scanning electron microscopy (Cryo-SEM)

Specimens prepared by freezing a small volume of sample between two brass rivets, which are plunged into slushed liquid nitrogen. Rivets transferred to a brass loading shuttle under liquid nitrogen and transferred under a nitrogen atmosphere to a preparation stage cooled to −120 °C. Anti-contaminator in preparation stage run at −190 °C. Fracture surface created in frozen specimen by pushing-off the upper rivet from the one held in the shuttle (using a liquid nitrogen cooled knife). Fracture surface coated with Pt in the preparation chamber, to make it conductive and specimen transferred to a cooled stage in the FIB/SEM (at −160 °C, with an anti-contaminator held at −190 °C). Specimens photographed using an in-chamber secondary electron detector Everart Thornley using either 1.5 or 10 keV and a beam current of 15 pA.

Powder X-ray diffraction (PXRD)

PXRD data were collected in transmission mode on a Panalytical X'Pert PRO MPD equipped with a high throughput screening (HTS) XYZ stage, X-ray focusing mirror and PIXcel detector, using Cu Kα radiation. Data were measured on loose powder samples held on thin Mylar film in aluminium well plates, over the range 4 to 40 ° in approximately 0.013 ° steps over 60 minutes.

2.7. Appendix

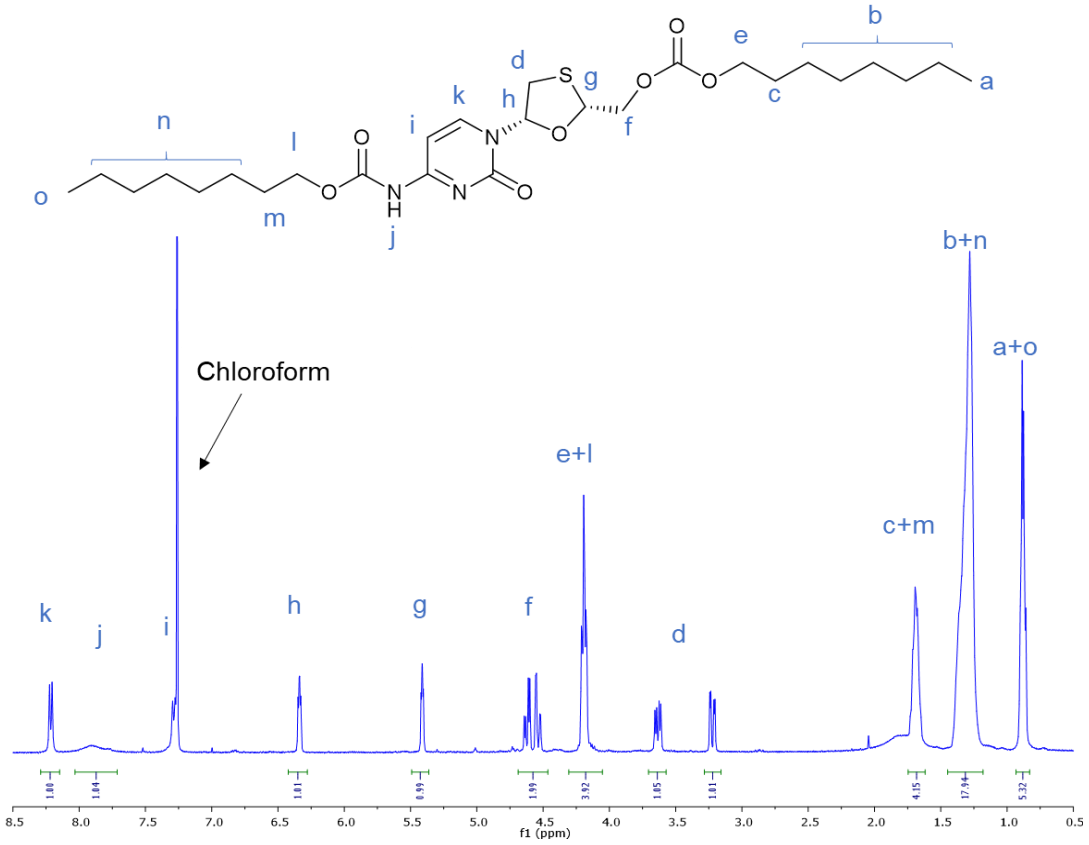

Appendix Figure 2.1- ^{1}H NMR (400 MHz) spectra of octyl drug analogue in $CDCl_3$

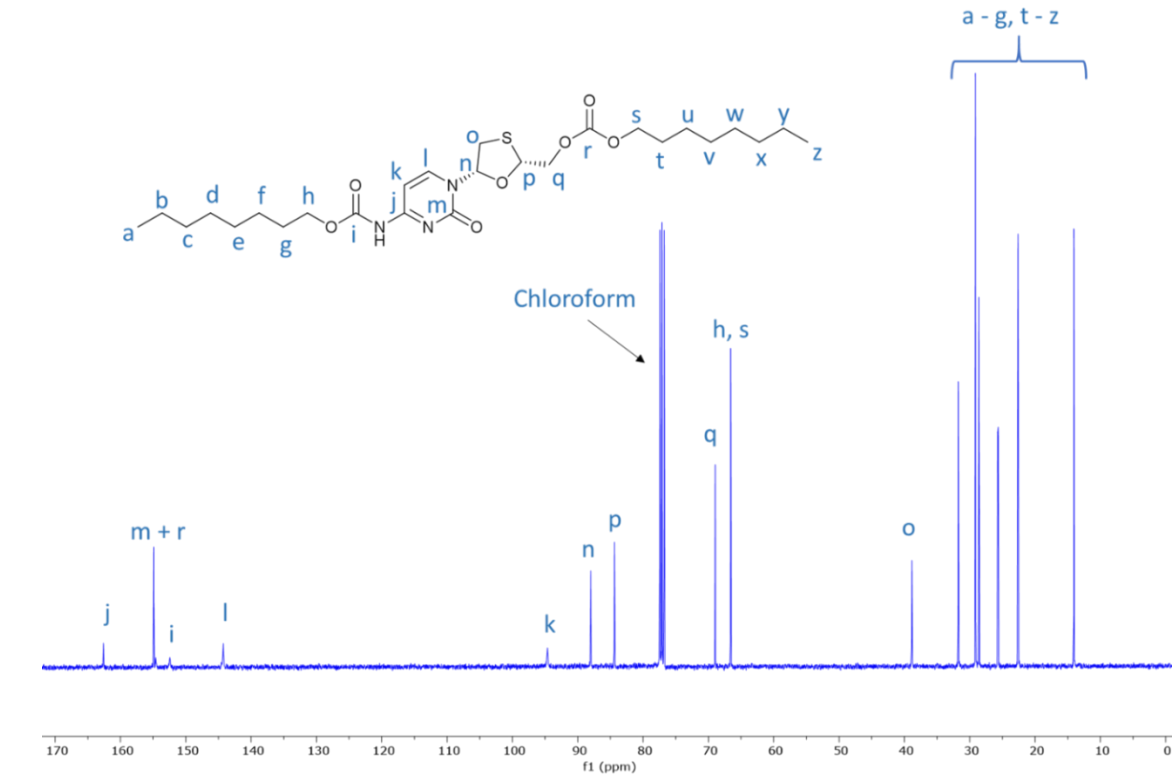

Appendix Figure 2.2-^{13}C NMR (400 MHz) spectra of octyl drug analogue in $CDCl_3$

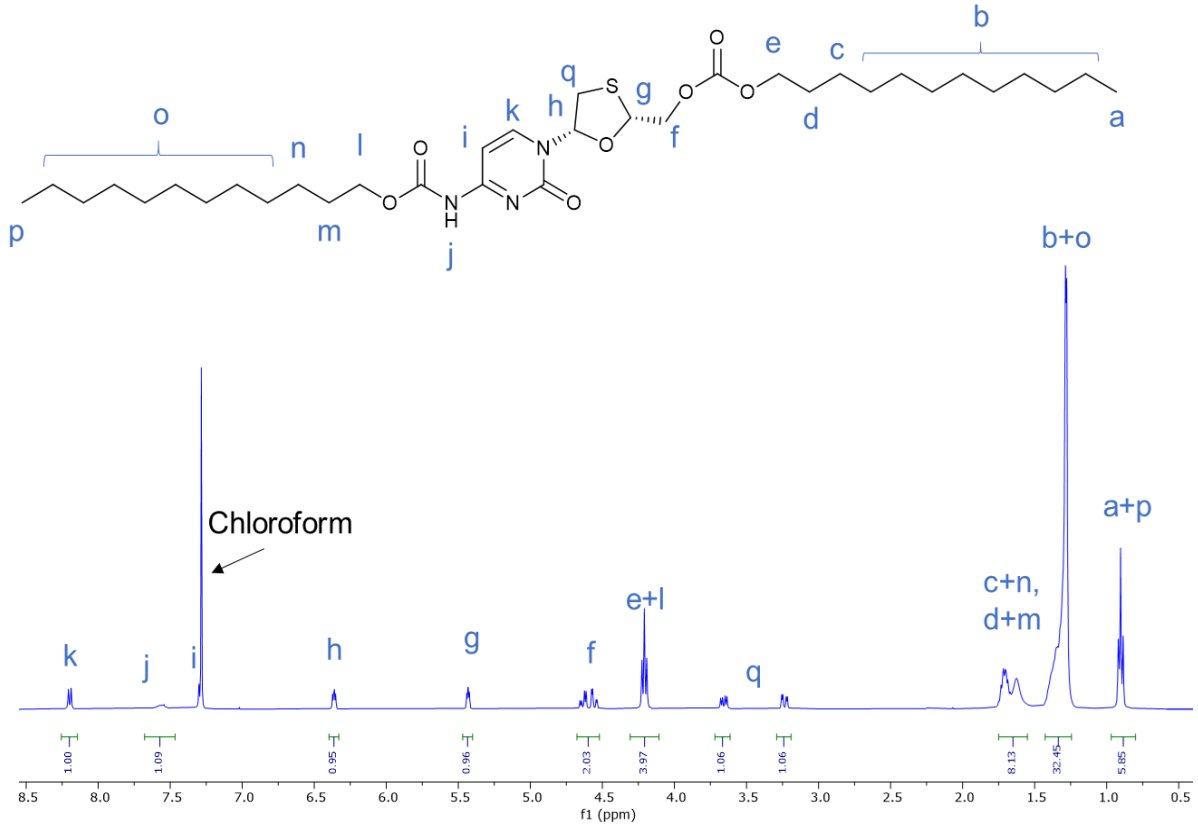

Appendix Figure 2.3-^{1}H NMR (400 MHz) spectra of dodecyl drug analogue in $CDCl_3$

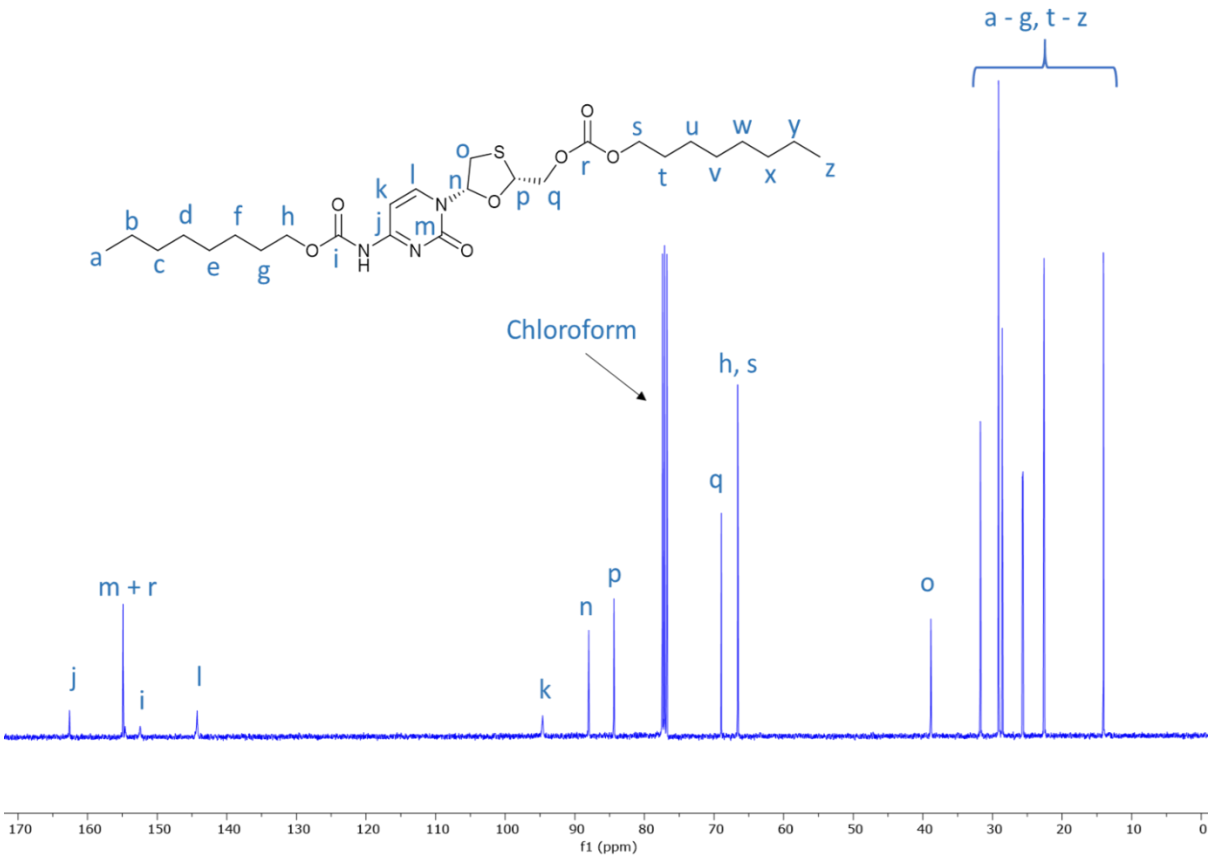

Appendix Figure 2.4-^{13}C NMR (400 MHz) spectra of dodecyl drug analogue in $CDCl_3$

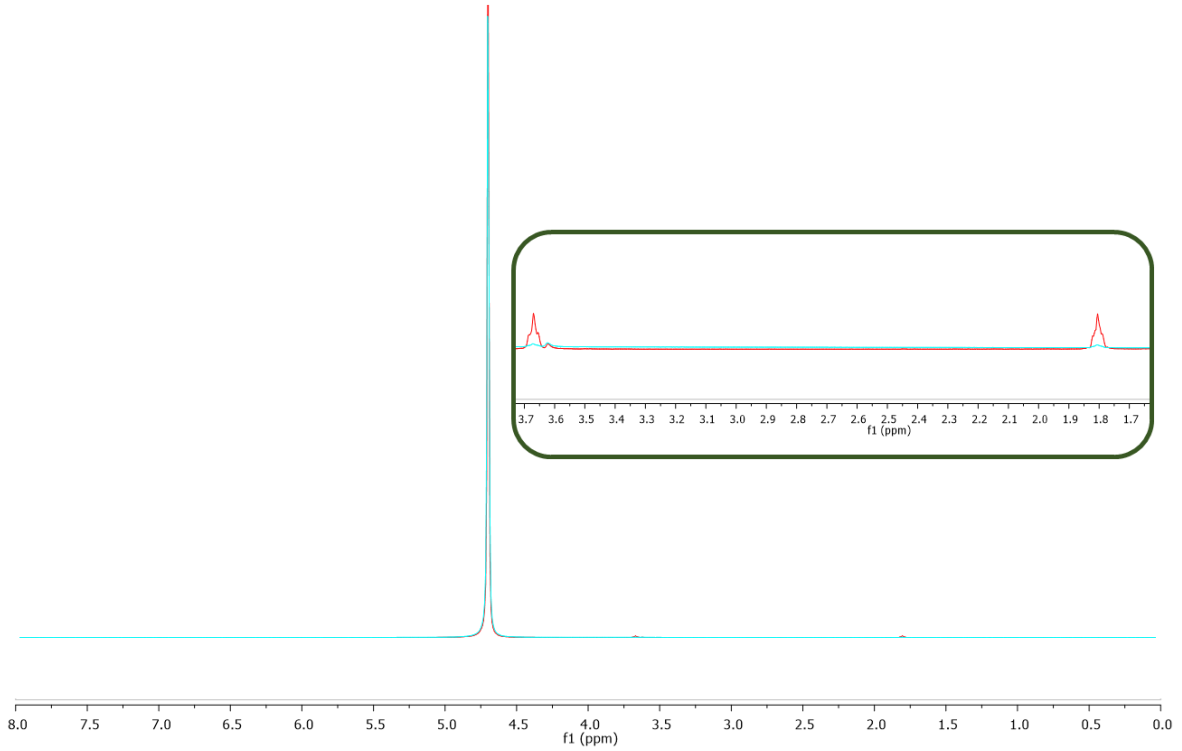

Appendix Figure 2.5-^{1}H NMR overlay of day 0 (red) and day 2 (cyan) showing disappearance of peaks for tetrahydrofuran (THF) at approximately 1.85 and 3.7 ppm indicating complete evaporation of THF for the 100 % dodecyl drug analogue nanoparticle formulation. Sample ran in D_2O.

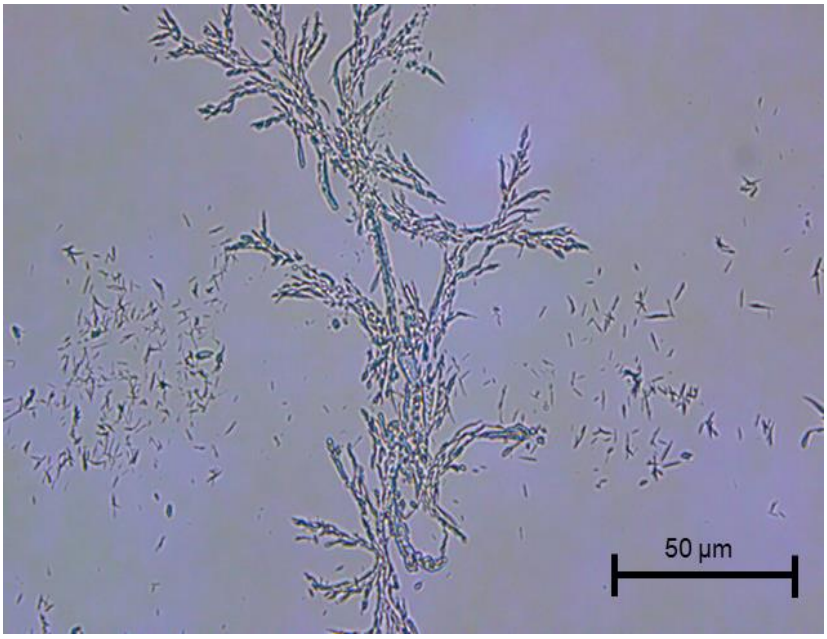

Appendix Figure 2.6- Optical Microscopy image confirming the presence of anisotropic crystals of Imwitor 900k indicating poor stability between day 6 and day 28

CHAPTER 3

The influence of surfactant type and surfactant composition on lipid nanoparticle formation and stability

Chapter 3 -The influence of surfactant type and surfactant composition on lipid nanoparticle formation and stability

3.1. Introduction

In the area of lipid nanoparticle formulations it is possible to categorise lipid surfactants into two distinct types; pegylated lipids and unpegylated lipids.[145] Pegylated lipids are typically a lipid which has been conjugated to a PEG chain. PEG is a material commonly employed as it is reported to enhance circulation times of nanoparticles *in vivo*, meanwhile also enhancing colloidal stability with the aid of a steric barrier.[146] Meanwhile, unpegylated lipids are typically ionically neutral i.e. zwitterionic phospholipids such as DOPE and therefore offer exceptional biocompatibility. Indeed, unpegylated lipids have been used to design and synthesise phospholipid polymer conjugates to improve biocompatiblity of polymers as well as formulation of drugs with low aqueous solubility.[147,148] Furthermore, unpegylated lipids phospholipids have been described by Schoenmaker *et al*. as 'helper lipids' due to their influence of enhancing delivery efficiency but more so in aiding nanoparticle formation.[7,146] Although, there is little information in literature on how unpegylated lipids aid nanoparticle formation. Nevertheless, surfactants may be characterised by their properties, for example their place on the HLB scale and their molecular weight. The hydrophilic lipohpilic balance (HLB) scale was designed to streamline the surfactant selection process to increase efficiency during formulation development. HLB defines non-ionic surfactants by their ratio of molecular weight of hydrophilic and hydrophobic components. Meanwhile, has been amended to accommodate ionic surfactants whereby an approximate HLB may be determined experimentally based on the surfactant's solubility or dispersibility in water; no dispersibility in water HLB 1-4, poor dispersion HLB 3-6, milky dispersion after vigorous agitation HLB 6-8, stable milky dispersion HLB 8-10, translucent to clear dispersion HLB 10-13 and a clear solution HLB 13+.[26] Unfortunately, despite advances in development lipid nanoparticle formulations, many typically suffer from low drug loading,[28] many of which can be attributed to being dominated by a large wt % of surfactant relative to the core material thus leading to formulations of low efficiency.

3.2. Chapter Aims

The aim of this chapter is to investigate how unpegylated lipids such as Lipoid S100 may aid nanoparticle formation over pegylated lipids. This will be done by employing a series of pegylated lipid surfactants which differ in the chain length of the hydrophilic component. Thus, providing a systematic investigation into how the properties of surfactants such as HLB influence nanoparticle lipid nanoparticle formation and stability by flash nanoprecipitation, Fig.3.1-A. Furthermore, we have also

made direct comparisons between the pegylated lipid surfactant Brij S20 and the unpegylated lipid surfactant Lipoid S100. Blends of both unpegylated and pegylated lipid surfactants were examined for benefits from each type of surfactant, as well as each blend's ability to achieve stable formulations with a higher wt % of core material thus increasing potential drug loading, Fig. 3.1-B. Finally, dodecyl prodrug was blended in the most promising formulations to demonstrate how high drug loading formulations can be achieved from the developed strategy.

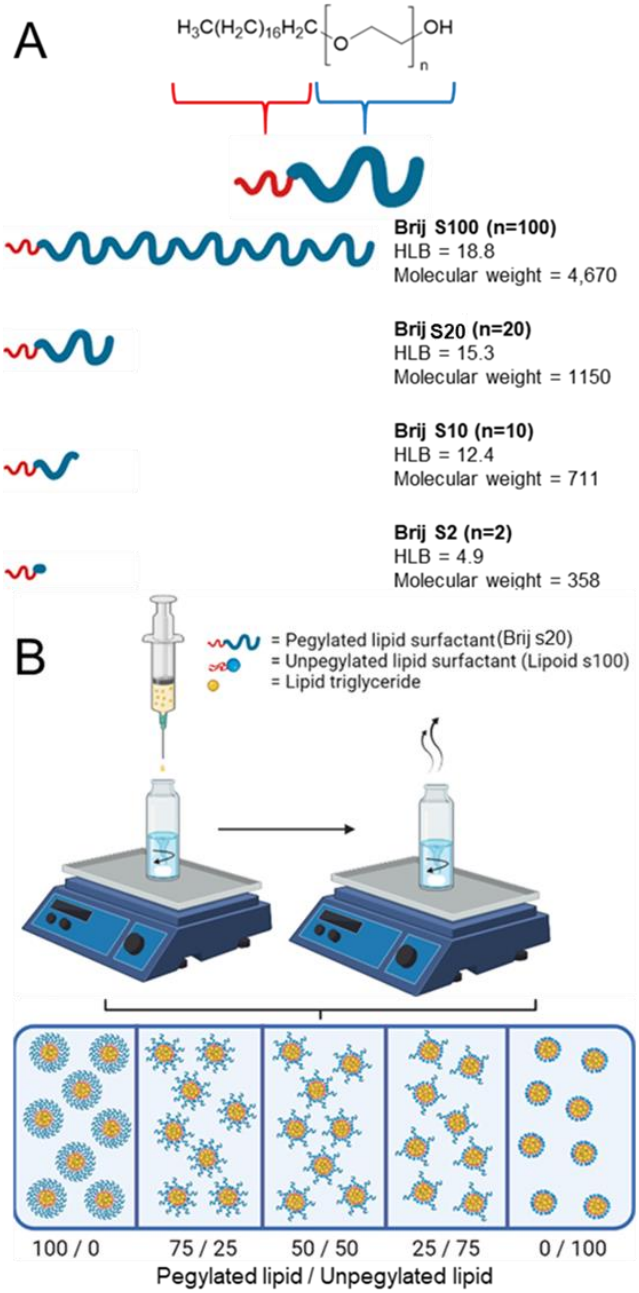

Figure 3.1- Schematic overview of strategy to investigate the role of surfactant and lipid type on the properties of the nanoparticles formed. A) Depicts a series of linear pegylated lipids to be formulated to investigate any trend in surfactant properties. Each surfactant is composed of the same stearyl hydrophobic component, while differ in the chain length of the hydrophilic polyethylene glycol block. B) Schematic overview of a strategy to blend both pegylated and unpegylated surfactants to assess nanoparticle formation control and stability at increased wt % of lipid triglyceride when formulating solid lipid nanoparticles.

3.3. Result and Discussion

3.3.1 Investigation into properties of helper lipid

The four linear pegylated lipid surfactants were used to formulate tricaprin at 14 wt %. To better understand the relationship between the HLB of the surfactant and the properties of the resulting lipid nanoparticles, Brij surfactants were selected. These surfactants were composed of the same stearyl chain for the lipophilic/hydrophobic components meanwhile varying the chain length of the polyethylene glycol from 2, 10, 20 and 100 units long to vary the hydrophilic component (information on the names and properties of the surfactants is shown in Fig.3.2). Tricaprin was nanoprecipitated into a fixed volume of each of the Brij surfactants Brij S20 and Brij S100. Due to aqueous solubility limits of the surfactants with shorter PEG chains, the Brij S2 and Brij S10 were instead dissolved in the organic phase along with the triglyceride tricaprin.

Upon injection the formulations were analysed by dynamic light scattering (DLS) to measure the size distribution of any particles formed. The DLS data in Fig.3.2 taken 10 minutes post formulation in shows a trend whereby both the diameter and PDI decreased with decreasing PEG chain length of the pegylated lipid surfactants.

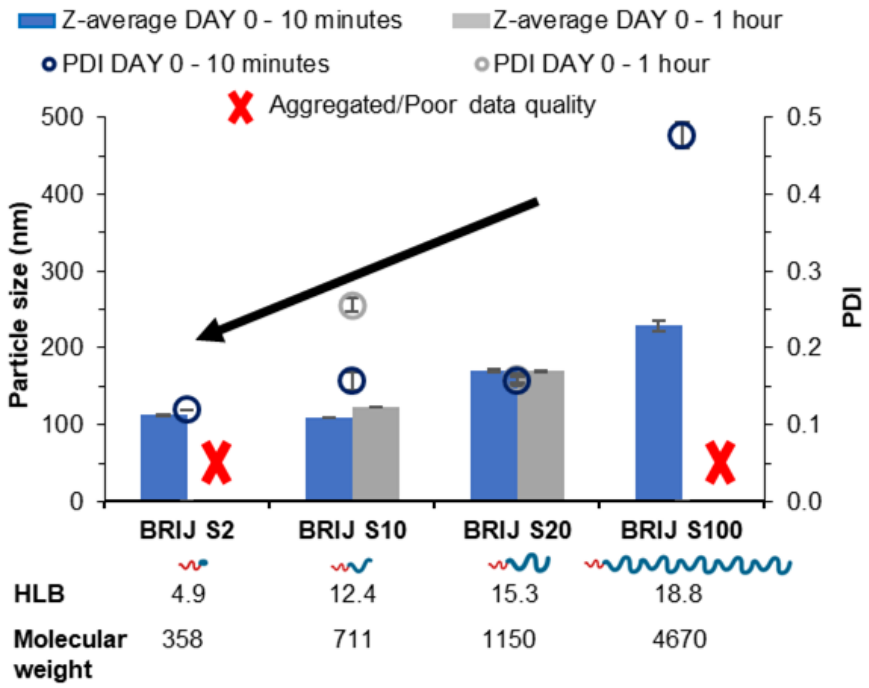

Figure 3.2- Data collected measuring both particle size and polydispersity of a series of tricaprin nanoparticle formulations stabilised by various Brij surfactants at equal mol %.

After an hour of particle formation, both samples stabilised by the Brij surfactant with the shortest and longest PEG chains were no longer suitable for DLS measurements; the formulation stabilised by Brij S2 possessed a shimmering effect (Fig.3.3-A), indicating the presence of anisotropic crystal

formation likely caused by insufficient steric stabilisation provided by the surfactant thus resulting in aggregation. Meanwhile, the formulation stabilised by Brij S100 contained aggregates (Fig.3.3-C), potentially caused by depletion flocculation due to the presence of excess polymer.[19] Meanwhile, the formulation of Brij S20 contained no visible particles (Fig.3.3-B), and was identified as the most efficient surfactant going forward due to providing a steric barrier against aggregation yet offering good control over the nanoparticle particle size and PDI. In combination, this data suggested that; as the HLB decreased towards the range of the Lipoid S100 (1-4), the surfactants were no longer soluble in the aqueous phase and thus share a 'nucleation' like behaviour similar to that of the triglyceride, which may in turn provides a decrease in initial nanoparticle size and PDI. Conversely, when the surfactant had a HLB of ~12.4 (~10 PEG repeat units), the nanoparticles were found to increase in diameter within 1 hour of production. This suggests that the chain length of PEG was too short to provide sufficient steric repulsion to stabilise the growing nuclei thus resulting in a large degree of aggregation events until a point whereby the system finds stability.

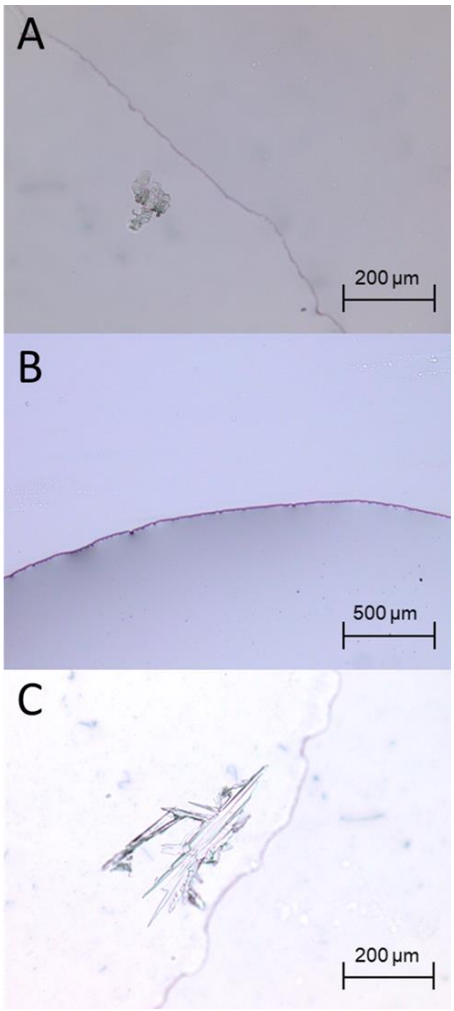

Figure 3.3- Optical microscopy images of formulations stabilised by the various Brij surfactants after 1 hour. A and C highlight the instability of the formulations containing Brij s2 and S100 respectively. Meanwhile, B shows no sign of visible aggregates when stabilised by Brij S20.

3.3.2 Nucleation behaviour of helper lipids

Nucleation of material has previously been attributed to the degree of supersaturation with greater supersaturation resulting in greater nucleation of material.[46] Furthermore, LogP has been shown as an indicator of nucleation with higher LogP resulting in a higher degree of nucleation of material and smaller and more uniform nanoparticle formulations.[149] We hypothesised that helper lipids may aid nanoparticle formation as they would nucleate alongside the other core components in a similar manner to Brij S2 due to sharing similar characteristics such as low HLB and high LogP, (Brij S2; CLogP = 6.5 , HLB = 4.9 and Lipoid S100; CLogP ~ 4.6 *, HLB ~ 1-4 *. *= Note Lipoid S100 is a natural blend of various alkyl chain length and saturation of phosphatidylcholine while is predominantly of linoleic acid at 65 %). In order to test this theory formulations were prepared in the absence of core material i.e. no triglyceride; therefore, the only components would be the surfactants Brij S20 and Lipoid S100. The two surfactants were prepared at equal mass ratios 100/0, 75/25, 50/50, 25/75 and 0/100. Particles with an average diameter and PDI of 174 nm at 0.3 were detected during a DLS measurement of Brij S20 solution indicating the presence of micelles, additionally this sample displayed a derived count rate of 488 kilo counts per second, such weak scattering also provided evidence of the sample being composed of micelles. On the other hand, as Lipoid S100 was introduced into the formulation nanoparticles were detected and grew as the proportion of Lipoid S100 was increased (Fig.3.4). At 100 % Lipoids S100 an average derived count rate of 64,607 kilo counts per second was detected. From this data it was plausible to assume that upon injection, Lipoid S100 nucleates to form nuclei which then grow to form nanoparticles.

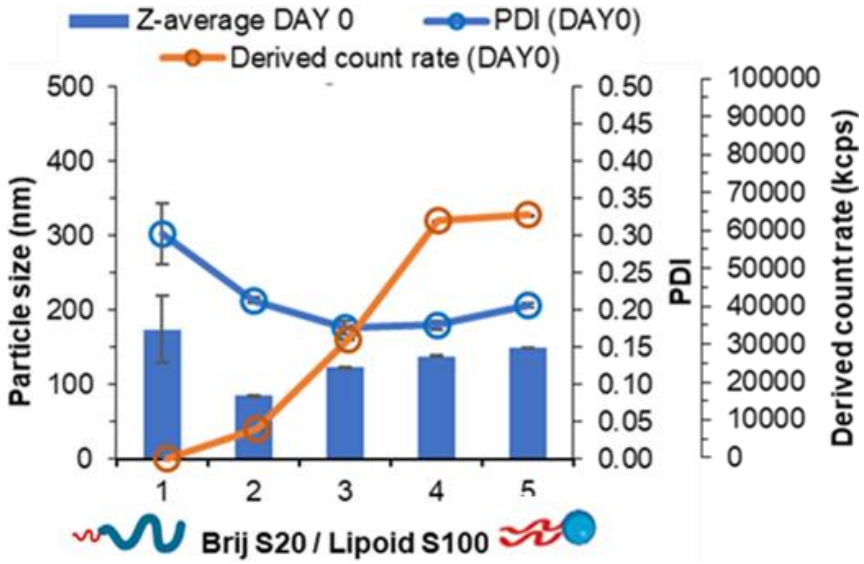

Figure 3.4- Data collected both particle size, polydispersity and derived count rate of a series of pegylated/unpegylated lipid surfactant blends with no triglyceride.

3.3.3 Investigation of pegylated vs unpegylated lipid surfactants

To further support the theory of how the nucleation behaviour of the unpegylated lipid surfactant Lipoid S100 aids nanoparticle formation. A direct comparison was made between the unpegylated lipid, Lipoid S100 and the pegylated lipid Brij S20. Both surfactants were used at an equal mol % to stabilise triglycerides of increasing LogP; tricaprin (CLogP, 13.1), trimyristin (CLogP, 19.5) and tristearin (CLogP, 25.8). Increasing the LogP of the core lipid would result in an increase the degree of supersaturation and therefore increase the degree of nucleation.[149] Therefore, it is plausible to assume increasing LogP would increase the number of nuclei and potential for aggregation events between nuclei if an inefficient or insufficient surfactant was used.[40] As a result, a comparison can be made how the properties of the different surfactants may enable more or less control.

The samples analysed by DLS (Fig.3.5-A) showing that increasing LogP from tricaprin to tristearin (Dynasan 118) while using the pegylated lipid Brij S20 resulted in poor DLS data quality due to errors in the fits to the correlation curves indicating the presence of aggregates. However, when formulated using Lipoid S100 formulations appeared to form nanoparticles and there was an increase in particle size and polydispersity with increasing LogP, Fig.3.5-B. A comparison between correlation curves for both samples of trimyristin (unpegylated and pegylated) are shown by Fig. 3.6. Overall, Lipoid S100 appeared to limit particle growth during nanoparticle formation and provided stability. All samples were analysed on day 2 once the organic solvent had evaporated to assess short term stability. Whereby the instability of the trimyristin (Dynasan 114) and tristearin (Dynasan 118) sample stabilised by Brij S20 had become more apparent due to noticeable sedimentation and precipitation. Meanwhile, trimyristin stabilised by unpegylated lipid (Lipoid S100) remained stable. Samples of both pegylated and unpegylated lipid stabilising tristearin contained visible aggregates and were therefore unsuitable for DLS measurement. Hence all four of these samples were characterised using optical microscopy Fig.3.7. This analysis clearly showed the presence of aggregates for each of the samples Brij S20/trimyristin (Fig.3.7-A), Brij S20/tristearin (Fig.3.7-C) and Lipoid S100/tristearin (Fig.3.7-D), while shows no sign of visible particle aggregates for the formulation of trimyristin stabilised by Lipoid S100 (Fig.3.7-B). This data set suggests the nucleation behaviour of unpegylated lipids such as Lipoid S100 results in greater stabilisation, which may be due to faster stabilisation of growing nuclei by limiting the number of aggregation events in comparison to pegylated lipids. Furthermore, suggests Lipoid S100 may be able to stabilise materials of higher LogP.

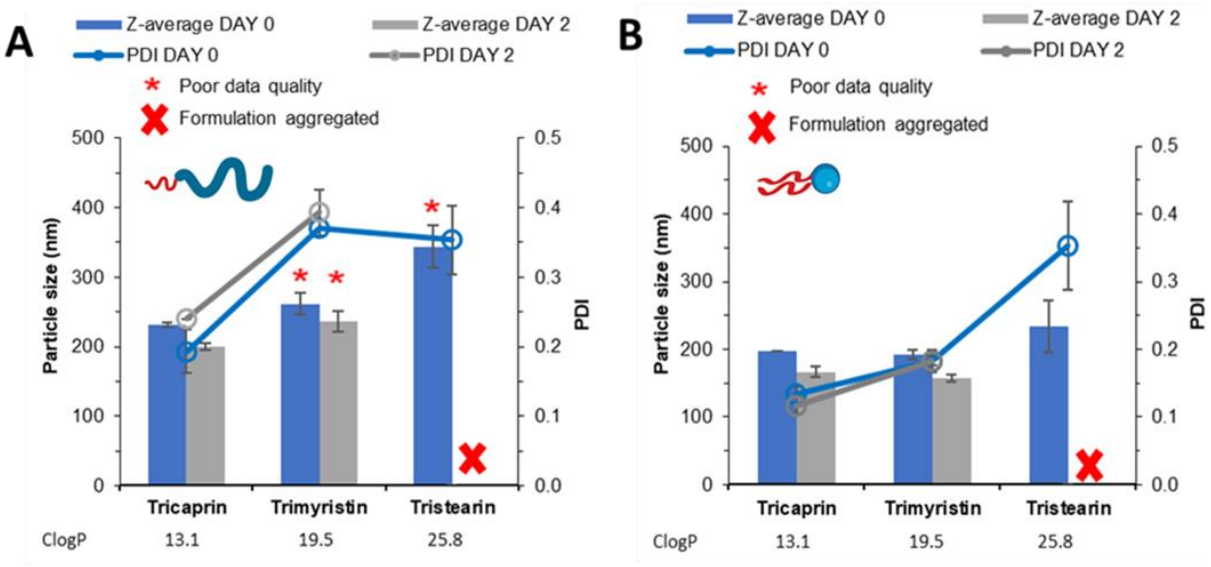

Figure 3.5- Data collected measuring both particle size and size distribution of a series of triglyceride formulations stabilised on an equal mol % by A) Pegylated lipid surfactant (Brij S20) B) Unpegylated lipid surfactamt (Lipoid S100)

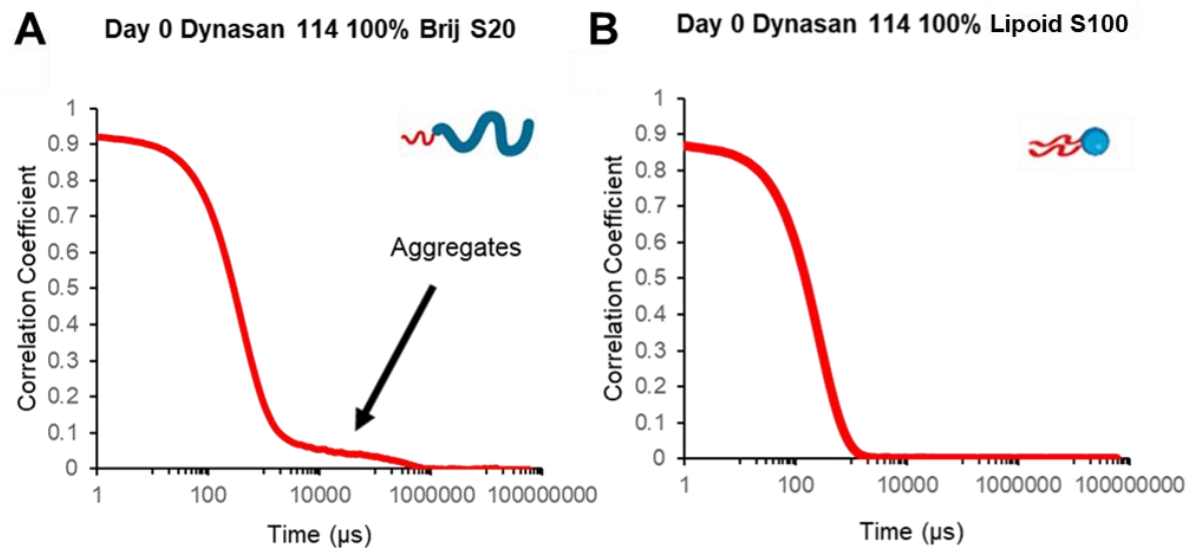

Figure 3.6- Data collected by DLS displaying size correlation curves of A) Dynasan 114 stabilised by pegylated lipid surfactant (Brij S20) showing signs of aggregation or sedimentation due to presence of hump on curve. B) Dynasan 114 stabilised by unpegylated lipid surfactant (Lipoid S100) day 0.

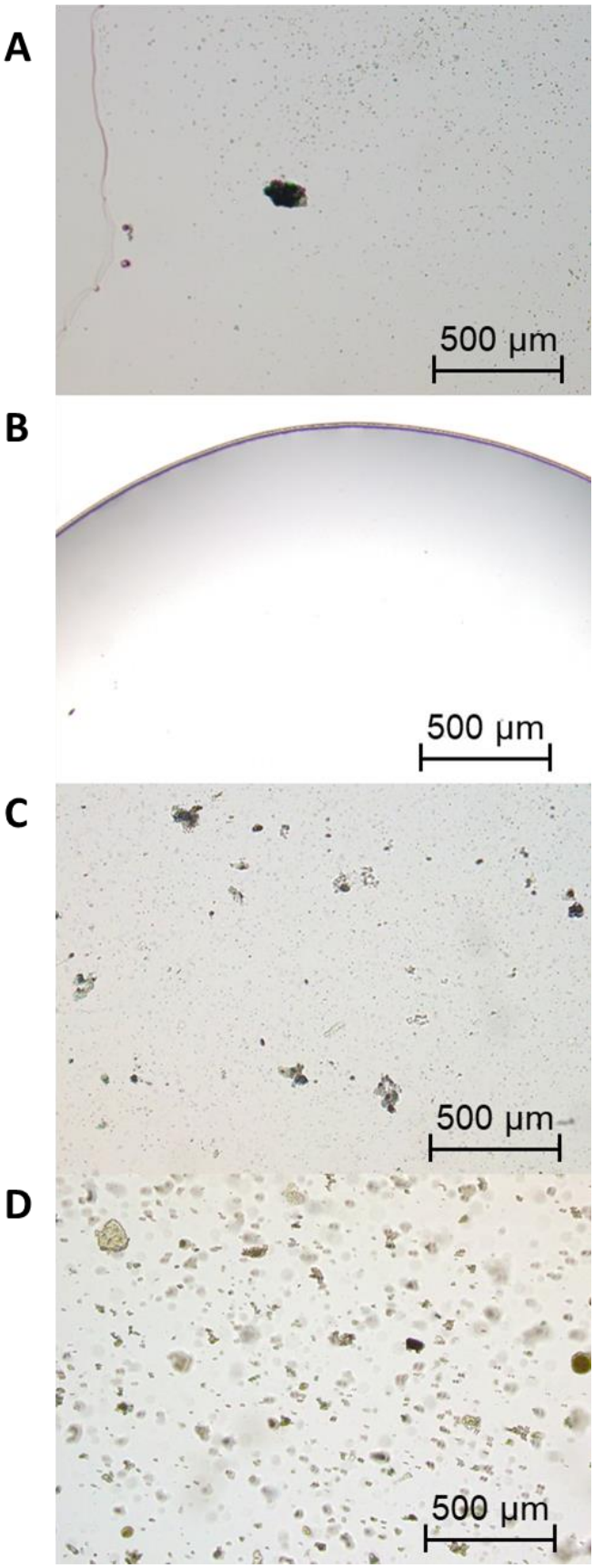

Figure 3.7- Data collected by optical microscopy on day 2 comparing samples prepared by both Brij S20 and Lipoid S100 for trimyristin and trimyristin. A) Brij S20/trimyristin, B) Lipoid S100/trimyristin, C) Brij S20/tristearin, D) Lipoid S100/tristearin.

As unpegylated lipid surfactants (Lipoid S100) limited growth of nanoparticles composed of materials at higher LogP, it was hypothesised that Lipoid S100 may also limit particle growth at higher wt % loadings of triglyceride, this would be attractive for a nanoformulation as the higher mass of lipid core in the formulation potentially offers the opportunity for also high drug loadings. Fig.3.8 displays DLS data obtained where Brij S20 and Lipoid S100 were compared on at equal mol % on their ability to form stable nanoparticle formulations at increased loading of tricaprin. The data in Fig.3.8 A shows how when the concentration of the tricaprin was doubled, tripled or quadrupled to achieve wt% of 25, 33 and 40 % tricaprin there was a sudden increase in particle size and polydispersity. There was also a loss of stability between day 0 and day 2 for formulations of 33 and 40 wt%. Meanwhile, Fig.3.8 B shows how the unpegylated lipid surfactant Lipoid S100 limited the occurrence of aggregation with a slight gradual increase in particle size and polydispersity and no loss of stability between day 0 and day 2. Overall this data set further supports how unpegylated lipid surfactants limit growth of nanoparticle formulations, and is likely due to their ability to nucleate alongside the triglyceride tricaprin and limit the number of aggregation events.

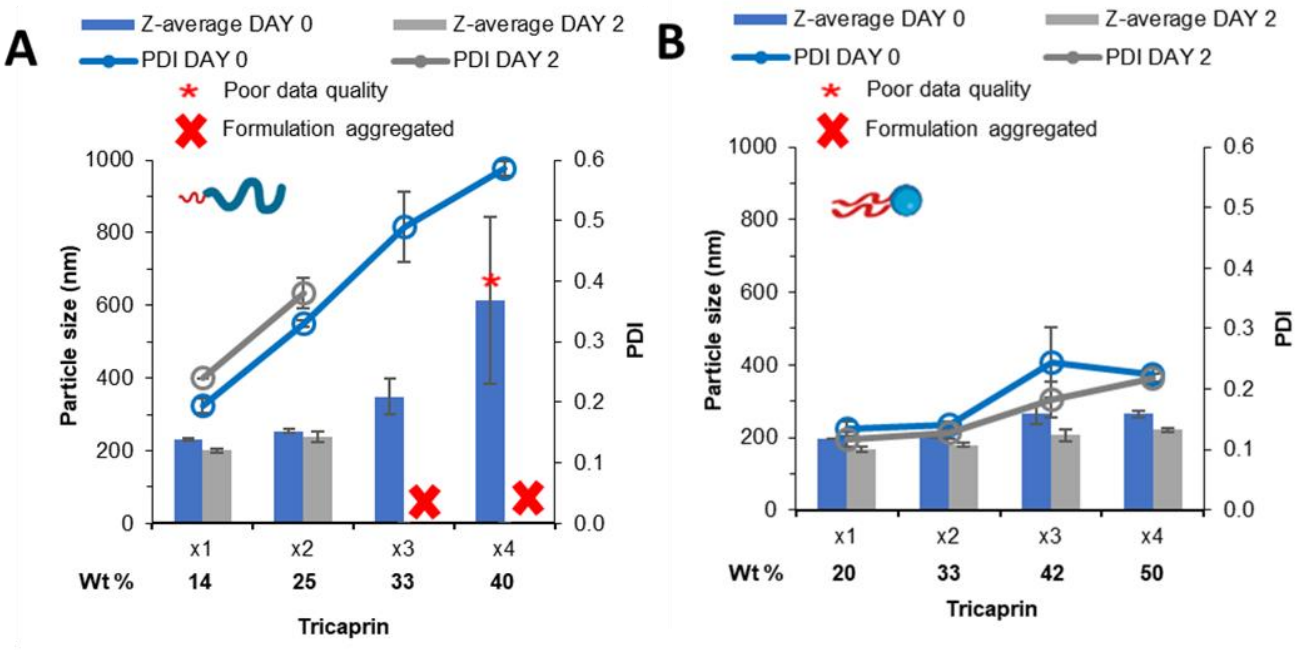

Figure 3.8- Data collected measuring both particle size and size distribution by DLS. A) Formulations of tricaprin at increasing wt % stabilised by A) Pegylated lipid surfactant Brij S20 B) Unpegylated lipid surfactant Lipoid S100

3.3.4 Investigation of pegylated/unpegylated lipid surfactant blends

Unpegylated lipids such a Lipoid S100 are zwitterionic phospholipids and have been demonstrated to produce relatively stable formulations below 25 °C,[150] consequently various lipid based nanoparticles stabilised by phospholipids have been marketed.[151] Nevertheless, formulation stability have improved by blending with pegylated lipid surfactants. Blending surfactants is a strategy that may be employed to formulate nanoparticles that offer the benefits of both the pegylated and unpegylated lipid surfactants, i.e. a blend may offer good control over the nanoparticle formation while maintaining steric stability enabling prolonged circulation time.[7] It was hypothesised that by employing the blend of lipid surfactants (pegylated and unpegylated) it may be possible to develop formulations of a higher wt % of core material. To investigate the effect of blending surfactants five formulations were prepared from 100 % pegylated surfactant to 100 % unpegylated surfactant with blends of surfactants produced at 25 % intervals. The formulation with a blend of 75 % Brij S20 (pegylated) to 25 % Lipoid S100 (unpegylated) yielded a formulation which was transparent suggesting a particularly small average particle size thus limited growth of nanoparticle formulations. Immediately, after injection obvious differences in the degrees of light scattering were noticeable due to a change in turbidity of the samples (Appendix Fig.3.1). Generally, the surfactant composition had a large influence on formulation turbidity at 14 wt %, meanwhile generally each formulation increased in turbidity as the wt % increased which made each blend indistinguishable, likely a consequence of increased particle size and/ or concentration of nanoparticles which resulted in a milky white appearance, Appendix Fig.3.1. Fig.3.9, displays the particle diameter and size distribution data obtained by DLS analysis over a 28 day period. Formulations varied in surfactant composition of pegylated and unpegylated lipid surfactant which were compared at an equal mass ratio, as well as wt % loading of tricaprin which was increased from 14 to 25, 33 and 40 wt %. Interestingly at 14 wt % tricaprin the inclusion of 25 % Lipoid S100 resulted in the nanoparticle formulation with the smallest size, which explained why this sample had the lowest turbidity (smaller particles have much weaker light scattering). When the amount of Lipoid S100 was increased in the formulation there was a slight increase in nanoparticle size. This was attributed to Lipoid S100 potentially including itself within the core of nanoparticles at 14 wt%. Nevertheless, the following observations were made; particle size and size distribution generally decreased with increasing unpegylated lipid surfactant within the surfactant ratio, as well as a generally increase in particle size and size distribution with increasing wt % of tricaprin (Fig.3.9). Although, over a prolonged period of 28 days the formulations at 100 % Lipoid S100 were found to be unstable due to the occurrence of phase separation in a similar manner to 100 % Brij S20 and 75 % Brij S20/ 25 % Lipoid S100 formulations at higher wt %, This could be seen by eye as visible particles and also by optical microscopy as non-spherical particles (Fig.3.10). Zeta potential measurements on

the samples revealed a charge less than ± 10 mV for each surfactant blend, Fig.3.11. These experiments showed the benefit of the use of blends of surfactants; formulations containing a high proportion of unpegylated lipid such as 50 % pegylated/50 % unpegylated or 25 % /75 % unpegylated were able to maintain stability likely a result of the steric stability provided by the Brij S20.

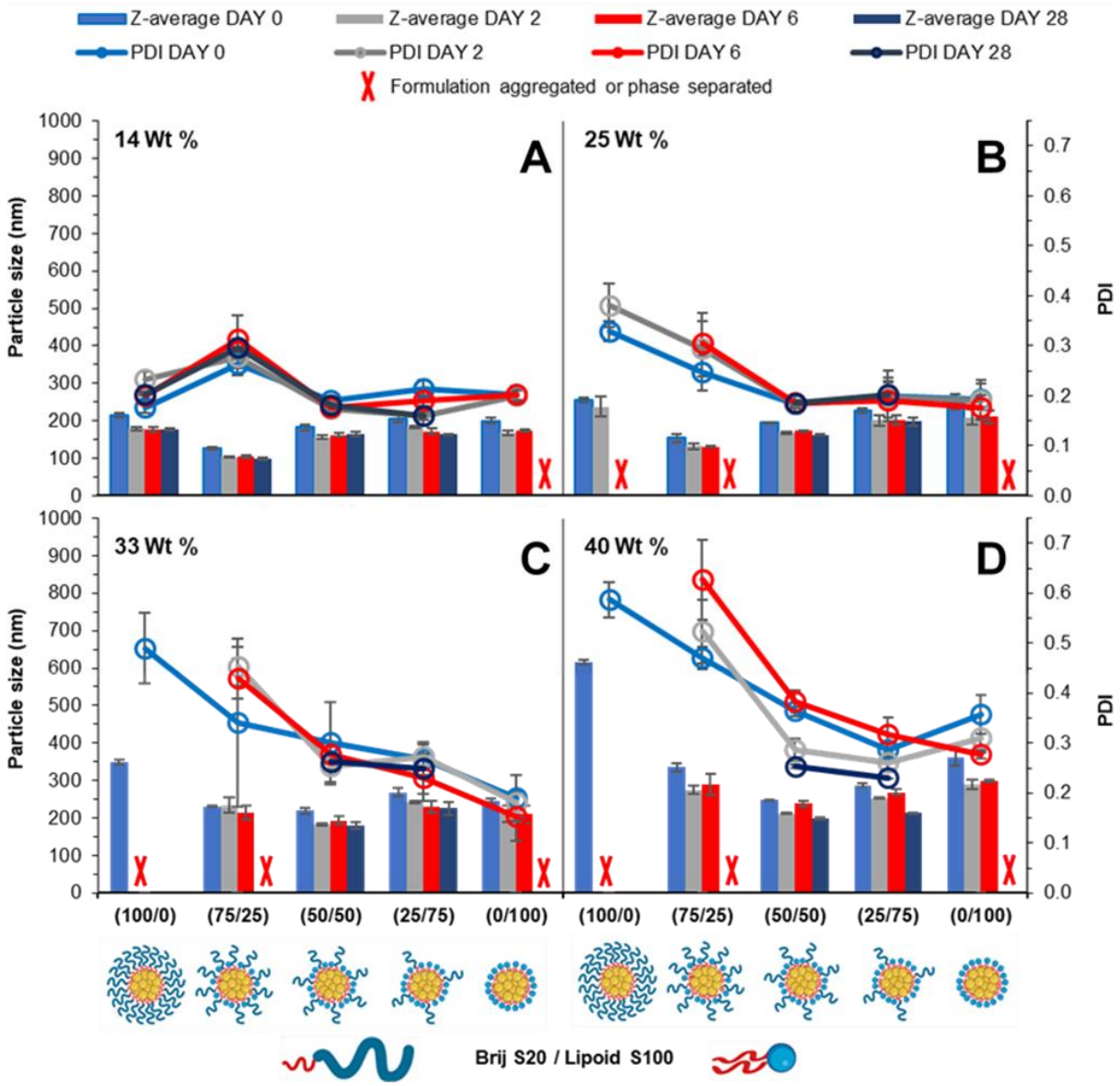

Figure 3.9- Particle size and size distribution obtained by DLS over a 28-day period. Formulations varied in pegylated/unpegylated lipid surfactant blends on a mass ratio. Data also examines the effect of increasing wt % of tricaprin 14 (A), 25 (B), 33 (C) and 40 (D) wt%. Samples were prepared in triplicate and error bars calculated on standard deviation between sample measurements. Samples were stored at 22 °C.

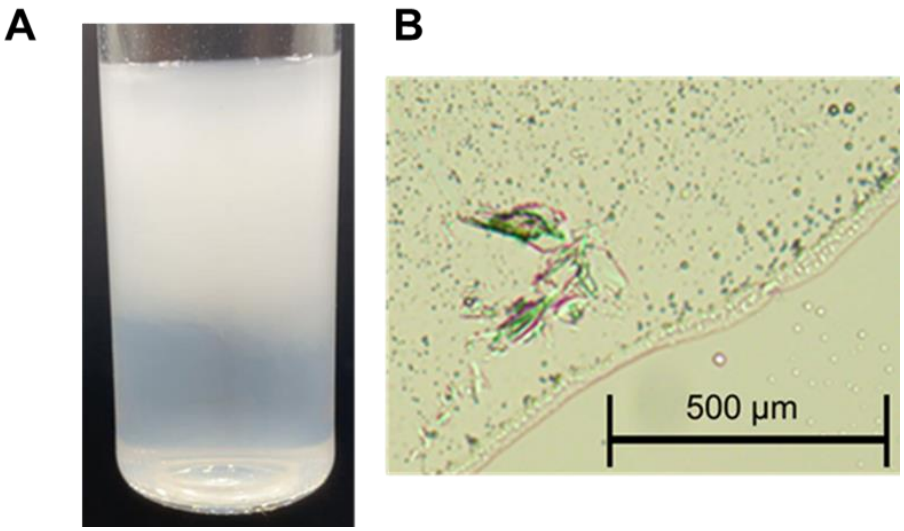

Figure 3.10- Displays A) Photo of 100 % Brij S20 33 wt % tricaprin formulation on day 6 which has experienced phase separation. B) Optical microscopy image of the top phase indicating the presence of aggregates.

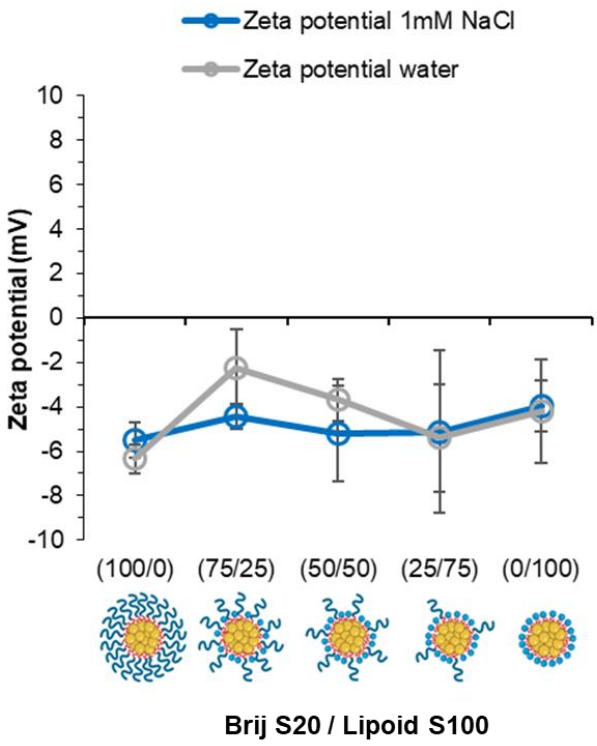

Figure 3.11- Zeta potential measurements on day 2 of formulation of tricaprin formulations measured at 14 wt% for each surfactant composition of Brij S20 and Lipoid S100.

Cryo-SEM was also employed to visualise the particles of the tricaprin nanoparticles at 14 wt% stabilised by 50 % Brij S20 50 % Lipoid S100. Measurement of the nanoparticles from the cryo-SEM shown in Fig.3.12 revealed an average particle diameter of 131 nm Fig.3.12 B, thus in agreement with

data obtained by DLS (157 nm). Fig.3.12 C displays an overlay comparing the data obtained from the cryo-SEM image which has been normalised for comparison with the size distribution data obtained by DLS which shows both cryo-SEM and DLS had a slight deviation. This may be due to the effects of solvation sphere that is included in the DLS diameter measurement, or the influence of a low number of larger particles not included in the smaller sample size of the SEM measurement.

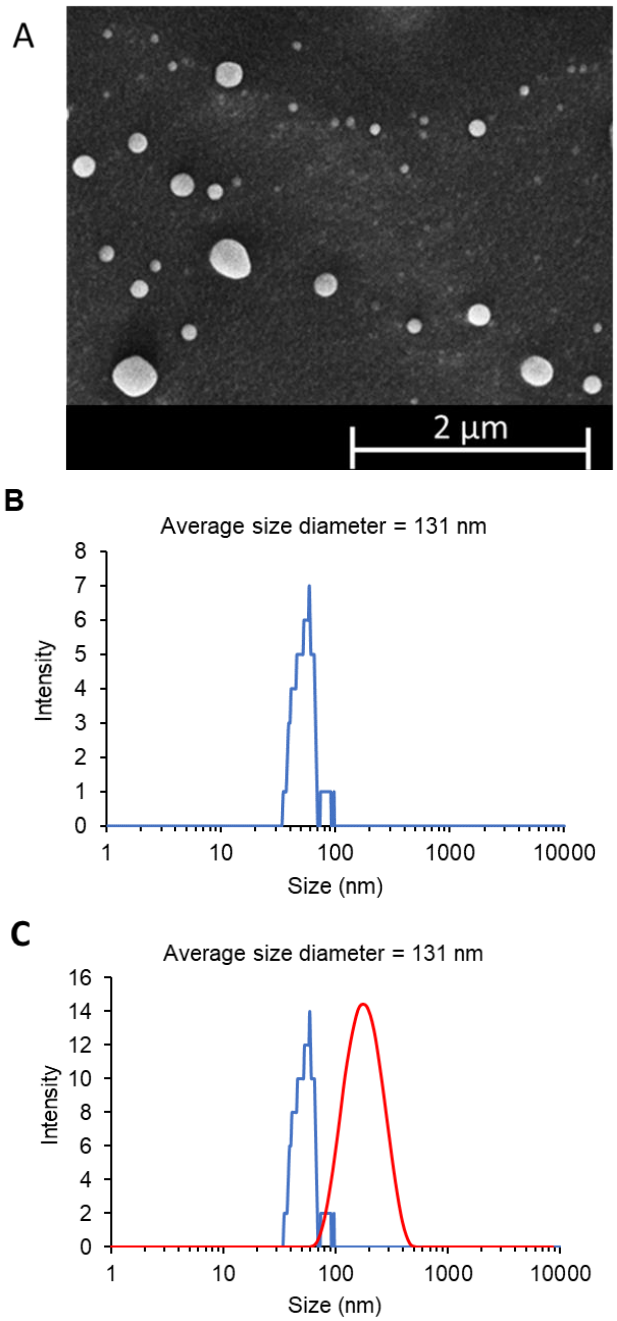

Figure 3.12- A) Cryo-SEM image of 100 % tricaprin nanoparticles at 14 wt % stabilised by 50 % Brij S20 50 % Lipoid S100. B) Size distribution graph using data calculated by Image J. A sample size of 98 particles and a bin size of 1 was used. C) An overlay of a normalised size distribution of the data obtained from the cryo-SEM image with the size distribution obtained by DLS.

The thermal properties of the various individual materials were analysed before formulations with various surfactant composition were investigated. Tricaprin had a melting point of ~ 32 °C Brij S20 showed a broad melting point of ~46 °C and Lipoid S100 had a melting point of ~160 °C (Appendix Fig. 3.2). The 14 wt % lipid formulations with varying surfactant compositions were then analysed by DSC. Fig.3.13 displays an overlay of the thermograms for each of the nanoparticle formulations and how the different transitions differ according to the surfactant composition. The endotherms occurring at approximately 28 °C correspond to tricaprin and, thus the core crystallinity. Interestingly, the core appeared virtually amorphous at a surfactant composition of 100% Lipoid S100, meanwhile is most intense when a blend of Brij S20 and Lipoid S100 was used.

As expected, the Lipoid S100 endotherm region peak intensity broadens and becomes less intense as the percentage of Lipoid S100 is decreased, meanwhile the endotherm for the alternative Brij S20 becomes sharper and increases in intensity. Smaller and broader melting endotherms suggest a reduction in crystallinity likely due to disruption of one surfactant by another. Fig.3.14 displays firstly how the crystallinity of tricaprin at 14 wt % is reduced relative to bulk tricaprin when nanoparticles are produced using either surfactant Brij S20 or Lipoid S100. This is likely the consequence of disruption of material crystallinity due to nanoformulation compared to a bulk material. Furthermore, Lipoid S100 appears to disrupt the crystallinity of tricaprin more than Brij S20. This may be a consequence of the two alkyl chains of the phospholipid causing greater disruption of the tricaprin within the core rather than the single alkyl chain of Brij S20. Alternatively, as Lipoid S100 has been proven to form nanoparticles of itself some Lipoid S100 may have blended within the core alongside tricaprin resulting in greater disruption, thus explaining the changes in the crystallinity in the different components of the formulations is shown in Fig.3.14.

Interestingly, as the surfactants were blended together the overall crystallinity of the tricaprin increased dramatically, Fig. 3.14. Bunjes *et al*. have previously suggested upon establishing a uniform surfactant layer, interactions between the surfactants are strong and the fluidity of the membrane layer is decreased. As a result, the crystalline tendencies of the core such as polymorphic transitions are reduced.[152] Therefore, it is possible that by blending the pegylated surfactant with the unpegylated lipid surfactant the phospholipid membrane is disrupted resulting in increased fluidity, and an overall increase in crystallinity due to less interactions between the hydrophobic tails of the surfactants and the core lipid. Nevertheless, further investigation would be required to understand the precise cause of this difference.

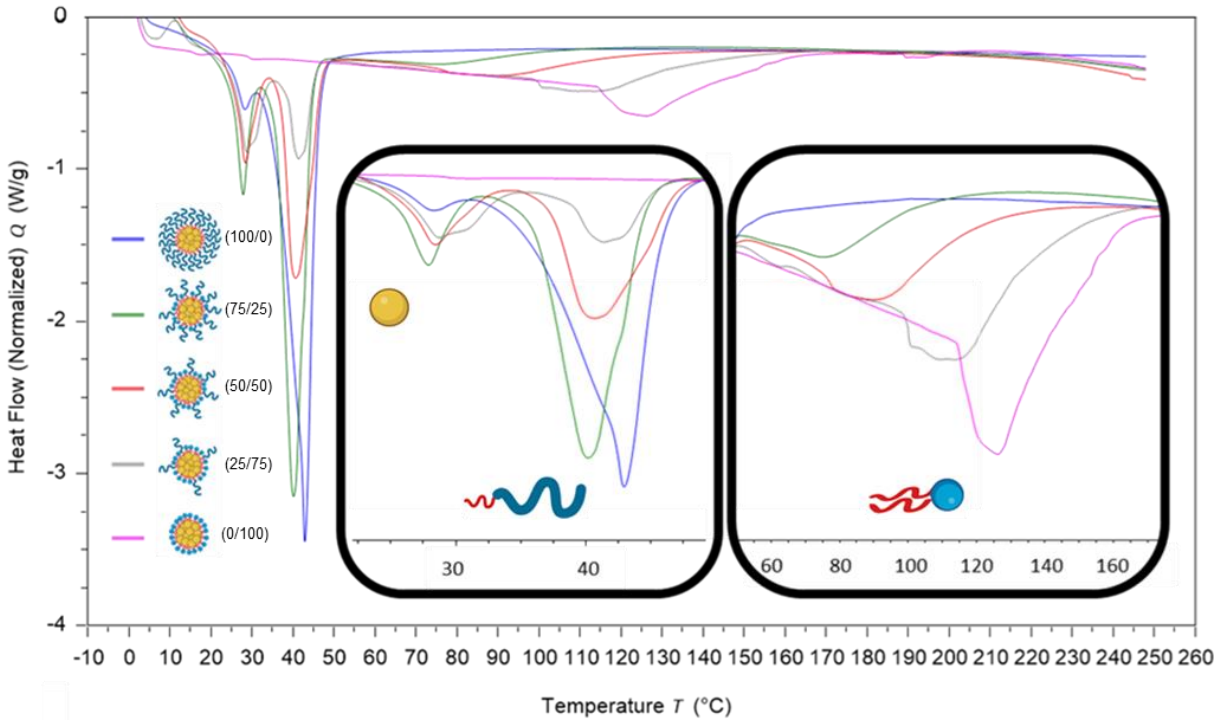

Figure 3.13- Overlay of DSC traces for each of the nanoparticle formulations at 14 wt % with a surfactant composition ratio (Brij S20/Lipoid S100). The two inserts show the regions for the melting of tricaprin and Lipoid S100. 22.5-50 °C, indicates the effect of surfactant composition on the crystallinity of the core (tricaprin) and pegylated lipid surfactant. 50-170 °C, indicates the effect of surfactant composition on the crystallinity of Lipoid S100.

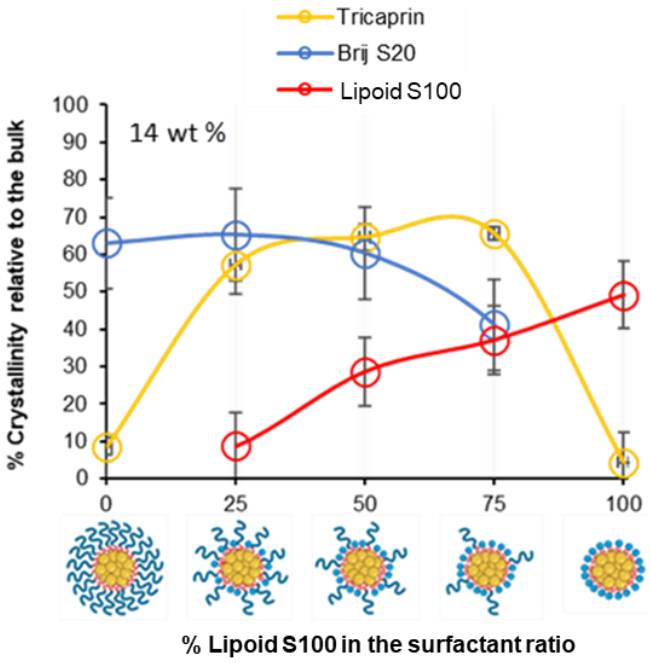

Figure 3.14- Graph showing the relationship between surfactant composition and crystallinity of tricaprin within the core at 14 wt %. Also informs of surfactant crystallinity.

Thermo-analysis was also performed on various formulations at higher wt % of 40 % tricaprin, to see how the lipid content of the formulation also influenced the crystallinity of the components (Fig.3.15). Only formulations containing at least 50 % of Lipoid S100 are shown as the formulations with lower amounts of Lipoid S100 did not display long term stability (Fig. 3.9-D). For the formulations tested, an increase in tricparin peak intensity was observed, meanwhile the surfactant peak intensity decreased and peaks underwent broadening. The peak for Lipoid S100 also appears to shift to a lower melting temperature. Overall, these changes suggested an increase in core crystallinity with increasing wt % from 14 to 40 %. In addition, at 40 wt % tricaprin was found to possess two peaks when stabilised by 100 % Lipoid S100 with the first at ~17 °C and the second at ~ 30 °C, Fig.3.15. Thus, suggesting the presence of two distinctly different crystal forms of tricaprin with the earlier being liquid at room temperature and the latter being solid. Therefore, the overall structure of the nanoparticle would adopt an NLC structure rather than a SLN.

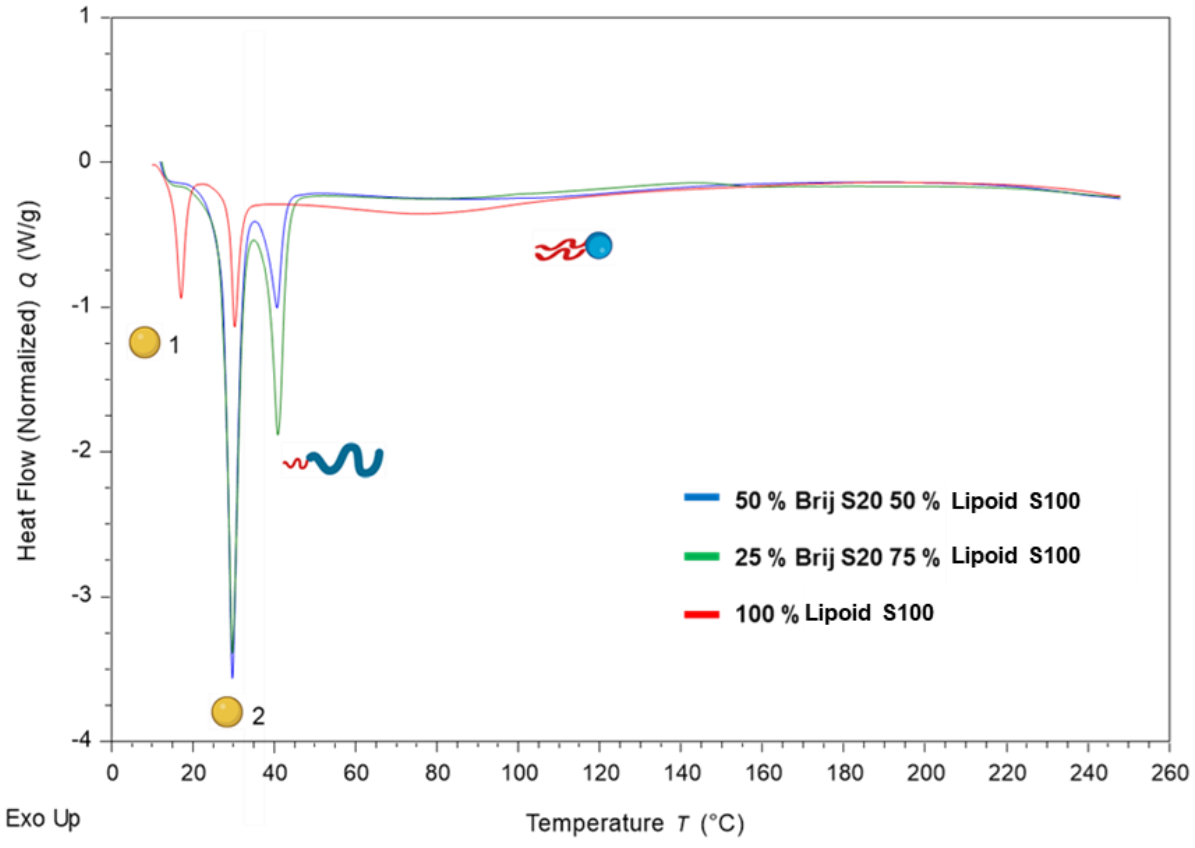

Figure 3.15- Displays an overlay of thermograms for each surfactant blend at 40 wt % tricaprin

The crystallinity values for individual components of the various blends relative to their bulk materials is shown in Fig.3.16. Overall, as the wt % of core materials (tricaprin) was increased, the crystallinity of surfactants decreased while the crystallinity of tricaprin increased. For example, at 50 % Brij S20 50 % Lipoid S100 there was an average increase in component crystallinity relative to bulk material for tricaprin of 9.9 % from 64.6 % to 74.5 %. Meanwhile, Brij S20 decreased on average by 14.5 % from 60.3 % to 45.8 % and Lipoid S100 decreased by 19.3 % from 28.5% to 9.2 %. The increase in core crystallinity of tricaprin was likely caused by a decrease in the overall disruption caused by the alkyl chains entering the core of the nanoparticle as the size of the core and/or number of nanoparticles is increased.

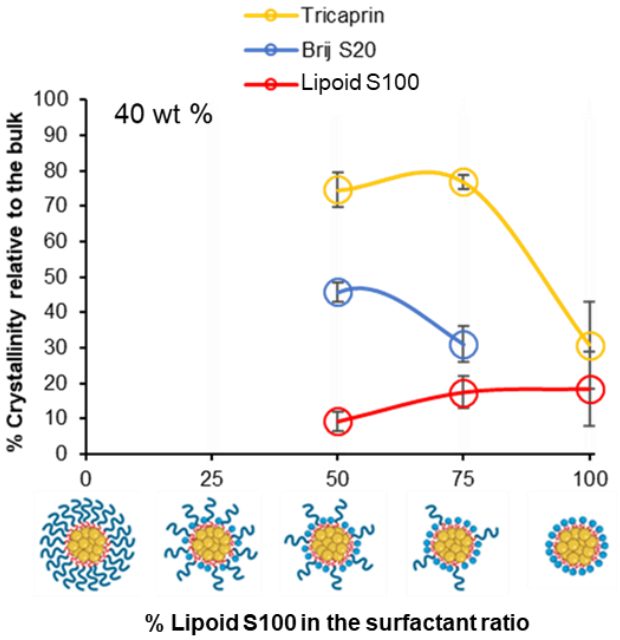

Figure 3.16- Graph showing the relationship between surfactant composition and relative crystallinity of tricaprin within the core at 40 wt%

3.3.5 Incorporation of prodrug into pegylated/unpegylated lipid surfactant blends

We have previously shown that the overall increase in core crystallinity may be overcome by the introduction of drug/prodrug into the core.[149] Given the stability of the 40 wt % lipid formulations with the surfactant ratios of 50% Brij S20/50 % Lipoid S100 and 25 % BrijS20/75 % Lipoid S100, these samples were identified as best candidates for formulating with a prodrug. Dodecyl prodrug/drug analogue previously developed in chapter 2 was employed in a blend of either 50 % tricaprin 50 % dodecyl prodrug or 25 % tricaprin 75 % dodecyl prodrug, with these two components making up to 40 wt % of the complete formulation. Zeta potential measurements revealed mean particle charge of less than ± 10 mV, thus suggesting the formulations were stabilised solely by steric stabilisation, Fig.3.17.

Fig.3.18 displays the particle size and size distribution data obtained by DLS analysis over a 28-day period. Each blend produced a particle formulation that was uniform in size and PDI with average particle size ranging between ~200-300 nm. The corresponding size distribution traces and correlation curves are also displayed by Fig.3.19. From the correlation curves it is apparent that there were some slight variations in size distribution graphs as the formulation of 75 % dodecyl prodrug 25 % tricaprin stabilised by 50 % Brij S20 50 % Lipoid S100 (Fig.3.19 – C1) appeared to be multimodal. Although, generally the size distribution graphs and correlation coefficient curves were deemed to be of good quality and reliable data.

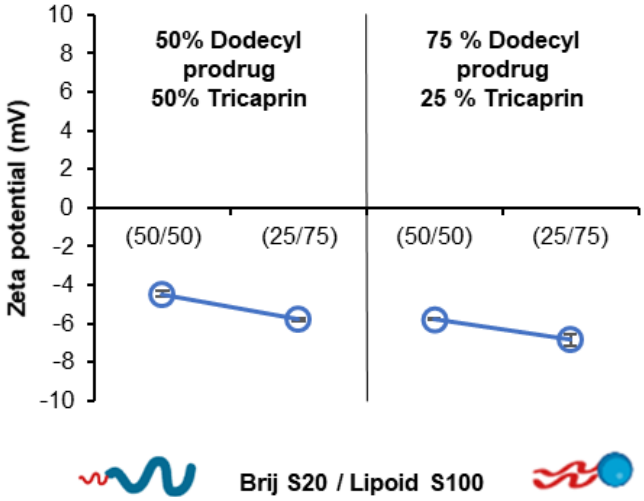

Figure 3.17- Data collected measuring zeta potential on day 2 of formulation of dodecyl prodrug/ tricaprin blend formulations measured at 40 wt % for each surfactant composition of Brij S20 and Lipoid S100

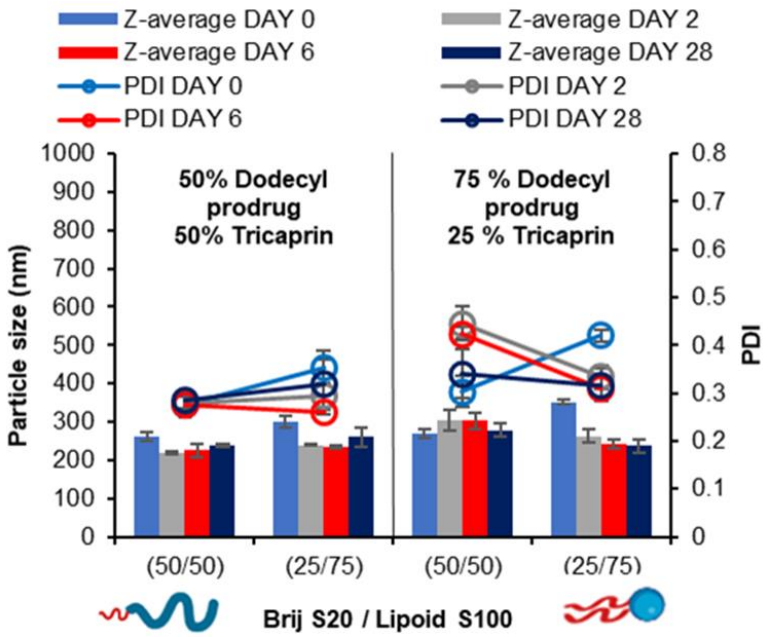

Figure 3.18- Particle size and size distribution obtained by DLS over a 28-day period. Formulations at 40 wt % core yet varied in core composition at both 50 % and 75 % dodecyl prodrug loading while also varied in surfactant composition 50% Brij S20/ 50 % Lipoid S100 and 75 % Brij S20/ 25 % Lipoid S100. Samples were prepared at in triplicate and error bars calculated on standard deviation between sample measurements. Samples were stored at 22 °C.

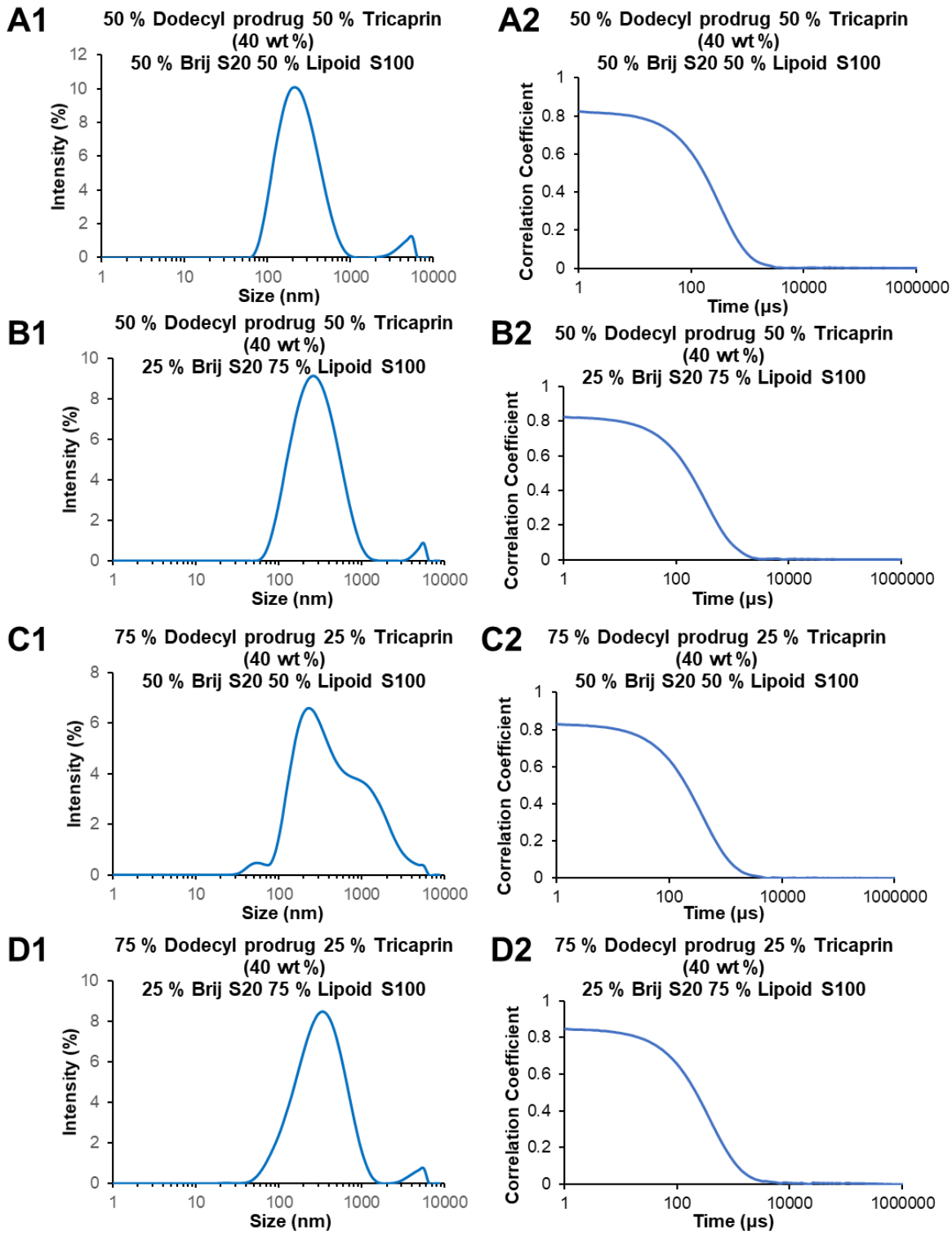

Figure 3.19- Size distribution graph and correlation coefficient curves corresponding to each of the formulations in Fig 3.18. Size distribution graphs were created by taking an average of the value for each of the triplicate measurements. Dodecyl prodrug was formulated at 50 % Dodecyl prodrug loading for A and B, at a surfactant blend of 50 % pegylated lipid 50 % unpegylated lipid surfactant (A); and 25 % pegylated lipid 75 % unpegylated lipid surfactant (B). At 75 % Dodecyl prodrug loading for C and D at a surfactant blend of 50 % pegylated lipid 50 % unpegylated lipid surfactant (C); and 75 % pegylated lipid 25 % unpegylated lipid surfactant (D).

Blending of core materials has previously been shown to influence the core crystallinity,[149] therefore DSC analysis was carried out to determine the impact of blending dodecyl prodrug alongside tricaprin. Fig.3.20, displays an overlay of DSC traces for formulations of 50 % dodecyl prodrug loading each at a surfactant composition of 50 % Brij S20/50 % Lipoid S100. Immediately, it is noticeable that tricaprin only possesses a singular melting peak which may suggest that the entirety of tricaprin is of a solid physical form. It was calculated the crystallinity of tricaprin reduced by ~21% from 74.9 % to 53.9 % crystallinity compared to the equivalent formulation at 100 % tricaprin. As a result, it can be deemed by blending the tricaprin with dodecyl prodrug the core crystallinity may be controlled even at an elevated core wt % of 40 %. Unfortunately, it was not possible to obtain an accurate value for the crystallinity of dodecyl prodrug could not be obtained due to overlapping of the dodecyl prodrug and Lipoid S100 peaks. Nevertheless, this study demonstrates how loading dodecyl prodrug at 50 % of the core mass at a surfactant composition of 50 % pegylated 50 % unpegylated lipid surfactant blend resulted in disruption of the crystallinity of the core due to a decrease in tricaprin relative crystallinity.

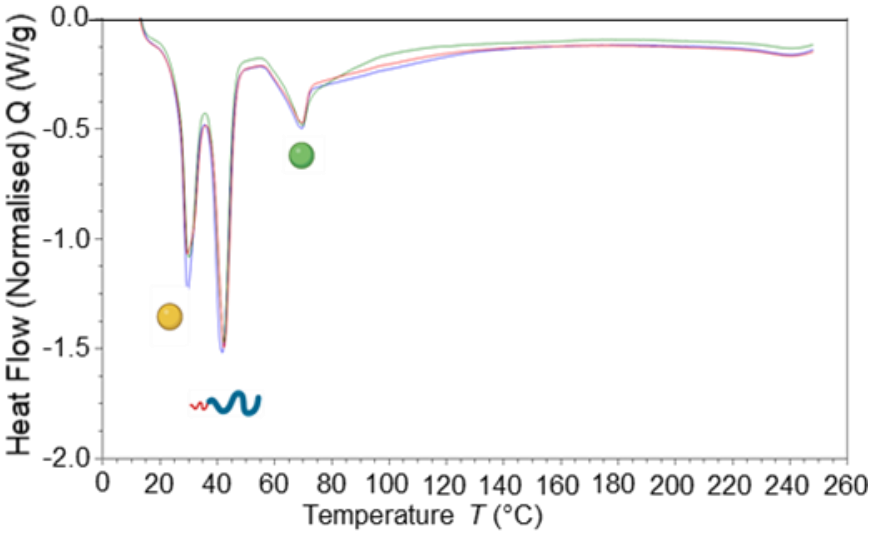

Figure 3.20- Displays an overlay of DSC traces for nanoparticle formulations prepared in triplicate with a core composition of 50 % Dodecyl prodrug/drug analogue and 50 % tricaprin while a surfactant composition of 50 % Brij S20 50 % Lipoid S100.

3.4. Conclusions

In this study the properties of lipid surfactants have been studied and suggested that their nucleation behaviour aids nanoparticle formation due to stabilising growing nuclei. In doing so, offers stabilisation earlier to growing nuclei/nanoparticles thus limiting nanoparticle size and size distribution of materials at elevated LogP or wt%. Unpegylated lipid surfactants have been investigated in blends with a pegylated lipid surfactant Brij S20 resulting in benefits such as enhanced stability at higher wt % of core material, thus enabling higher drug loading formulations. In addition, blends of prodrug and lipid at the elevated core wt % have been shown to disrupt core crystallinity.

Overall, this work provides greater understanding of how the properties of lipid materials determine behaviour in specific environments and translate into a beneficial attribute during application of formulation development of lipid nanoparticles. For example, the investigation of different blends across various ratios enabled the conclusion that the hydrophobic nature of the unpegylated lipid surfactant which results in its nucleation upon nanoprecipitation enabled rapid stabilisation of the growing nuclei at even much higher drug loadings and thus limited growth by aggregation, meanwhile the steric stabilisation of the pegylated lipid surfactant provided the formulation with greater long term colloidal stability. In literature there was a clear lack of understanding for the role of unpegylated lipid surfactants other than aiding in nanoparticle formation and how this was achieved, as a result this work may be used as a guide to better inform of their role and how this understanding may be applied in order to tune and optimise nanoparticle formulations in the future.

3.4. Future work

In the future it would be interesting to broaden the understanding further by exploring a wide variety of unpegylated lipid surfactants other than Lipoid S100 for example unpegylated lipid surfactants that possess a net charge such as DOTAP-Cl which may nucleate in a similar manner yet provide electrostatic stabilisation and thus greater control over nanoparticle formulation by flash nanoprecipitation. Likewise, it is also plausible to investigate other forms of pegylated lipid surfactants such as those shown in Fig.1.33. e.g. DSPE-MPEG-2K. One aspect we identified is pegylated lipid surfactants with lower HLB display nucleation behaviour, although those with a short PEG chain may not provide sufficient steric stabilisation. As a result, it is plausible to investigate other pegylated lipid surfactants which are of lower HLB yet possess a PEG chain which is efficient enough to provide sufficient steric stabilisation upon formulation. DSPE-MPEG-2K may be a potential example as DSPE-MPEG-2K is a pegylated phospholipid which is

composed of two alkyl chains conjugated to a 2K PEG chain. It may be that the additional alkyl chain may worsen the solubility of the pegylated lipid surfactant resulting in nucleation behaviour if introduced *via* the organic solvent.

3.7. Experimental

Materials

Dodecyl prodrug/drug analogue was used as synthesised by previous publication. Brij S10, Brij S20, Brij S100, tetrahydrofuran and deuterated solvents ($CDCl_3$ and D_2O) were all purchased from Sigma Aldrich. Each were used as received apart from $CDCl_3$ where 0.1 % tetramethylsilane was added. Lipoid S100 was purchased from Lipoid and used as received. Tricaprin was purchased from Tokyo chemical industry and used as received. Dynasan 114 (trimyrisitn) and Dynasan 118 (tristearin) was kindly gifted from IOI Oleochemical, Hamburg. Lamivudine was purchased from Top Well Medipharma Group.

Methods

Preparation of lipid nanoparticle formulations varying in pegylated lipid and unpegylated lipid Lipoid S100

Method adopted for nanoparticle formulation was nanoprecipitation. For the aqueous phase, the surfactant Brij S20 was dissolved to prepare a 1000 ml stock solution in distilled water (1 mg/ml) and left overnight at 21 degrees Celsius under mechanical stirring (300 rpm). Portions of the stock solution were taken and potentially diluted further with distilled water, compositions shown by Table 3.1.

For the organic phase stock solutions of tricaprin (4 mg/mL) and Lipoid S100 (24 mg/mL) were prepared in tetrahydrofuran (THF). Compositions are shown by Table 3.2. The organic phase was charged dropwise into the vortex of the aqueous phase contained in a 40 mL vial while mechanically stirring (800 rpm). To ensure consistency in time of injection the shot was charged by removing the plunger of a clamped syringe resulting in a steady flow through the hypodermic needle. The combined mixture was left stirring to allow evaporation of tetrahydrofuran over 2 days at a room temperature (~21 °C) in a fume cupboard with an average air velocity of 0.35 m/s. Samples were then stored at 21 °C.

Table 3.1- Aqueous phase composition depending on surfactant blend.

Surfactant composition	Volume Brij S20 stock solution (mL)	Volume distilled water (mL)	Total volume aqueous phase (mL)
100 % Brij S20	24	0	24
75 % Brij S20 25 % Lipoid S100	18	6	24
50 % Brij S20 50 % Lipoid S100	12	12	24
25 % Brij S20 75 % Lipoid S100	6	18	24
100 % Lipoid S100	0	24	24

Table 3.2- Organic phase composition depending on surfactant blend.

Surfactant composition	Volume tricaprin stock solution (mL)	Volume Lipoid S100 stock solution (mL)	Volume neat THF (mL)	Total volume organic phase injectable shot (mL)
100 % Brij S20	1	0	1	2
75 % Brij S20 25 % Lipoid S100	1	0.25	0.75	2
50 % Brij S20 50 % Lipoid S100	1	0.5	0.5	2
25 % Brij S20 75 % Lipoid S100	1	0.75	0.25	2
100 % Lipoid S100	1	1	0	2

Preparation of lipid nanoparticle formulations varying in pegylated lipid and unpegylated lipid Lipoid S100 at elevated wt %

Formulations prepared in the same way as at 14 wt% although the concentration of the tricaprin stock solution was increased i.e. (25 wt %, 8 mg/mL; 33 wt%, 12 mg/mL; 40 wt %, 16 mg/mL)

Preparation of lipid nanoparticle formulations varying in pegylated lipid and unpegylated lipid Lipoid S100 at elevated wt % varying in dodecyl drug analogue loading

General preparation method the same although composition of organic phase adjusted see Table 5 for example of blends of tricaprin and dodecyl drug analogue at 40 wt %. Stock solution concentrations; tricaprin (16 mg/mL) and dodecyl drug analogue (16 mg/mL). (Table 3.3.)

Table 3.3- Organic phase composition depending on blends of tricaprin, dodecyl drug analogue as well as surfactant blends

Core composition	Surfactant composition	Volume tricaprin stock solution (mL)	Volume dodecyl drug analogue stock solution (mL)	Volume Lipoid S100 stock solution (mL)	Volume neat THF (mL)	Total volume organic phase injectable shot (mL)
50 % tricaprin 50 % dodecyl drug analogue	50 % Brij S20 50 % Lipoid S100	0.5	0.5	0.5	0.5	2
50 % tricaprin 50 % dodecyl drug analogue	25 % Brij S20 75 % Lipoid S100	0.5	0.5	0.75	0.25	2
25 % tricaprin 75 % dodecyl drug analogue	50 % Brij S20 50 % Lipoid S100	0.25	0.75	0.5	0.5	2
25 % tricaprin 75 % dodecyl drug analogue	25 % Brij S20 75 % Lipoid S100	0.25	0.75	0.75	0.25	2

Analytical techniques

Dynamic light scattering (DLS) and Zeta potential

Samples were analysed by DLS using The Malvern ZetaSizer Nano S DLS obtain a Z-average and size distribution (PDI) and zeta potential of nanoparticle dispersion. 2 ml of each sample was measured in standard 3 ml fluorimeter cuvettes with a pathlength of 10 mm. All measurements were carried out at 25 °C with a fixed backscattering angle of 173° using automated setting. Each sample was measured once although formulations were done in triplicate. Zeta potential was also measured using Malvern ZetaSizer Nano S. Samples were measured using automated settings and samples were measured in triplicate in a Malvern zetasizer nano series disposable folded capillary cell. All measurements were carried out at 25 °C.

Differential scanning calorimetry (DSC)

Nanoparticle formulations were dried down in a glass vial before weighing out into Aluminium pans. Performed by a TA DSC25. The freeze-dried nanoparticle formulations were equilibrated at 10 °C before heating to 100 °C at a rate of 10 °C/minute. The bulk samples were heated to 100 °C at a rate of 10 °C/minute before being cooled back down to 0 °C at a rate of 5 °C/minute and again heating back up to 100 °C at a rate of 10 °C/minute. Measurements were carried out in triplicate.

Cryogenic scanning electron microscopy (cryo-SEM)

Specimens prepared by freezing a small volume of sample between two brass rivets, which are plunged into slushed liquid nitrogen. Rivets transferred to a brass loading shuttle under liquid nitrogen and transferred under a nitrogen atmosphere to a preparation stage cooled to -120 °C. Anti-contaminator in preparation stage run at -190 °C. Fracture surface created in frozen specimen by pushing-off the upper rivet from the one held in the shuttle (using a liquid nitrogen cooled knife). Fracture surface coated with Pt in the preparation chamber, to make it conductive and specimen transferred to a cooled stage in the FIB/SEM (at -160 °C, with an anti-contaminator held at -190°C). Specimens photographed using an in-chamber secondary electron detector Everart Thornley using either 1.5 or 10 KeV and a beam current of 15 pA

3.8. Appendix

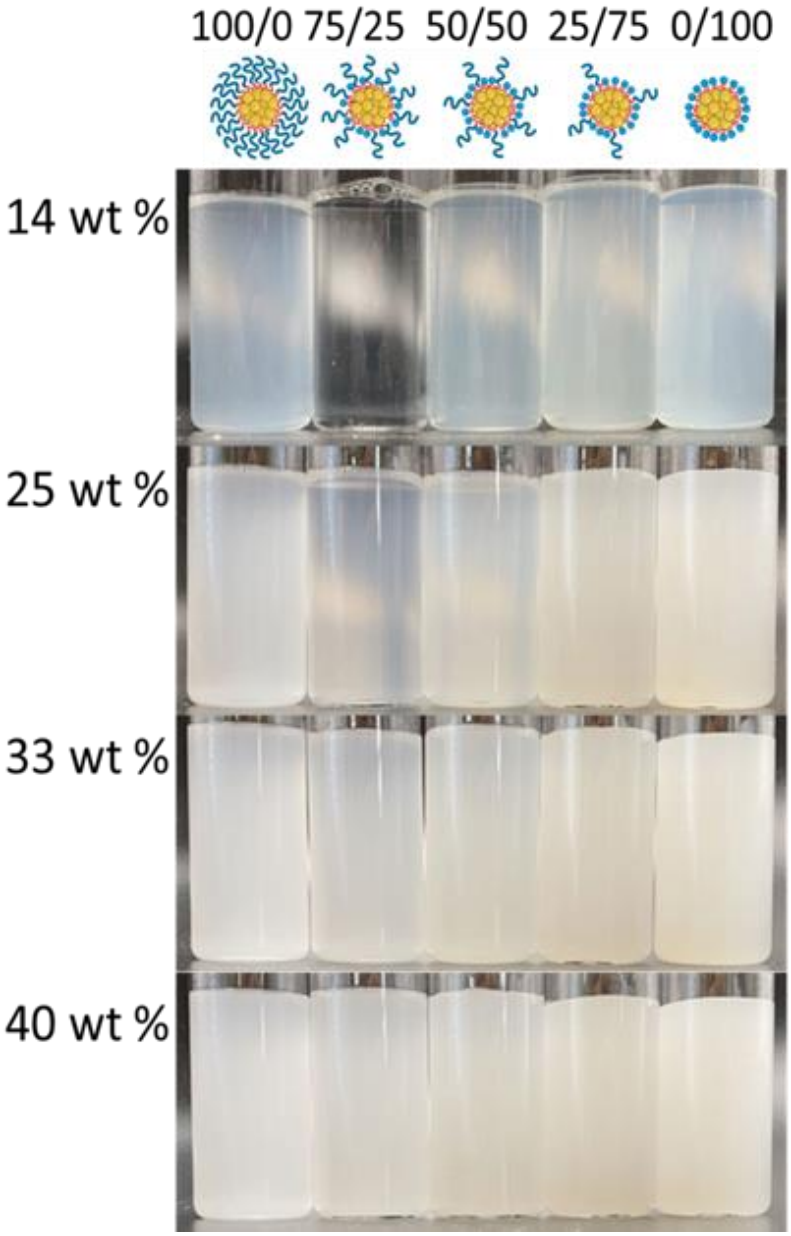

Appendix Figure 3.1- Displays visual changes in the appearance of formulations. From left to right displays variation between surfactant composition within the formulation, while from top to bottom displays variation between wt % of tricaprin in formulation (% dry mass of tricaprin in formulation). Overall images display how surfactant composition and wt % may influence formulation turbidity as a result of varying degrees of light scattering caused by means of particle size and concentration of particles.

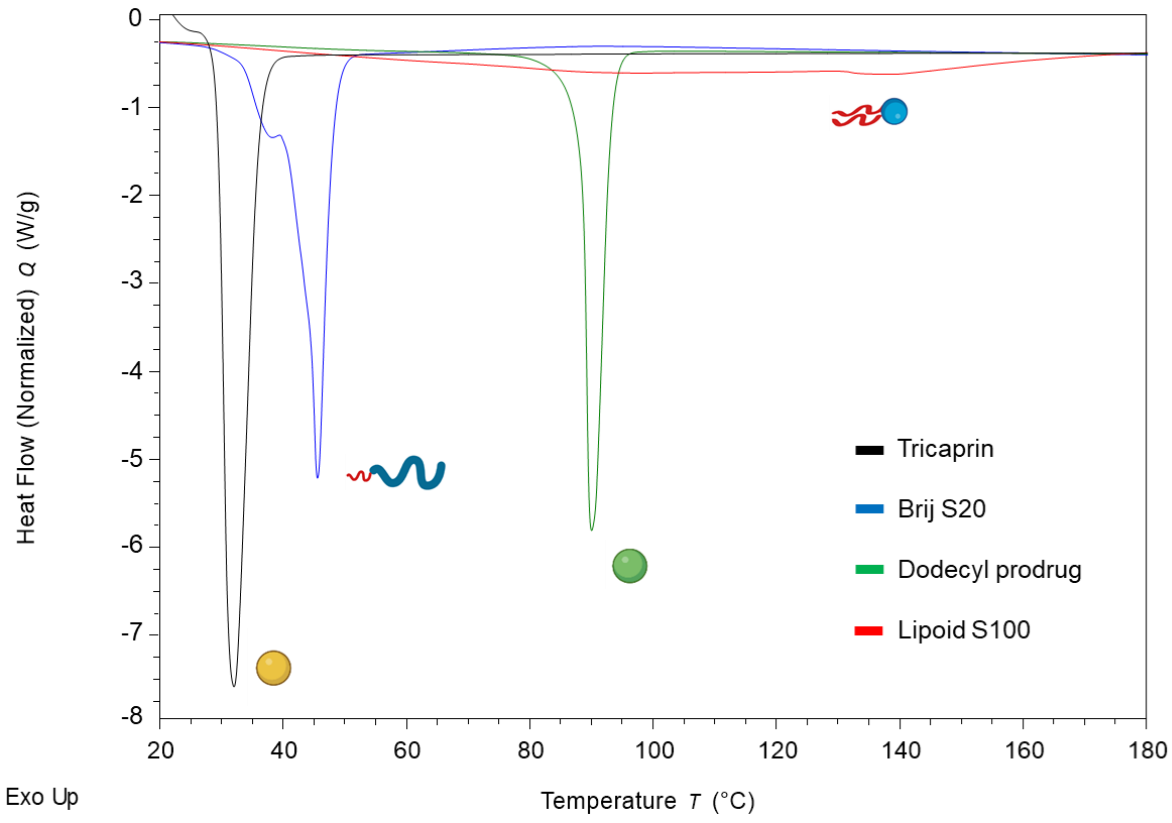

Appendix Figure 3.2- Displays the thermal properties of each of the materials in bulk.

CHAPTER 4

Cryopreservation methods of lipid nanoparticles

Chapter 4 Cryopreservation methods of lipid nanoparticles

4.1. Introduction

Cryopreservation techniques such as freeze drying/lyophilization have been identified as a potential route to improve the long-term stability of lipid nanoparticles, however the stress induced by cryopreservation on colloidal formulations is severe and can cause irreversible aggregation. In order to streamline the process, freeze thaw- another method of cryopreservation has been commonly employed to test the stability of colloidal formulations against the stresses of freezing to indicate which candidates may be potentially stable during freeze drying.[69] Nevertheless, the stresses implemented during the freezing step are also substantial, during sample freezing the growth of the ice crystals the nanoparticles may be concentrated in areas of unfrozen solution.[64] This causes close contact between nanoparticles facilitating attractive particle-particle interactions and potentially particle aggregation.[65] Studies by Schwarz *et al*. have been focused on improving the stability of formulations against the stresses of freezing. One parameter they investigated was the method of freezing and found that freezing the sample into liquid nitrogen compared to using a freezer may limit particle aggregation during freezing. It was believed that using liquid nitrogen to freeze samples resulted in a rapid and homogenous freeze whereby particles are not concentrated to as much an extent compared to a slow freezing method.[64,66,67]

During the freeze-drying process, the frozen water within samples is sublimed under vacuum resulting in the formation of a cake. This cake is typically a porous structure formed from the solutes such as particles and additives (i.e. cryoprotectants or lyoprotectants) being spatially arranged during freezing. Work by Patel and Sylvester *et al*. has investigated how the structure and stability of cakes translates to a formulation's ability to redisperse upon rehydration. Their findings indicate that cake stability correlates with the quality of redispersion; with occurrences of cake collapse indicating that the likelihood of successful redispersion was low. Markers of cake collapse such depression in cake may be visible by a simple visual appearance, meanwhile more detailed analysis by SEM may reveal holes in the cake structure.[78,80]

A parameter commonly discussed in literature is how the use of cryoprotectants and lyoprotectants may be incorporated to address colloidal stability issues during freezing and drying. Sylvester *et al*. clearly investigated how the ratio of liposome to cryoprotectant impacts the cake stability and thus redispersion quality.[80] As a result, a wide range of materials have been investigated at various concentrations to test their performance as a cryoprotectant/lyoprotectant- with sugars such as sucrose being favoured in literature.[66,75,86] Allison *et al*. have suggested that sugars efficiently stabilise formulations during freeze drying by three methods; by establishing a protective layer, forming a glass

matrix and/or by isolating particles. The result is a cake which is formed with minimal/no aggregation of nanoparticles which can easily redissolve and redisperse the particles to restore a colloidal formulation.[84,85] As a result of variation in the quality of formulation redispersion, some studies such as that by Amis *et al*. have implemented a grading system.

4.2. Chapter Aims

As discussed, much research has investigated the parameters surrounding freeze drying such as various cryoprotectants/lyoprotectants or methods of freezing or redispersion. However, there is a lack of data on how the properties of a formulation may impact the overall stability of a formulation against the stresses of freezing and drying. As a result, the overall aim of this work is to gain further understanding surrounding the fundamentals behind cryopreservation techniques such as freeze thaw and freeze drying. In addition, investigate in detail how properties of formulations (such as surfactant properties) may influence the ability of a formulation to redisperse once freeze dried. The desired outcome was to design a formulation that could withstand the stresses of freezing and drying steps that contains only lipid and then apply the same design to a formulation that contained a high level of dodecyl prodrug-synthesised in Chapter 2.

The chapter uses the nanoprecipitation method of lipid nanoparticle formulation developed in earlier chapters (Fig.1-A) to develop nanoparticle formulation varying in material composition for both core and surfactant. Key formulation factors investigated were the ratio of pegylated and unpegylated lipid nanoparticles, thus varying the degree of steric stabilisation of the formulation and its effect on preventing/limiting aggregation events during cryopreservation methods. Additionally, the wt % of formulation was investigated again to determine how formulation stability may changes with degree of stabilisation. To achieve this, a freeze thaw method was employed to examine formulation stability against the stresses of freezing before examining against the stresses of drying during lyophilization. Formulations were prepared varying the concentration of the cryo/lyoprotectant sucrose and assessed using a combination of visual observations, DLS and microscopy, Fig.1-B. Upon establishing fundamental design rules formulations were modified to include the active ingredient dodecyl prodrug before further assessment.

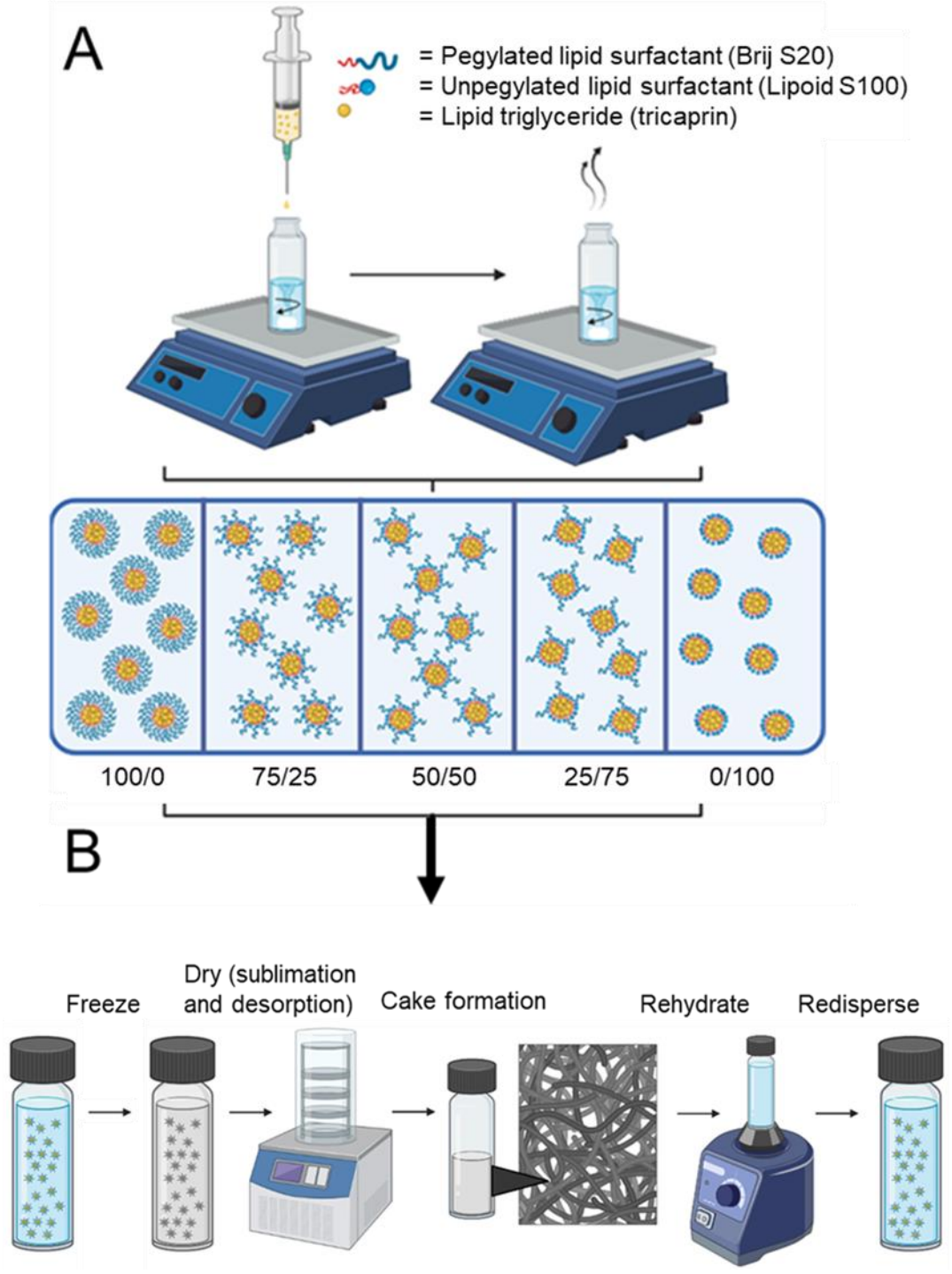

Figure 4.1-Schematic overview depicting strategy to investigate the fundamentals of cryopreservation. A) Variations in formulation properties B) Assessment of stability during freeze drying into order to develop a formulation that contains drug at a high wt % while can withstand the stresses of freeze drying

4.3. Result and Discussion

4.3.1. Cryopreservation of lipid-based formulations varying degree of pegylated lipid surfactant and zwitterionic unpegylated lipid surfactant

Formulations of tricaprin at 14 wt % varying in surfactant composition of Brij S20 and Lipoid S100 from Chapter 3 were tested for stability against the stresses during freeze thaw and freeze drying/lyophilization.

4.3.1.1. Freeze thaw

Freeze-thaw experiments were used to examine how surfactant composition may determine nanoparticle formulation stability against the stresses of freezing. This approach was used to accelerate the identification of favourable surfactant compositions as formulations that were unstable during this first step of lyophilization were highly unlikely to be stable after the second stage. The studies were conducted at various cryoprotectant concentrations 1, 5 and 10 % w/v sucrose, with no cryoprotectant as a control. Each formulation was examined for changes which could be observed by the naked eye. Fig.4.2-A displays a compiled series of photos of each formulation at each concentration before and after freeze thaw. Immediately the formulation without any cryoprotectant at 100 % Lipoid S100 (100% unpegylated lipid surfactant) adopted a highly glittery appearance indicating the presence of crystals in solution likely the result of aggregation. Formulation was examined under an optical microscope and confirmed the presence of crystals, Fig.4.2-B. When 1 % w/v of sucrose was used as the cryoprotectant then the visual appearance of the samples was similar to pre-freezing, with the exception that the formulation made with 100 % Lipoid S100 was more turbid, potentially indicating larger particles due to an increase in light scattering. Each formulation was then examined for changes in particle size, size distribution and derived count rate by DLS. The data presented in Fig.4.3-A highlights how when no cryoprotectant was present there was an increase in particle size and PDI as the ratio of pegylated lipid surfactant was decreased. However the formulation stabilised by 100 % Lipoid S100 which possessed anisotropic crystals produced a correlation coefficient curve of poor quality indicating the DLS data for this formulation was unreliable, appendix Fig.4.1. Appendix Fig.4.1-A displays an overlay of correlation coefficient curves before and after freeze thaw indicating reliable data for the formulation 25 % Brij S20 75 % Lipoid S100, which did not have anisotropic crystals present, meanwhile Fig.4.1-B displays a large shift in correlation coefficient curve after freeze thaw suggesting the presence of large aggregates and poor data quality. Furthermore, there was no clear increase in derived count rate except the formulation stabilised by 100 % Lipoid S100 thus suggesting the presence of anisotropic crystals led to an increase in light scattering, Fig.4.3-B. In addition, it is plausible someof the anisotropic crystals may be above the detectable size limit of the DLS, and as a result formulations that possessed the glittery effect were

deemed incompatible with DLS. In the presence of cryoprotectant even as low at 1 % w/v sucrose there was no clear indication of aggregation. There was noteworthy difference between the DLS data and the visual observations for the sample stabilised by 100 % Lipoid S100 with 0 % w/v sucrose; the visual observation revealed particles on the micron scale, while the DLS provided a mean diameter of ~240 nm. This difference is likely due to the micro-sized particles being above the size that can be measured by DLS. Therefore, it must be considered that although the DLS data supports the narrative the data of size, PDI and derived count rate is not a true reflection of the overal sample and the degree of aggregation is likely suppresed by these values. As a result, this data showed the importance of using multiple methods of characterisation for the formulations.

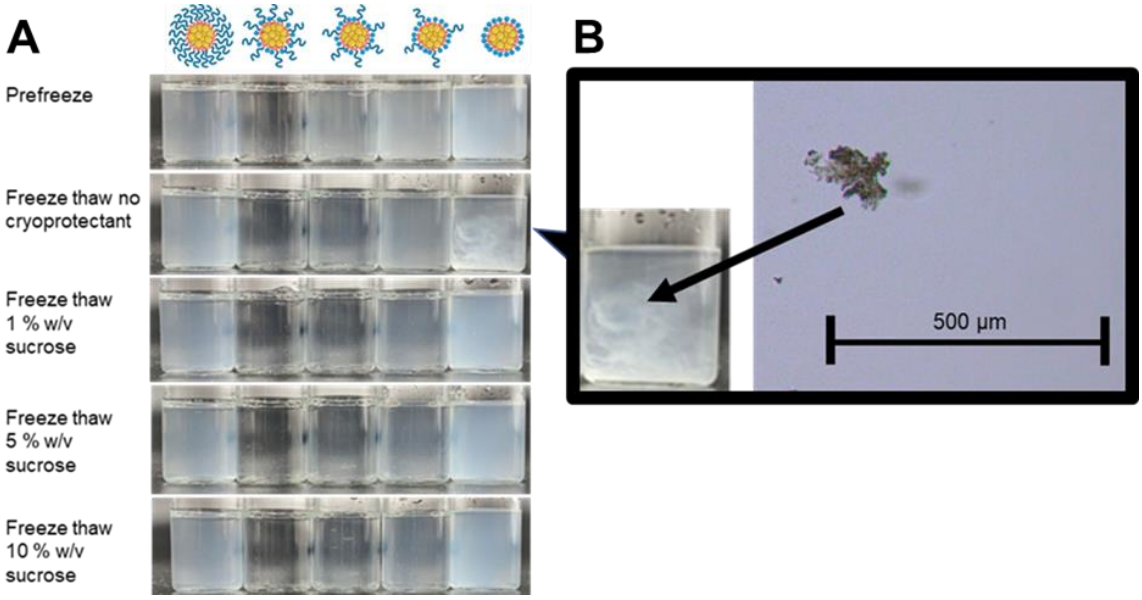

Figure 4.2- Effect of cryoprotectant concentration on appearance of the formulations after freeze-thaw on Day 2 after formulation. A) Compiled photos of each formulation before freeze thaw as well as at each concentration of cryoprotectant (no cryoprotectant, 1, 5, 10 % w/v sucrose) after freeze thaw. B) Enlarged image of formulation displaying a slight glittery effect of stabilised by 100 % Lipoid S100 (unpegylated lipid) without any cryoprotectant present after freeze thaw including an optical microscope image confirming the presence of crystals as a result of aggregation due to the stress of freezing.

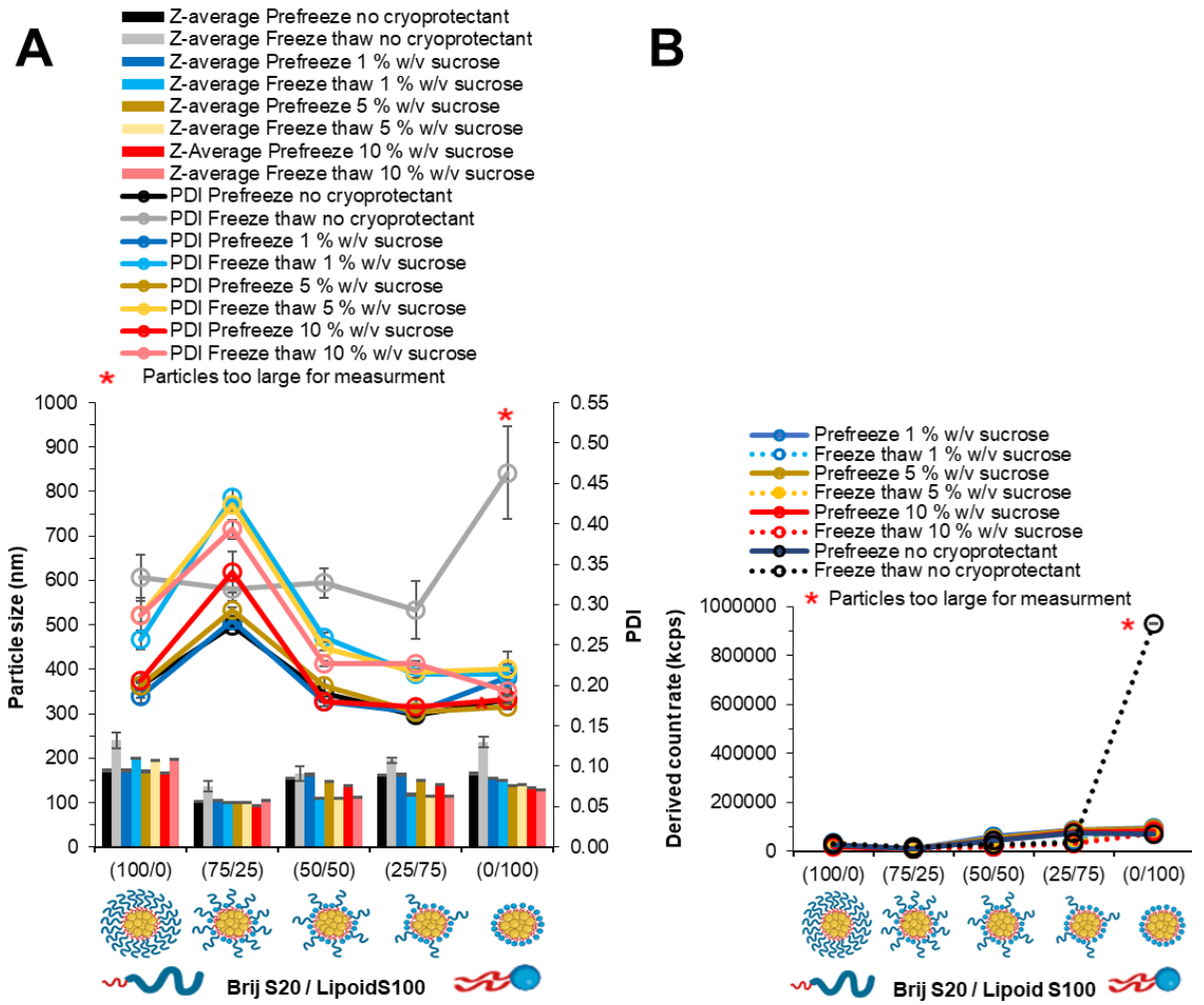

Figure 4.3- Particle size, size distribution and derived count rate data obtained by DLS on Day 2 after formulation. A) size and size distribution. B) Derived count rate. Formulations of tricaprin at 14 wt % varied in pegylated/unpegylated lipid surfactant blends on a mass ratio. Data examines how the ratio of pegylated/unpegylated lipid surfactant determines stability during freeze thaw at various concentrations 0, 1, 5 and 10 % w/v of the cryoprotectant sucrose and suggests the presence of pegylated lipid surfactant is essential to prevent aggregation events during freeze thaw in the absence of any cryoprotectant during. Measurements made at a fixed position of 4.65 mm.

4.3.1.2. Freeze drying/Lyophilization

The sample formulation blends were then subjected to lyophilization to assess the ability to withstand the stresses of drying as well as freezing. Again, the studies were conducted at various cryoprotectant concentrations 1, 5 and 10 % w/v sucrose as well as no cryoprotectant as a control. After complete drying each formulation was examined for changes which could be observed by the naked eye. Fig.4.4-A displays a compiled series of photos of each formulation once dried down to form their 'cake'. There was a noticeable trend as the ratio of pegylated lipid is reduced the cake size/density decreased until the lyophilized material at 100 % Lipoid S100 is a lump of sticky material suggesting lack of cake formation. Furthermore at 0 and 1 % w/v sucrose there was a noticeable degree of cake collapse, however cakes appeared to maintain integrity at 5 and 10 % w/v sucrose. Furthermore, for each formulation there was an increase in the size of the cake produced with increased concentration of sucrose. Fig. 4.4-B displays each of the formulations before and after lyophilization and redispersing in the presence of the different sucrose concentrations. Each of the formulations without any cryoprotectant adopted a highly glittery appearance similar to that shown by Fig.4.2-B, thus indicating the presence of crystals in suspension likely the result of aggregation. Interestingly, each of the formulation stabilised by 50, 75 and 100 % Lipoid S100 at 1 % w/v sucrose also showed signs of aggregation with the glittery effect increasing with increasing Lipoid S100 composition. On the other hand, those stabilised by a high proportion 100 % Brij S20 appeared stable and showed no clear sign of large particles. This suggests the pegylated lipid surfactant Brij S20 provided necessary steric stabilisation to prevent/limit aggregation of nanoparticles. Furthermore, Brij S20 helped in cake formation and limit cake collapse which likely helped in redispersibility which is in agreement with Patel and Sylvester *et al* who suggested cake integrity and stability is essential to ensure efficient redispersion of a formulation.[78,80] Table 1 summarises the re-dispersibility of each formulation by a grading system.

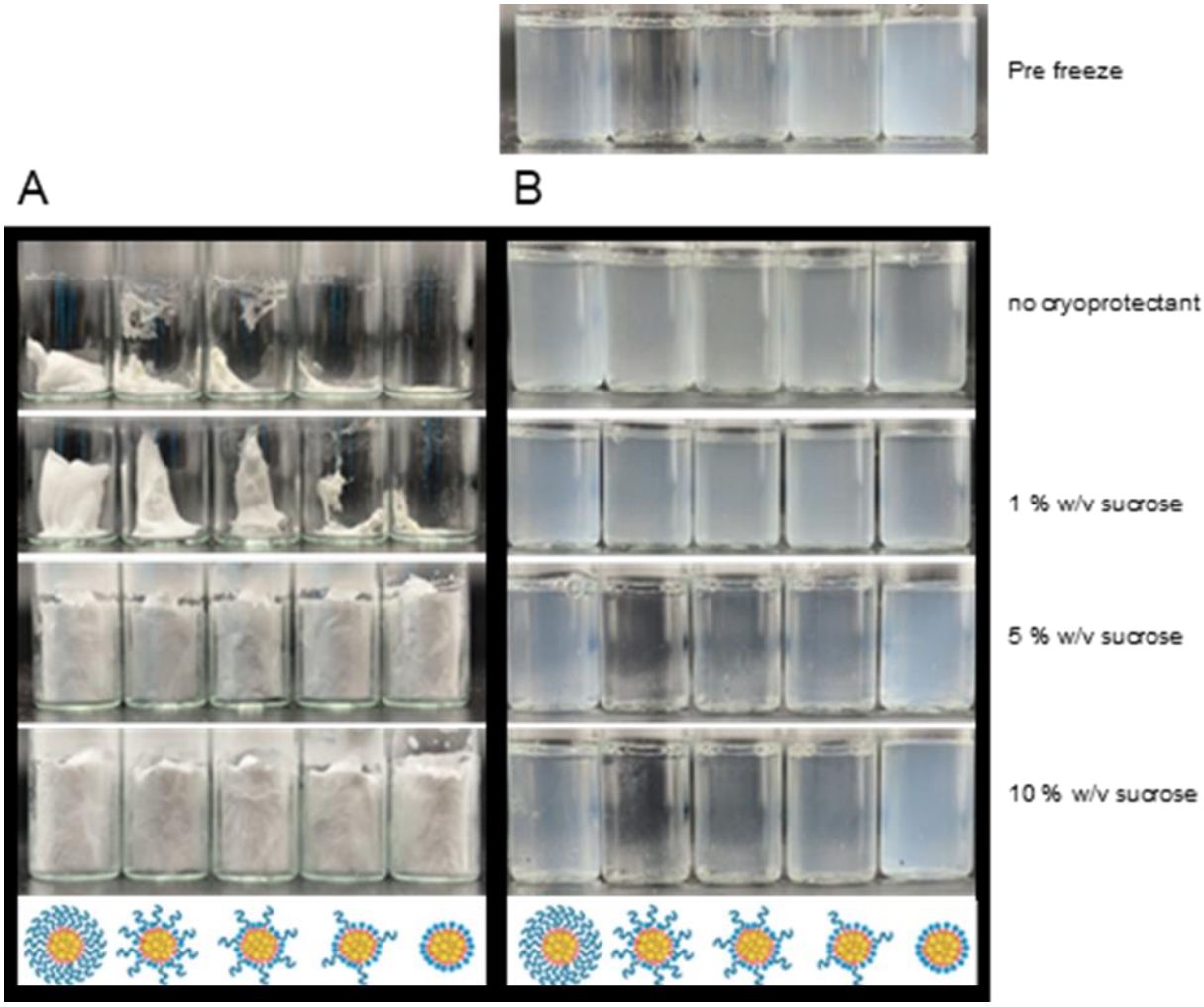

Figure 4.4- Effect of cryoprotectant concentration and surfactant composition on appearance of the formulations after freeze-drying and after redispersion samples were freeze-dried on Day 2 after formulation. A) Compiled photos of each formulation's cake once freeze-dried down highlighting differences based on sucrose concentration as well as surfactant composition. B) Compiled photos of each formulation before and after lyophilization. Suggests 5 and 10 % w/v sucrose may be sufficient at stabilising each formulation despite surfactant composition.

Table 4.1 - Table of grades of redispersion of formulations varying in surfactant composition (Brij S20/Lipoid S100) at 14 wt % tricaprin. (1= Appears the same as prior to freezing and lyophilization, 2= increase in turbidity, 3= glittery effect, 4= visible aggregates)

	100 % Brij S20	75 % Brij S20 25 % Lipoid S100	50 % Brij S20 50 % Lipoid S100	25 % Brij S20 75 % Lipoid S100	100 % Lipoid S100
No sucrose	3	3	3	3	3
1 % w/v sucrose	1	2	3	3	3
5 % w/v sucrose	1	1	1	1	1
10 % w/v sucrose	1	1	1	1	1

SEM was employed to further investigate the effect of surfactant composition on cake formation, the aim of this was to gain further insight of the cake structure between formulations stabilised by 100 % pegylated lipid (Brij S20), 50 % pegylated lipid (Brij S20) 50 % unpegylated lipid (Lipoid S100) and 100 % unpegylated lipid (Lipoid S100) surfactants. Fig. 4.5 displays the key structural differences between the three lyophilized formulations. When the formualtion was stabilised by 100 % Lipoid S100 the nanoparticles appeared to aggregate to one mass which is a sticky material similar to that of bulk Lipoid S100 (Fig 4.5-A). Meanwhile, Fig.4.5-B shows how even at a ratio of 50 % Brij S20 50 % Lipoid S100 the freeze dried material appears to adopt a scaffold struture. Likewise the formulation stabilised by 100 % Brij S20 results in what appears to be a polymer scaffold network with pores where water may have once been similar to that shown by Zhang *et al*. (Fig.4.5-C).[71] Although, the cake produced by the blend of 50 % Brij S20 50 % Lipoid S100 was more collapsed than the 100 % Brij S20 formulation. This difference in sturcture may suggest key properties of what a desirable cake/scaffold may look like. Although, formulations higher in BrijS20 appear to have greater stability, it is plausible that there was an excess of surfactant Brij S20 (i.e. more than required to stabilise the nanoparticles) and this excess solbule polymer could also act as a cryoprotectant/lyoprotectant. It is important to remember that previous reports have shown that the quality of the cake produced may determine the quality of redispersion. In an effort to improve cake formation and stability the samples were then freeze dried with the addition of 10 % w/v sucrose, images of the sakes and SEM images of the cakes are shown in Fig-4.6-A (50 % BrijS20 50 % Lipoid S100) and Fig-4.6-B (100 % Lipoid S100). This experiment showed how a high concentration of sucrose can overcome structural differences between surfactant compositions as both display an array of crystal structures most likely to be sucrose. In addition, appeared that the presence of many small crystals of sucrose was due to homgenous freezing of the formulation and upon drying the crystals become stacked.[67,68]

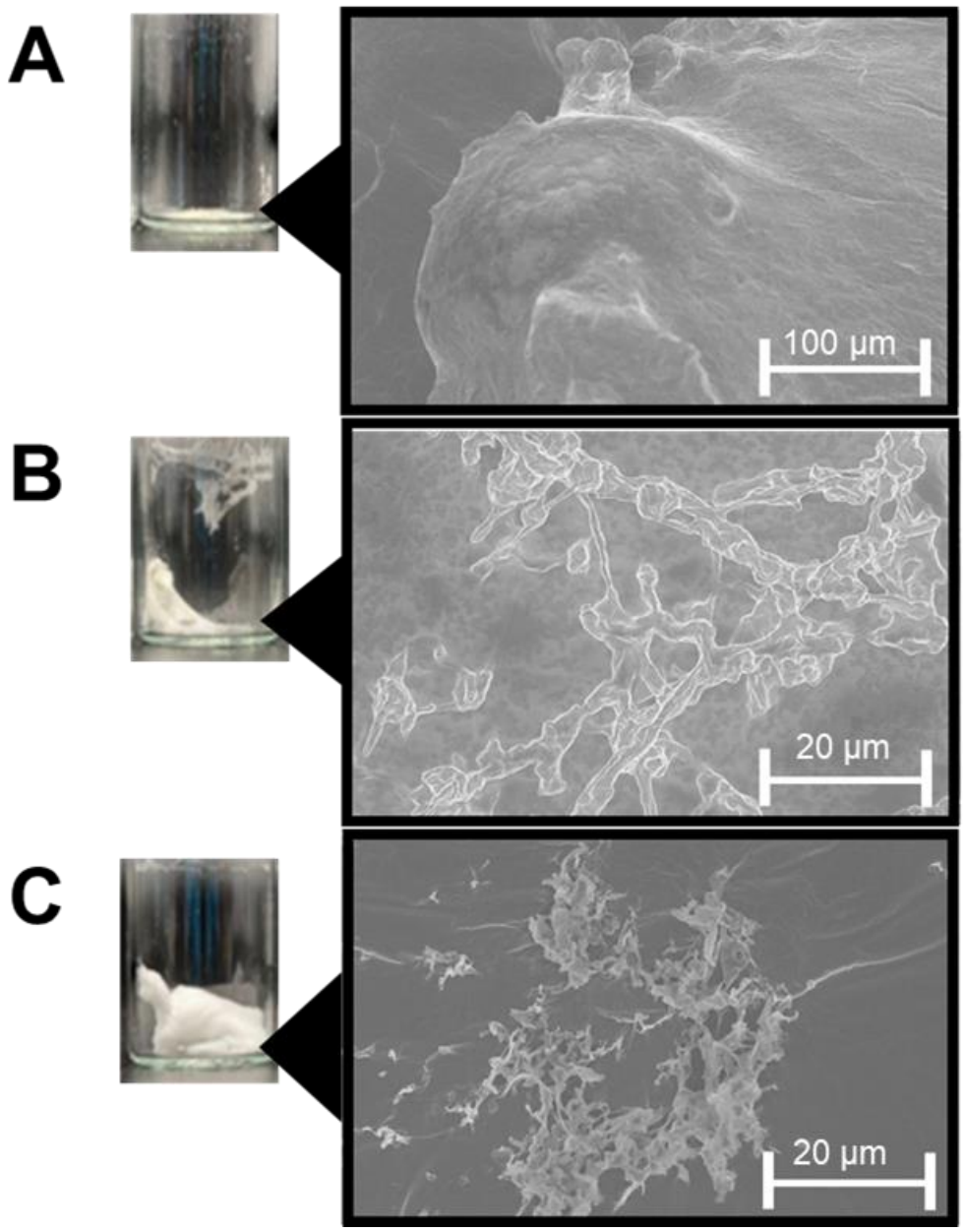

Figure 4.5- SEM of freeze-dried materials comparing formulations of 14 wt % tricaprin with no cryoprotectant present and stabilised by a surfactant composition of A) 100% Lipoid S100 and B) 50 % Brij S20 50 % Lipoid S100 C) 100% Brij S20. Highlights differences in structure between 100% Brij S20 and Lipoid S100 suggesting the PEG chain of Brij S20 acts as a steric stabiliser while also forming a polymer scaffold. Although it is plausible Brij S20 may be in excess and thus any Brij S20 not attached to the nanoparticles may be acting as a cryoprotectant. Nevertheless, at 50 % Brij S20 50 % Lipoid S100 the presence of Brij S20 seems to still provide a polymer scaffold.

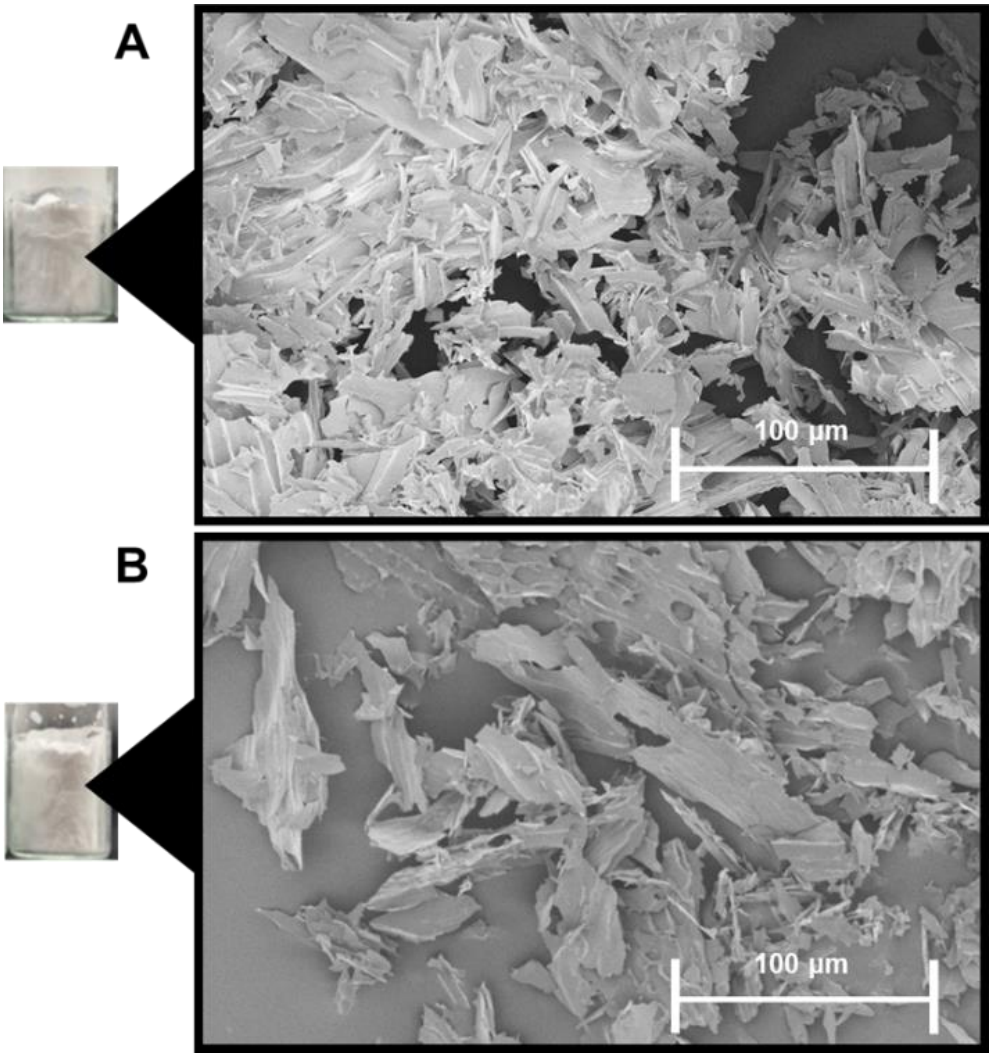

Figure 4.6- SEM of freeze-dried formulation of 14 wt % tricaprin at a cryoprotectant concentration of 10 % w/v sucrose and surfactant compositions of A) 50 % Brij S20 50 % Lipoid S100 B) 100 % Lipoid S100. Highlights similarities in cake appearance due to high concentration of sucrose. Likely the crystal structure visible are crystals of sucrose with nanoparticles between/within. Thus, leading to prevention/limitation of the number of aggregation events during freeze drying.

Nevertheless, in order to investigate the properties of the freeze-dried formulations after redispersion they were examined for changes in particle size, size distribution and derived count rate by DLS. Three different concentrations of sucrose were investigated as the cryoprotectant (1, 5 and 10 % w/v). The data presented in Fig.4.7-A highlighted that when 1 % w/v sucrose cryoprotectant was used then the lower ratios of pegylated lipid surfactant resulted in an increase in PDI. There are no clear deviations in particle size or derived count rate in Fig.4.7-B. This is likely a result of aggregates forming which are beyond the size that is detectable by DLS.

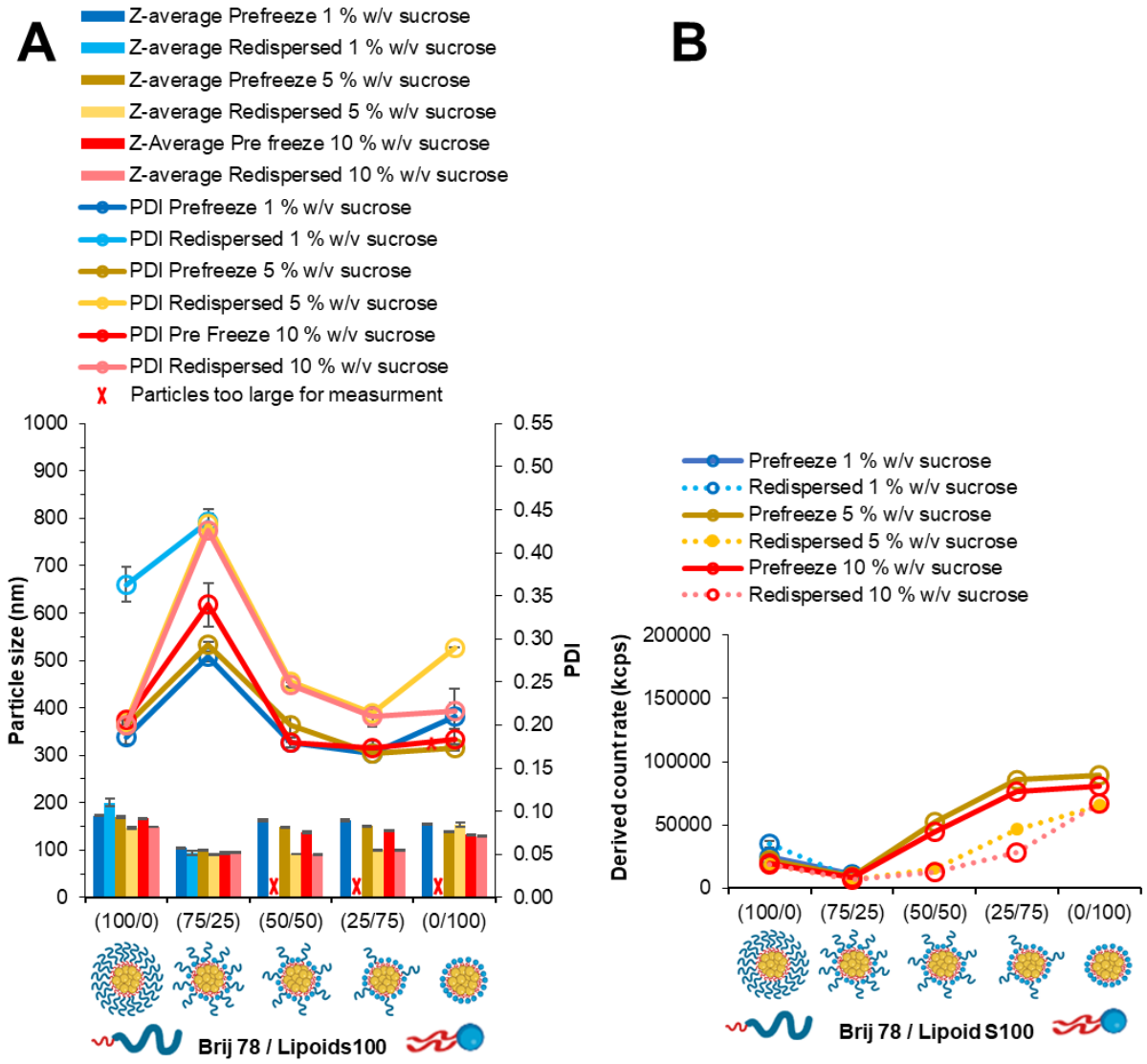

Figure 4.8- Particle size, size distribution and derived count rate data obtained by DLS. A) Particle size and size distribution. B) Derived count rate. Formulations of tricaprin at 14 wt % varied in pegylated/unpegylated lipid surfactant blends on a mass ratio. Data examines how the ratio of pegylated/unpegylated lipid surfactant determines stability during freeze-drying at various concentrations 1, 5 and 10 % w/v of the cryoprotectant sucrose and suggests the presence of pegylated lipid surfactant is essential to prevent aggregation events during freeze-drying at lower concentrations of 1 % w/v sucrose. Measurements made at a fixed position of 4.65 mm.

Fig.4.8, displays particle size distribution graphs and corelograms for formulations stabilised by 100 % Brij S20 and 100 % Lipoid S100 before and after freeze drying at 1 and 10 % w/v sucrose concentration. Firstly, it is clear at the lower concentration of 1 % w/v sucrose the stability of both formulations was poor after freeze drying due to the drastic changes in particle size distribution graphs (Fig.4.8-A1 and D1) which showed broadening as well as secondary peaks of higher Z-average suggesting the presence of aggregates. Furthermore, correlograms in Fig.4.8- A2 and D2 showed a shift to the right as well as contained peaks suggesting the presence of aggregates post lyophilization, therefore indicating poor quality DLS likely due to the presence of aggregates.[153] Although, as the concentration of sucrose was increased the differences in the size distributions before and after for formulations stabilised by 100 % Lipoid S100 was less pronounced (Fig.4.8- D1, E1 and F1), the same was true for the correlograms, Fig.4.8- D2, E2 and F2. The blends of Brij S20 and Lipoid S100 at 10 % w/v sucrose also show good stability due to little difference in size distribution graphs and correlation coefficient curves as shown by, appendix Fig.4.2. Overall, it was deemed formulations in the presence of 10 % w/v sucrose limited/prevented aggregation events the most during the process of freeze drying. This was likely due to sufficient separation of nanoparticles provided by sucrose at higher concentrations of preventing aggregation during the ice crystal formation of the freezing phase as well as the during the sublimation of ice during drying phase.

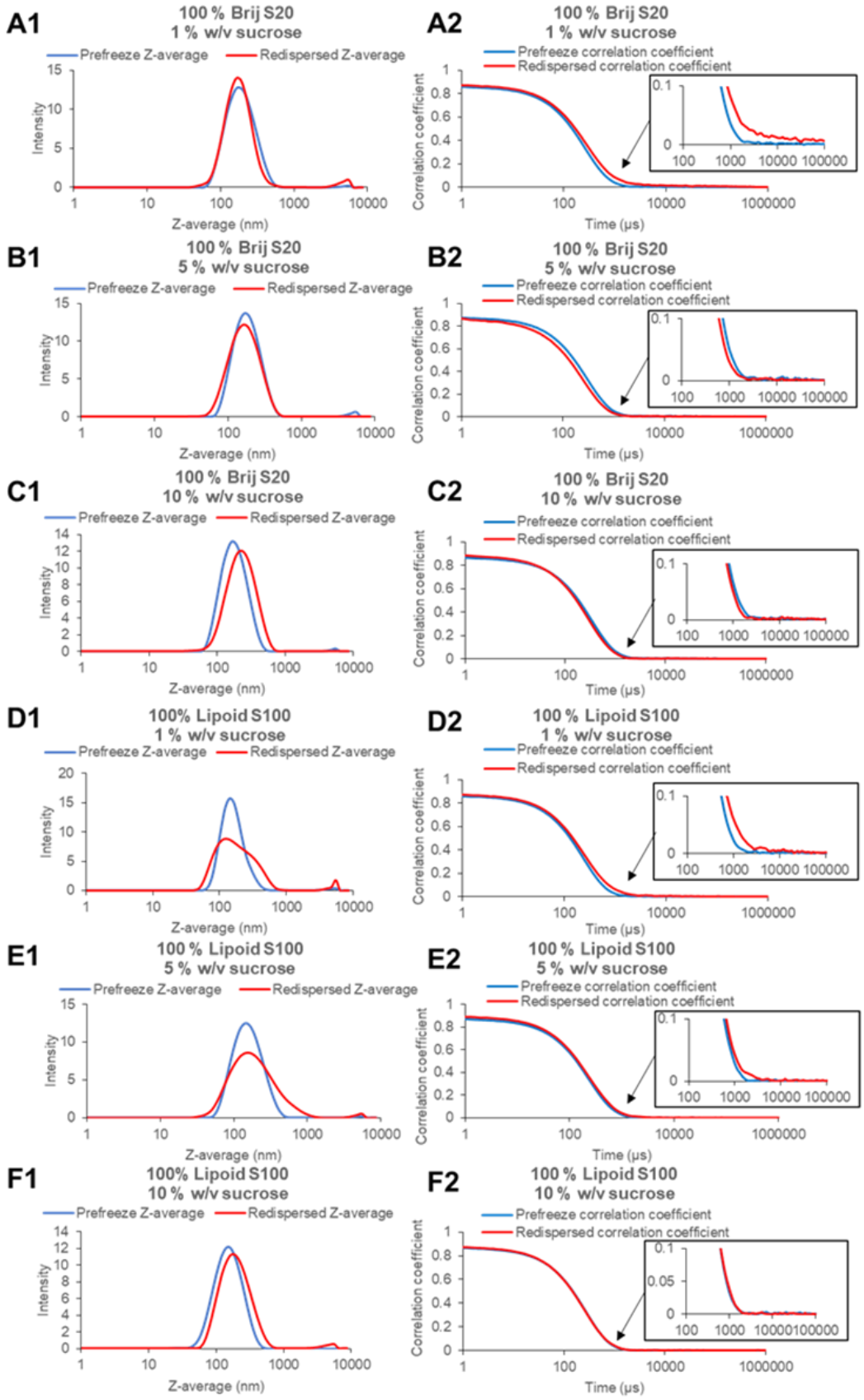

Figure 4.8- Particle size distribution graphs and correlation coefficient graphs before and after freeze drying and redispsersion for 14 wt % tricaprin formulations stabilised by both 100 % Brij S20 (A1, A2, B1, B2, C1 and C2) and 100 % Lipoid S100 (D1, D2, E1, E2, F1 and F2) at both 1, 5 and 10 % w/v sucrose. Overall displays how the stability of formulations increases with increasing sucrose concentration.

4.3.2. Cryopreservation of lipid-based formulations varying the ratio of pegylated lipid and cationic unpegylated lipid surfactants

It was hypothesised formulations high in Lipoid S100 (a blend of various forms of phosphatidylcholine) may have had poor stability due to not possessing a net charge shown in Chapter 3 Fig.3.11, thus present little/no electrostatic barrier to aggregation during the stresses of cryopreservation. As a result, Lipoid S100 was replaced by the cationic unpegyalted lipid surfactant 1,2-dioleoyl-3-trimethylammonium-propane chloride salt (DOTAP-Cl). DOTAP-Cl shares similarities with the zwitterionic unpegylated surfactant Lipoid S100 as both are insoluble in water and therefore should theoretically nucleate upon injection during flash nanoprecipitation. On the other hand, DOTAP-Cl possess a net positive charge compared to the net neutral charge of Lipoid S100 (Fig.4.9), and thus has potential to increase the level of stabilisation to formulations. Furthermore, the presence of electrostatic stabilisation in combination with pegylated lipid surfactants would provide an electrosteric barrier to particle aggregation.

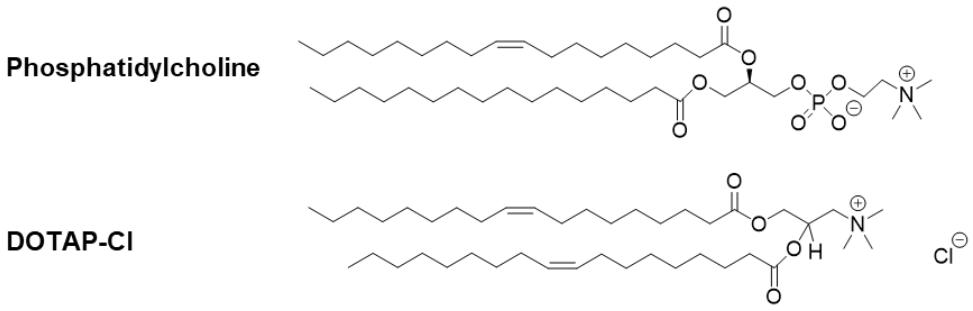

Figure 4.9- Chemical structures of both phosphatidylcholine and DOTAP-Cl, highlighting the differences in charge as phosphatidylcholine is zwitterionic and DOTAP-Cl has a net charge.

As a result, Brij S20 was blended with DOTAP-Cl in the formulation of tricaprin at 14 wt % on a 1:1 mass ratio to investigate the resultant formulations prior to cryopreservation. The particle size and size distribution values are shown in Fig.4.10 and display a clear trend of decreasing particle size from ~190 nm to 100 nm with increasing percentage of DOTAP-Cl, suggesting DOTAP-Cl provides stabilisation to the growing particles at a smaller stage than Brij S20. Unlike Lipoid S100 which in Fig. 3.9-A of Chapter 3 we observe a substantial reduction in particle size at 75 % Brij S20 25 % Lipoid S100 before an increase in particle size with further increase in the proportion of Lipoid S100. This suggests that the net positive charge of DOTAP-Cl results in repulsion between DOTAP-Cl molecules during the growth stage of particle formation, thus limiting the number of aggregation events between growing nuclei thus better controlling particle size. This theory is further supported by Fig.4.11 which displays a clear increase in zeta potential and decrease in derived count rate with increasing DOTAP-Cl content. Formulations stabilised by 100 % Brij S20 possessed a charge less than ± 10 mV, however at 75 % Brij S20 25 % DOTAP-Cl the formulation possesses a zeta potential of ~ 64 mV. This generally increased

with increased percentage of DOTAP-Cl within the surfactant composition, until a zeta potential of ~ 81 mV was recorded for the formulation stabilised by 100 % DOTAP-Cl.

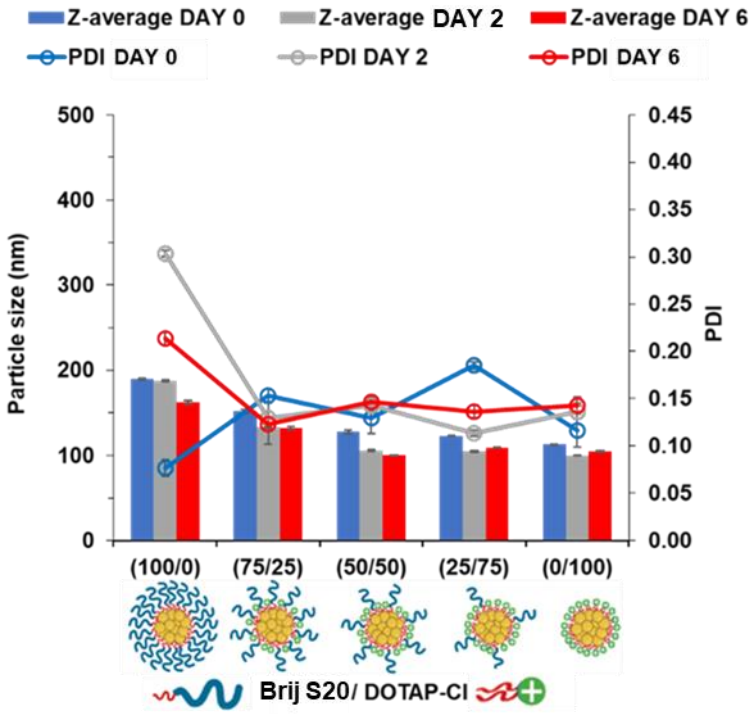

Figure 4.10- Particle size and size distribution obtained by DLS over a 6-day period. Formulations varied in pegylated/cationic unpegylated lipid surfactant blends on a mass ratio. Samples were prepared at in triplicate and error bars calculated on standard deviation between sample measurements. Samples were stored at 22 °C.

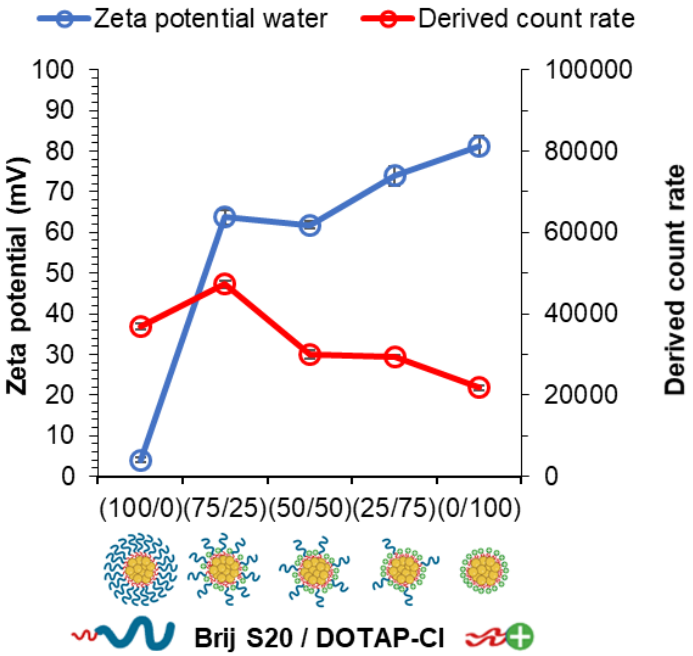

Figure 4.11- Zeta potential and Derived count rate obtained by DLS on day 2 of formulation. Formulations varied in pegylated/cationic unpegylated lipid surfactant blends on a mass ratio. Samples were prepared in triplicate and error bars calculated on standard deviation between sample measurements. Samples were stored at 22 °C.

4.3.2.1. Freeze thaw

Freeze-thaw experiments were conducted to examine how surfactant composition between pegylated lipid surfactants and cationic unpegylated lipid surfactants may determine nanoparticle formulation stability against the stresses of freezing. The studies were conducted at various cryoprotectant concentrations 1, 5 and 10 % w/v sucrose as well as no cryoprotectant as a control.

Each formulation was first examined for changes which could be observed by the naked eye. Fig.4.12 displays photos of each formulation at each concentration before and after freeze thaw. Immediately the formulation without any cryoprotectant at 100 % DOTAP-Cl (100% cationic unpegylated lipid surfactant) adopted a highly glittery appearance indicating the presence of crystals in solution in a similar manner to 100 % Lipoid S100, thus likely the result of aggregation. Furthermore, blends containing DOTAP-Cl had also adopted a glittery appearance post freeze thaw.

The formulations were then examined for changes in particle size, size distribution and derived count rate by DLS. The data presented in Fig.4.13-A highlights how in the presence of 5 and 10 % w/v sucrose each of the formulations appeared stable as there was no increase in particle size or PDI. Meanwhile, at 1 % w/v sucrose there was an increase in PDI which became more pronounced with decreasing concentration of Brij S20 in the formulation. In addition, there was no clear increase in derived count rate at either surfactant composition or sucrose concentration Fig.4.13-B. As a result, the data obtained by DLS alongside the compilation of photos in Fig.4.12 highly suggested that the steric stabilisation provided by the pegylated lipid surfactant was more efficient than electrostatic stabilisation provided by DOTAP-Cl at stabilising particle formulations against the stresses of freeze thaw. Nevertheless, again there was a clear need for a cryoprotectant as upon addition of 1 % w/v sucrose each surfactant composition appears stable post freeze thaw.

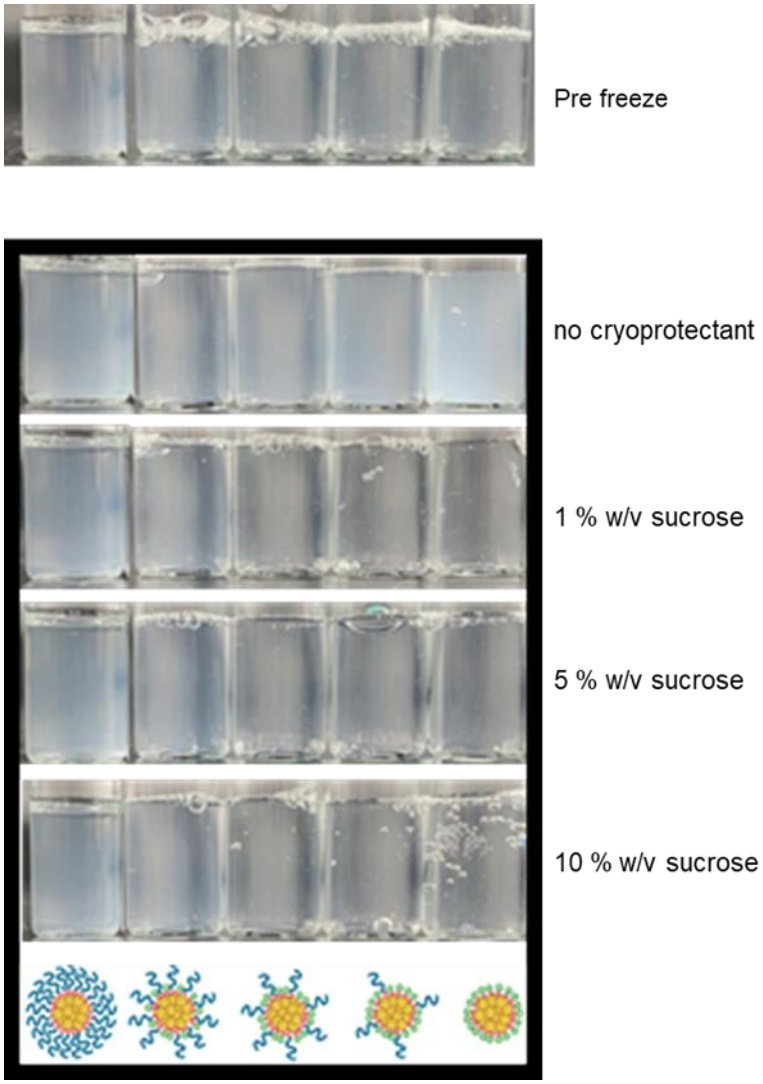

Figure 4.12- Displays compiled photos of each formulation before freeze thaw as well as at each concentration of cryoprotectant (no cryoprotectant, 1, 5, 10 % w/v sucrose) after freeze thaw. Photos highlight the need for cryoprotectant to preserve stability during freezing despite the presence of electrostatic or electrosteric stabilisation.

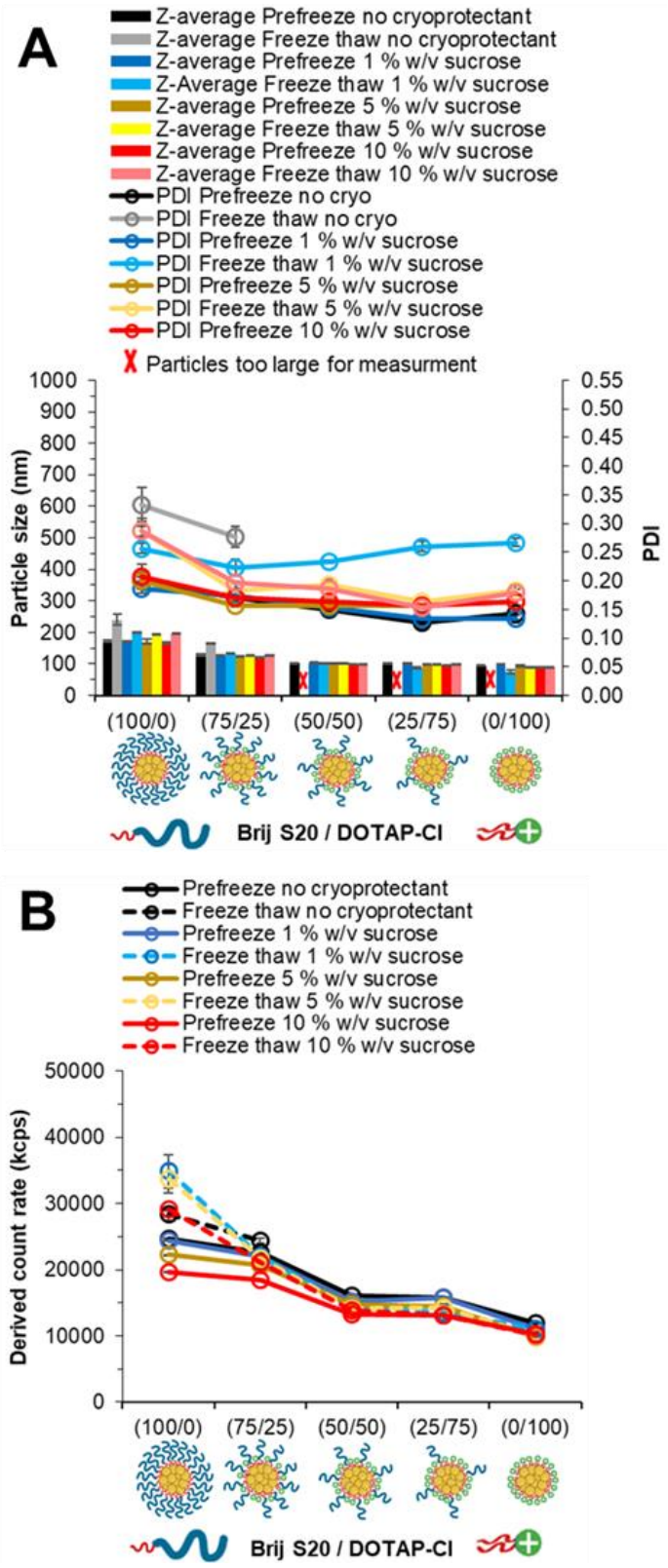

Figure 4.13- Particle size, size distribution and derived count rate data obtained by DLS. A) size and size distribution. B) Derived count rate. Formulations of tricaprin at 14 wt % varied in pegylated/cationic unpegylated lipid surfactant blends on a mass ratio. Data examines how the ratio of pegylated/cationic unpegylated lipid surfactant determines stability during freeze thaw at various concentrations 0, 1, 5 and 10 % w/v of the cryoprotectant sucrose and suggests the presence of pegylated lipid surfactant is essential to prevent aggregation events during freeze thaw in the absence of any cryoprotectant during. Measurements made at a fixed position of 4.65 mm.

4.3.2.2. Freeze drying/Lyophilization

The sample formulation blends were then subjected to freeze-drying/lyophilization to assess the ability to withstand the stresses of drying as well as freezing. Again, the studies were conducted at various cryoprotectant concentrations 1, 5 and 10 % w/v sucrose as well as no cryoprotectant as a control.

Fig.4.14-A displays a compiled series of photos of each formulation once dried down to form their 'cake'. In a similar manner to the blends of Brij S20 and Lipoid S100 there is a noticeable trend as the ratio of pegylated lipid is reduced the cake size/density decreases dramatically until the lyophilized material at 100 % DOTAP-Cl is a small lump of material. Interestingly, the cake formation/stability is much greater at 1 % w/v sucrose while using DOTAP-Cl rather than Lipoid S100. This is also reflected by the redispersion appearance shown by Fig. 4.14-B which displays each of the formulation blends pre and post freeze-drying to allow for comparison of the effect of surfactant composition and cryo/lyoprotectant concentration at 0, 1, 5 and 10 % w/v sucrose. Immediately, each of the formulations without any cryoprotectant adopted a highly glittery appearance, thus indicating the presence of crystals in solution likely the result of aggregation. Although, unlike with the unpegylated lipid surfactant Lipoid S100 each of the formulation stabilised by 50 and 75 % unpegylated lipid DOTAP-Cl at 1 % w/v sucrose did not show any signs of aggregation with the glittery effect only appearing at 100 % DOTAP-Cl. This suggests that the DOTAP-Cl may be more efficient than Lipoid S100 when blended with Brij S20 at maintaining cake stability and thus redispersion quality (samples containing Lipoid S100 were found to display a glittery effect indicating the presence of large isotropic crystals likely due to aggregation during freeze drying). Upon increasing the concentration of sucrose further it appeared the stability of the formulation stabilised by 100 % DOTAP-Cl could be preserved. Grades for each of redispersion quality for each of the formulation blends at each sucrose concentration are listed in Table 4.2. In addition, the differences in redispersion grade compared to those containing Lipoid S100 are displayed in brackets.

Formulations containing sucrose were examined for changes in particle size, size distribution and derived count rate by DLS. The data presented in Fig.4.15-A highlights how formulations at 1 % w/v sucrose appear stable with the exception of 100 % DOTAP-Cl which experiences an increase by ~100 nm in average particle size. Nevertheless, stability at 100 % DOTAP-Cl appears to be maintained once the concentration of sucrose is increased to 5 % w/v sucrose. Despite a a slight increase in turbidity and a notable increase in average particle size the formulation at 100 % DOTAP-Cl experiences no obvious increase in derived count rate, Fig.4.15-B.

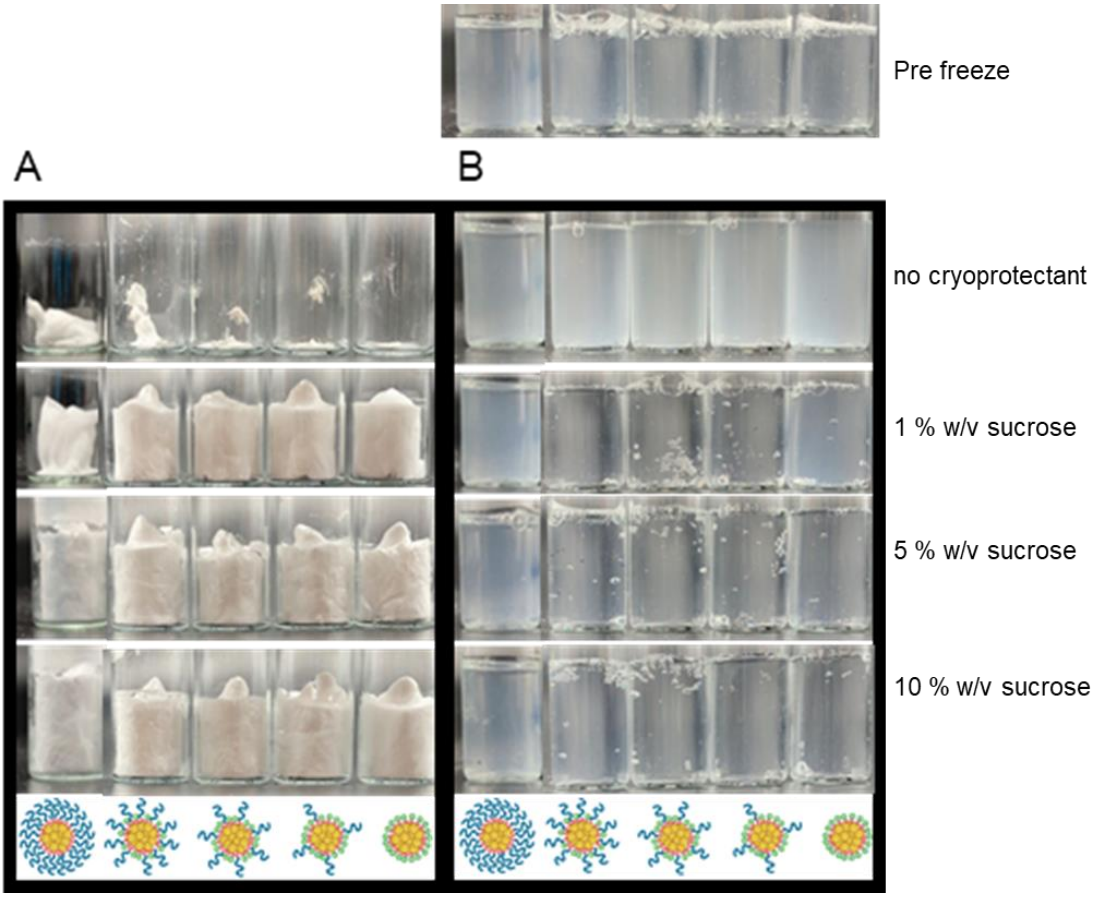

Figure 4.14- Effect of cryoprotectant concentration and surfactant composition on appearance of the formulations after freeze -drying and after redispersion samples were freeze-dried on Day 2 after formulation. A) Compiled photos of each formulation's cake once freeze-dried down highlighting differences based on sucrose concentration as well as surfactant composition. B) Compiled photos of each formulation before and after lyophilization. Suggests 5 and 10 % w/v sucrose may be sufficient at stabilising each formulation despite surfactant composition.

Table 4.2- Table of grades of redispersion of formulations varying in surfactant composition (Brij S20/DOTAP-Cl) at 14 wt % tricaprin. (1= Appears the exact same, 2= increase in turbidity, 3= glittery effect, 4= visible aggregates) – In brackets indicates the difference in redispersion grade compared to formulations containing Lipoid S100 i.e., 1(+1) = DOTAP grade 1, Lipoid S100 grade 2.

	100 % Brij S20	75 % Brij S20 25 % DOTAP-Cl	50 % Brij S20 50 % DOTAP-Cl	25 % Brij S20 75 % DOTAP-Cl	100 % DOTAP-Cl
No sucrose	3	3	3	3	3
1 % w/v sucrose	1	1 (+1)	1 (+2)	1 (+2)	2 (+1)
5 % w/v sucrose	1	1	1	1	1
10 % w/v sucrose	1	1	1	1	1

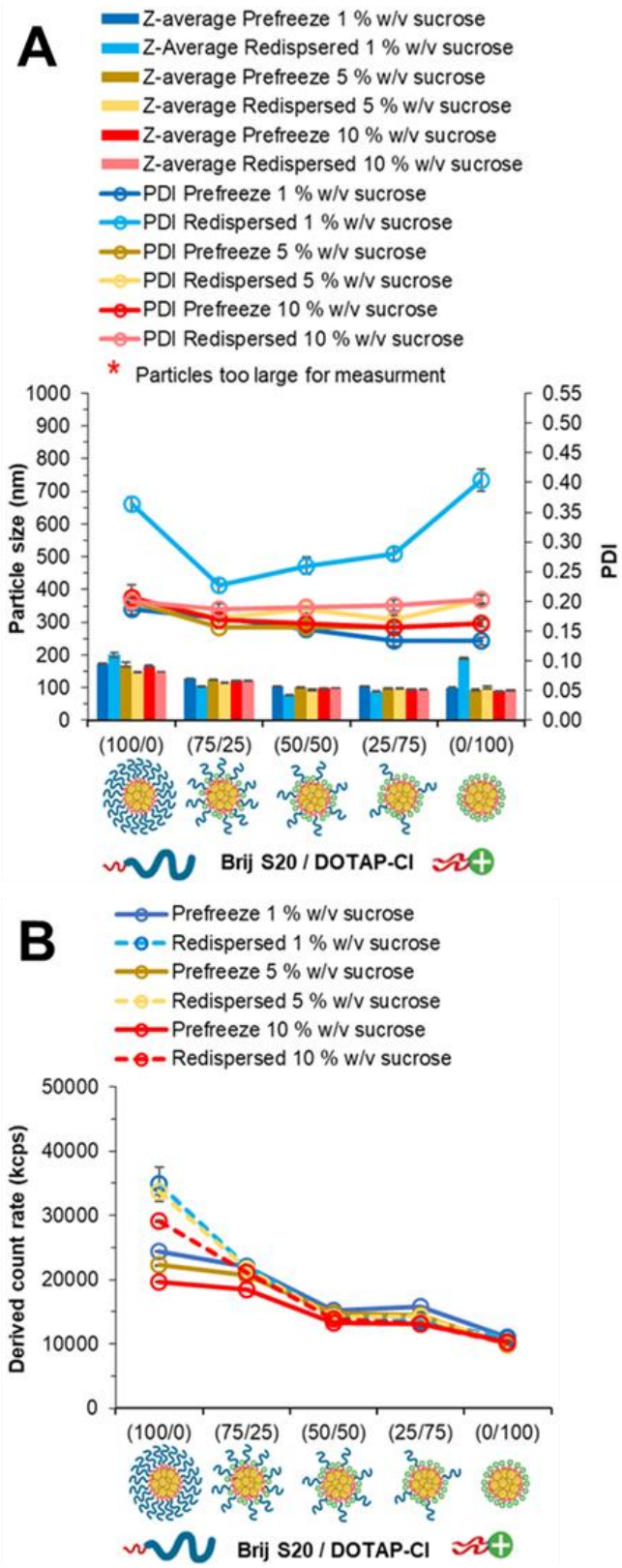

Figure 4.15- Particle size, size distribution and derived count rate data obtained by DLS. A) Size and size distribution. B) Derived count rate. Formulations of tricaprin at 14 wt % varied in pegylated/cationic unpegylated lipid surfactant blends on a mass ratio. Data examines how the ratio of pegylated/cationic unpegylated lipid surfactant determines stability during freeze-drying at various concentrations 1, 5 and 10 % w/v of the cryoprotectant sucrose and suggests the presence of pegylated lipid surfactant is essential to prevent aggregation events during freeze-drying at lower concentrations of 1 % w/v sucrose. Measurements made at a fixed position of 4.65 mm.

To further explore the redispersion quality of the formulation stabilised by 100 % DOTAP-Cl size distribution graphs and correlation graphs were overlaid before and after freeze drying, Fig.4.16. The graphs A, B and C present overlays at sucrose concentrations of 1 , 5 and 10 % w/v respectively. From Graphs A1, B1 and C1 there is a clear trend that with increasing sucrose concentration the quality of the size distribution graph increases due to disappearance of the secondary peak (which suggests the presence of aggregates) and the distribution curve becomes more symmetrical and of higher intensity similar to that prior to freeze drying. Furthermore, for A2, B2 and C2 the correlation curve generally did not show any aggregation peaks i.e. irregular peaks in the correlation coefficient and instead shifts to the left towards that of prior freeze drying with increasing concentration of sucrose. In addition, size distribution graphs and correlation curves for blends of Brij S20 and DOTAP-Cl also appeared to support formualtion redispersion due to minimal/no clear difference in number and shape of peaks and curves of graphs before and after freeze drying, appendix Fig.4.3. Overall, taking into consideration all aspects of the data characterising formulation redispersion it can be concluded DOTAP-Cl does slightly improve the stability of blends with Brij S20 compared to Lipoid S100. Nevertheless, it is plausible to argue that 10 % w/v sucrose should be used going forward whether a blend of Brij S20 with Lipoid S100 or DOTAP-Cl as it was identified as the most efficient concentration out of those trialled at preventing the occurance of signs of instability such as the glittery effect which indicates the presence of large isotropic crystals which form within formulations during lyophilization.

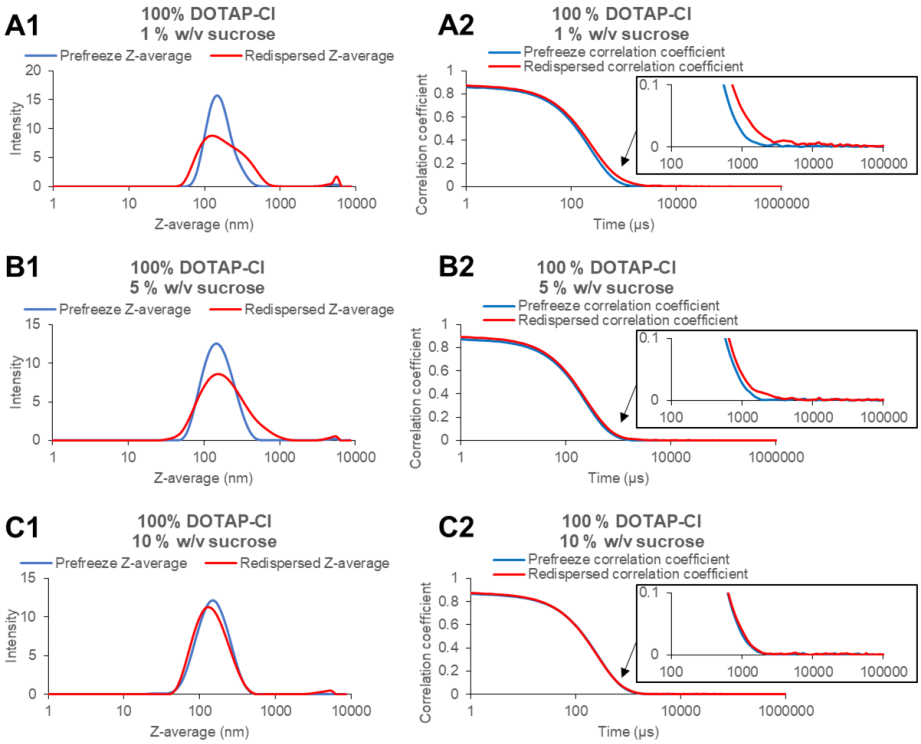

Figure 4.16- Particle size distribution graphs and correlation coefficient graphs before and after freeze drying and redispsersion for 14 wt % tricaprin formulations stabilised by 100 % DOTAP-Cl at 1, 5 and 10 % w/v sucrose. Overall displays how the stability of formulations increases with increasing sucrose concentration.

4.3.3. Cryopreservation of lipid-based formulations at increasing wt % of core material

After establishing 10 % w/v was the best concentration of sucrose for enabling formulations of 14 wt % tricaprin to be freeze dried and redispersed, attention was turned to increasing the wt % of the core material. Here the aim was to determine how the ratio of core material to surfactant at different surfactant compositions may impact stability during the stresses of freezing and drying. Attempts were made to freeze dry and redisperse the 40 wt % formulations of tricaprin at 50/50 25/75 and 0/100 Brij S20/ Lipoid S100 from Chapter 3. Unfortunately, each of the formulations resulted in a glittery effect indicating grade 3- poor redispersibility. Fig.4.17 displays the vast amount of crystals within the formulation post redispersion while employing 10 % w/v sucrose. It was hypothesised by increasing the wt % of the core materials not only may the particle size have increased but the surface coverage may have decreased as shown by the illustration in Fig.4.18. If so then the degree of stabilisation would reduce and thus the barrier to nanoparticle aggregation. This data also suggested despite using a high concentration of 10 % w/v sucrose the lack of stabilisation by the surfactants may dominate. Attempts were made to freeze dry and redisperse using 20 % w/v sucrose however resulted in a similar outcome shown in Fig.4.17. This suggests it may not always be possible to overcome poor redispersibility by increasing the cryo/lyoprotectant concentration.

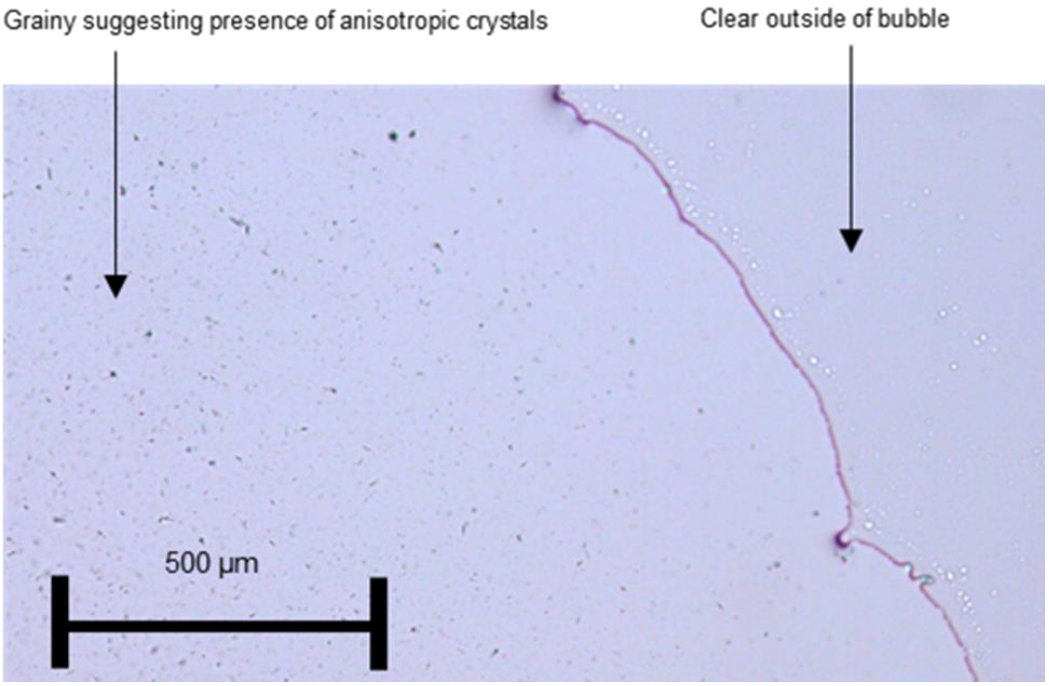

Figure 4.17- Optical microscopy image highlighting the presence of a large amount of aggregates formed upon lyophilization and redispersion of tricaprin at 40 wt % stabilised by 50 % BrijS20 50 % Lipoid S100.

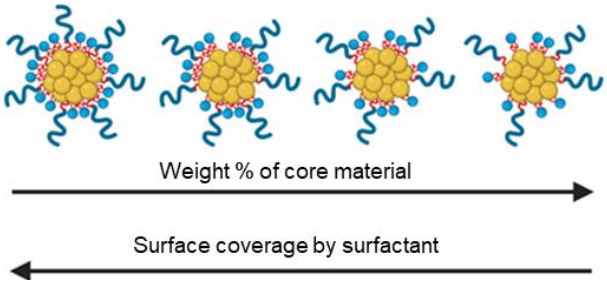

Figure 4.18- Illustration depicting the relationship between wt % of core material and surface coverage by surfactant.

Assuming that particle size remains constant, as the wt% of core material was increased the number of nanoparticles would also increase. Attempts were made to investigate the impact of an increased concentration of particles on redispersion quality, formulations were prepared with four times the mass of both surfactant and core material. In doing so, the mass of tricaprin within the formulation would be equal to that at 40 wt %. In theory by increasing the mass of surfactant as well as the core material the number of nanoparticles would be increased while maintaining surface coverage. Formulations were freeze dried in the presence of 10 % w/v sucrose and assessed for stability upon redispersion. Immediately, there was a clear difference as formulations of blends BrijS20/Lipoid S100 at ratios of 75/25, 50/50, 25/75, 0/100 were given grades of 1,1,2,2 respectively. Note- formulation at 100 % Brij S20 did not produce a stable formulation suitable for freeze drying due to the presence of visible aggregates on Day 0. The DLS data in Fig.4.19 showed how the formulation with surfactant blend 75 % Brij S20 25 % Lipoid S100 appeared to redisperse due to no change in particle size or PDI. While at 50 % Brij S20 50 % Lipoid S100 there was a slight decrease in particle size after redispersion, this trend in diameter reduction from freeze drying was more pronounced as the percentage of Lipoid S100 was further increased in the surfactant composition. It is plausible that the decrease in particle size was due to aggregation of particles resulting in aggregates too large to be detected by the DLS. This hypothesis is supported by the fact formulations lower in Brij S20 which experienced the largest decrease in particle size also were given a grade 2 for redispersion due to an increase in formulation turbidity post redispersion. As the increase in turbidity may be due to greater light scattering caused by the presence of larger aggregates. Nevertheless, the overall redispersion quality has improved compared to 40 wt %, as there was no visible glittery effect for each of the formulations at elevated core material and surfactant concentration. Overall, it was hypothesised an increase the concentration of core material and surfactant increased the number of particles, however due to the particles possessing sufficient stability due to maintaining surface coverage formulations improved in redispersion quality. Furthermore, the decrease in redispersion quality at 40 wt % was likely due to a decrease in surface coverage by surfactant. Going forward the ratio of surfactant to core material was identified as a key parameter impacting formulations ability to redisperse due to the degree of stabilisation provided by both the surfactant composition and surfactant coverage.

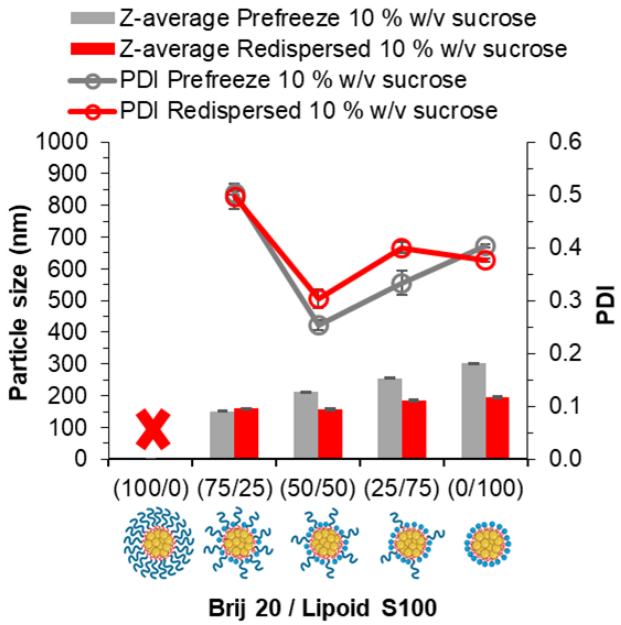

Figure 4.19- Particle size and size distribution obtained by DLS. Formulations with the mass of surfactant and tricaprin quadrupled for an overall of tricaprin at 14 wt % while varied in pegylated/unpegylated lipid surfactant blends on a mass ratio. Data examines how the increased concentration of nanoparticles and ratio of pegylated/unpegylated lipid surfactant determines stability during freeze-drying at 10 % w/v of sucrose.

Attempts were made to freeze dry a lower wt % of core material, 33 % tricaprin were made. Upon initial observation each formulation appeared to redisperse. Grades for each of the formulations redispersions were as follows; 75 % Brij S20 25 % Lipoid S100 – grade 2, 50 % Brij S20 25 % Lipoid S100 –grade 1, 25 % Brij S20 75 % Lipoid S100- grade 1 and 100 % Lipoid S100- grade 2. Although, formulations were graded on appearance to the naked eye as the wt % of core material was increased so did the turbidity as shown in Chapter 3 Appendix Fig.3.1, therefore making redispersion grading more difficult. As a result, samples were analysed by DLS to gain more insight on redispersion quality. Fig 4.20-A displays the particle size and size distribution data for formulations at 33 wt %. Note at 100 % Brij S20 samples were not stable prior to cryopreservation techniques. The data suggests that samples stabilised by 75 % Brij S20 25 % Lipoid S100 displayed a degree of aggregation due to an average increase in particle size by ~ 125 nm. Additionally, the 100 % Lipoid S100 formulation also displayed some aggregation which was shown by a slight increase in particle size, large increase in PDI from ~0.15 to 0.35 and a large decrease in light scattering shown by derived count rate, Fig.4.20-B. This reduction in derived count rate may have been due to the sedimentation of micron-sized particles in the sample. Nevertheless, samples stabilised by 50 % Brij S20 50 % Lipoid S100 and 25 % Brij S20 75 % Lipoid S100 appeared to be stable despite a slight increase in PDI. Analysis of the DLS size distribution and correlation coefficients confirmed the findings shown for the mean diameter and PDI data; 75 % Brij S20 25 % Lipoid S100 and 100 % Lipoid S100 showed aggregation as a result of freeze drying and redispersion. The 75 % Brij S20 25 % Lipoid S100 formulation showed aggregation peaks

on both the particle size distribution graph and the correlation coefficient curve (Fig.4.21-A1 and A2) indicating that exposure to the stresses of freeze-drying had caused aggregation. In addition, at 100 % Lipoid S100 there was a clear change in particle size distribution as well as a shift in the correlation coefficient curve suggesting the presence of aggregates (Fig.4.21- D1 and D2). Meanwhile, both formulations 50 % Brij S20 50 % Lipoid S100 and 25 % Brij S20 75 % Lipoid S100 appear to suffer from slight aggregation but to a much lower extent (Fig.4.21- B1, B2, C1 and C2). As a result, formulations containing surfactant compositions of 50 % Brij S20 50 % Lipoid S100 and 25 % Brij S20 75 % Lipoid S100 were identified as the formulations with highest potential going forward due to high wt % of core material relative to surfactants and may be freeze dried and redispersed with few aggregation events.

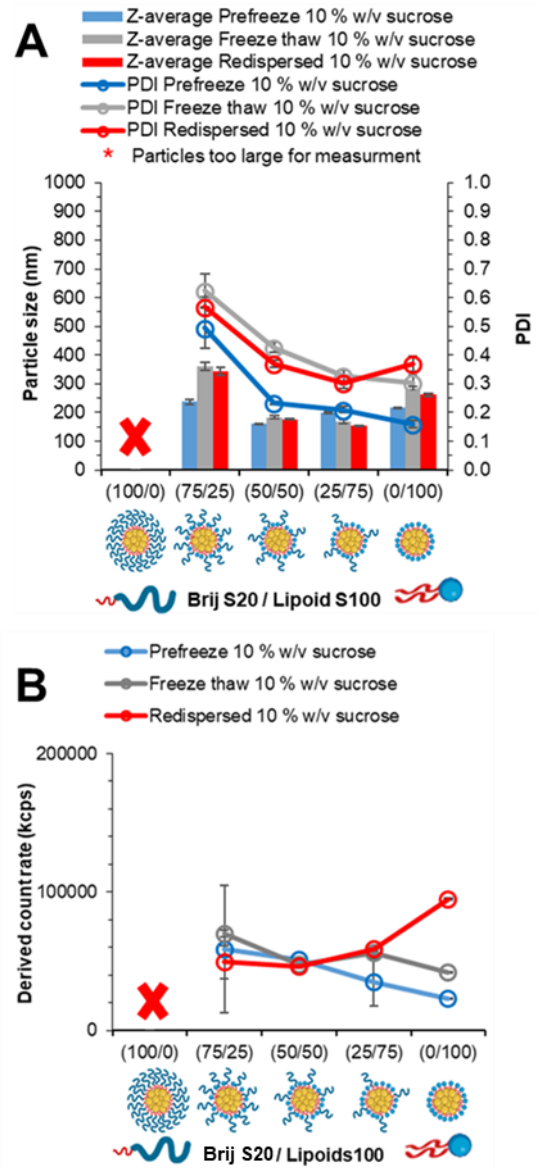

Figure 4.20- Particle size, size distribution and derived count rate data obtained by DLS.A) Size and size distribution. B) Derived count rate. Formulations of tricaprin at 33 wt % varied in pegylated/unpegylated lipid surfactant blends on a mass ratio. Data examines how the ratio of pegylated/unpegylated lipid surfactant determines stability during freeze-thaw and freeze-drying at 10 % w/v of sucrose. Measurements made at a fixed position of 4.65 mm

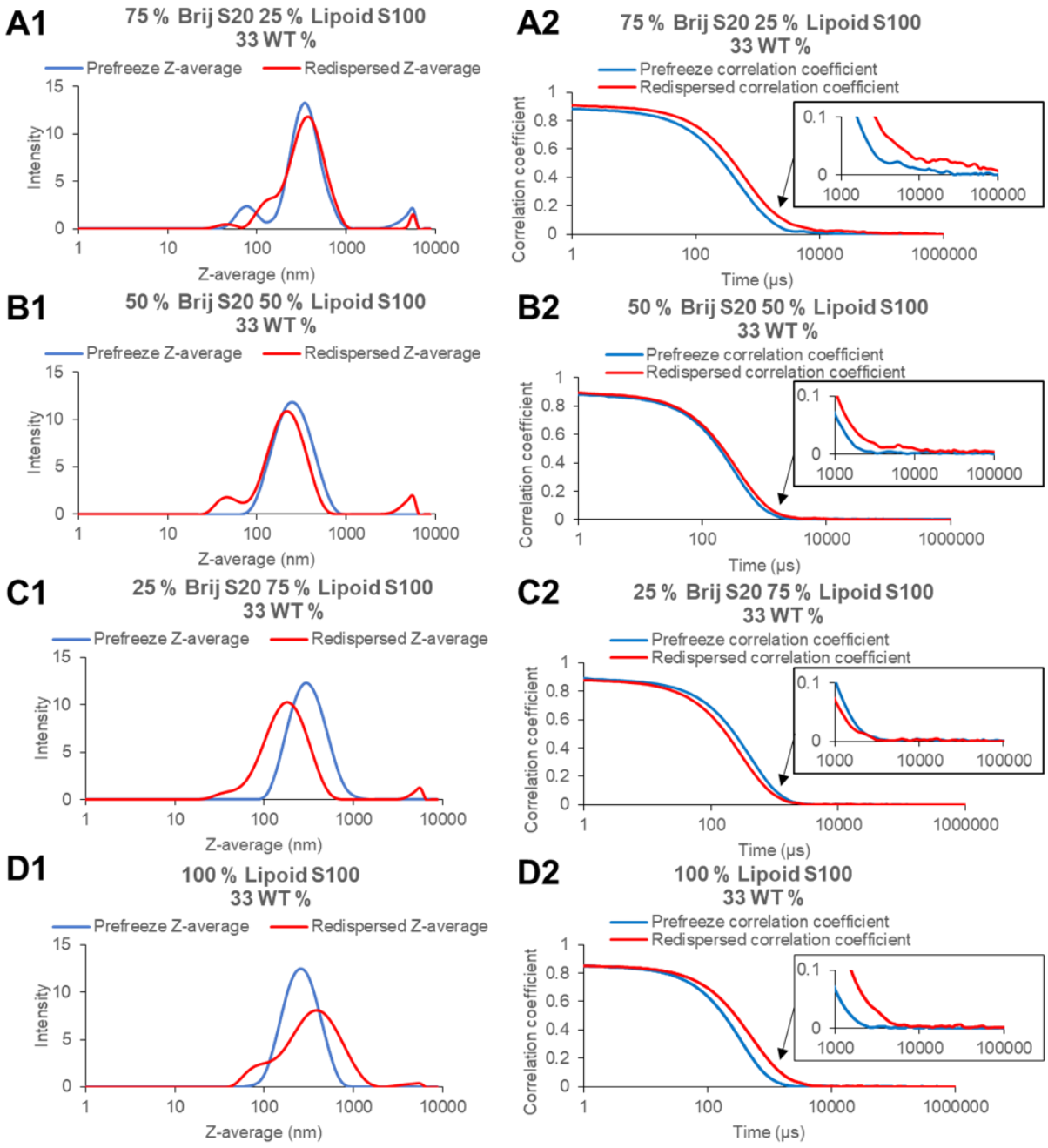

Figure 4.21- Particle size distribution graphs and correlation coefficient graphs before and after freeze drying and redispsersion for 33 wt % tricaprin formulations stabilised by 75% Brij S20 25 % Lipoid S100 (A1 and A2), 50 % Brij S20 50 % Lipoid S100 (B1 and B2), 25 % Brij S20 75 % Lipoid S100 (C1 and C2) and 100 % Lipoid S100 (D1 and D2) at 10 % w/v sucrose. Overall displays how the stability of formulations increases with increasing sucrose concentration.

4.3.4. Cryopreservation of lipid-based formulations containing dodecyl prodrug

The conditions for freeze drying and formulation surfactant combination that showed promise in redispersion of a high wt % of core material lipid nanoparticle formulation were employed in a formulation containing active material. The dodecyl prodrug developed in Chapter 2 was blended at ratios of 50/50 and 75/25 (dodecylprodrug/tricaprin) for an overall 33 wt % core material. Fig.4.22 displays the particle size and size distribution for each of the formulations over 28- day period suggesting sufficient stability in aqueous conditions due to no obvious deviation in values. Each of the formulations were taken forward and freeze dried and redispersed and assessed for redispersion quality. In doing so any effects of blending the core material on the formulation properties and ability to withstand the stresses of freeze drying would be revealed. In a similar manner to formulations in 4.3.2. observing any changes in formulation appearance was difficult as the formulations were already turbid, Fig.4.23 due to the large degree of light scattering by the enhanced concentration of particles. Nevertheless, none of the formulations tested showed visible particles or anisotropic crystals. As a result, we proceeded to characterise each formulation by DLS.

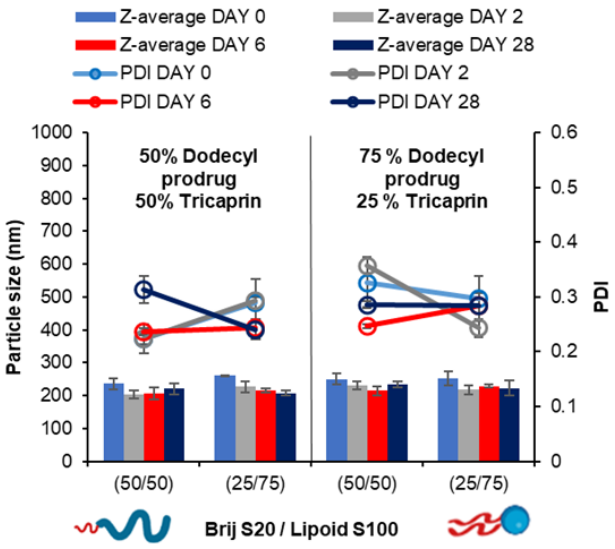

Figure 4.22- Particle size and size distribution obtained by DLS. Formulations of dodecyl prodrug/tricaprin blends at an overall 33 wt % varied in pegylated/unpegylated lipid surfactant blends on a mass ratio. Data examine stability of each formulation in aqueous solution over a 28-day period.

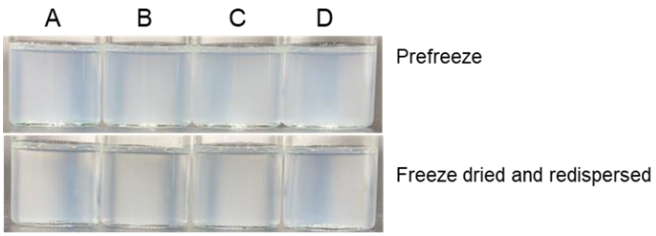

Figure 4.23- Photographs of each formulation containing various blends post redispersion. A) 50 % dodecyl prodrug 50 % tricaprin 50 % Brij S20 50 % Lipoid S100, B) 50 % dodecyl prodrug 50 % tricaprin 25 % Brij S20 75 % Lipoid S100, C) 75 % dodecyl prodrug 25 % tricaprin 50 % Brij S20 50 % Lipoid S100 and D) 75 % dodecyl prodrug 25 % tricaprin 25 % Brij S20 75 % Lipoid S100.

Each formulation was characterised by DLS, Fig.4.24-A displays particle size and polydispersity index while Fig.4.24-B displays derived count rate for each formulation before and after freeze-drying. The data from each figure further suggested that each of the formulations redispersed at grade 1 as there was no clear increase in particle size or derived count rate. On the other hand, each formulation independent of surfactant or core composition experienced an increase in PDI except for that of 75 % Dodecyl prodrug 25 % tricaprin 50 % Brij S20 50 % Lipoid S100, Fig, 4.24-A. Fig.4.25 displays overlays of particle size distribution graphs and correlation curves for each of the formulations before and after freeze drying and redispersion, (Fig.4.25-A and C with a surfactant composition of 50 % Birj S20 50 % Lipoid S100, B and D 25 % Brij S20 75 % Lipoid S100; A and B with a core composition 50 % dodecyl prodrug 50 % tricaprin, C and D 75 % dodecyl prodrug 25 % tricaprin). Each again support redispersion. On the contrary to reports by Schwarz *et al*.[67] it appears from the data in Fig.4.23-4.25 the inclusion of drug/prodrug does not always impair the redispersion quality. Although this may be due to similarities between tricaprin and dodecyl prodrug such as molecular weight and LogP causing the resultant formulations are also relatively similar, thus explaining comparable redispersion quality.

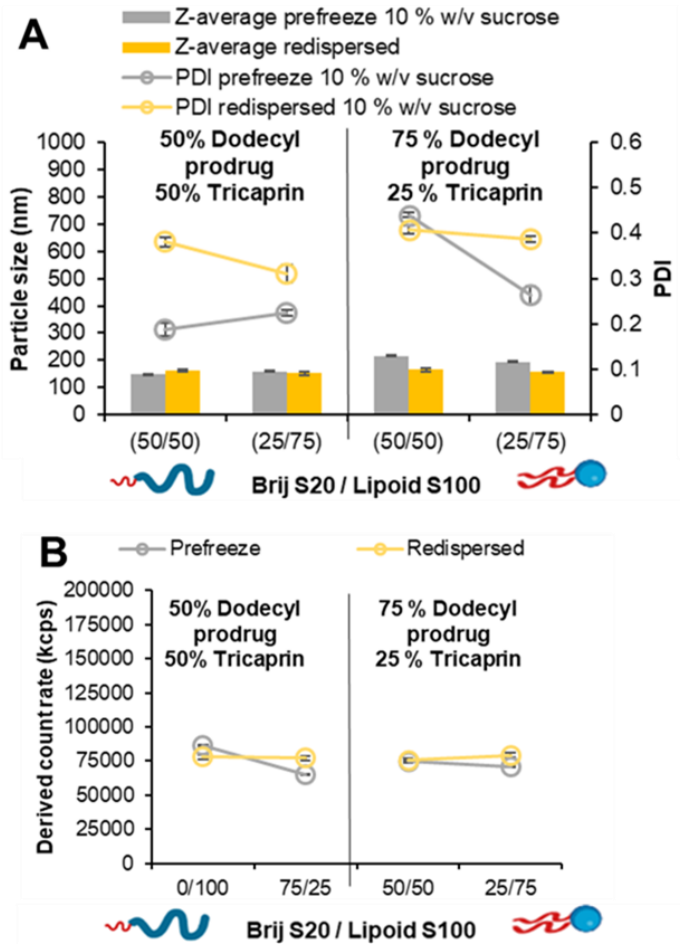

Figure 4.24- Particle size, size distribution and derived count rate data obtained by DLS. Formulations of dodecyl prodrug/tricaprin blends at an overall 33 wt % varied in pegylated/unpegylated lipid surfactant blends on a mass ratio. Data examine stability of each formulation against the stresses of freeze drying at 10 % w/v sucrose. A) Particle size and size distribution. B) Derived count rate measurements at a fixed measurement position of 4.65 mm.

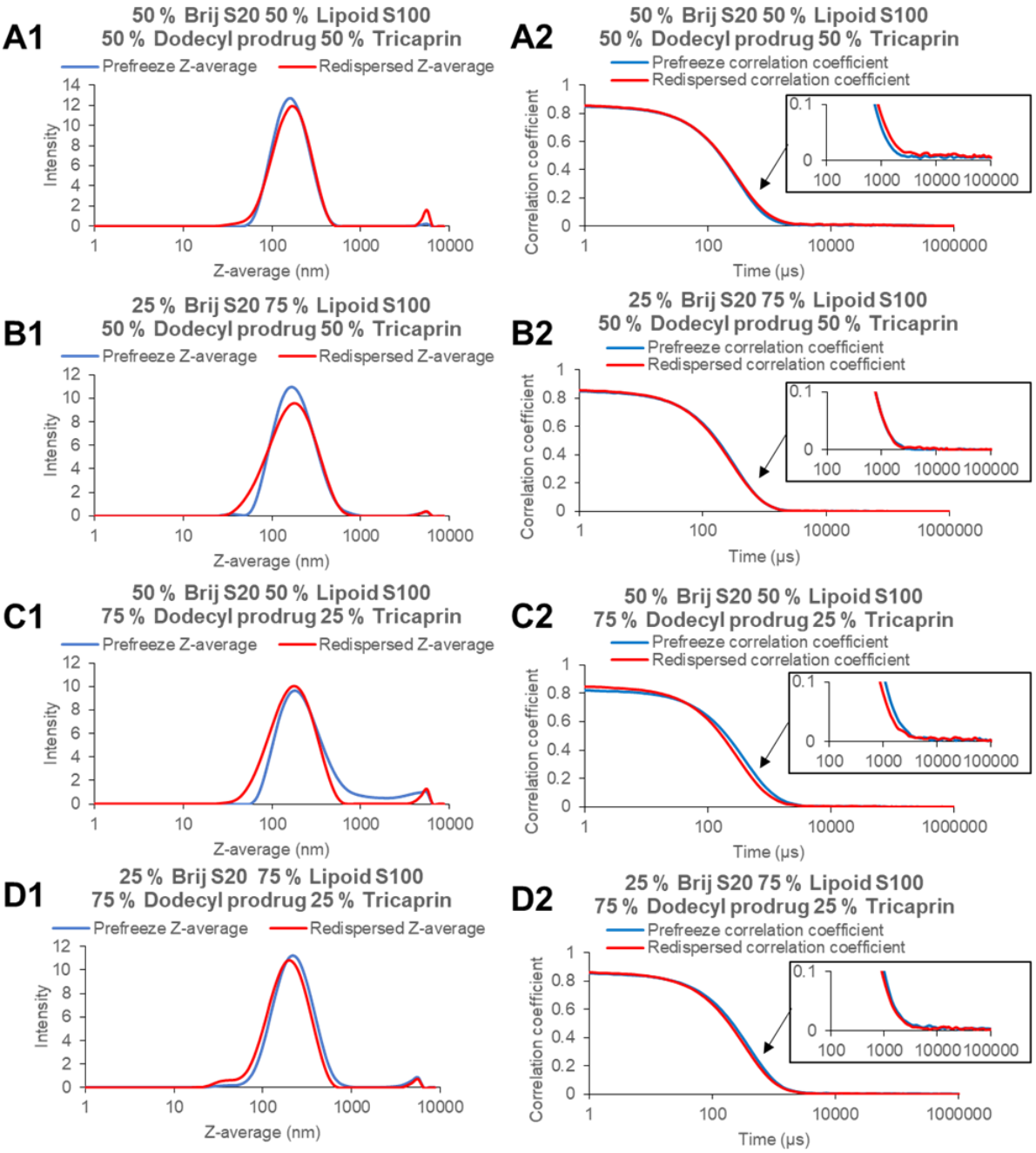

Figure 4.25- Particle size distribution graphs and correlation coefficient graphs before and after freeze drying and redispsersion for 33 wt % blends of dodecyl prodrug and tricaprin in the presence of 10 % w/v sucrose. 50 % dodecyl prodrug 50 % tricaprin formulations stabilised by 50% Brij S20 50 % Lipoid S100 (A1 and A2), 25 % Brij S20 75 % Lipoid S100 (B1 and B2). Blends of 75 % dodecyl prodrug 25 % tricaprin stabilised at 50 % Brij S20 50 % Lipoid S100 (C1 and C2) and 25 % Brij S20 75 % Lipoid S100 (D1 and D2). Overall supports redispersion.

The formulation containing dodecyl prodrug at the elevated wt % of 33 % that had successfully been redispersed were then examined by cryo-SEM. Fig. 4.26-A and 4.26-B display cryoSEM images taken of the formulation prior to freeze drying. Fig.4.26-A clearly displays the formation of a freeze-dried cake while Fig.4.26-B reveals the presence of nanoparticles on the surface of the cake. Furthermore, Fig.4.26-C reveals a similar cake formation by the same formulation after undergoing the process of freeze-drying and redispersion. While, Fig.4.26-D visualises nanoparticles on the surface of the cake. The visualisation of nanoparticles in Fig.4.26-D therefore suggests nanoparticles were stable against the stresses of freeze drying and redispersion. The measurement of 150 particles from each cryo-SEM image revealed average particle diameters of 94 and 81 nm and standard deviations of 28 and 22 for prefreeze dry and redispersed retrospectively, appendix Fig.4.4. The data obtained from the microscopy images was deemed in agreement with the data obtained by DLS- (216 and 166 nm before and after freeze drying) after factoring in the solvent layer which adheres to the surface of nanoparticles in solution thus making particles appear bigger than when measured by microscopy.

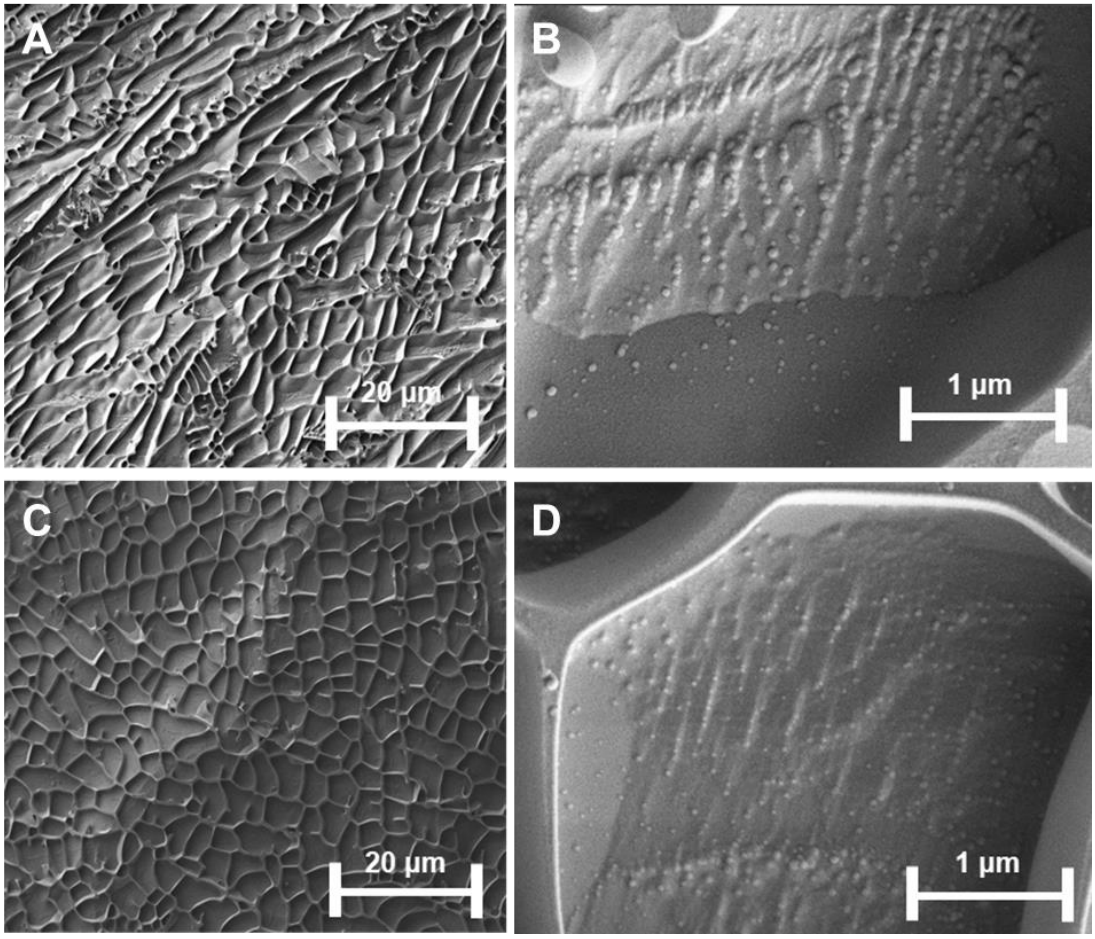

Figure 4.26- CryoSEM images of the formulation at 33 wt % with a core composition of 75 % dodecyl prodrug 25 % Lipoid S100 and a surfactant composition of 50 % Brij S20 50 % Lipoid S100, while also in the presence of 10 % w/v sucrose. Images A and B are images of the formulation taken prior to freeze drying and redispersion, while C and D are after freeze drying and redispersion. Images A and C highlight the network structure formed upon drying, while B and D clearly display the presence of nanoparticles embedded within the network, thus support successful redispersion of nanoparticles.

4.4. Conclusions

In conclusion, the type of surfactant and surfactant composition plays a big role in the stability of formulations against the stresses of cryopreservation techniques such as freeze thaw and freeze drying/lyophilization. As formulations containing the cationic unpegylated lipid surfactant DOTAP-Cl rather than the zwitterionic unpegylated lipid surfactant Lipoid S100 appear to maintain the cake structure more efficiently, resulting in higher redispersion quality. Although, generally formulations stabilised by more pegylated lipid surfactant appeared to maintain stability over those higher in unpegylated lipid surfactant. As a result, suggests the steric stabilisation provided by Brij S20 was much more efficient at stabilising formulations than the electrostatic stabilisation provided by DOTAP-Cl. In all formulations the addition of more sucrose resulted in improved cake formation/stability. As a result, it was possible to enhance formulation stability and quality against the stresses of freeze thaw and freeze drying with the aid of a cryoprotectant and/or lyoprotectant such as sucrose.

On the contrary to reports by Schwarz *et al*.[67] the inclusion of drug/prodrug does not always impair the redispersion quality. Furthermore, it is likely due to the similarities between tricaprin and dodecyl prodrug the resultant formulations are also relatively similar, thus explaining comparable redispersion quality. As a result, the key findings of this work are the successful exploration of conditions to enable a lipid nanoparticle formulation at 33 wt % tricaprin to be freeze dried and redispersed were achieved. In addition, these conditions were successfully applied to a formulation which had blended dodecyl prodrug with tricaprin in the core at a ratio of 75/25.

Aspects such as method of freezing and method of redispersion have been investigated in literature although there is a lack of understanding of how aspects of the formulation may impact its stability against the stresses of freezing and drying. Overall, this work demonstrates a systematic approach to gain necessary insight and understanding that was lacking in literature of how the different types and blends of surfactants used in lipid nanoparticle formulations impact formulation stability against the stresses of cryopreservation methods such as freeze drying. Furthermore, demonstrates how the ratio of core material to surfactant, surfactant composition, and cryoprotectant concentration may be tuned to develop a high drug loading formulation which is able to be freeze dried and redispersed which may improve the long-term stability of formulations upon storage. This work may be employed as a guide for anyone attempting to produce a lipid nanoparticle formulation with the goal of it being successfully cryopreserved such as mRNA containing lipid nanoparticles.

4.5. Future work

It would be interesting to further expand on the work in this study by investigating various chain lengths of pegylated lipid surfactants; would an increase in PEG chain length would result

in sufficient steric stabilisation? This might offer the potential to reduce the cryoprotectant/lyoprotectant concentration required in order to maintain formulation stability during cryopreservation techniques such as freeze drying and/or enable formulations of higher wt % to be freeze dried and redispersed. Furthermore, other types of cryoprotectants/lyoprotectants may also be explored.

4.6. Experimental

Materials

Dodecyl prodrug/drug analogue was synthesised as shown in chapter 2. Brij S20 and deuterated solvent D_2O were obtained by Sigma Aldrich, while tetrahydrofuran was obtained from Fisher Scientific. Lipoid S100 was purchased from Lipoid and used as received. DOTAP-Cl was kindly gifted by Lipoid and used as received. Tricaprin was purchased from Tokyo chemical industry and used as received.

Methods

Preparation of lipid nanoparticle formulations varying in pegylated lipid and unpegylated lipid Lipoid S100

Method adopted for nanoparticle formulation was nanoprecipitation. For the aqueous phase, the surfactant Brij S20 was dissolved to prepare a 1000 ml stock solution in distilled water (1 mg/ml) and left overnight at 21 degrees Celsius under mechanical stirring (300 rpm). Portions of the stock solution were taken and potentially diluted further with distilled water, compositions shown by Table 4.3.

For the organic phase stock solutions of tricaprin (4 mg/mL) and Lipoid S100 (24mg/mL) were prepared in tetrahydrofuran (THF). Compositions are shown by Table 4.4. The organic phase was charged dropwise into the vortex of the aqueous phase contained in a 40 mL vial while mechanically stirring (800 rpm). To ensure consistency in time of injection the shot was charged by removing the plunger of a clamped syringe resulting in a steady flow through the hypodermic needle. The combined mixture was left stirring to allow evaporation of tetrahydrofuran over 2 days at a room temperature (~21 °C) in a fume cupboard with an average air velocity of 0.35 m/s. Samples were then stored at 21 °C.

Table 4.3- Aqueous phase composition depending on surfactant blend.

Surfactant composition	Volume Brij S20 stock solution (mL)	Volume distilled water (mL)	Total volume aqueous phase (mL)
100 % Brij S20	24	0	24
75 % Brij S20 25 % Lipoid S100	18	6	24
50 % Brij S20 50 % Lipoid S100	12	12	24
25 % Brij S20 75 % Lipoid S100	6	18	24
100 % Lipoid S100	0	24	24

Table 4.4- Organic phase composition depending on surfactant blend.

Surfactant composition	Volume tricaprin stock solution (mL)	Volume Lipoid S100 stock solution (mL)	Volume neat THF (mL)	Total volume organic phase injectable shot (mL)
100 % Brij S20	1	0	1	2
75 % Brij S20 25 % Lipoid S100	1	0.25	0.75	2
50 % Brij S20 50 % Lipoid S100	1	0.5	0.5	2
25 % Brij S20 75 % Lipoid S100	1	0.75	0.25	2
100 % Lipoid S100	1	1	0	2

Preparation of lipid nanoparticle formulations varying in pegylated lipid and unpegylated lipid Lipoid S100 at elevated wt %

Formulations prepared in the same way as at 14 wt% although the concentration of the tricaprin stock solution was increased i.e. (33 wt%, 12 mg/mL; 40 wt %, 16 mg/mL)

Preparation of lipid nanoparticle formulations varying in pegylated lipid and unpegylated cationic lipid DOTAP-Cl

Same as with Lipoid S100 although concentration of unpegylated lipid stock solution was adjusted for an equal mol % comparison.

Preparation of lipid nanoparticle formulations varying in pegylated lipid and unpegylated lipid Lipoid S100 at quadruple the concentration of surfactant and core material

Same as with Lipoid S100 although concentration of the Brij S20, unpegylated lipid and tricaprin stock solutions were all quadruple.

Preparation of lipid nanoparticle formulations varying in pegylated lipid and unpegylated lipid Lipoid S100 at elevated wt % varying in dodecyl drug analogue loading

General preparation method the same although composition of organic phase adjusted see Table 4.5 for example of blends of tricaprin and dodecyl drug analogue at 33 wt %. Stock solution concentrations; tricaprin (12 mg/mL) and dodecyl drug analogue (12 mg/mL).

Table 4.5- Organic phase composition depending on blends of tricaprin, dodecyl drug analogue as well as surfactant blends

Core composition	Surfactant composition	Volume tricaprin stock solution (mL)	Volume dodecyl drug analogue stock solution (mL)	Volume Lipoid S100 stock solution (mL)	Volume neat THF (mL)	Total volume organic phase injectable shot (mL)
50 % tricaprin 50 % dodecyl drug analogue	50 % Brij S20 50 % Lipoid S100	0.5	0.5	0.5	0.5	2
50 % tricaprin 50 % dodecyl drug analogue	25 % Brij S20 75 % Lipoid S100	0.5	0.5	0.75	0.25	2
25 % tricaprin 75 % dodecyl drug analogue	50 % Brij S20 50 % Lipoid S100	0.25	0.75	0.5	0.5	2
25 % tricaprin 75 % dodecyl drug analogue	25 % Brij S20 75 % Lipoid S100	0.25	0.75	0.75	0.25	2

Cryopreservation methods

Freeze thaw 2 ml of each sample was mixed 1:1 with sucrose stock solution i.e. for 1, 5 or 10 % w/v sucrose; 2 ml of formulation with mixed with 2 ml of 2, 10 or 20 % w/v sucrose stock solution in a 12 ml vial. Vials were then placed into liquid nitrogen for ~5 minutes until completely frozen. For freeze thaw samples were allowed to thaw out at ~ 21 degrees. For freezedrying samples were then immediately freezedried in a VirTis Bench Top K freeze dryer (SP Scientific, Ipswich UK). Condenser temperature was set to – 100 °C and vacuum of < 40 µbar. All samples remained in the freeze dryer for 72 hours prior to immediate reconstitution in distilled water.

Redispersion method

Upon reconstitution in distilled water. Samples were then redispersed using a Vortex-Genie 2 on setting 5 for 2 minutes.

Analytical techniques

Dynamic light scattering (DLS) and Zeta potential

Samples were analysed by DLS using The Malvern Zetasizer Nano S DLS obtain a Z-average and size distribution (PDI) and zeta potential of nanoparticle dispersion. 2 ml of each sample was measured in standard 3 ml fluorimeter cuvettes with a pathlength of 10 mm. All measurements were carried out at 25 °C with a fixed backscattering angle of 173° using automated setting. Each sample was measured once although formulations were done in triplicate. Zeta potential was also measured using Malvern zetasizer Nano S. Samples were measured using automated settings and samples were measured in triplicate in a Malvern zetasizer nano series disposable folded capillary cell. All measurements were carried out at 25 °C.

For prefreeze and redispersion measurements the measurement position was fixed at 4.65 mm.

Scanning electron microscopy (SEM)

Freeze dried materials were loaded onto an aluminium SEM specimen stub (12.5 mm diameter) using carbon adhesive tab before using aluminium solution to coat the rim of the carbon tab. Samples were then left overnight for the aluminium coating to dry. This was followed by coating with gold (EMITECH K550X) with a deposition current of 25 mA for 100 s before imaging. The morphology of the freeze-dried materials was then investigated using a Hitachi S-4800 FE-SEM at 2 and 5 kV.

Cryogenic scanning electron microscopy (cryo-SEM)

Specimens prepared by freezing a small volume of sample between two brass rivets, which are plunged into slushed liquid nitrogen. Rivets transferred to a brass loading shuttle under liquid nitrogen and transferred under a nitrogen atmosphere to a preparation stage cooled to -120 °C. Anti-contaminator in preparation stage run at -190 °C. Fracture surface created in frozen specimen by pushing-off the upper rivet from the one held in the shuttle (using a liquid nitrogen cooled knife). Fracture surface coated with Pt in the preparation chamber, to make it conductive and specimen transferred to a cooled stage in the FIB/SEM (at -160 °C, with an anti-contaminator held at -190°C).

Specimens photographed using an in-chamber secondary electron detector Everart Thornley using either 1.5 or 10 KeV and a beam current of 15 pA.

4.7. Appendix

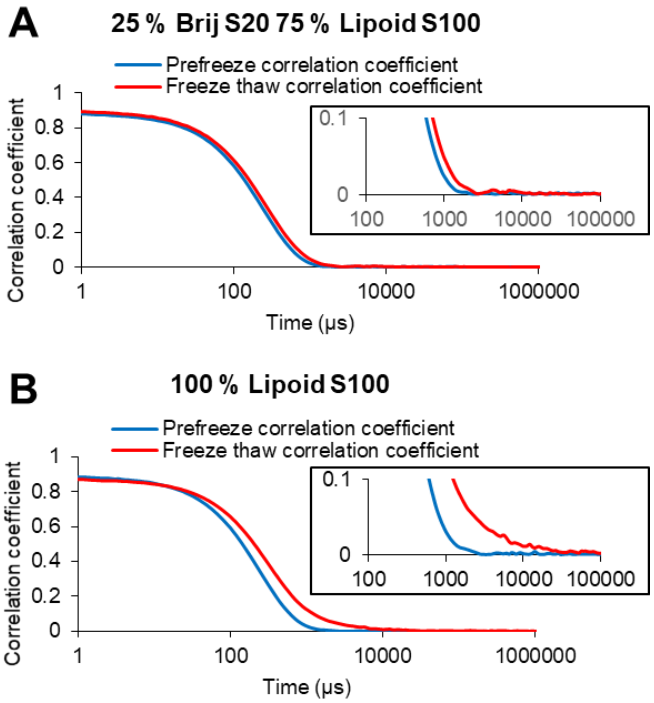

Appendix Figure 4.1- Correlation coefficient data obtained by DLS. Overlay of graphs before and after freeze thaw for 14 wt % tricaprin formulations stabilised by 75 % Brij S20 25 % Lipoid S100 (A), 100% Lipoid S100 (B). Note no cryoprotectant was present.

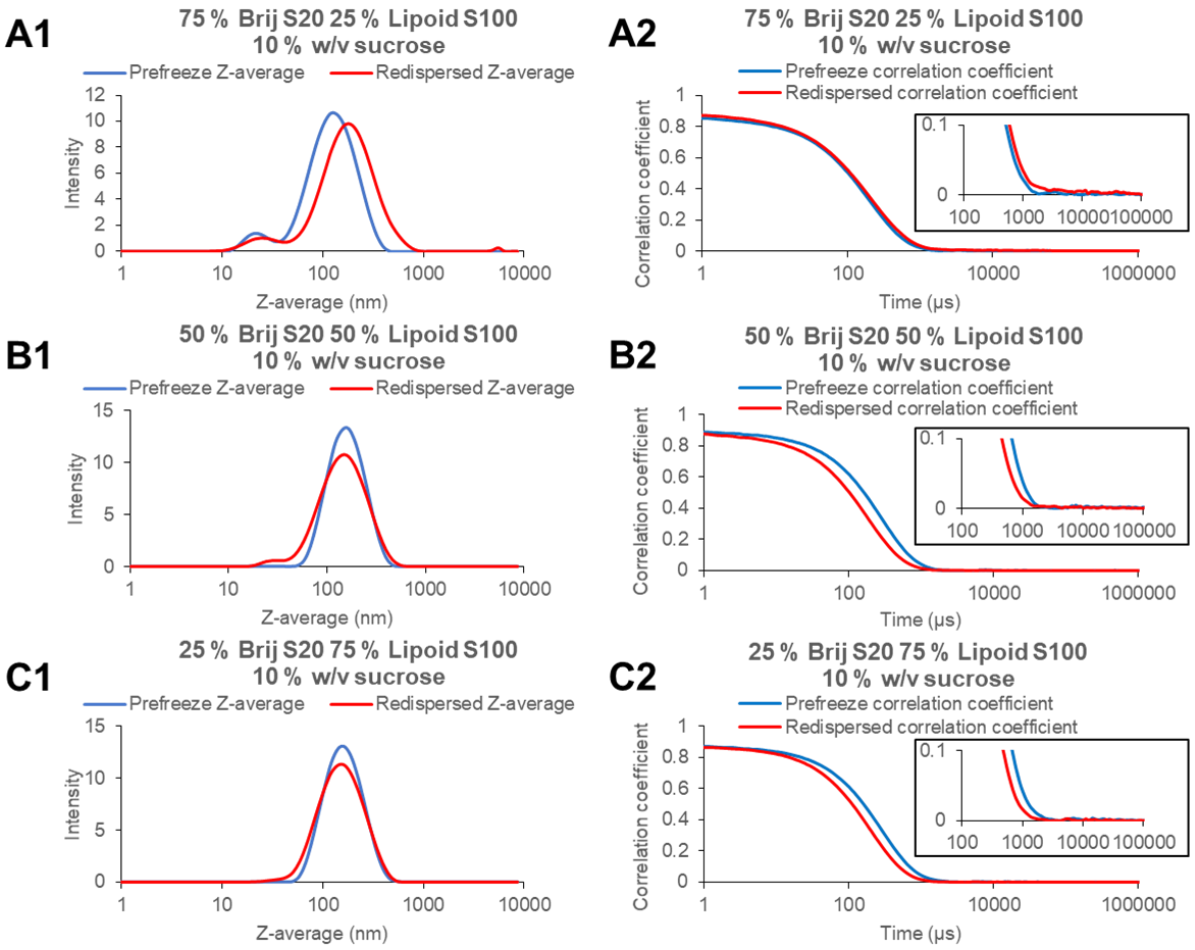

Appendix Figure 4.2- Particle size distribution graphs and correlation coefficient graphs before and after freeze drying and redispsersion for 14 wt % tricaprin formulations stabilised by 75 % Brij S20 25 % Lipoid S100 (A), 50 % Brij S20 50 % Lipoid S100 (B), 25 % Brij S20 75 % Lipoid S100 (C) at 10 % w/v sucrose.

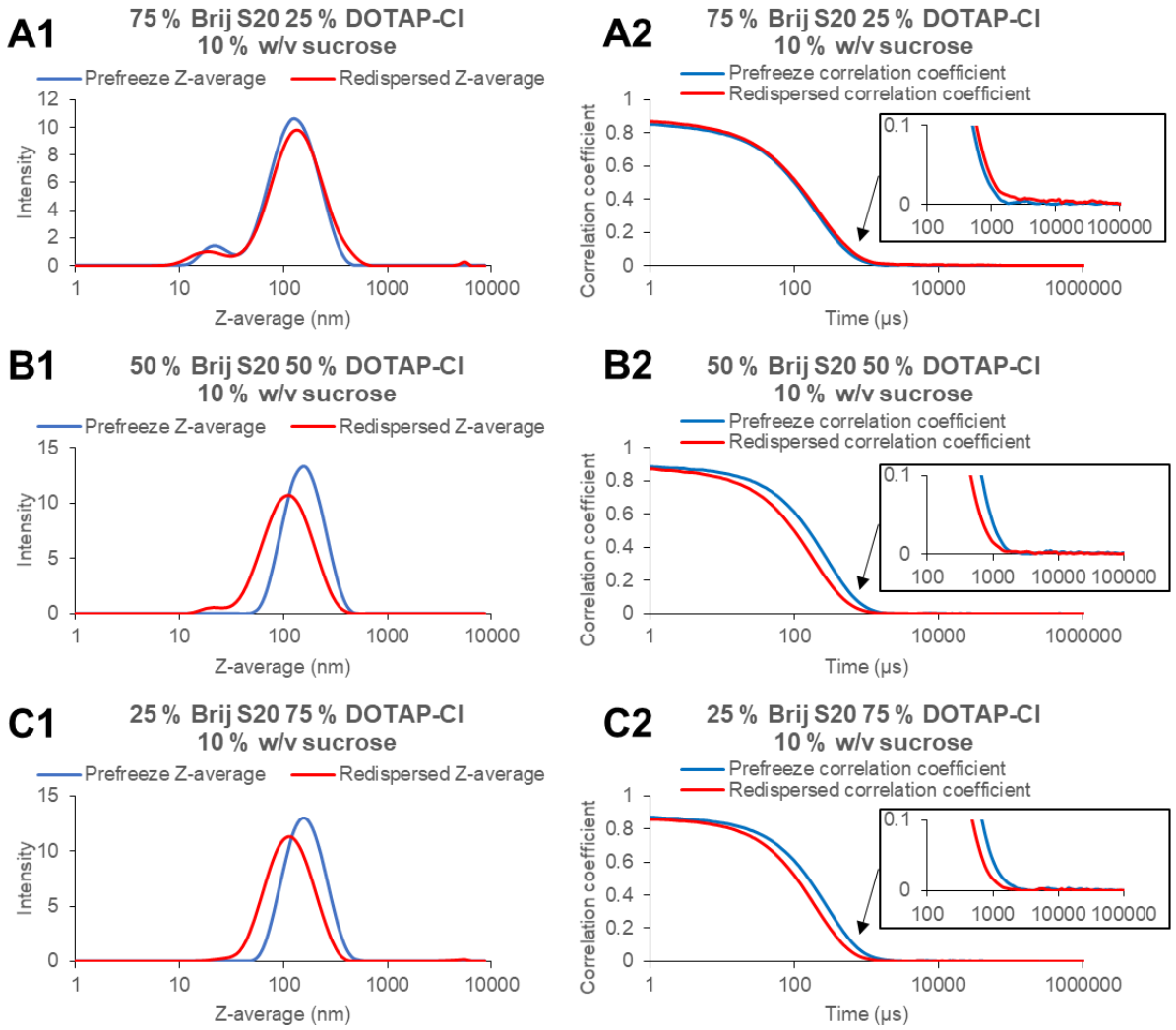

Appendix Figure 4.3- Particle size distribution graphs and correlation coefficient graphs before and after freeze drying and redispsersion for 14 wt % tricaprin formulations stabilised by 75 % Brij S20 25 % DOTAP-Cl (A), 50 % Brij S20 50 % DOTAP-Cl (B), 25 % Brij S20 75 % DOTAP-Cl (C) at 10 % w/v sucrose.

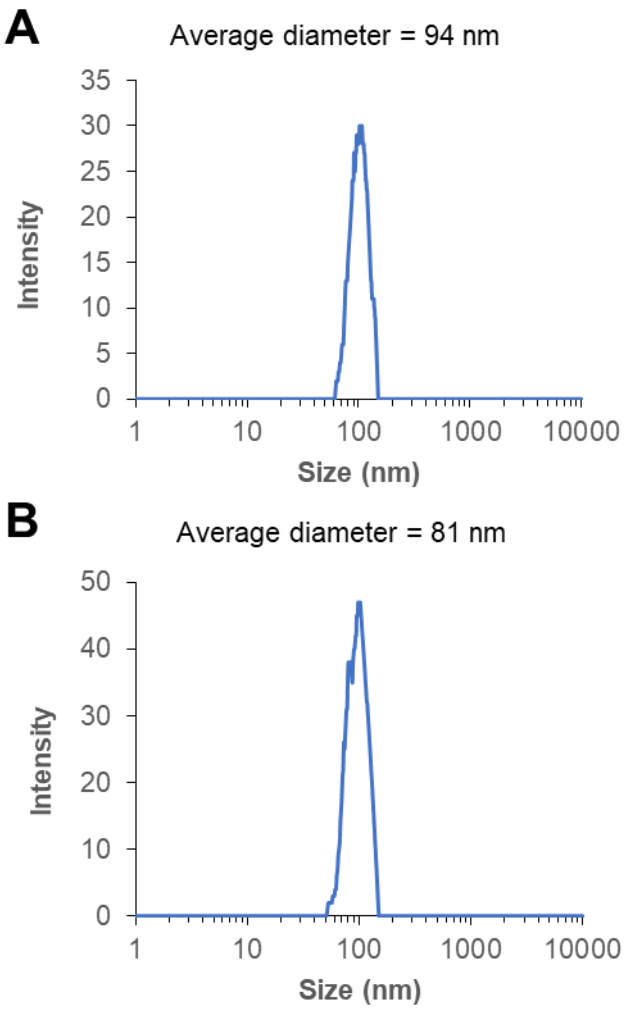

Appendix Figure 4.4- Size distribution graphs using data calculated by ImageJ for the formulation with a core at 33 wt % and composition of 50 % dodecyl prodrug 50 % tricaprin, while a surfactant composition of 50 % Brij S20 50 % Lipoid S100; A) Pre-freeze drying. B) Freeze dried and redispersed. Measured 100 nanoparticles per image and a bin size of 1

CHAPTER 5

Prodrug activation by enzymatic cleavage

Chapter 5 Prodrug activation by enzymatic cleavage

5.1. Introduction

As previously suggested by Zhu *et al*. and Hogarth *et al*., drugs with a LogP greater than ~ 11 may be formulated to allow stable nanoparticle formulations to be produced.[33,149] Furthermore, it has been possible to use a prodrug synthesis approach to chemically modified drugs with a low LogP, altering their physical properties with the ultimate aim of producing lipid-based nanoparticle formulations of high stability and enhanced drug loading.[149] The benefits of prodrugs also include potential to improve the pharmacokinetic properties of drugs.[51,53]

The data from Chapter 3 also suggested that drug loading of lipid nanoparticles may be further enhanced by investigating various types of surfactant blends. Formulations of tricaprin and a dodecyl prodrug stabilised by a blend of the pegylated lipid Brij S20 and the unpegylated lipid surfactant Lipoid S100 were demonstrated with an overall combined wt % of tricaprin and dodecyl prodrug of 40 % relative to the surfactants. In addition, as shown in Chapter 4, similar formulations at 33 wt % of tricaprin and dodecyl prodrug appear to be stable against the stresses of freezing and drying during cryopreservation, allowing the formulation to be successfully freeze dried and redispersed. Although, in order for a modified drug to function as a prodrug, the prodrug must be able to revert back to release the drug. As a result, during the design of prodrugs it is imperative to consider how the prodrug may be activated to release the drug once exposed to physiological conditions *in vivo*.[17] Typically this is first tested is by first exposing prodrug formulations to physiological conditions *in vitro*.[17,54] A study by Shi *et al*. has also demonstrated how the prodrug strategy of irinotecan conjugated to cholesterol was employed to allow the formulation of the prodrugs within liposomes before testing *in vitro*. Results revealed that the formulation could successfully release drug over time at physiological conditions *via* UV detection.[54] Furthermore, the rate of drug release was dependant on the presence of porcine liver esterase enzyme. Hobson *et al*. previously demonstrated how the release of drug may be monitored by HPLC whereby the UV signal from the drug is quantified and compared to a standard calibration curve in order to calculate the concentration of drug at various time points.[17] Overall, prodrugs appear to be a potential solution for many therapeutic drugs which face challenges during formulation or biological barriers once inside the body.

5.2. Chapter Aims

The aims of this study were to employ the strategies developed of previous chapters 2, 3 and 4 to develop of formulation of dodecyl prodrug and reveal the stability of the prodrug at physiological conditions as well as in the presence of enzyme and monitor any release of drug over time.

In order to achieve this goal, the dodecyl prodrug from Chapter 2 was formulated using the knowledge from Chapter 3 surrounding surfactant compositions to develop a formulation of high drug loading. The selected formulation was then freeze dried using the parameters defined by Chapter 3 and redisperse into phosphate buffered saline (PBS), Fig. 5.1-A. 0.1 M PBS was selected as the redispersion media in order to mimic physiological salt conditions within the body. Furthermore, the formulation was monitored for release at physiological temperature of 37 °C, as well as in the presence and absence of enzyme porcine liver esterase, Fig.5.1-B. It was hypothesised upon cleavage of the carbamate ester and carbonate ester bonds the dodecyl prodrug would degrade to release dodecanol, carbon dioxide and the drug lamivudine. The same ratio of enzyme to prodrug in the experiment (98,100 units of porcine liver esterase per mM of prodrug) was employed as used by Shi *et al*. Furthermore, aliquots were taken over various time points and analysed by HPLC to reveal any release of drug, Fig.5.1-B.

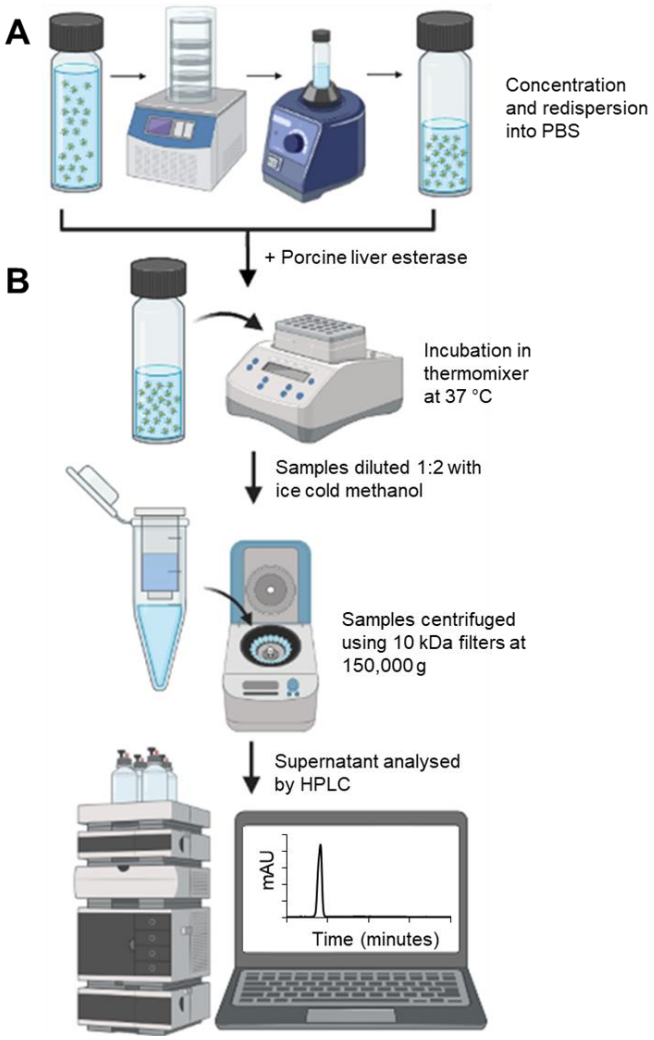

Figure 5.1- Schematic overview illustrating the various steps of the following study from employing freeze drying for concentrating and redispersing sample in PBS to the drug release experiment monitored by HPLC. A) Preparation of formulation which is freeze dried and redispersed into 0.1 M PBS. B) Prodrug activation experiment at physiological conditions with and without porcine liver esterase, samples taken and centrifuged in preparation for HPLC analysis.

5.3. Result and Discussion

5.3.1. Concentration of selected formulation

The formulation with a core composition of 75 % dodecyl prodrug 25 % tricaprin and a surfactant composition of 50 % Brij S20 50 % Lipoid S100 was selected due to its ability to redisperse back to its initial concentration with ease as well as containing a high loading of drug, Chapter 4.3.4. The formulation was prepared and taken forward to trial redispersion into a smaller volume ($1/8^{th}$ of original) while also redispersing into 0.1 M PBS rather than water as 0.1 M PBS was the buffer solution chosen for the *in vitro* experiments to mimic physiological conditions. Unfortunately, due to the high concentration of sucrose (80 % w/v) samples could no longer obtain accurate DLS measurements. Although, figures 4.28-4.30 of Chapter 4 have shown upon dilution samples may be analysed by DLS and indicated successful redispersion. A similar approach has been demonstrated by Hobson *et al*. whereby nanoparticle formulation prepared by nanoprecipitation were dried and redispersed into a smaller volume to concentrate the formulation for use as a long acting delivery injectable. In addition, another study by Hobson *et al*. examined candidates by their ability to redisperse at a dilute and standardised concentration of 1 mg mL^{-1}.[154]

Furthermore, upon redispersion into 0.1 M PBS samples were subjected to visual inspection and there were no signs of aggregates or a glittery effect which had been previously identified as signs of poor redispersion quality, Fig.5.2. The formulation had increased in turbidity, although it is plausible to assume this may be due to the increased concentration of particles resulting in an increased degree of light scattering which had previously been witnessed in Chapter 3 Appendix fig.3.1. As a result, it was deemed there were no clear signs of aggregation and the study progressed with the chosen formulation and strategy.

Figure 5.2- Photo graphs of 75 % dodecyl prodrug/25 % tricaprin stabilised by 50 % Birj S20 50 % Lipoid S100 which has been freeze dried with an initial concentration of 10 % w/v sucrose before redispersion into $1/8^{th}$ of the initial volume. Redispersion was also performed in 0.1 M PBS. Photos indicate no sign of aggregates therefore deemed successful.

5.3.2. Preliminary investigation- method development on HPLC

In order to monitor the release of drug over time HPLC was employed to measure the UV signal of the drug. Firstly, method development was required in order to measure absorbance of lamivudine across a range of concentrations that the drug release experiment will be performed. Figure.5.3-A displays an overlay of HPLC traces varying in the concentration of lamivudine from 0.454545455 mg/ml to 0.000887782 mg/ml. Lamivudine shows absorbance maxima at ~270 nm,[155] therefore samples were monitored on HPLC at a UV detection of 270 nm. Furthermore Fig.5.3-B displays the corresponding data plotted as a calibration line with an R^2 value of 0.99 ensuring a linear relationship. The method was developed aiming to determine 1 % release of drug within the calibration plot.

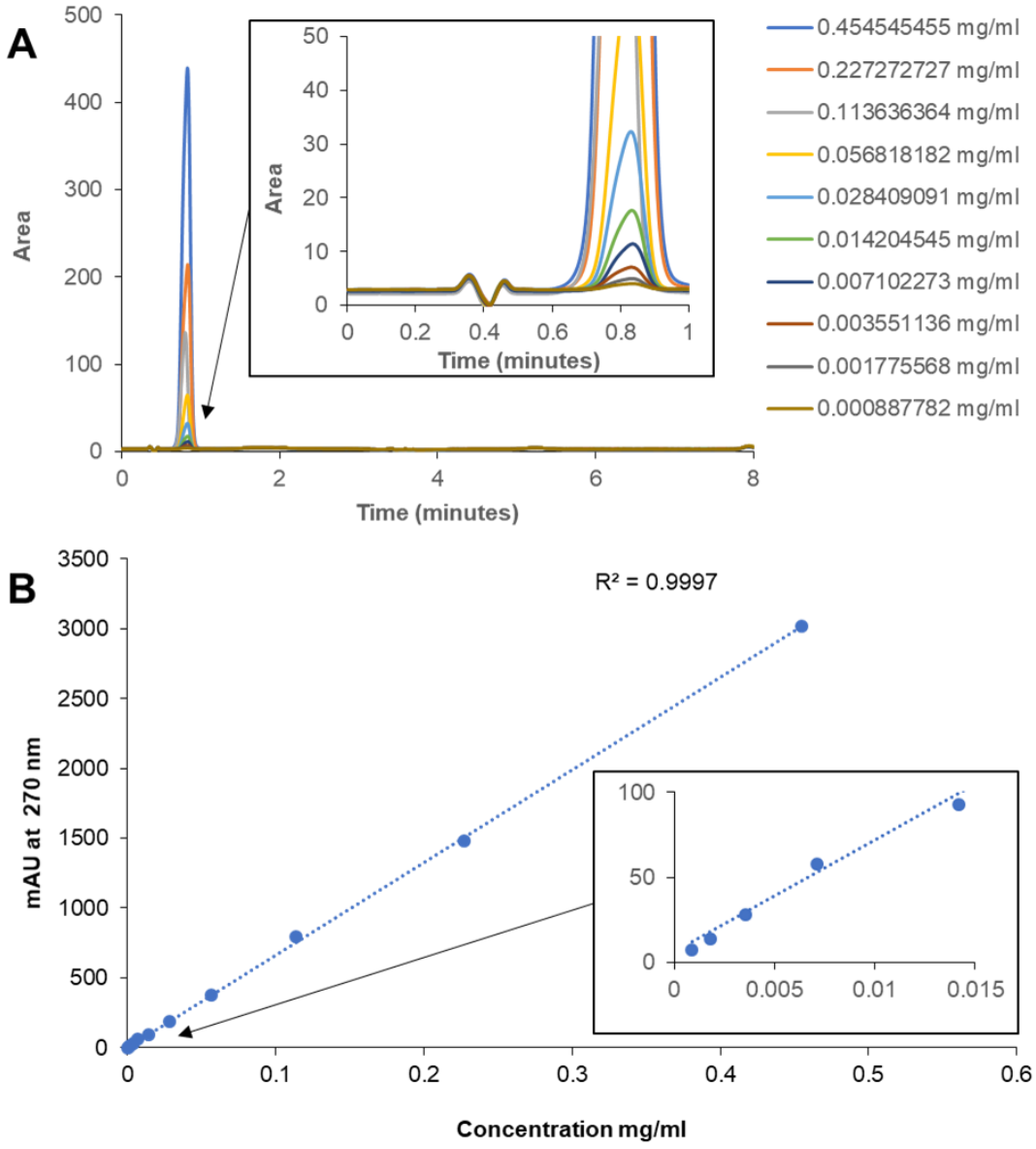

Figure 5.3- HPLC analysis of lamivudine A) Overlay of HPLC traces varying in lamivudine concentration. B) Calibration plot of UV signal vs concentration of lamivudine drug.

5.3.3. Enzymatic degradation of dodecyl prodrug from lipid nanoparticle *in vitro*

The formulation of 75 % dodecyl prodrug 25 % tricaprin stabilised by 50 % Brij S10 50 % Lipoid S100 was prepared so that studies with and without enzyme could be performed in triplicate. Each formulation contained a theoretical 18 mg of prodrug thus 5.76 mg drug for overall concentration at 100 % release of 0.2304 mg/ml. As lamivudine has a solubility of 70 mg/ml in water ensuring that sink conditions would be maintained throughout the release experiment.[156] For the samples investigating the effect of enzymes 130 mg (2465 U) of enzyme was used. Samples were taken at various time points and was quenched by dilution with ice cold methanol. The dissolved drug was then separated from the enzyme and any nanoparticles by the use of centrifuge filters with a 10 kDa cut off. The samples were collected using this process over a period of 9 weeks and were analysed by HPLC. The drug release behaviour data shown in Fig.5.4-A. When no enzyme was used (PBS alone) then no drug release was detected. In the presence of enzyme ~3.7 % release was detected after 24 hours, ~14.5 % was measured after one week and ~ 37 % after 9 weeks, Fig.5-A. A sample from week 9 was also analysed by HPLC-MS which found 230.05 $[M+H]^+$ for the peak at ~0.85 minutes, thus indicating the presence of lamivudine.

Between weeks 1-5 the difference in drug release was ~ 17.98 % over four weeks translating to ~4.5 % per week. There was a linear relationship of drug release over weeks 1-5 as seen in Fig.5.4-B. After week 5, the rate of release began to reduce, with an average release of 4.26 % released between weeks 5 and 9 (~1 % per week). As a result, there was an overall average drug release of ~ 37 % after 9 weeks, Fig.5.4-A. The reduction of drug release may be explained by suicide inhibition of the enzymes, whereby a degradation product irreversibly binds to the enzyme by forming a covalent bond.[157] Yan *et al*. have highlighted potential suicide inhibition occurrence of esterase's in the presence of sugars such as sucrose in a process known as glycation.[158,159] The difference between the drug release behaviour in the absence of enzyme (~ 0 % drug release detected after 9 weeks) clearly showed that the enzyme was driving the drug release fig.5.4-C, by hydrolysing the carbamate and carbonate ester linkages on the prodrug. Furthermore, this shows that the prodrug was stable at physiological conditions when encapsulated within this formulation and release may only be triggered in the presence of an enzyme. Appendix Fig.5.1 displays raw data for with and without enzyme over various timepoints of the drug release experiment. It is clear that no peak evolves at the targeted retention time of the drug 0.85 minutes. On the other hand, it is clear that a peak evolves when in the presence of enzyme. In addition, in the presence of enzyme other peaks also evolve over time alongside that of the drug. It is plausible to assume the peaks correspond to free pegylated lipid surfactant that may become free in solution as a result of desorbing from the nanoparticle surface as

the prodrug is activated. Furthermore, the ester bonds of the triglyceride tricaprin within the nanoparticles may also undergo hydrolysis releasing water soluble products such as glycerol.

After sampling on week 5 formulations containing enzyme were divided into two with one set maintaining the original enzyme concentration, meanwhile another set investigating the effect of fresh enzyme, Fig.5.4-A. The addition of fresh enzyme; resulted in greater drug release than the samples that only contained the original enzymes, with ~43 % drug release measured by week 9. This data further suggests that the enzyme than had been added at the start of the experiment had begun to lose activity. It is plausible to assume ~100 % drug release could hypothetically be achieved upon continuous additions of fresh enzyme. This work shows that the prodrug contained within the nanoparticles can be accessed by an esterase and is slowly activated to form the drug molecule.

Other researchers have shown different release behaviour in their studies of activation of prodrug from nanoparticles. The drug release by Shi *et al*. for a similar approach resulted in ~ 50 % drug release after 12 hours.[54] A potential explanation may be the difference in formulation as Shi *et al*. incorporated their prodrug within the membrane of liposomes with a nanoparticle size of 125 nm, therefore the difference in particle size and structure may have made the SN-38 prodrug employed by Shi *et al*. more accessible than the dodecyl prodrug found within slightly larger particles (150 nm when redispersed into water, Chapter 4) the core of lipid nanoparticles. Another potential cause for the difference in rates of drug release experienced compared to Shi *et al*. may be that the prodrug synthesised by Shi *et al*. was only conjugated at one site. Furthermore, for the *in vitro* release experiment Shi *et al*. employed dialysis whereby the formulation and enzyme were more concentrated within a dialysis bag which may contribute to an increase rate of prodrug activation. Alternatively, the high concentration of sucrose leading to suicide inhibition used in our study may have also played a role in the slow rate of release. As a result, the rate of release may be largely impacted by the nanoparticle and/or prodrug structure as well as the experimental set up. Nevertheless, the overall rate of drug release from the formulation is deemed to be slow and therefore has potential application as a long acting injectable.

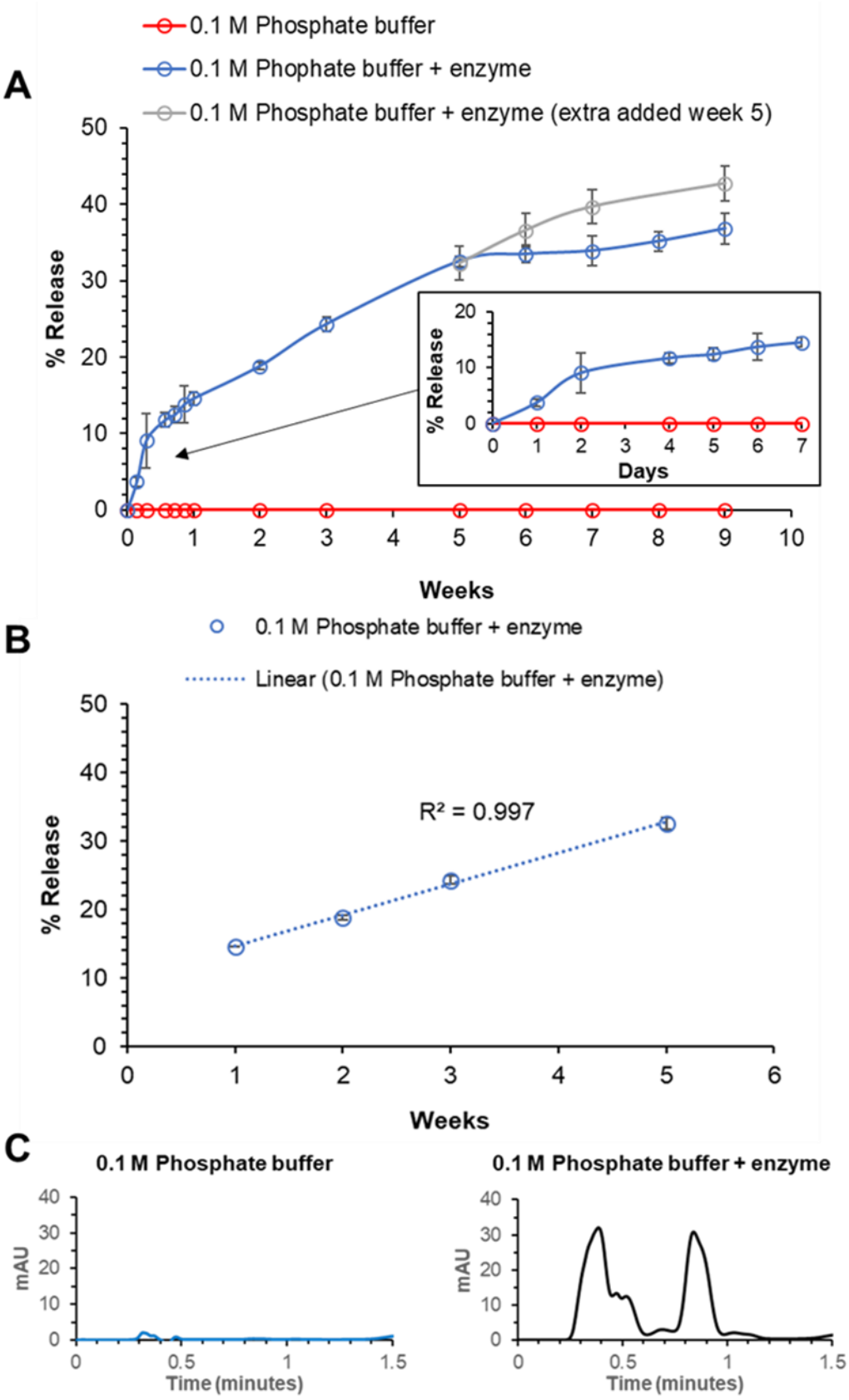

Figure 5.4- HPLC analysis of drug release A) Graph displaying % drug release over 9 weeks with and without porcine liver esterase enzyme. B) Linear relationship between drug release over 4 weeks between week 1 and 5. C) Raw data obtained by HPLC after 9 weeks displaying no peak development in the absence of enzyme, while in the presence of enzyme a peak for drug is present after ~0.85 minutes.

5.4. Conclusions

The dodecyl prodrug of lamivudine synthesised and employed over various studies throughout this thesis can be activated to release the original drug lamivudine. Activation was achieved at physiological conditions of 37 °C, 0.1 M phosphate buffer in the presence of porcine liver esterase enzyme. Prodrug activation was only found in the presence of enzyme and not solely in the presence of physiological temperature and buffer. This suggests high stability of the dodecyl prodrug and the release may be triggered once exposed to enzyme. Overall average drug release of ~ 14 % after one week and 37 % was achieved with one batch of enzyme after nine weeks. Although, the porcine liver esterase enzyme showed signs of potential suicide inhibition *via* glycation caused by the high concentration of sucrose in the solution due to a decrease in rate of release at week 5. Nevertheless, upon addition of more enzyme drug release could be sustained, thus suggesting potential for higher percentages of drug release to be achieved if the study was continued or if performed *in vivo*. Overall, the strategy of prodrugs for encapsulation within lipid nanoparticles is promising due to successful prodrug activation translating to a sustained release of drug. Thus, reinforces the contribution made to the field by each of the other chapters 2, 3 and 4.

5.5. Future work

It would be plausible to attempt to dilute the concentration of sucrose prior to studying enzyme activation, which would provide greater insight into the extent of suicide inhibition induced by glycation of enzyme. As a result, would reveal whether the slow release is due to the formulation or the occurrence of suicide inhibition of the enzyme.

Additionally, other enzymes that may be found within the body as well as different concentrations of enzyme could be investigated to test for different release profiles, before finally investigating release *in vivo*.

5.6. Experimental

Materials

Brij S20, sucrose, porcine liver esterase and 0.1 M phosphate buffered saline solution were all purchased and used as received from Sigma Aldrich. Tricaprin was purchased from Tokyo chemical industry and used as received. Lipoid S100 was purchased and used as received from Lipoid.

Methods

Preparation of formulation

The formulation as described in Chapter 4 was prepared multiple times for a total volume of 288 mL which was then diluted 1:1 with 20 % w/v sucrose and freeze dried in volumes of 8 mL in 12 mL vials over 4 days using a VirTis Bench Top K freeze dryer (SP Scientific, Ipswich UK). Condenser temperature was set to – 100 °C and vacuum of < 40 µbar. The contents of each vial were reconstituted immediately using 1 mL 0.1 M phosphate buffered saline solution per vial. Redispersion was achieved using a Vortex-Genie 2 on setting 5 for 10 minutes. 12 vials containing redispersed formulations were then combined in a 14 mL vial.

In vitro drug release

12 mL of prodrug formulated lipid nanoparticles in 0.1 M phosphate buffered saline (PBS) containing (or not) were loaded into 14 mL vials. Vials were continuously and vigorously shaken at 500 rpm in an incubator shaker with a fixed incubation temperature of 37 ± 0.5 °C. 0.2 mL aliquots were collected and quenched with 0.4 mL ice cold methanol then centrifuged at 150,000 x g for 1 hour using 0.5 mL regenerated cellulose membrane spin filters with a molecular weight cut off of 10 kDa. The filtrate was then analysed by HPLC analysis as described. *In vitro* release experiments were performed in triplicate.

Analytical techniques

HPLC

HPLC analysis was performed on a Hypersil gold C_{18} column (50 x 4.6 mm 3 µm) using the following method: 95 % solvent A 5 % solvent B for 30 seconds before switching to 5 % solvent A 95 % solvent B over 1 minute before holding at 5 % solvent A 95 % solvent B for a further 6 minutes at a flow rate of 2 mL min^{-1} (solvent A: 20 mM ammonium formate aqueous solution prepared in distilled water, solvent B: acetonitrile).

For calibration plot various concentrations of drug were dissolved in 10:1 methanol: 20 mM ammonium formate solution and run using same method as above.

HPLC-MS

Samples were analysed using the same HPLC method as above. HPLC-MS was performed on an Agilent 1290 Infinity II UHPLC coupled to Agilent 6540 UHD Accurate-Mass Q-TOF LC/MS with electrospray ionisation source.

5.7. Appendix

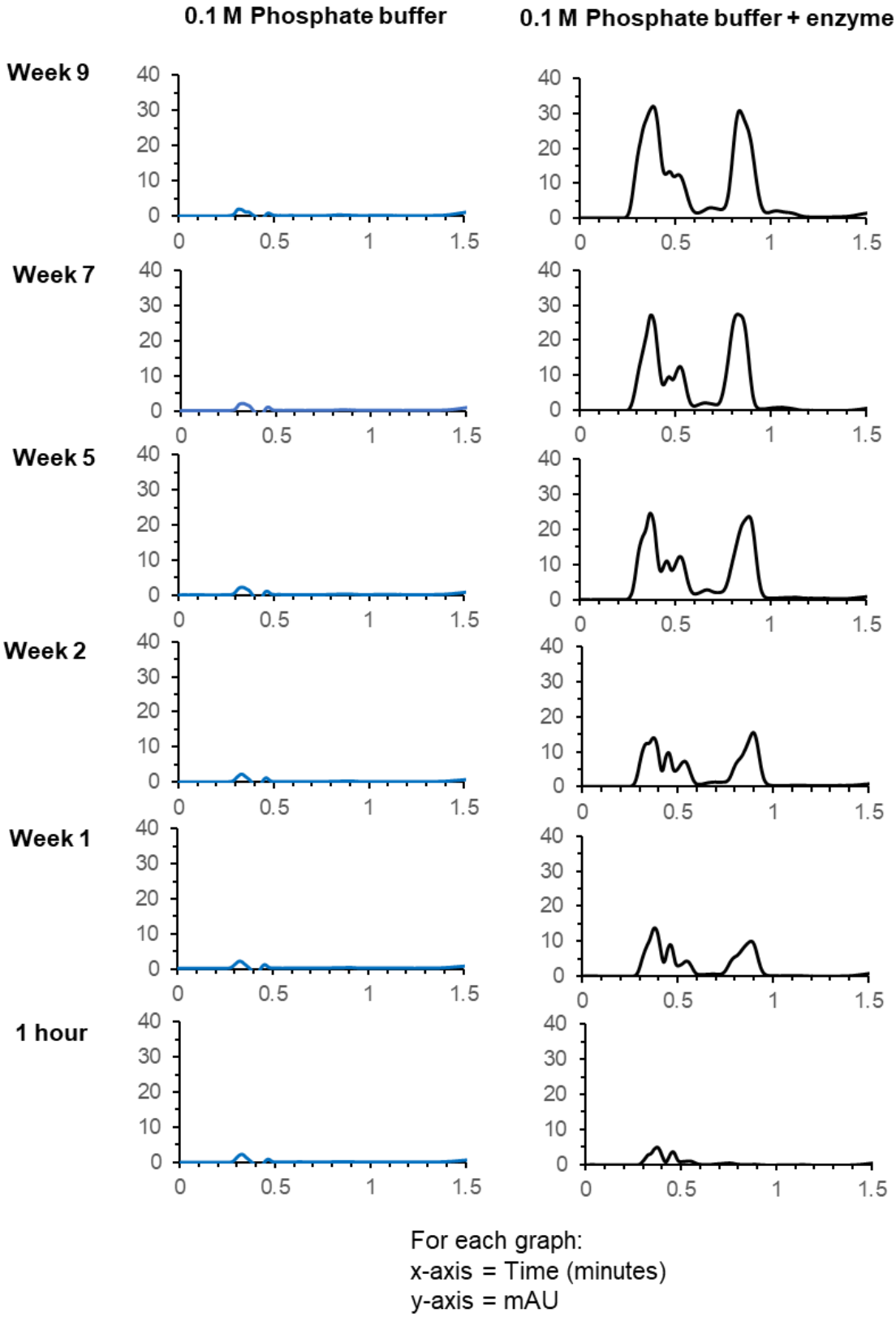

Appendix Figure 5.1- Raw data obtained by HPLC from drug release experiments over various periods of time to monitor release with and without porcine liver esterase

CHAPTER 6

mRNA formulation

Chapter 6 mRNA formulation

6.1. Introduction

The success of the BioNTech/Pfizer and Moderna mRNA COVID-19 vaccines has provided a successful route out of the global COVID pandemic.[7] Additionally, lipid nanoparticles for the delivery of mRNA are now being studied for a wide range of indications including cancer and various neurological conditions and neurological diseases such as multiple-sclerosis and Parkinson's.[88–90] Despite vast amounts of research already performed in the development of lipid nanoparticles for the delivery of nucleic acids there appears to be a large degree of potential for further optimisation and development. A few key challenges yet to face are mRNA degradation by means of hydrolysis or oxidation.[7] Furthermore, there are outstanding questions over the delivery efficiency of nucleic acids as some systems report less than ~ 5 % of nucleic acid cargo actually being delivered to the cytoplasm.[107] As a result, strategies to investigate how structural components may be modified and or new materials synthesised may enable further advance the technology. One method commonly employed is the investigation of structural property relationships in order to gain further insight into what parameters are detrimental to formulation performance. As previously discussed in 1.6.2.1., a great deal of research has taken place looking into how the components of the lipid nanoparticle formulations may influence parameters by investigating structure property relationships in order to optimise formulation efficacy and limit toxicity and preserve nucleic acid activity.[97,106,108,111,112] The ionisable cationic lipid upon addition to acidic pH becomes protonated and thus cationic, and is responsible for the entrapment of mRNA within lipid nanoparticle by complexing with the anionic backbone of the mRNA.[102] Thus, the ionisable cationic lipid has received immense amounts of interest surrounding structure and pKa, which has been found to be detrimental to mRNA vaccine performance. For example, during development Moderna identified SM-102 which had a pKa of 6.68 as a lead candidate due to possessing desirable properties such as good biodegradability, tolerability, protein expression as well as immunogenicity,[113,114]encapsulation efficiency, stability and particle membrane permeability. Again, another structure property relationship identified which has been previously discussed in 1.6.2.4. is the pegylated lipid, which has vast influence on formulation performance. The pegylated lipid has been found to be essential for colloidal stability during formulation and storage, however has also been found to be crucial once the formulation enters a biological system. [123,124] Although, studies by Mui *et al*. have suggested formulations with a high degree of surface coverage by pegylated lipids and/or pegylated lipids of high chain length have shown poor cellular uptake and endosomal escape due to limiting the interaction between the ionisable cationic lipid and the cell membrane.[160] As a result, PEG chain length and degree of pegylation are areas of interest. Studies by Suk *et al*. has investigated the favouritism of a PEG chain length

corresponding to a molecular weight of 2000 Daltons (Da) in the COVID-19 vaccines. Suk *et al*. revealed particularly short circulation times of pegylated lipids with very short PEG chain lengths < 1000 Da. Whereas, pegylated lipids with long peg i.e. > 5000 Da led to a clear increase in circulation time. Alternatively, when the molecular weight of PEG was between 350 -2000 Da the differences in circulation time were negligible.[130] Research by Mui *et al*. has investigated how structure properties relationships with respect to changing aspects around the lipid tails/unit of the pegylated surfactant may influence the tendency of the pegylated lipid desorb from the lipid nanoparticle, thus affecting particle circulation time as well as membrane permeability.[123,128] Furthermore, there are also reports by Kim *et al*. of how cleavable PEG chains of pegylated lipids result in greater cellular uptake.[131] Nonetheless, there appears to be a lack of research investigating how the peg chain length of the pegylated lipid may affect the formulation performance with respect to cellular uptake/endosomal escape. Mui *et al*. has suggested that PEG may act as a steric barrier to endocytosis and endosomal escape. As a result, this remains an area that requires further research.

A common method to investigate cellular accumulation/uptake is incorporating a lipophilic dye such as DiI into nanoparticle formulations. For example, Harade *et al*. employed fluorescence within nanoparticles and measured the fluorescence emitted to provide a quantitative and qualitive indication of the cellular uptake/association of the nanoparticles.[134] This strategy of dye loading has been successfully reported by Kim *et al*. who monitored the accumulation/internalisation of lipid based formulations to a cell line at various pH over a period of time.[131] Furthermore, fluorescence measured by flow cytometry suggesting intracellular accumulation of nanoparticles has been correlated with the secretion of chemokines such as Interleukin 8 (IL-8).[133] It is believed that IL-8 secretion may be the result of oxidative stress by cells as a consequence of intracellular accumulation of nanoparticles.[133,134]

6.2. Chapter Aims

The aims of this chapter were to systematically vary the chain length of PEG of the pegylated lipid surfactant and reveal any impact on the formulation's ability to accumulate at the cell and enter the cell. In order to do so a standard formulation employing a common pegylated lipid surfactant (DSPE-MPEG-2K) used in mRNA lipid nanoparticle vaccine formulations were employed as a standard. In addition, in order to investigate a range of PEG chain length various PEG octadecyl ether surfactants varying in PEG chain length were trialled. The PEG chain lengths selected for trial were 10, 20 and 100 units long thus investigating above and below that of the DSPE-MPEG-2K. Fig.6.1-A illustrates the difference in PEG cain length with the various pegylated lipid surfactants. The lipid particles also included the lipophilic fluorescent dye DiO (3,3'Dioctadecyloxacarbocyanine perchlorate), Fig.6.1-B. The lipid used in the particles was SM-102 as well as trimyristin (Dynasan 114) which was selected to

mimic SM-102 while being a neutral lipid, (Fig.6.1-C). We investigated how the changes in the formulation influenced the particle size, size distribution, zeta potential and fluorescence before testing formulations on cell lines for indications of cellular uptake. This approach examines the effect of PEG chain length on cellular accumulation and uptake and would allow a more informative decision on pegylated lipid going forward.

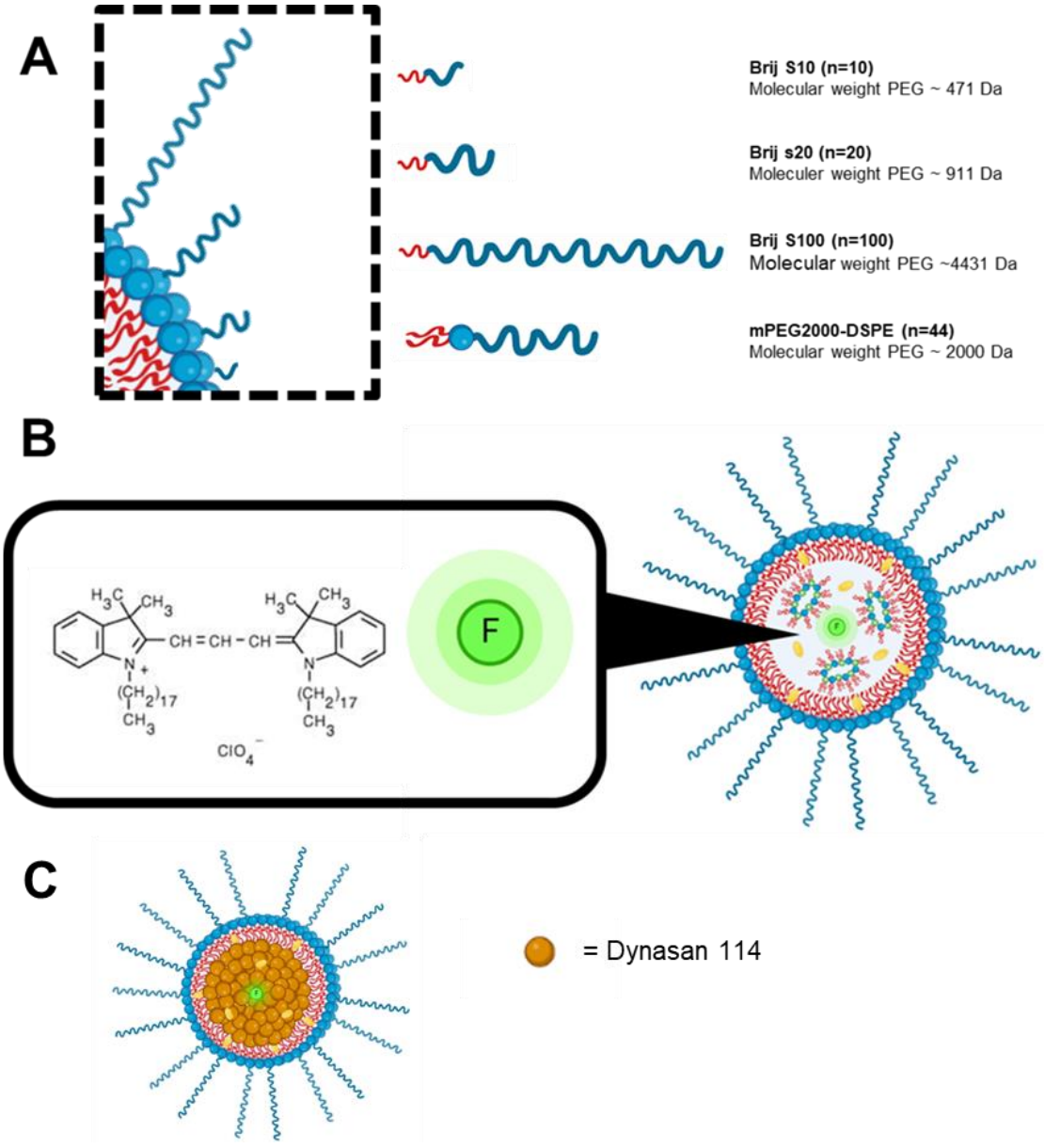

Figure 6.1- Schematic summary of research. A) Illustration displaying the difference in chain length of PEG depending on surfactant as well as the various pegylated lipids to be tested showing a clear variation in PEG chain length. B) Structure of DiO fluorescent dye. C) stucture of nanoparticle formulation using Dnasan 114 as a mimic for SM-102

6.3. Result and Discussion

6.3.1. Preliminary studies

6.3.1.1. Scale down

The first issue to address was the scale of previous formulations as the volume of 24 ml was considered too high as it would require large quantities of the expensive materials (ionisable cationic lipid, SM-102, dye, DiO and further down the line mRNA). As a result, the previous flash nanoprecipitation method was adapted to suit this separate study. The scale was reduced to a total volume of aqueous phase of 1.5 ml, 1/16th of that used in previous chapters as this was deemed the lowest possible volume that was practical with respect to vial and stirrer size, while having enough material for analysis such as DLS, zeta potential and fluorescence. Fig.6.2 displays a comparison between the two scales using 100 % Lipoid S100 as the stabiliser and Dynasan 114 as the core lipid. Dynasan 114 was employed as the core mimic as it was of similar LogP and molecular weight to the ionisable cationic lipid selected for this study (SM-102). The data presented in Fig.6.2 indicates that particles of a similar size and PDI were achieved despite the difference in scale. As a result, it was deemed the difference in scale had little effect on the formulation. ^{1}H NMR was also employed to prove THF solvent disappearance by evaporation after ~ 24 hours- Appendix Fig.6.1.

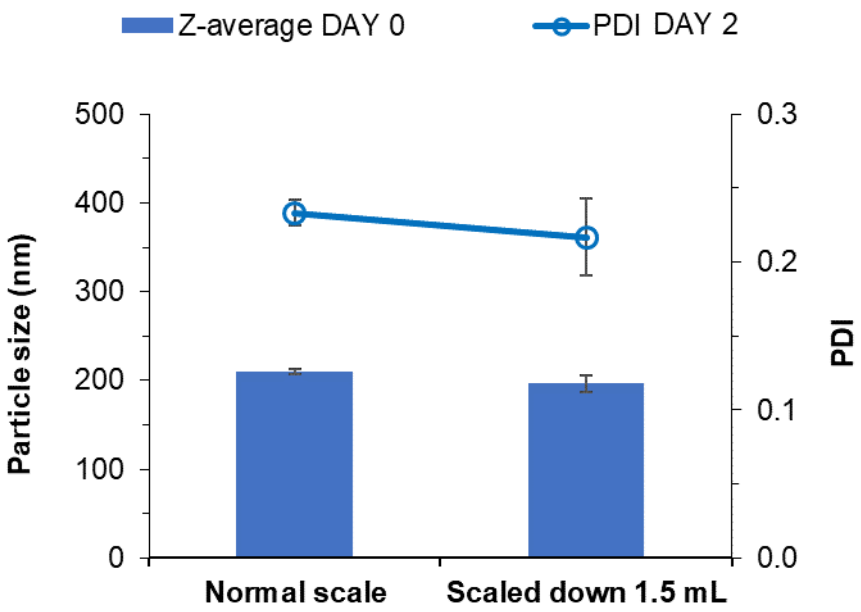

Figure 6.2- Particle size and size distribution obtained by DLS. Formulations of trimyristin stabilised by 100 % Lipoid S100 at the normal scale of 24 ml aqueous phase vs the scaled down at 1.5 ml aqueous phase.

Following successfully scaling down the formulation an attempt was made to replicate the ratio of materials employed in a typical mRNA containing lipid nanoparticle. The ratio of lipid nanoparticle components (ionisable cationic lipid: helper lipid : cholesterol : pegylated lipid, 46.3 : 9.4 : 42.7 : 1.6) was employed while using Dynasan 114 as a mimic for the ionisable cationic lipid. The data presented in Fig.6.3 indicates that particles of ~ 150 nm in average particle size and ~ 0.15 in polydispersity were formed which appeared stable over a one day while the organic solvent THF evaporated from the formulation. As a result, it was deemed the flash nanoprecipitation method had been successfully modified to account for the adjustment in scale and change in overall formulation components and ratio of components.

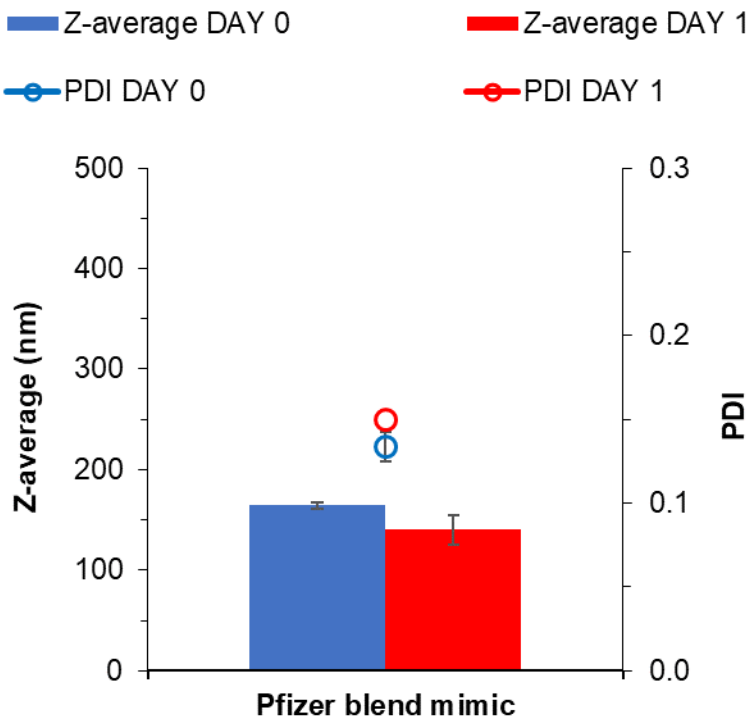

Figure 6.3- Mimic of Pfizer formulation blend at a molar ratio of while employing Lipoid S100, Brij S20 and Dynasan 114 as helper lipid, pegylated lipid and a mimic for SM-102 (Ionisable cationic lipid)

6.3.1.2. Inclusion of Ionisable cationic lipid SM-102

Dynasan 114 was selected as a mimic of SM-102 due to similar properties such as LogP and molecular weight (Dynasan 114; CLogP 19.49, Molecular weight = 723.2; SM-102; CLopP = 17.8, Molecular weight = 708.21). LogP was identified as a key parameter due to studies in previous chapters suggesting

tricaprin and dodecyl prodrug produce similar nanoparticle sizes and are of similar stability due to similar LogP.[33,149] Meanwhile, molecular weight was also identified to ensure similar molarity.

Fig.6.4 shows how substituting Dynasan 114 for SM-102 and then formulating SM-102 in the presence of an acidic buffer (thus protonating SM-102) each resulted comparable particle size and size distribution. Thus, it was deemed due to relatively similar properties, Dynasan 114 was successfully employed as a mimic for SM-102 and any conditions developed should in theory be compatible for SM-102.

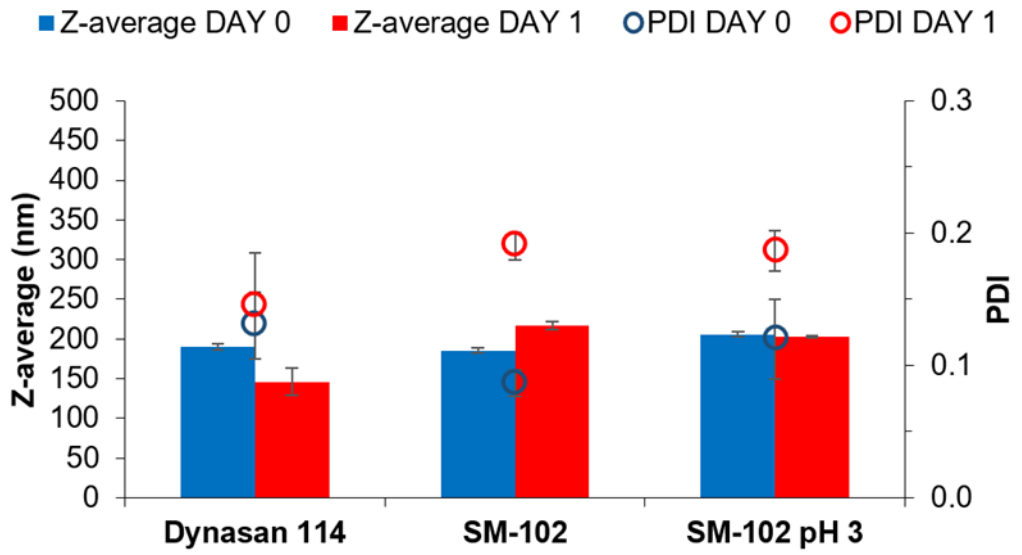

Figure 6.4- Size and size distribution data obtained by DLS for samples of Dynasan 114, SM-102 and SM-102 in the presence of a citrate buffer at pH 3.

6.3.1.3. Determining dye loading

It was important to maximise the loading of dye into the lipid nanoparticles in order to give a strong fluorescence signal upon accumulation of the nanoparticles in cells. Therefore, a range of dye concentrations were trialled for loading into nanoparticles. Fig.6.5 displays how upon loading dye into the nanoparticle formulations there appears to be no apparent implication for the formulation size and size distribution up to 1.87 µg DiO per mg of Dynasan 114 (µg/mg) (Fig.6.6-A). Although, once at a loading of 18.7 µg/mg there was a large increase in particle size measured as well as the difference in correlation coefficient graphs in Fig.6.6-B. Furthermore, fluorescence data (Fig.6.7) shows how a detectable level of excitation and emission was measured while using the dye loading of 1.87 µg/mg; there was a considerable decrease in fluorescence signal at lower levels of dye loading. As a result, 1.87 µg DiO/mg Dynasan 114 was identified as the most suitable dye loading for future formulations.

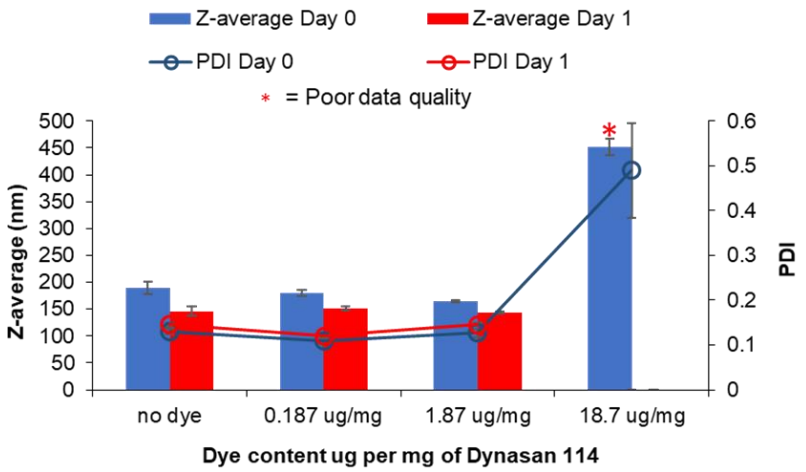

Figure 6.5- Particle size and size distribution data obtained by DLS. Formulations varying in DiO dye loading. Formulated using Pfizer ratio with Brij S20 as pegylated lipid.

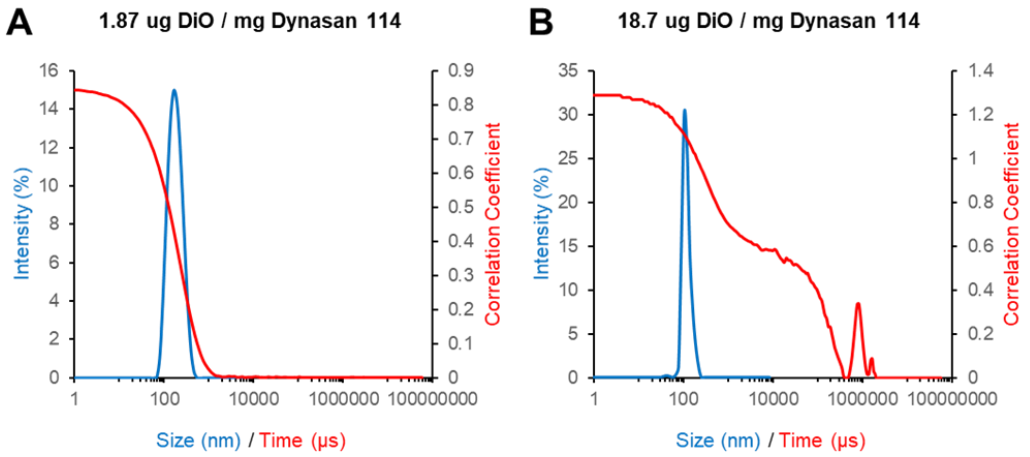

Figure 6.6- Overlay of particle size distribution graphs and correlation coefficient for DiO dye loading at; A) 1.87 ug DiO/mg Dynasan 114, B) 18.7 ug/mg DiO/mg Dynasan 114.

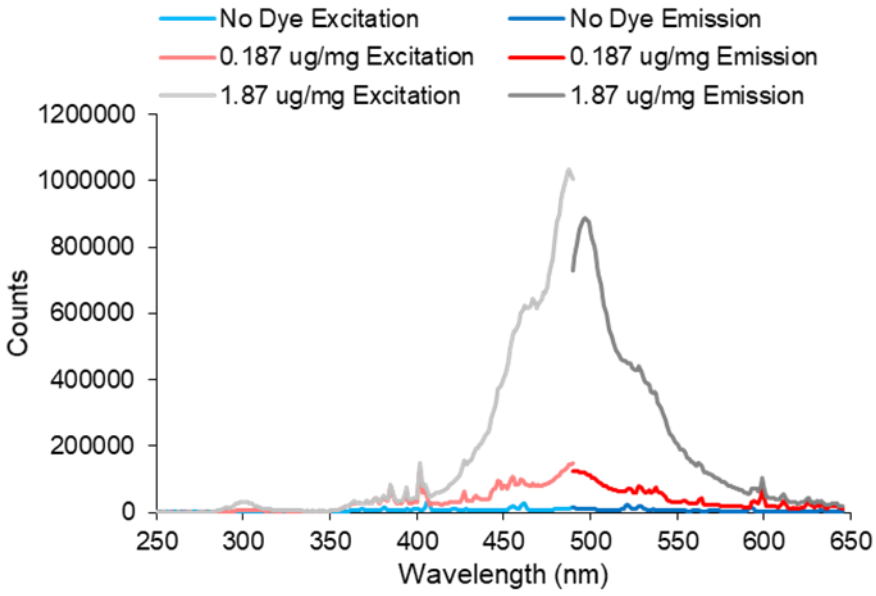

Figure 6.7- Overlay of excitation and emission for various concentrations of dye loaded into the formulations as well as a blank formulation with no dye. Excitation and emission wavelengths were set to 484 and 501 nm during measurements.

6.3.1.4. Determining buffer concentration

The purpose of the following study was to investigate various concentrations of citrate buffer to gauge level of ionisable lipid protonation while also assessing stability of each sample. It was necessary to determine if formulations could also be generated using other pegylated lipids as well as examine differences in stability due to the differences in degree of steric stabilisation provided by the various pegylated lipids. To assess the stability DLS was employed to measure size and PDI of samples at pH 3 (pH of formulation conditions) and pH 7 (physiological pH) as prior to cell testing it was necessary to elevate the pH after formulation by dilution with TRIS buffer in order to make formulations compatible with cell lines.

Formulations were conducted using both SM-102 and Dynasan 114, Fig.6.8 displays formulation size and size distribution data obtained by DLS. From the graphs in Fig.6.8- A- F it is clear that formulations of either Dynasan 114 or SM-102 using Brij S100 as the pegylated lipid were stable throughout each buffer concentration due to sufficient steric stabilisation provided by the longer chain length of PEG. Although when SM-102 was used as the lipid, the buffer concentration of 1 and 10 mM resulted in samples that showed an increased mean diameter at pH 7. This trend may be due to incomplete protonation of the ionisable cationic lipid SM-102. This would lead to a lack of electrostatic stabilisation due to a lack of stability upon elevating pH for formulations stabilised by a pegylated lipid with a lower PEG chain length (Brij S20 and DSPE-MPEG-2K). Meanwhile, once the buffer concentration is increased to 100 mM formulations stabilised by Brij S20 and DSPE-MPEG-2K appear stable. Furthermore, the electrostatic stabilisation alone at 100 mM was not sufficient alongside the lowest degree of steric stabilisation such as that provided by the short PEG chain length of Brij S10. As a result, formulations of Dynasan 114 using Brij S10 were also not stable enough to form nanoparticles.

Dynasan 114 is not ionisable and therefore does not offer any electrostatic stabilisation at any concentration of buffer and thus solely relies on steric stabilisation of the pegylated lipid. Fig.6.8-D-F show that when the longest chain length of PEG is employed in the form of Brij S100 formulations are stable at each concentration of buffer. While, a reduction in chain length with Brij S20 and DSPE-MPEG-2K results in poor stability reflected by formulation aggregation resulting in incompatibility with DLS or poor data quality. Although DSPE-MPEG-2K formulations were slightly better than that of Brij S20 which is likely due to the electrostatic stabilisation provided by the net negative charge of DSPE-MPEG-2K. The difference in stability of Dynasan 114 formulations is also clear from the size distribution and correlogram overlays (Fig.6.9), whereby the formulation of Dynasan 114 stabilised by DSPE-MPEG-2K adopted a multi modal size distribution and the correlogram undergoes a clear shift to the right both indicating the presence of large aggregates upon increasing the pH, (Fig.6.9-A1 and

A2). On the other hand, the longer PEG chain length of Brij S100 appears to maintain control which is reflected by no noticeable differences in size distribution graph or correlogram, Fig.6.9- B1 and B2.

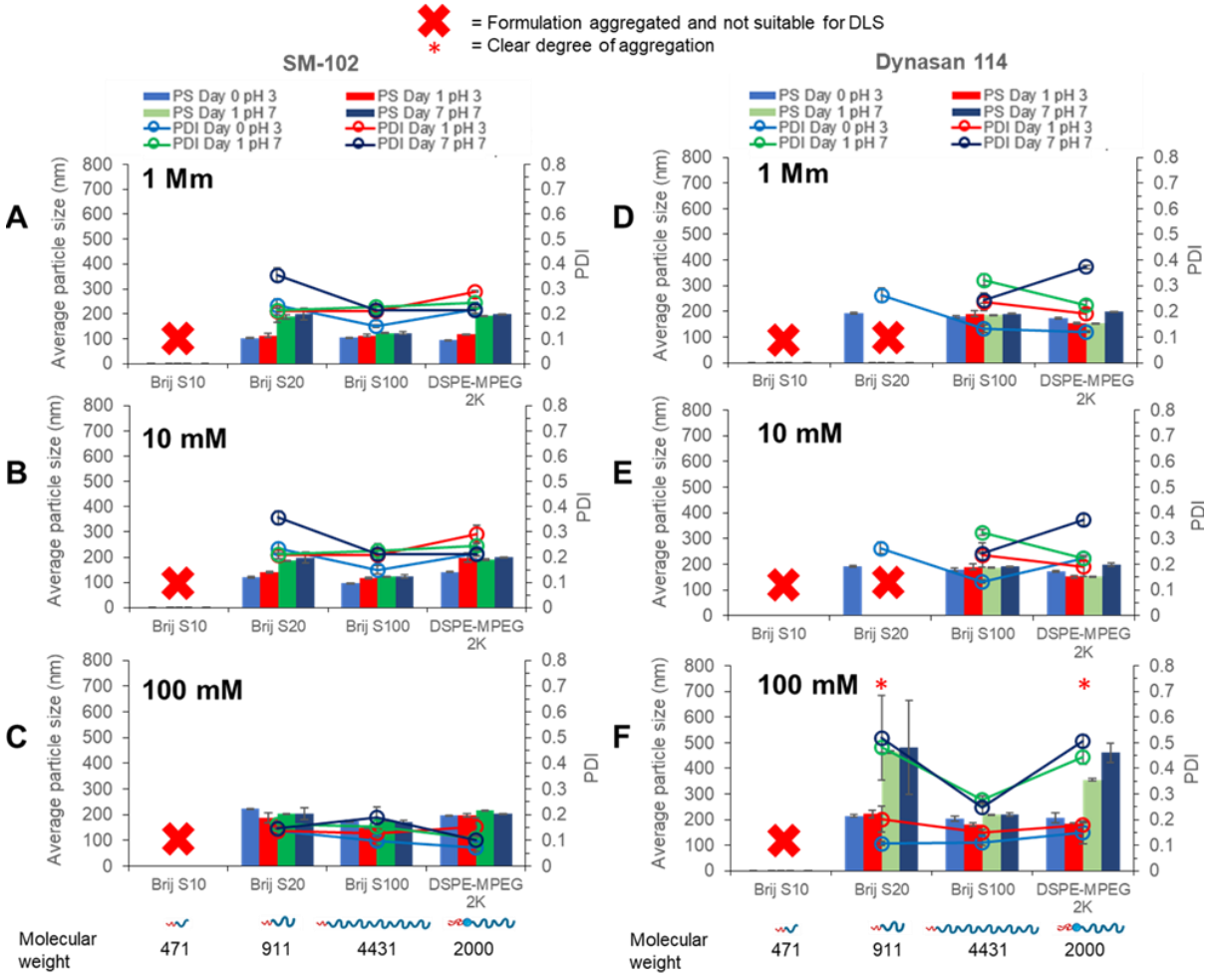

Figure 6.8- Particle size and size distribution data obtained by DLS for formulations varying in; pegylated lipid, buffer concentration and core lipid (Dynasan 114 or SM-102) at different durations after nanoprecipitation and pH values.

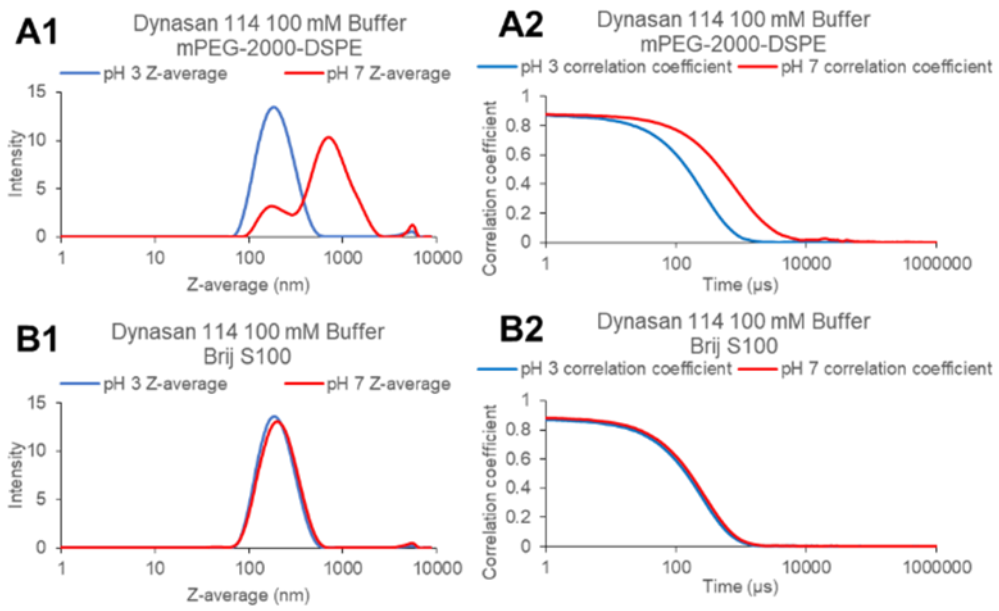

Figure 6.9- Size distribution graph and correlogram overlays displaying the steric stabilisation provided by Brij S100 may stabilise formulations of Dynasan 114.

The data from Fig.6.10 displays the size distribution graphs (1) and corresponding correlation coefficient plots (2) for various formulations of SM-102 varying in pegylated lipid and buffer concentration at both pH 3 and pH 7. The graphs A-C display the effect of changing the pegylated lipid while at an initial citrate buffer concentration of 1 mM. Immediately, it is clear from the graphs A1 and A2 there is a large degree of instability of formulations stabilised by Brij S20 due to a clear shift in size distribution and correlation coefficient to larger particles being detected which may suggest aggregation. Although, this effect is much less for formulations stabilised by DSPE-MPEG-2K and Brij S100, suggesting formulations are potentially more stable with a longer chain length of PEG. On the other hand, graphs D-F display the effect of changing pegylated lipid at an initial citrate buffer concentration of 100 mM. It is clear at an elevated buffer concentration there is no obvious shift in size distribution or correlation coefficient. This further supports the presence of stronger electrostatic stabilisation at higher citrate buffer concentration, which is likely due to a higher degree of protonation of the ionisable cationic lipid SM-102.

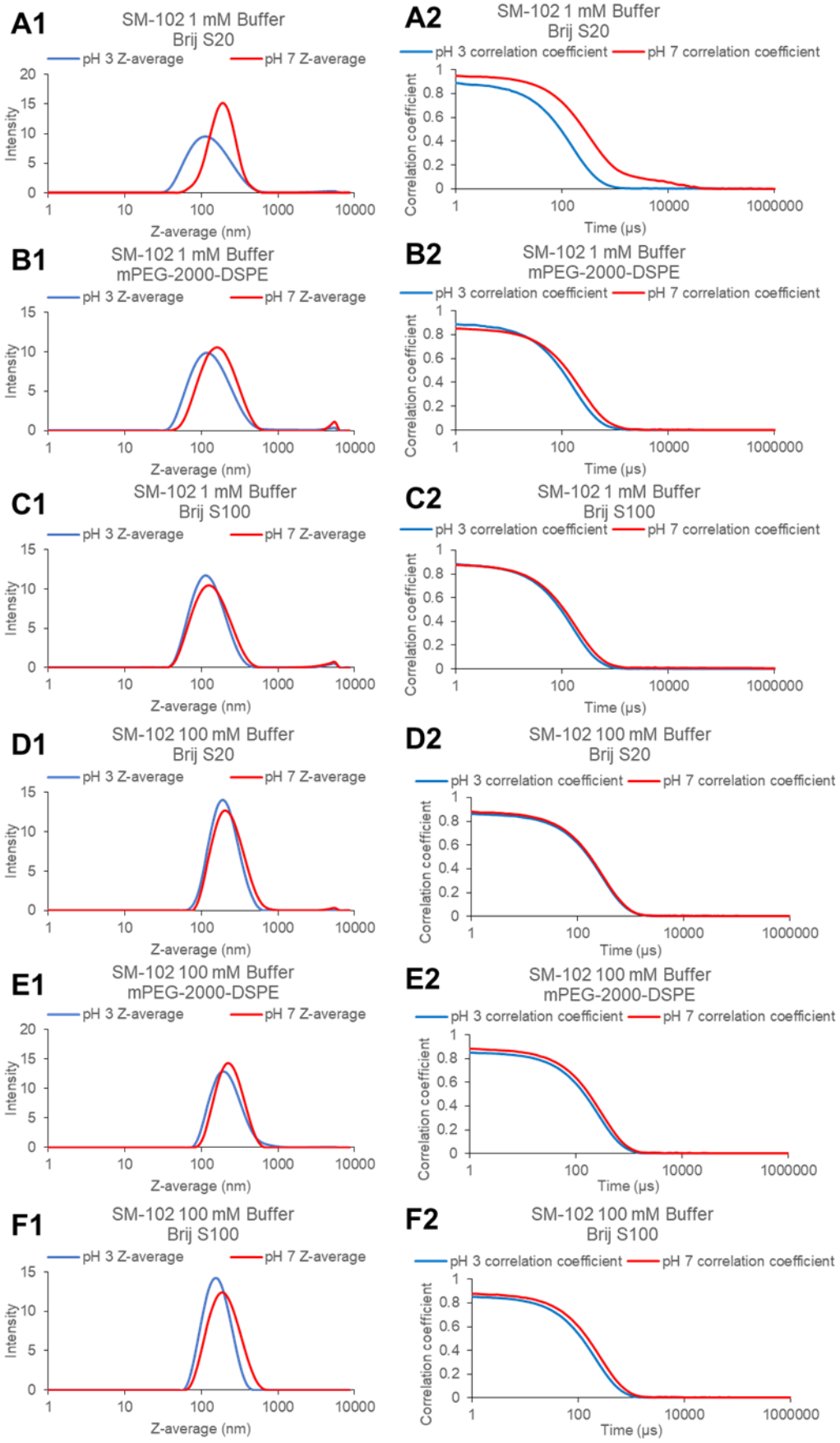

Figure 6.10- Size distribution graph and correlogram overlays displaying the effect of pegylated lipid at both 1- and 10-mM citrate buffer.

To further investigate how the changes in buffer concentration and pegylated lipid influence the formulations the zeta potentials of samples were measured at both pH 3 and pH 7. When there was an increase in buffer concentration there was generally a reduction in the total charge on the particles (Fig.6.11). For the particles with SM-102 which started with a cationic charge due to protonation of the amine on the surfactant this was seen as a reduction in zeta potential at both pH 3 (Fig.6.11-A) and pH 7 (Fig.6.11-B). Although, this appears to initially contradict the earlier hypothesis at lower buffer concentration as one would expect SM-102 to be more protonated at higher buffer concentration resulting in a more positive zeta potential. However, it is worth noting that at 100 mM citrate buffer concentration the signal to noise ratio of the zeta potential measurement was poor and it is likely the decrease in zeta potential with increasing buffer concentration is the result of a screening effect by the buffer which drowns out the signal from the particles making it appear less positive than at lower buffer concentration. This is supported by Fig.6.11-C which shows a lack of zeta potential at either buffer concentration for formulations stabilised by Brij S20 or Brij S100. More evidence supporting the theory of buffer drowning out the zeta potential from the particles within the formulation is the suppression of the negative charge of DSPE-MPEG-2K. DSPE-MPEG-2K possesses a net negative charge and therefore formulations of Dynasan 114 possess a negative zeta potential, which becomes less negative with increasing buffer concentration, Fig.6.11-C. In addition, DSPE-MPEG-2K appears to decrease the zeta potential further due to the negative net charge on DSPE-MPEG-2K which cancels out some of the charge of the SM-102 resulting in a suppressed zeta potential, Fig.6.11-A.

The data presented by Fig.6.11 clearly displays various relationships between pegylated lipid, buffer concentration and how they impact zeta potential. Another observation is how at higher PEG molecular weight the zeta potential appears to decrease, Fig.6.11-A. A similar trend was found by Hashizaki *et al*. whereby zeta potential of liposomes decreased with increasing PEG chain length of PEG-DSPE.[161] This suggests that the PEG chains disrupting/limiting the formation of the electrostatic cloud of counter ions in solution limiting the zeta potential measurement. Zeta potential signals are weakened further upon adjustment of pH, which is a likely consequence of dilution, Fig.6.11- B and D.

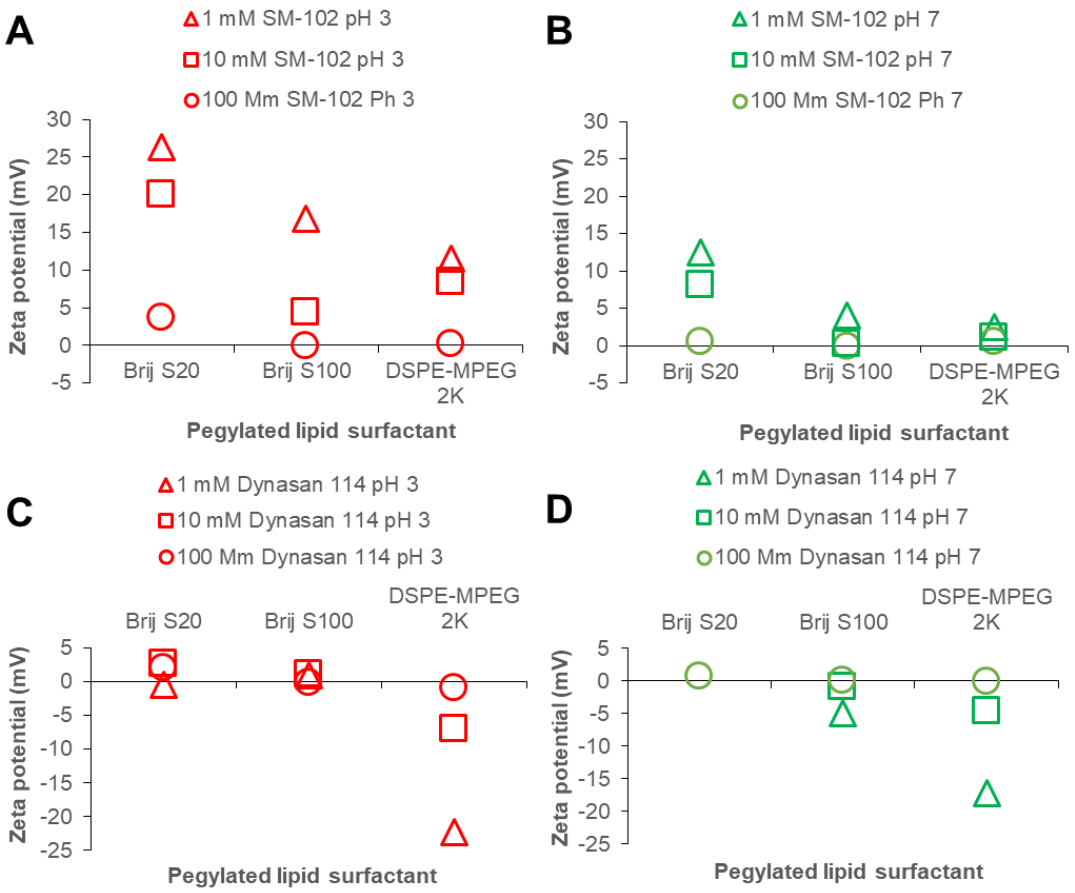

Figure 6.11- Zeta potential data for each of the formulations varying in pegylated lipid, buffer concentration and core lipid (SM-102 or Dynasan 114) while at both pH 3 and pH 7.

The fluorescence of each sample was measured once the pH had been elevated to physiological levels of 7 to ensure a level of fluorescence could be detected before testing on cell lines. Immediately, it was apparent those samples that had experienced a degree of aggregation (Dynasan 114 stabilised by Brij S20 or DSPE-MPEG-2K, at 100 mM buffer) were weak in fluorescence emission relative to the stable samples which is likely a consequence of fluorescence quenching and/or sedimentation of particles, Fig.6.12. Meanwhile, there was only a slight deviation in the degree of fluorescence between samples of SM-102 when varying pegylated lipid, Fig.6.13. Another observation between samples stabilised by Brij S100 is a weaker emission fluorescence from samples containing SM-102 (~5.E+6) compared to those prepared with Dynasan 114 (8.E+6). This is likely the result of fluorescence quenching by O-H bonds in water,[162] as the formulation containing SM-102 will contain pockets of buffer solution to stabilise the ionisable cationic lipid within the nanoparticle as suggested by the model created by Leung *et al.*[102] Whereas, the samples containing Dynasan 114 will likely form a solid core.

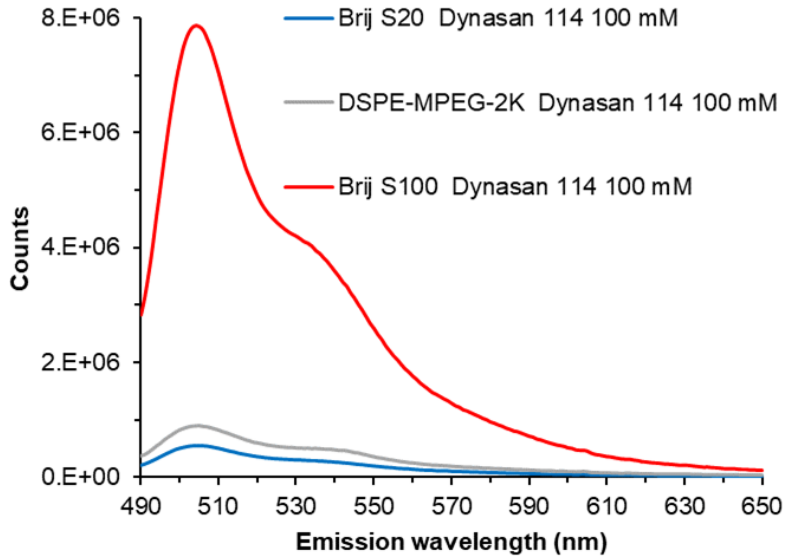

Figure 6.12- DiO fluorescence data displaying emission wavelength from samples containing Dynasan 114 at pH 7. Samples were formulated using an initial citrate buffer concentration of 100 mM. Samples were excited at 484 nm.

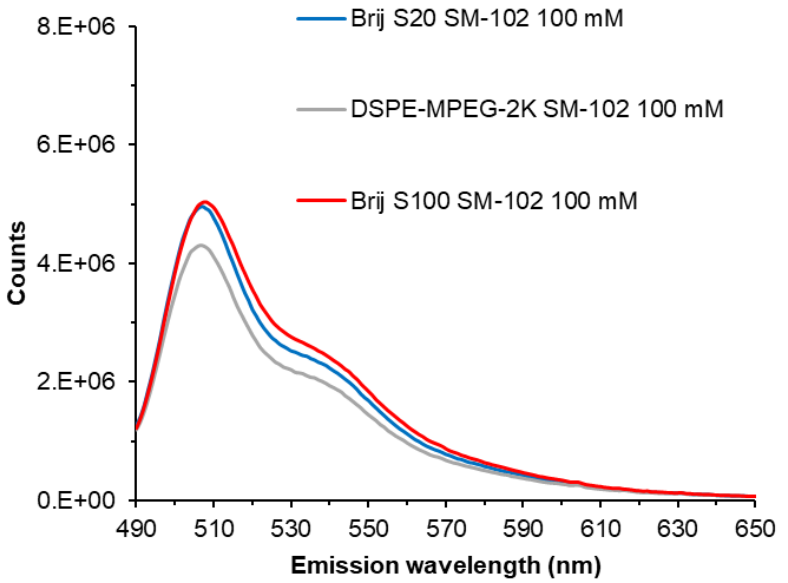

Figure 6.13- DiO fluorescence data displaying emission wavelength from samples containing SM-102 at pH 7. Samples were formulated using an initial citrate buffer concentration of 100 mM. Samples were excited at 484 nm.

There was also a noticeable effect on fluorescence induced by increasing the concentration of buffer solution suggesting a lower degree of quenching. This effect was consistent and independent on pegylated lipid as shown by Fig.6.14-A-D. Although, the exact reasoning is unknown. Nevertheless, along with the data from DLS and Zeta potential it was deemed 100 mM citrate buffer was most suitable going forward as it produced samples with highest fluorescence while also producing stable nanoparticle formulations with a higher potential of protonating the ionisable cationic lipid SM-102.

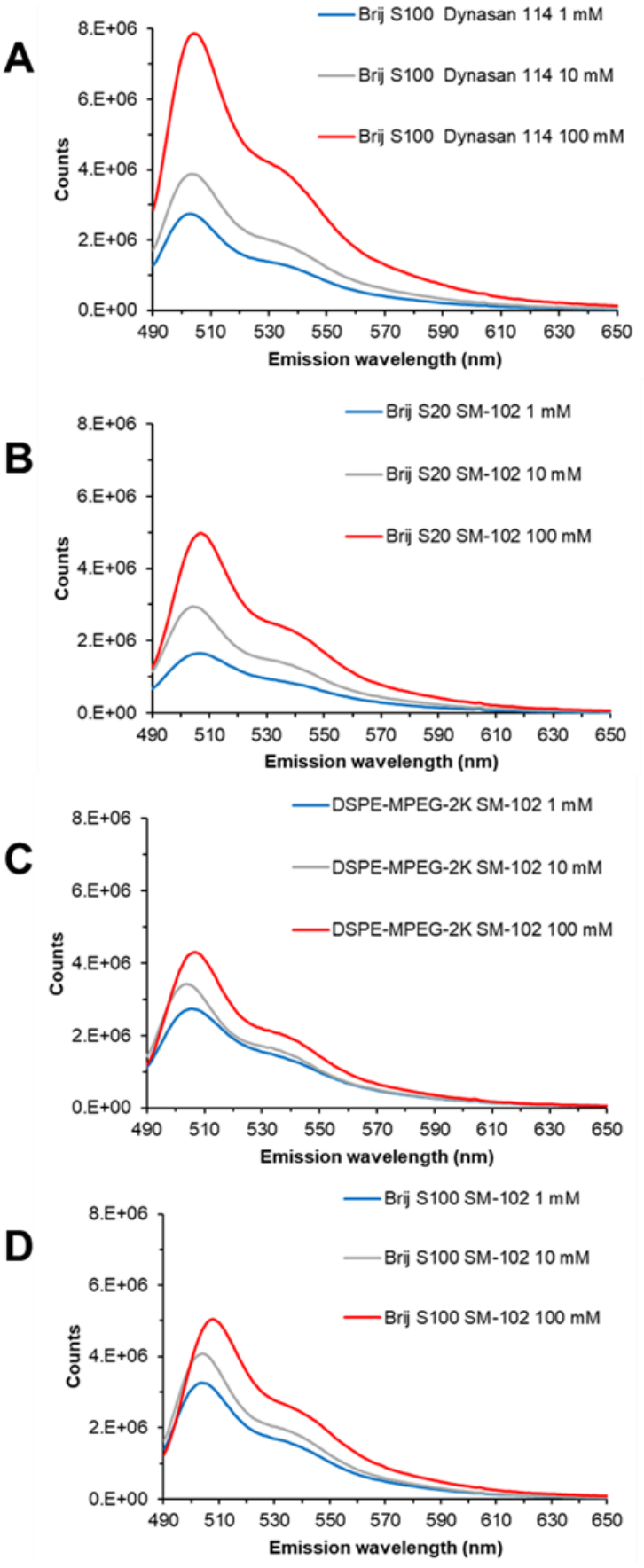

Figure 6.14- DiO fluorescence data displaying the consistent effect of buffer concentration increasing emission intensity. Samples were excited at 484 nm.

To ensure the dye had in fact been encapsulated within the particle and was not existing as a solute dissolved in solution, formulations were centrifuged at 150,000 g for 20 minutes using centrifuge filters to remove the particles from solution. The supernatant was then analysed for fluorescence and for formulations of both Dynasan 114 and SM-102 the emission was lost, as shown by Fig.6.15. As a result, it was deemed that the dye DiO had been successfully encapsulated within the particles and therefore any visible emission was coming from within the particles.

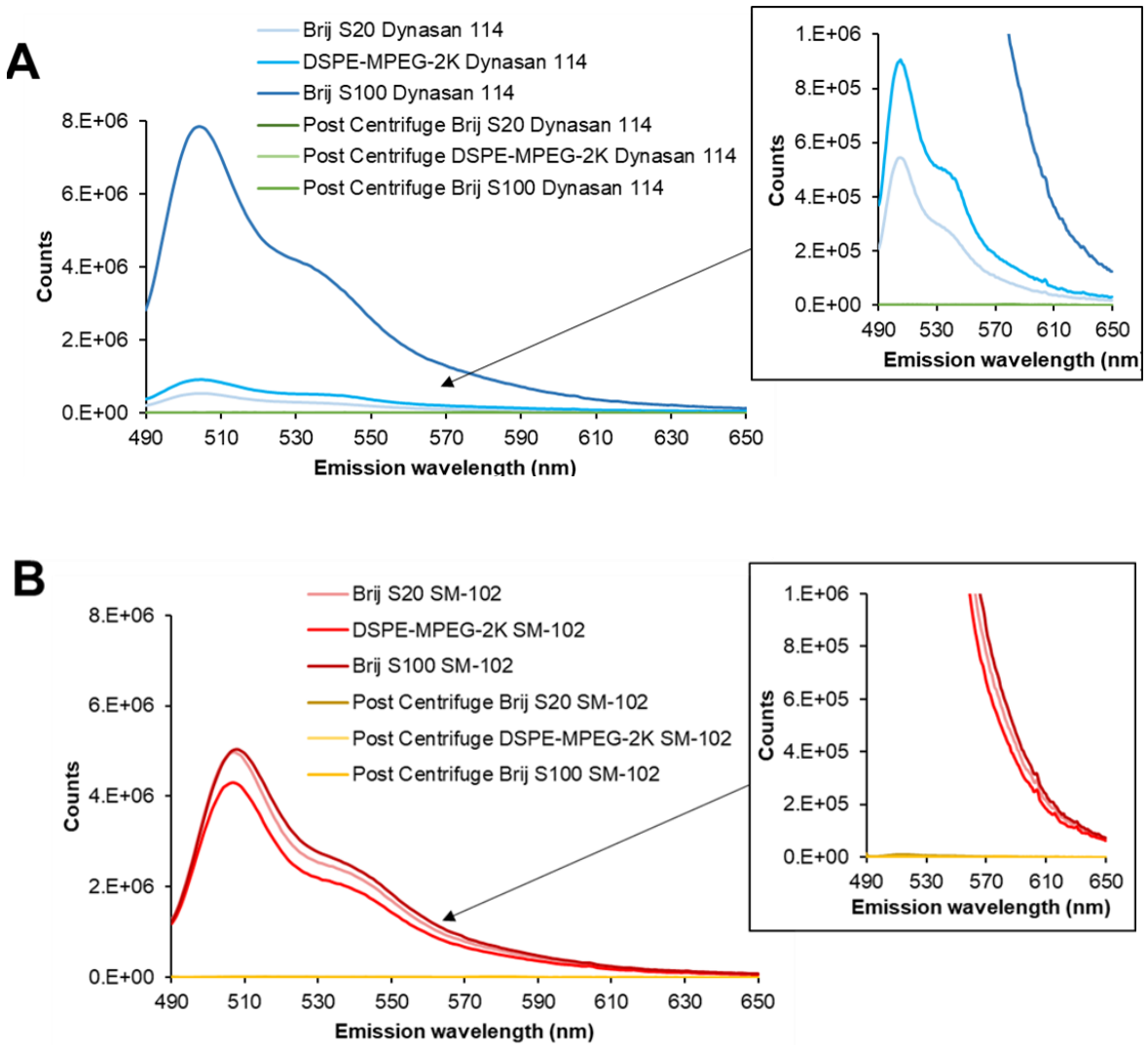

Figure 6.15- DiO fluorescence data displaying loss of emission signal upon removal of particles from suspension by centrifuge. Samples were excited at 484 nm.

6.3.2. *In vitro* studies

THP-1 cell lines were exposed to lipid nanoparticle formulations developed at 1.87 ug DiO loading per mg of Dynasan 114 or SM-102, and an intial citrate buffer concentration of 100 mM. Lipid nanoparticle formulations were tested at four various concentrations; 0.01, 0.1, 1 and 10 ug/mL. After an incubation period of 24 hours (37 °C, 5 % CO_2 and humidified) cell suspensions were collected, culture supernatants stored at -80 °C and cells suspended in running buffer. Fluorescence was then measured by flow cytometry. Fig.6.16, displays the results of fluorescence for the various formulations tested- samples that showed significant fluorescence were then normalised against the intensity of fluorescence obtained in Fig.6.12 and 6.13. Immediately, it is clear that formulations of Dynasan 114 stabilised by Brij S100 (black), SM-102 stabilised by Brij S100 (green) and SM-102 stabilised by Brij S20 (red) resulted in significant fluorescence at the highest concentration. Thus, suggesting these formulations had accumulated and/or permeated within the cells.

Formulations of Dynasan 114 stabilised by Brij S20 and DSPE-MPEG-2K displayed very little to no fluorescence suggesting failure to accumulate and or permeate within the cell. It was believed due to the aggregation of these formulations while elevating pH to physiological pH 7 the formulations exceeded the size limitations in order to permeate within the cell. Interestingly the formulation of SM-102 stabilised by DSPE-MPEG-2K also showed no fluorescence and thus no indication of accumulation and/or permeation within cells. It was hypothesised the negative charge of DSPE-MPEG-2K may have impacted the particles ability to accumulate/permeate within. As previously discussed, positive charge and not just size of particles plays a key role in influencing accumulation/permeation.[103]

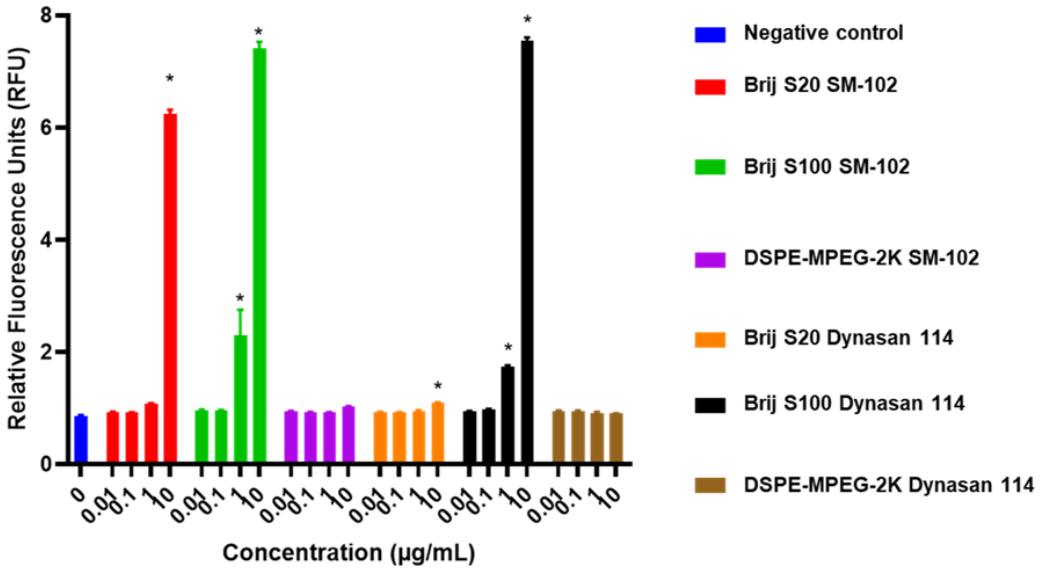

Figure 6.16- Fluorescence data obtained after THP-1 cell lines were exposed to lipid nanoparticle formulations. Data was normalised against that in Fig.6.12 and Fig.6.13.

Multiplex analysis of the culture supernatants was then performed using various analytes (IFN-γ, IL-6, IL-18, IL-1β, IL-8 and TNF-α), although the only quantifiable differences observed were in IL-8. Fig.6.17 displays the data obtained while analysing IL-8. The data suggests potential secretion of IL-8 by cells treated with nanoparticle formulations composed of SM-102 and stabilised by either Brij S20 or Brij S100, whereas the formulation of Dynasan 114 stabilised by Brij S100 does not. As a result, this data suggests formulations of SM-102 stabilised by either Brij S20 or Brij S100 may have resulted in successful cell membrane permeation and thus intracellular accumulation due to the correlation identified between cytokine/chemokine release and cellular uptake of nanoparticles by Avila *et al*.[133] On the other hand, due to the formulation of Dynasan 114 stabilised by Brij S100 only showing signs of fluorescence yet no IL-8 secretion, this formulation is expected to only accumulate on the exterior of the cell. The hypothetical ability of formulations to enter cells is illustrated by Fig.6.18.

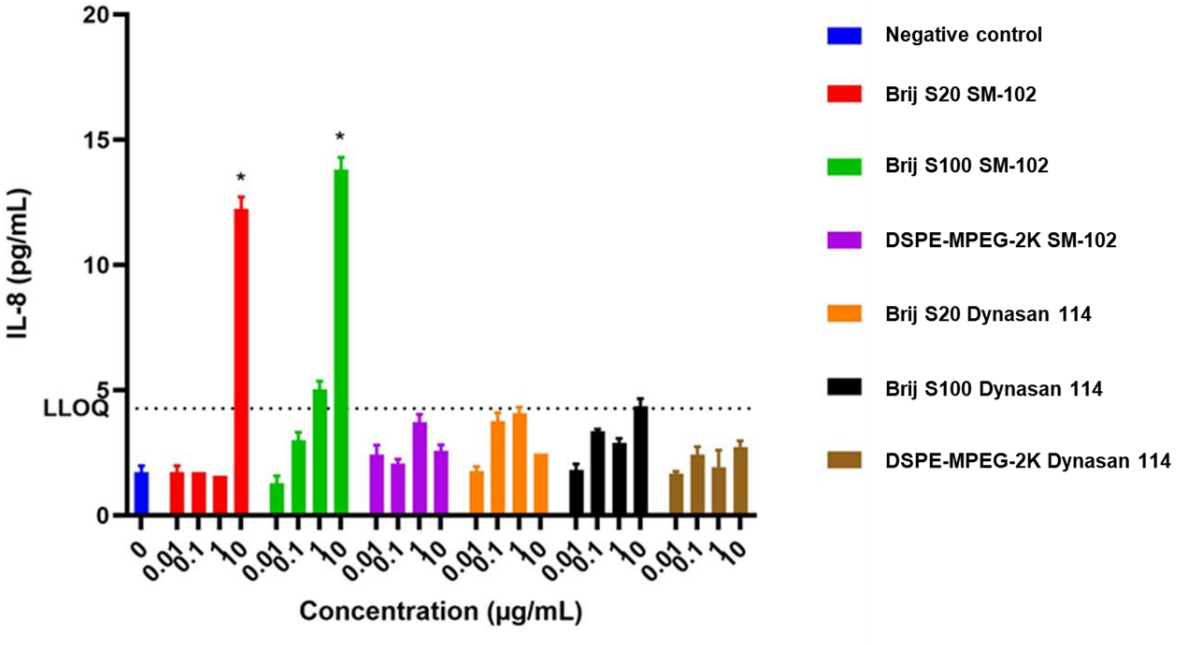

Figure 6.17- Results from multiplex analysis of cell culture supernatant analysing Interleukin 8 (IL-8) chemokine.

Thus far the data presented only suggests that charge appears to be critical with regards to intra or extracellular accumulation. This is due to formulations containing ionisable cationic SM-102 which are stabilised by a non-ionic pegylated lipid surfactant appearing to accumulate within the cell while similar formulations containing the neutal lipid Dynasan 114 accumulate outside of the cell. The ability of the SM-102 formulations stabilised by Brij S20 and Brij S100 to escape from the endosomes once successfully accumulated within the cell is unknown. As a result, it is still unclear whether the difference in PEG chain length between Brij S20 and Brij S100 would have an impact on the delivery

of nucleic acids such as mRNA- assuming nanoparticles formulations would behave the same once mRNA is incorporated.

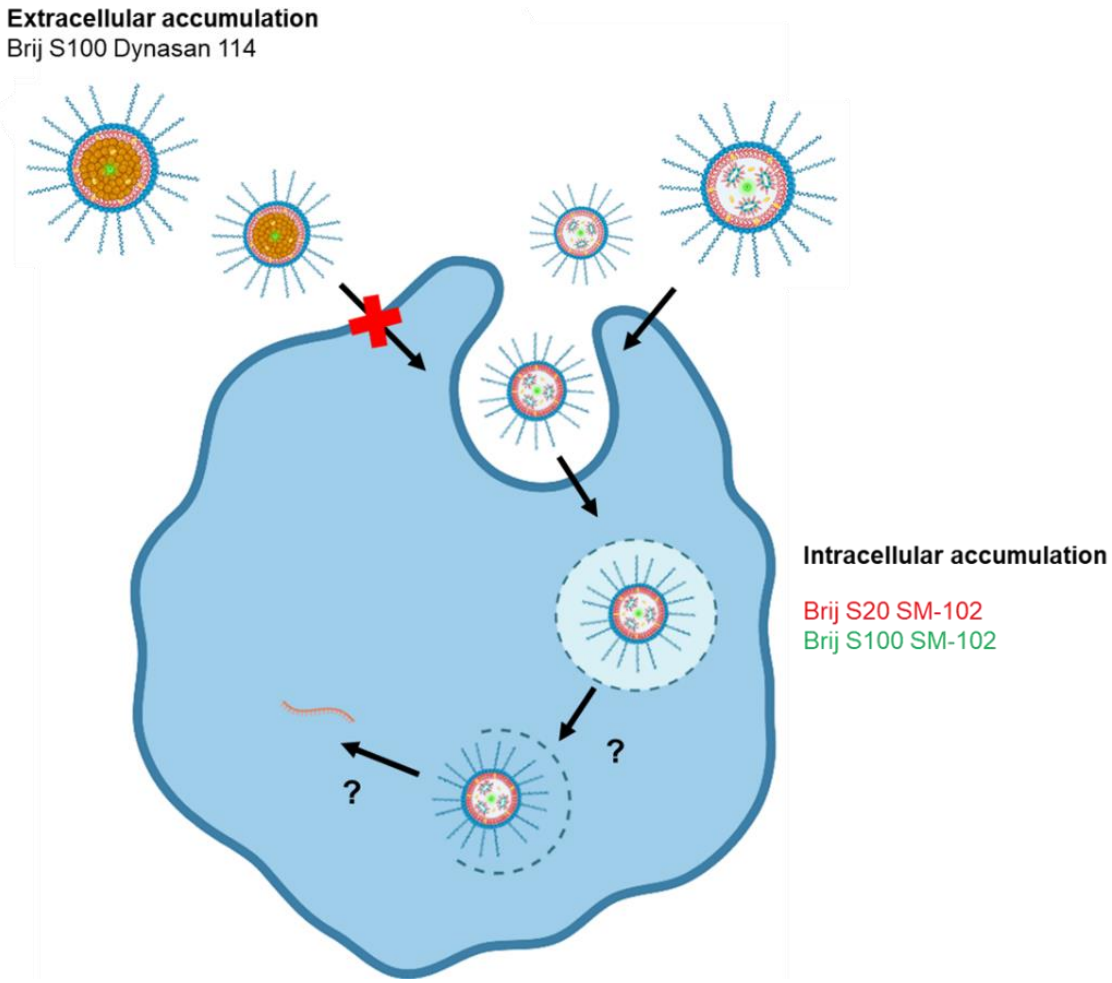

Figure 6.18- Illustration summarising the hypothetical ability of each formulation to enter cells.

6.4. Conclusions

In conclusion, for formulations containing SM-102 the data obtained by fluorescence flow cytometry and by multiplex analysis of IL-8 indicated intracellular accumulation due to significant fluorescence signal and secretion of IL-8. On the other hand, only extracellular accumulation was achieved with formulations containing the neutral trimyristin lipid Dynasan 114. Furthermore, in both cases accumulation was only possible when stabilised by a neutral pegylated lipid, as formulations stabilised by the anionic DSPE-MPEG-2K failed to produce any fluorescence or IL-8. It was hypothesised accumulation failed due to the negative charge suppressing the positive charge from the ionisable

cationic lipid SM-102. Furthermore, formulations of Dynasan 114 with a shorter chain length of PEG were unstable and failed to accumulate likely due to size limitations and/or sedimentation. Overall, out of the formulations that were stable there was no clear difference in the degree of intracellular accumulation between samples varying in chain length (Brij S20 and Brij S100).

Formulations stabilised by pegylated lipids of shorter PEG mw experienced instability when Dynasan 114 was incorporated although appeared stable upon incorporation of SM-102, therefore it was deemed the positive charge of the ionisable lipid SM-102 appeared to play a crucial role not only in cellular uptake but also the colloidal stability of the lipid nanoparticle formulation. This work further supports the understanding of the roles of materials within lipid nanoparticles formulations and how they may play a role in intracellular accumulation.

It was previously believed in literature that ~ 10 % of ionisable cationic lipid still carries a positive charge once the formulation is at near neutral pH,[101] and that may play a role in the particles ability to accumulate within the cell. This work supports and further builds on the knowledge that due to the direct comparison between a formulation containing ionizable cationic lipid with another containing only a neutral lipid, as the combination of both the fluorescence and data of IL-8 secretion suggests that only formulations containing the ionisable cationic lipid could successfully accumulate within the cell. As a result, this work further advances understanding of the role of the ionisable cationic lipid and can be used in the future development of mRNA containing lipid nanoparticles.

Future work

It would be interesting to incorporate mRNA with a fluorescent tracer for example EGFP mRNA. EGFP mRNA can be directly visualised and may be used to determine mRNA delivery and accumulation independent of translation,[163] therefore it may be possible to determine any differences in mRNA delivery efficiency between the two different PEG chain lengths of Brij S20 and Brij S100. If successful It would also be plausible to increase number of neutral pegylated lipid of varying PEG chain length should be trialled to further explore how the molecular weight of PEG may have an impact on the delivery of nucleic acids such as mRNA to the cytoplasm. In doing so a greater understanding of the relationship of ho the PEG chain length of pegylated lipid impacts permeability of membranes such as in the events of internalisation and endosomal escape. Furthermore, would provide a greater idea of the trade-off between formulation steric stability and ability to permeate cell membranes.

Additionally, formulations could be investigated for circulation times depending on PEG chain length. As a result, all aspects could be considered when developing a formulation for the delivery of mRNA.

6.5. Experimental

Materials

Deuterated solvent (D_2O), tris buffer, citric acid, sodium citrate dihydrate, Brij S10, Brij S20, Brij S100 and cholesterol were all purchased from Sigma Aldrich and used as received. Tetrahydrofuran solvent were reagent grade and purchased from Fischer Scientific and used as received. Lipophilic dye 3,3'-Dioctadecyloxacarbocyanine (DiO) and a solution of SM-102 in ethanol was also purchased from Cambridge Biosciences. Dynasan 114 (trimyristin) was kindly gifted from IOI Oleochemical, Hamburg. Lipoid S100 was purchased from Lipoid and used as received. DSPE-MPEG-2K was kindly gifted from Lipoid. Cell work was performed by Pharmacology department and source of materials is thus unknown. CleanCap cyanine 5 EGFP mRNA provided by Pharmacology who purchased from Trilink Biotechnologies.

Preparation of initial scale down trial in Fig.2

Method adopted for lipid nanoparticle formulation was nanoprecipitation. For the aqueous distilled water was used at a volume of 24 (normal) and 1.5 mL (scaled down). For the organic phase stock solutions of Dynasan 114 (4 mg/ml) and Lipoid S100 (24 mg/ml) were prepared in tetrahydrofuran (THF). 0.5 mL portions of each stock solution were combined to produce an injectable shot of 2 mL- for scaled down these volumes were reduced to 0.0625 mL for an overall shot of 0.125 mL. At normal scale organic shot was added dropwise into the vortex of the aqueous solution by removing the plunger from a clamped syringe. When scaled down the solution was rapidly injected into the vortex of the aqueous phase contained in a 4 mL vial. Each were mechanically stirred at 800 rpm by a PTFE stirrer bar (Stirrer bar size- 10 mm scaled down, 20 mm normal scale). The combined mixture was left stirring to allow evaporation of tetrahydrofuran over ~24 hours at a room temperature of ~ 21 °C in a fume cupboard with an average air velocity of 0.35 ms^{-1}

Preparation of lipid nanoparticles varying in dye loading

Method adopted for lipid nanoparticle formulation was nanoprecipitation. For the aqueous phase stock solutions of pegylated lipid and citrate buffer pH 3 were prepared and portions combined for a total volume of 1.5 mL. For the organic phase stock solutions of ionisable cationic lipid (SM-102), Dynasan 114, Helper lipid (Lipoid S100), cholesterol and lipophilic dye (DiO) were prepared in tetrahydrofuran (THF). Note aliquots of SM-102 were taken and dried down to remove ethanol prior to dissolving in (THF). In addition, formulations contained either Dynasan 114 or SM-102 not both. 0.031 mL portions of stock solutions were combined for a total injection volume of 0.124 mL. Organic phase was rapidly injected into the vortex of the aqueous phase contained in a 4 mL vial. Mechanically stirred by a 10 mm PTFE stirrer bar at 800 rpm. The molar ratio of materials employed was 46.3 : 1.6

: 9.4 : 42.7 (Dynasan 114/SM-102 : pegylated lipid : helper lipid : cholesterol). The overall concentration of the formulations was approximately ~ 0.165mg/mL. The combined mixture was left stirring to allow evaporation of tetrahydrofuran over ~24 hours at a room temperature of ~ 21 °C in a fume cupboard with an average air velocity of 0.35 ms^{-1}.

Samples that underwent pH adjustment were performed by dilution with Tris buffer until pH 7.

Uptake of lipid nanoparticles by THP-1 cell line

THP-1 cell lines were exposed to lipid nanoparticle formulations. Nanoparticle formulations were tested at four concentrations: 0.01, 0.1, 1 and 10 ug/mL. THP-1 were washed once in HBSS, suspended in Opti-MEM (2×10^5 cells/mL), and seeded to a 24-well microplate (500 µL). 100 µL of nanoparticle dilutions (prepared in Opti-MEM) was added to respective wells, and incubated 24 hours (37°C, 5% CO_2, humidified). Cell suspensions were collected, culture supernatants stored at -80°C, and cells suspended in running buffer. Release of IL-8 was also determined from culture supernatants.

Analytical techniques

Fluorescence

Fluorescence excitation and emission spectra were recorded using a FLS 1000 with a Xenon lamp at 68.75 °C. Each sample was measured using set conditions of a 1 mm scan slit for 5 scans. Excitation and emission were set to 484/501 nm.

Fluorescence measurements of formulations containing lipophilic dye were obtained upon treatment to cell lines were obtained by flow cytometry using a B1 channel, excitation 488 nm and emission 525/50.

Nuclear Magnetic Resonance Spectroscopy

^1H NMR spectra were recorded using a Bruker DPX-400 spectrometer operating at 400 MHz for ^1H NMR. Solvents used for NMR spectroscopy were D_2O. Chemical shifts (δ) are reported in parts per million (ppm).

Dynamic light scattering (DLS) and Zeta potential

Samples were analysed by DLS using The Malvern ZetaSizer Nano S DLS obtain a Z-average and size distribution (PDI) and zeta potential of nanoparticle dispersion. 2 ml of each sample was

measured in standard 3 ml fluorimeter cuvettes with a pathlength of 10 mm. All measurements were carried out at 25 °C with a fixed backscattering angle of 173° using automated setting. Each sample was measured once although formulations were done in triplicate. Zeta potential was also measured using Malvern ZetaSizer Nano S. Samples were measured using automated settings and samples were measured in triplicate in a Malvern zetasizer nano series disposable folded capillary cell. All measurements were carried out at 25 °C.

LogP

Calculated LogP values were predicted using ChemDrawProfessional version 18.1 software.

6.6. Appendix

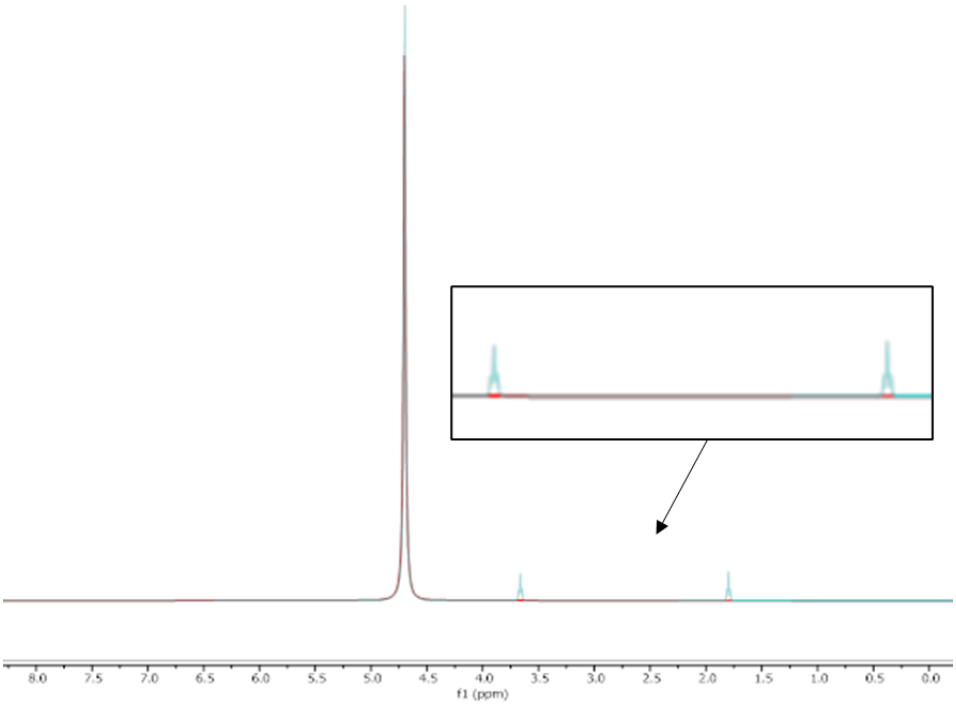

Appendix Figure 6.1- 1H NMR overlay of day 0 (cyan) and day 1 (red) showing disappearance of peaks for tetrahydrofuran (THF) at approximately 1.85 and 3.7 ppm indicating complete evaporation of THF for the scaled down nanoparticle formulation.

CHAPTER 7

Conclusions and Future work

Chapter 7 Conclusions and Future Work

Chapter 2 explored the use of LogP as a model for nanoparticle formation and stability *via* flash nanoprecipitation. Furthermore, prodrugs of lamivudine were synthesised strategically varying the LogP of carbamate and carbonate-based prodrug before assessment of the formation and stability of SLN and SPN were investigated. As per the LaMer model, it was found with increasing LogP (and the likely higher degree of supersaturation and faster rate of nucleation) smaller nanoparticles with reduced standard deviation were produced. Furthermore, the prodrug with the highest LogP (11.44) resulted in highly stable formulations which maintained size and dispersity for up to at least 4 weeks. Meanwhile prodrugs of lower LogP experienced considerable growth resulting in micron sized aggregates as a result of Ostwald ripening. This work agrees with Zhu et al. that molecules of a LogP between 9-12 may form potentially stable nanoparticles by nanoprecipitation,[33] while demonstrates a more systematic approach and in depth understanding that molecules with an elevated LogP may be formulated to form stable particles of a small size and narrow size distribution. As a result, demonstrates how LogP can be used as a tool to tune and optimise nanoparticle formulations in the future. Additionally, this work demonstrates how poorly water-soluble drugs may be formulated with or without the need of prodrug synthesis to achieve high drug loading formulations. This work also opens the door to potential combination nanoparticles with both hydrophilic and hydrophobic drugs. Meanwhile, this work builds on that of Jennings *et al*.,[13] and Bunjes *et al*.,[34] by demonstrating how blending drug/prodrug with a lipid such as Imwitor 900k tackles issues such as high crystallinity of the

On the back of this work it would be interesting for more studies to be performed using this strategy, while employing other model drugs and chemistries to strengthen the hypothesis. In doing so, LogP could be deemed as a universal indicator for stable nanoparticle formulation with regards to prodrugs.

Chapter 3 explored the properties of lipid surfactants and the study suggested that their nucleation behaviour aids nanoparticle formation due to providing stabilisation during the growth phase of nanoparticle formation. In doing so, potentially offers stabilisation earlier to growing nuclei/nanoparticles thus limiting nanoparticle size and size distribution of materials at elevated LogP or wt%.

Blends of unpegylated lipid surfactants with pegylated lipid surfactant revealed how harnessing the stabilisation provided by both types of surfactant enabled formulations of tricaprin at higher wt % to be produced that were stable. This strategy along with that developed in chapter 2 were employed to produce nanoparticle formulations of high drug loading. Overall, this work provides greater understanding of how the properties of lipid materials determine behaviour in specific environments and translate into a beneficial attribute during application of formulation development of lipid

nanoparticles. For example, the investigation of different blends across various ratios enabled the conclusion that the hydrophobic nature of the unpegylated lipid surfactant which results in its nucleation upon nanoprecipitation enabled rapid stabilisation of the growing nuclei at even much higher drug loadings and thus limited growth by aggregation, meanwhile the steric stabilisation of the pegylated lipid surfactant provided the formulation with greater long term colloidal stability. In literature there was a clear lack of understanding for the role of unpegylated lipid surfactants other than aiding in nanoparticle formation and how this was achieved, as a result this work may be used as a guide to better inform of their role and how this understanding may be applied in order to tune and optimise nanoparticle formulations in the future.

In the future it would be interesting to broaden the understanding further by exploring a wide variety of unpegylated lipid surfactants other than Lipoid S100 for example unpegylated lipid surfactantsthat possess a net charge such as DOTAP-Cl which may nucleate in a similar manner yet provide electrostatic stabilisation and thus greater control over nanoparticle formulation by flash nanoprecipitation. Likewise, it is also plausible to investigate other forms of pegylated lipid surfactants such as those shown in Fig.1.33 e.g. DSPE-MPEG-2K. One aspect we identified is pegylated lipid surfactants with lower HLB display nucleation behaviour, although those with a short PEG chain may not provide sufficient steric stabilisation. As a result, it is plausible to investigate other pegylated lipid surfactants which are of lower HLB yet possess a PEG chain which is efficient enough to provide sufficient steric stabilisation upon formulation. DSPE-MPEG-2K may be a potential example as DSPE-MPEG-2K is a pegylated phospholipid which is composed of two alkyl chains conjugated to a 2K PEG chain. It may be that the additional alkyl chain may worsen the solubility of the pegylated lipid surfactant resulting in nucleation behaviour if introduced *via* the organic solvent.

Chapter 4 examined how aspects of formulation design that had been developed in chapters 2 and 3 i.e. ratio of pegylated lipid to unpegylated lipid surfactant and wt % of core material impacted the stability of a formulation during cryopreservation.

It was concluded that the type of surfactant and surfactant composition played a big role in the stability of formulations against the stresses of cryopreservation techniques such as freeze thaw and freeze drying/lyophilization. As formulations containing the cationic unegylated lipid surfactant DOTAP-Cl rather than the zwitterionic unpegylated lipid surfactant Lipoid S100 appear to maintain the cake structure more efficiently, resulting in higher redispersion quality. Although, generally formulations stabilised by more pegylated lipid surfactant appeared to maintain stability over those higher in unpegylated lipid surfactant. As a result, suggests the steric stabilisation provided by Brij S20 was much more efficient at stabilising formulations than the electrostatic stabilisation provided by

DOTAP-Cl. This was likely due to the PEG chain of the Brij S20 which contributed to cake formation and stability. In all formulations the addition of more sucrose resulted in improved cake formation/stability. As a result, it was possible to enhance formulation stability and quality against the stresses of freeze thaw and freeze drying with the aid of a cryoprotectant and/or lyoprotectant such as sucrose.

Surfactant blends of pegylated lipid to unpegylated lipid surfactant at a ratio of (50:50) or (25:75) to stabilise formulations of tricaprin at 33 wt % were developed with the ability to withstand the stress of freeze drying. This approach was then employed while blending in dodecyl prodrug into the formulation. As a result, the strategy of chapters 2, 3 and 4 demonstrated how a formulation of high drug loading may be achieved which may also withstand the stress of cryopreservation, thus potentially enabling long term storage. Aspects such as method of freezing and method of redispersion have been investigated in literature although there is a lack of understanding of how aspects of the formulation may impact its stability against the stresses of freezing and drying. Overall, this work demonstrates a systematic approach to gain necessary insight and understanding that was lacking in literature of how the different types and blends of surfactants used in lipid nanoparticle formulations impact formulation stability against the stresses of cryopreservation methods such as freeze drying. Furthermore, demonstrates how the ratio of core material to surfactant, surfactant composition, and cryoprotectant concentration may be tuned to develop a high drug loading formulation which is able to be freeze dried and redispersed which may improve the long-term stability of formulations upon storage. This work may be employed as a guide for anyone attempting to produce a lipid nanoparticle formulation with the goal of it being successfully cryopreserved such as mRNA containing lipid nanoparticles.

It would be interesting to further expand on the work in this study by investigating various chain lengths of pegylated lipid surfactants; would an increase in PEG chain length result in sufficient steric stabilisation? This might offer the potential to reduce the cryoprotectant/lyoprotectant concentration required in order to maintain formulation stability during cryopreservation techniques such as freeze drying and/or enable formulations of higher wt % to be freeze dried and redispersed. Furthermore, other types of cryoprotectants/lyoprotectants may also be explored. Again, it would be interesting to investigate whether a different prodrug of different chemistry yet same/similar LogP could also prodrug a formulation which was of high drug loading and withstand the stress of cryopreservation.

Chapter 5 incorporates each strategy of chapters 2, 3 and 4 to develop a highly concentrated formulation before monitoring drug release. The study revealed that formulations of the dodecyl prodrug can be activated to release the original drug lamivudine. Activation was achieved at

physiological conditions of 37 °C, 0.1 M phosphate buffer in the presence of porcine liver esterase enzyme. Prodrug activation was only found in the presence of enzyme and not solely in the presence of physiological temperature and buffer. This suggested high stability of the dodecyl prodrug and the release may be triggered once exposed to enzyme. Overall, an average drug release of ~ 14 % after one week and 37 % was achieved with one batch of enzyme after nine weeks. Although, the porcine liver esterase enzyme showed signs of potential suicide inhibition *via* glycation caused by the high concentration of sucrose in the solution due to a decrease in rate of release at week 5. Nevertheless, upon addition of more enzyme drug release could be sustained, thus suggesting potential for higher percentages of drug release to be achieved if the study was continued or if performed *in vivo*. This study also validated the strategy of prodrugs for encapsulation within lipid nanoparticles as a method for delivering a sustained release of drug.

It would be interesting to attempt to dilute the concentration of sucrose prior to studying enzyme activation, which would provide greater insight into the extent of suicide inhibition induced by glycation of enzyme. As a result, would reveal whether the slow release is due to the formulation or the occurrence of suicide inhibition of the enzyme. Additionally, other enzymes that may be found within the body as well as different concentrations of enzyme could be investigated to test for different release profiles, before finally investigating release *in vivo*. Furthermore, prodrugs of other chemistries could be investigated and formulated to investigate any potential differences in rate of release.

Chapter 6 investigated how different aspects of lipid nanoparticle formulations for the delivery of nucleic acids such as mRNA impact the overall formulation's ability to function. Formulations containing the ionisable cationic lipid SM-102, the data obtained by fluorescence flow cytometry and by multiplex analysis of IL-8 indicated intracellular accumulation due to significant fluorescence signal and secretion of IL-8. Unfortunately, we could distinguish a difference between the cellular uptake or endosomal escape for formulations of the ionisable cationic lipid SM-102 when stabilised by Brij S20 or Brij S100. Formulation of the neutral lipid Dynasan 114 stabilised by Brij S100 was found to accumulate extracellularly. This was believed to be because the absence of positive charge which further supports the theory that positively charge facilitate membrane permeability. Interestingly, formulations stabilised by DSPE-MPEG-2K failed to accumulate which was attributed to the negative charge it introduced to the nanoparticle formulations.

During formulation development PEG chain length and the presence of SM-102 were found to be instrumental in the stability of formulations as formulations of the neutral lipid stabilised by a shorter PEG chain length pegylated lipid were unstable likely due to the absence of electrostatic stabilisation

and insufficient steric stabilisation. Whereas formulations of SM-102 were stable with shorter PEG chain length pegylated lipid stabilisers.

This work further supports the understanding of lipid nanoparticles with respect to membrane permeability due to the clear differences in variables surrounding lipid nanoparticle composition such as containing an ionisable cationic lipid. Furthermore, provides greater insight into how different aspects of the formulation design such as charge and various forms and degree of stabilisation impact formulation size and size distribution which is key in the development of lipid nanoparticles which are designed to permeate cell membranes such as in the delivery of mRNA.

It was previously believed in literature that ~ 10 % of ionisable cationic lipid still carries a positive charge once the formulation is at near neutral pH,[101] and that may play a role in the particles ability to accumulate within the cell. This work supports and further builds on the knowledge that due to the direct comparison between a formulation containing ionizable cationic lipid with another containing only a neutral lipid, as the combination of both the fluorescence and data of IL-8 secretion suggests that only formulations containing the ionisable cationic lipid could successfully accumulate within the cell. As a result, this work further advances understanding of the role of the ionisable cationic lipid and can be used in the future development of mRNA containing lipid nanoparticles.

In the future it would be interesting to expand this study by incorporating mRNA which can produce a fluorescent protein upon translation. As a result, any differences in delivery efficiency of mRNA could be revealed. Furthermore, the scope of pegylated surfactants could be expanded to further broaden the understanding of the role and impact of PEG chain length on delivery efficiency.

Overall, the contents of this thesis demonstrate how drugs may be chemically modified to synthesise prodrugs which can be formulated by flash nanoprecipitation to produce stable and high drug loading lipid nanoparticle formulations. These formulations have also been proven to be capable of enhanced drug loading and providing formulations with greater stability. Furthermore, the importance of surfactant composition and cryoprotectant/lyoprotectants is displayed for cryopreservation methods such as freeze thaw and freeze drying. Finally, the method of prodrug formulation is used to facilitate sustained drug release over a prolongued period but only when exposed to physiological conditions and the presence of a biological agent such as an enzyme. In addition, the knowledge gained has also been translated to develop formulations with the potentially to deliver other drug forms such as mRNA. This provides greater insight and understanding surrounding lipid nanoparticle formulation and may be used in the design of formulations in the future.

In conclusion, the contents of this thesis may provide other researchers with specific insight into formulation design to overcome various challenges faced by lipid nanoparticle development. This work may also be built on by other researchers to further develop the strategies outlined in this thesis.

CHAPTER 8

References

Chapter 8 References

1 O. Escalona-Rayo, P. Fuentes-Vázquez, G. Leyva-Gómez, B. Cisneros, R. Villalobos, J. J. Magaña and D. Quintanar-Guerrero, *Drug Dev. Ind. Pharm.*, 2017, **43**, 871–888.

2 A. Fahr and X. Liu, *Expert Opin. Drug Deliv.*, 2007, **4**, 403–16.

3 J. M. Custodio, C.-Y. Wu and L. Z. Benet, *Adv. Drug Deliv. Rev.*, 2008, **60**, 717–733.

4 Y. (Chezy) Barenholz, *J. Control. Release*, 2012, **160**, 117–134.

5 U. Bulbake, S. Doppalapudi, N. Kommineni and W. Khan, *Pharmaceutics*, 2017, **9**, 12.

6 N. Muhamad, T. Plengsuriyakarn and K. Na-Bangchang, *Int. J. Nanomedicine*, 2018, **Volume 13**, 3921–3935.

7 L. Schoenmaker, D. Witzigmann, J. A. Kulkarni, R. Verbeke, G. Kersten, W. Jiskoot and D. J. A. Crommelin, *Int. J. Pharm.*, 2021, **601**, 120586.

8 H. Wen, H. Jung and X. Li, *AAPS J.*, 2015, **17**, 1327–1340.

9 W. Mehnert and K. Mäder, *Adv. Drug Deliv. Rev.*, 2012, **64**, 83–101.

10 K. Westesen, H. Bunjes and M. H. . Koch, *J. Control. Release*, 1997, **48**, 223–236.

11 M. Koroleva, I. Portnaya, E. Mischenko, I. Abutbul-Ionita, L. Kolik-Shmuel and D. Danino, *J. Colloid Interface Sci.*, 2022, **610**, 61–69.

12 T. Helgason, T. S. Awad, K. Kristbergsson, D. J. McClements and J. Weiss, *J. Am. Oil Chem. Soc.*, 2008, **85**, 501–511.

13 V. Jenning, K. Mäder and S. H. Gohla, *Int. J. Pharm.*, 2000, **205**, 15–21.

14 Z. HUANG, S. HUA, Y. YANG and J. FANG, *Acta Pharmacol. Sin.*, 2008, **29**, 1094–1102.

15 R. Shah, D. Eldridge, E. Palombo and I. Harding, *Lipid Nanoparticles: Production, Characterization and Stability*, Springer International Publishing, Cham, 2015.

16 M. Baptista, I. Cuccovia, H. Chaimovich and M. Politi, *J. Phys. Chem.*, 1992, **96**, 6442–6449.

17 J. J. Hobson, A. Al-khouja, P. Curley, D. Meyers, C. Flexner, M. Siccardi, A. Owen, C. F. Meyers and S. P. Rannard, *Nat. Commun.*, 2019, **10**, 1413.

18 S. Pouralhosseini, J. Shaw and S. Sajjad, *J. Mater. Sceince*.

19 A. Jones and B. Vincent, *Colloids and Surfaces*, 1989, **42**, 113–138.

20 B. Vincent, J. Edwards, S. Emmett and A. Jones, *Colloids and Surfaces*, 1986, **18**, 261–281.

21 D. . Napper, *J. Colloid Interface Sci.*, 1977, **58**, 390–407.

22 D. J. Meier, *J. Phys. Chem.*, 1967, **71**, 1861–1868.

23 T. F. Tadros, *Polym. J.*, 1991, **23**, 683–696.

24 BYK Additives & Instruments, Wetting and Dispersing Additives, https://ebooks.byk.com/en/wetting-and-dispersing/electrostatic-stabilization/, (accessed 17 February 2023).

25 C. M. Goodman, C. D. McCusker, T. Yilmaz and V. M. Rotello, *Bioconjug. Chem.*, 2004, **15**, 897–900.

26 *The HLB SYSTEM Croda's Time-Saving Guide to Surfactant Selection Personal Care Edition*, .

27 J. Davies, *Proceedings of the Second International Congress of Surface Activity- A quantitative kinetic theory of emulsion type. I . Physical chemistry of the emulsifying agent*, Butterworths Scientific, 1957.

28 V.-A. Duong, T.-T.-L. Nguyen and H.-J. Maeng, *Molecules*, 2020, **25**, 4781.

29 A. Deshpande, M. Mohamed, S. B. Daftardar, M. Patel, S. H. S. Boddu and J. Nesamony, in *Emerging Nanotechnologies for Diagnostics, Drug Delivery and Medical Devices*, Elsevier, 2017, pp. 291–330.

30 M. E. Gindy, B. Feuston, A. Glass, L. Arrington, R. M. Haas, J. Schariter and S. M. Stirdivant, *Mol. Pharm.*, 2014, **11**, 4143–4153.

31 Z. Zhang, Z. Wang, S. He, C. Wang, M. Jin and Y. Yin, *Chem. Sci.*, 2015, **6**, 5197–5203.

32 T. J. Wooster, M. Golding and P. Sanguansri, *Langmuir*, 2008, **24**, 12758–12765.

33 Z. Zhu, *Mol. Pharm.*, 2014, **11**, 776–786.

34 H. Bunjes, K. Westesen and M. H. J. Koch, *Int. J. Pharm.*, 1996, **129**, 159–173.

35 V. Jenning, A. F. Thünemann and S. H. Gohla, *Int. J. Pharm.*, 2000, **199**, 167–177.

36 H. Salminen, A.-S. Stübler and J. Weiss, *Eur. Food Res. Technol.*, 2020, **246**, 599–608.

37 M. Schubert, *Eur. J. Pharm. Biopharm.*, 2003, **55**, 125–131.

38 J. M. Taylor, K. Scale, S. Arrowsmith, A. Sharp, S. Flynn, S. Rannard and T. O. McDonald, *Nanoscale Adv.*, 2020, **2**, 5572–5577.

39 A. Gdowski, K. Johnson, S. Shah, I. Gryczynski, J. Vishwanatha and A. Ranjan, *J. Nanobiotechnology*, 2018, **16**, 12.

40 W. S. Saad and R. K. Prud'homme, *Nano Today*, 2016, **11**, 212–227.

41 A. J. Mahajan and D. J. Kirwan, *J. Cryst. Growth*, 1994, **144**, 281–290.

42 V. K. Lamer and R. H. Dinegar, *J. Am. Chem. Soc.*, 1950, **72**, 4847–4854.

43 J. Tao, S. F. Chow and Y. Zheng, *Acta Pharm. Sin. B*, 2019, **9**, 4–18.

44 B. K. Johnson, W. Saad and R. K. Prud'homme, 2006, pp. 278–291.

45 K. M. Pustulka, A. R. Wohl, H. S. Lee, A. R. Michel, J. Han, T. R. Hoye, A. V. McCormick, J. Panyam and C. W. Macosko, *Mol. Pharm.*, 2013, **10**, 4367–4377.

46 S. V. Dalvi and R. N. Dave, *Ind. Eng. Chem. Res.*, 2009, **48**, 7581–7593.

47 Y. Liu, K. Kathan, W. Saad and R. K. Prud'homme, *Phys. Rev. Lett.*, 2007, **98**, 036102.

48 R. Mannhold, G. Cruciani, K. Dross and R. Rekker, *J. Comput. Aided. Mol. Des.*, 1998, **12**, 573–

81.

49 A. Pyka, M. Babuska and M. Zachariasz, *Acta Pol Pharm.*, 2006, **63**, 159–67.

50 J. Rautio, H. Kumpulainen, T. Heimbach, R. Oliyai, D. Oh, T. Järvinen and J. Savolainen, *Nat. Rev. Drug Discov.*, 2008, **7**, 255–270.

51 R. Walther, J. Rautio and A. N. Zelikin, *Adv. Drug Deliv. Rev.*, 2017, **118**, 65–77.

52 D. Irby, C. Du and F. Li, *Mol. Pharm.*, 2017, **14**, 1325–1338.

53 F. Zaragoza Dörwald, *Lead Optimization for Medicinal Chemists*, Wiley, 2012.

54 L. Shi, X. Wu, T. Li, Y. Wu, L. Song, W. Zhang, L. Yin, Y. Wu, W. Han and Y. Yang, *Nanoscale Adv.*, 2022, **4**, 952–966.

55 C. Olbrich, A. Gessner, O. Kayser and R. H. Müller, *J. Drug Target.*, 2002, **10**, 387–396.

56 K.-M. Wu, *Pharmaceuticals*, 2009, **2**, 77–81.

57 T. Huang, A. Székács, T. Uematsu, E. Kuwano, A. Parkinson and B. Hammock, *Pharm. Res.*, 1993, **10**, 639–648.

58 P. Zhao, X. Hou, J. Yan, S. Du, Y. Xue, W. Li, G. Xiang and Y. Dong, *Bioact. Mater.*, 2020, **5**, 358–363.

59 S. Daniel, Z. Kis, C. Kontoravdi and N. Shah, *Trends Biotechnol.*, 2022, **40**, 1213–1228.

60 Y. Suzuki, T. Miyazaki, H. Muto, K. Kubara, Y. Mukai, R. Watari, S. Sato, K. Kondo, S. Tsukumo, K. Yasutomo, M. Ito and K. Tsukahara, *Mol. Ther. - Nucleic Acids*, 2022, **30**, 226–240.

61 R. Ball, P. Bajaj and K. Whitehead, *Int. J. Nanomedicine*, 2016, **Volume 12**, 305–315.

62 Moderna, Storing Vaccine Vials, https://eua.modernatx.com/covid19vaccine-eua/providers/storage-handling, (accessed 11 February 2023).

63 T. Saey, Here's why COVID-19 vaccines like Pfizer's need to be kept so cold, https://www.sciencenews.org/article/coronavirus-covid-19-why-vaccines-cold-freeze-pfizer-moderna.

64 W. Abdelwahed, G. Degobert and H. Fessi, *Eur. J. Pharm. Biopharm.*, 2006, **63**, 87–94.

65 E. Trenkenschuh and W. Friess, *Eur. J. Pharm. Biopharm.*, 2021, **165**, 345–360.

66 W. ABDELWAHED, G. DEGOBERT, S. STAINMESSE and H. FESSI, *Adv. Drug Deliv. Rev.*, 2006,

58, 1688–1713.

67 C. Schwarz and W. Mehnert, *Int. J. Pharm.*, 1997, **157**, 171–179.

68 F. Susa, G. Bucca, T. Limongi, V. Cauda and R. Pisano, *Cryobiology*, 2021, **98**, 46–56.

69 P.-F. Yue, G. Li, J.-X. Dan, Z.-F. Wu, C.-H. Wang, W.-F. Zhu and M. Yang, *Int. J. Pharm.*, 2014, **475**, 35–48.

70 P. V. Date, A. Samad and P. V. Devarajan, *AAPS PharmSciTech*, 2010, **11**, 304–313.

71 U. Wais, A. W. Jackson, Y. Zuo, Y. Xiang, T. He and H. Zhang, *J. Control. Release*, 2016, **222**, 141–150.

72 K. R. Ward and P. Matejtschuk, 2021, pp. 99–127.

73 S. Yeotikar, Lyophilization or Freeze drying: The Definitive Guide, https://pharmagxp.com/process-engineering/lyophilization/#Radiation.

74 Physical & Theoretical Chemistry, https://chem.libretexts.org/Bookshelves/Physical_and_Theoretical_Chemistry_Textbook_Maps/Supplemental_Modules_(Physical_and_Theoretical_Chemistry)/Physical_Properties_of_Matter/States_of_Matter/Phase_Transitions/Phase_Diagrams.

75 T. M. Amis, J. Renukuntla, P. K. Bolla and B. A. Clark, *Pharmaceutics*, 2020, **12**, 892.

76 K. Schersch, O. Betz, P. Garidel, S. Muehlau, S. Bassarab and G. Winter, *J. Pharm. Sci.*, 2012, **101**, 2288–2306.

77 K. Schersch, O. Betz, P. Garidel, S. Muehlau, S. Bassarab and G. Winter, *J. Pharm. Sci.*, 2010, **99**, 2256–2278.

78 S. M. Patel, S. L. Nail, M. J. Pikal, R. Geidobler, G. Winter, A. Hawe, J. Davagnino and S. Rambhatla Gupta, *J. Pharm. Sci.*, 2017, **106**, 1706–1721.

79 R. Esfandiary, S. K. Gattu, J. M. Stewart and S. M. Patel, *J. Pharm. Sci.*, 2016, **105**, 1427–1433.

80 B. Sylvester, A. Porfire, P.-J. Van Bockstal, S. Porav, M. Achim, T. De Beer and I. Tomuţă, *J. Pharm. Sci.*, 2018, **107**, 139–148.

81 D. L. Teagarden and D. S. Baker, *Eur. J. Pharm. Sci.*, 2002, **15**, 115–133.

82 K. Kasraian and P. . DeLuca, *Pharm. Res.*, 1995, **12**, 1491–495.

83 Y. Koyama, M. Kamat, R. J. De Angelis, R. Srinivasan and P. P. DeLuca, *J. Pharm. Sci. Technol.*, 1988, **42**, 47–52.

84 S. D. Allison, A. Dong and J. F. Carpenter, *Biophys. J.*, 1996, **71**, 2022–2032.

85 S. D. Allison, M. d. . Molina and T. J. Anchordoquy, *Biochim. Biophys. Acta - Biomembr.*, 2000, **1468**, 127–138.

86 A. Almalik, I. Alradwan, M. A. Kalam and A. Alshamsan, *Saudi Pharm. J.*, 2017, **25**, 861–867.

87 Food and Drug Administration, What is Gene Therapy?, https://www.fda.gov/vaccines-blood-biologics/cellular-gene-therapy-products/what-gene-therapy, (accessed 11 February 2023).

88 D. Correddu and I. K. H. Leung, *Drug Discov. Today*, 2019, **24**, 1295–1303.

89 BioNTech Reports Breakthrough In Treating Multiple Sclerosis With Another mRNA Vaccine, https://khn.org/morning-breakout/biontech-reports-breakthrough-in-treating-multiple-sclerosis-with-another-mrna-vaccine/.

90 E. Winstead, Can mRNA Vaccines Help Treat Cancer?, https://www.cancer.gov/news-events/cancer-currents-blog/2022/mrna-vaccines-to-treat-cancer.

91 T. Wei, W. Tao and Q. Cheng, *Life Med.*, 2022, **1**, 21–23.

92 M. Voysey, S. A. C. Clemens, S. A. Madhi and et al, *Lancet*, 2021, **397**, 99–111.

93 L. R. Baden, H. M. El Sahly, B. Essink, K. Kotloff, S. Frey, R. Novak, D. Diemert, S. A. Spector, N. Rouphael, C. B. Creech, J. McGettigan, S. Khetan, N. Segall, J. Solis, A. Brosz, C. Fierro, H. Schwartz, K. Neuzil, L. Corey, P. Gilbert, H. Janes, D. Follmann, M. Marovich, J. Mascola, L. Polakowski, J. Ledgerwood, B. S. Graham, H. Bennett, R. Pajon, C. Knightly, B. Leav, W. Deng, H. Zhou, S. Han, M. Ivarsson, J. Miller and T. Zaks, *N. Engl. J. Med.*, 2021, **384**, 403–416.

94 F. P. Polack, S. J. Thomas, N. Kitchin, J. Absalon, A. Gurtman, S. Lockhart, J. L. Perez, G. Pérez Marc, E. D. Moreira, C. Zerbini, R. Bailey, K. A. Swanson, S. Roychoudhury, K. Koury, P. Li, W. V. Kalina, D. Cooper, R. W. Frenck, L. L. Hammitt, Ö. Türeci, H. Nell, A. Schaefer, S. Ünal, D. B. Tresnan, S. Mather, P. R. Dormitzer, U. Şahin, K. U. Jansen and W. C. Gruber, *N. Engl. J. Med.*, 2020, **383**, 2603–2615.

95 M. Sun, U. J. Dang, Y. Yuan, A. M. Psaras, O. Osipitan, T. A. Brooks, F. Lu and A. J. Di Pasqua, *AAPS PharmSciTech*, 2022, **23**, 135.

96 A. K. K. Leung, I. M. Hafez, S. Baoukina, N. M. Belliveau, I. V. Zhigaltsev, E. Afshinmanesh, D. P.

Tieleman, C. L. Hansen, M. J. Hope and P. R. Cullis, *J. Phys. Chem. C*, 2012, **116**, 18440–18450.

97 M. J. W. Evers, J. A. Kulkarni, R. van der Meel, P. R. Cullis, P. Vader and R. M. Schiffelers, *Small Methods*, 2018, **2**, 1700375.

98 P. R. Cullis and M. J. Hope, *Mol. Ther.*, 2017, **25**, 1467–1475.

99 N. M. Belliveau, J. Huft, P. J. Lin, S. Chen, A. K. Leung, T. J. Leaver, A. W. Wild, J. B. Lee, R. J. Taylor, Y. K. Tam, C. L. Hansen and P. R. Cullis, *Mol. Ther. - Nucleic Acids*, 2012, **1**, e37.

100 S. T. LoPresti, M. L. Arral, N. Chaudhary and K. A. Whitehead, *J. Control. Release*, 2022, **345**, 819–831.

101 C. Hald Albertsen, J. A. Kulkarni, D. Witzigmann, M. Lind, K. Petersson and J. B. Simonsen, *Adv. Drug Deliv. Rev.*, 2022, **188**, 114416.

102 A. Leung, The University of British Coloumbia, 2014.

103 V. Francia, R. M. Schiffelers, P. R. Cullis and D. Witzigmann, *Bioconjug. Chem.*, 2020, **31**, 2046–2059.

104 M. CP Mendonça, A. Kont, P. S. Kowalski and C. M. O'Driscoll, *Drug Discov. Today*, 2023, 103505.

105 P. J. C. Lin, Y. Y. C. Tam, I. Hafez, A. Sandhu, S. Chen, M. A. Ciufolini, I. R. Nabi and P. R. Cullis, *Nanomedicine Nanotechnology, Biol. Med.*, 2013, **9**, 233–246.

106 S. C. Semple, A. Akinc, J. Chen, A. P. Sandhu, B. L. Mui, C. K. Cho, D. W. Y. Sah, D. Stebbing, E. J. Crosley, E. Yaworski, I. M. Hafez, J. R. Dorkin, J. Qin, K. Lam, K. G. Rajeev, K. F. Wong, L. B. Jeffs, L. Nechev, M. L. Eisenhardt, M. Jayaraman, M. Kazem, M. A. Maier, M. Srinivasulu, M. J. Weinstein, Q. Chen, R. Alvarez, S. A. Barros, S. De, S. K. Klimuk, T. Borland, V. Kosovrasti, W. L. Cantley, Y. K. Tam, M. Manoharan, M. A. Ciufolini, M. A. Tracy, A. de Fougerolles, I. MacLachlan, P. R. Cullis, T. D. Madden and M. J. Hope, *Nat. Biotechnol.*, 2010, **28**, 172–176.

107 G. Sahay, W. Querbes, C. Alabi, A. Eltoukhy, S. Sarkar, C. Zurenko, E. Karagiannis, K. Love, D. Chen, R. Zoncu, Y. Buganim, A. Schroeder, R. Langer and D. G. Anderson, *Nat. Biotechnol.*, 2013, **31**, 653–658.

108 K. J. Hassett, K. E. Benenato, E. Jacquinet, A. Lee, A. Woods, O. Yuzhakov, S. Himansu, J. Deterling, B. M. Geilich, T. Ketova, C. Mihai, A. Lynn, I. McFadyen, M. J. Moore, J. J. Senn, M. G. Stanton, Ö. Almarsson, G. Ciaramella and L. A. Brito, *Mol. Ther. - Nucleic Acids*, 2019, **15**, 1–11.

109 S. Cui, Y. Wang, Y. Gong, X. Lin, Y. Zhao, D. Zhi, Q. Zhou and S. Zhang, *Toxicol. Res. (Camb).*, 2018, **7**, 473–479.

110 H. Lv, S. Zhang, B. Wang, S. Cui and J. Yan, *J. Control. Release*, 2006, **114**, 100–109.

111 M. Packer, D. Gyawali, R. Yerabolu, J. Schariter and P. White, *Nat. Commun.*, 2021, **12**, 6777.

112 K. Hashiba, Y. Sato, M. Taguchi, S. Sakamoto, A. Otsu, Y. Maeda, T. Shishido, M. Murakawa, A. Okazaki and H. Harashima, *Small Sci.*, 2022, 2200071.

113 R. Verbeke, I. Lentacker, S. C. De Smedt and H. Dewitte, *J. Control. Release*, 2021, **333**, 511–520.

114 J. Kim, Y. Eygeris, M. Gupta and G. Sahay, *Adv. Drug Deliv. Rev.*, 2021, **170**, 83–112.

115 M. R. Krause and S. L. Regen, *Acc. Chem. Res.*, 2014, **47**, 3512–3521.

116 W.-C. Hung, M.-T. Lee, F.-Y. Chen and H. W. Huang, *Biophys. J.*, 2007, **92**, 3960–3967.

117 Avanti Polar Lipids, Phase Transition Temperatures for Glycerophospholipids, https://avantilipids.com/tech-support/physical-properties/phase-transition-temps.

118 S. C. Semple, A. Chonn and P. R. Cullis, *Biochemistry*, 1996, **35**, 2521–2525.

119 B. G. Tenchov, R. C. MacDonald and D. P. Siegel, *Biophys. J.*, 2006, **91**, 2508–2516.

120 A. Akinc, M. A. Maier, M. Manoharan, K. Fitzgerald, M. Jayaraman, S. Barros, S. Ansell, X. Du, M. J. Hope, T. D. Madden, B. L. Mui, S. C. Semple, Y. K. Tam, M. Ciufolini, D. Witzigmann, J. A. Kulkarni, R. van der Meel and P. R. Cullis, *Nat. Nanotechnol.*, 2019, **14**, 1084–1087.

121 M. P. Lokugamage, D. Vanover, J. Beyersdorf, M. Z. C. Hatit, L. Rotolo, E. S. Echeverri, H. E. Peck, H. Ni, J.-K. Yoon, Y. Kim, P. J. Santangelo and J. E. Dahlman, *Nat. Biomed. Eng.*, 2021, **5**, 1059–1068.

122 F. Sebastiani, M. Yanez Arteta, M. Lerche, L. Porcar, C. Lang, R. A. Bragg, C. S. Elmore, V. R. Krishnamurthy, R. A. Russell, T. Darwish, H. Pichler, S. Waldie, M. Moulin, M. Haertlein, V. T. Forsyth, L. Lindfors and M. Cárdenas, *ACS Nano*, 2021, **15**, 6709–6722.

123 T. Suzuki, Y. Suzuki, T. Hihara, K. Kubara, K. Kondo, K. Hyodo, K. Yamazaki, T. Ishida and H. Ishihara, *Int. J. Pharm.*, 2020, **588**, 119792.

124 E. Dams, P. Laverman, W. Oyen, G. Storm, G. Scherphof, J. Van der Meer, F. Corstens and O. Boerman, *J. Pharmacol. Exp. Ther.*, 2000, **292**, 1071–1079.

125 G. Besin, J. Milton, S. Sabnis, R. Howell, C. Mihai, K. Burke, K. E. Benenato, M. Stanton, P. Smith, J. Senn and S. Hoge, *ImmunoHorizons*, 2019, **3**, 282–293.

126 M. D. McSweeney, M. Mohan, S. P. Commins and S. K. Lai, *Front. Allergy*, , DOI:10.3389/falgy.2021.715844.

127 V. Sampath, G. Rabinowitz, M. Shah, S. Jain, Z. Diamant, M. Jesenak, R. Rabin, S. Vieths, I. Agache, M. Akdis, D. Barber, H. Breiteneder, S. Chinthrajah, T. Chivato, W. Collins, T. Eiwegger, K. Fast, W. Fokkens, R. E. O'Hehir, M. Ollert, L. O'Mahony, O. Palomares, O. Pfaar, C. Riggioni, M. H. Shamji, M. Sokolowska, M. Jose Torres, C. Traidl-Hoffmann, M. Zelm, D. Y. Wang, L. Zhang, C. A. Akdis and K. C. Nadeau, *Allergy*, 2021, **76**, 1640–1660.

128 B. L. Mui, Y. K. Tam, M. Jayaraman, S. M. Ansell, X. Du, Y. Y. C. Tam, P. J. Lin, S. Chen, J. K. Narayanannair, K. G. Rajeev, M. Manoharan, A. Akinc, M. A. Maier, P. Cullis, T. D. Madden and M. J. Hope, *Mol. Ther. - Nucleic Acids*, 2013, **2**, e139.

129 X. Ge, L. Chen, B. Zhao and W. Yuan, *Front. Pharmacol.*, , DOI:10.3389/fphar.2020.598175.

130 J. S. Suk, Q. Xu, N. Kim, J. Hanes and L. M. Ensign, *Adv. Drug Deliv. Rev.*, 2016, **99**, 28–51.

131 C. H. Kim, C.-K. Sa, M. S. Goh, E. S. Lee, T. H. Kang, H. Y. Yoon, G. Battogtokh, Y. T. Ko and Y. W. Choi, *Int. J. Nanomedicine*, 2018, **Volume 13**, 6661–6675.

132 J. Wu and S. R. Jaffrey, *Curr. Opin. Chem. Biol.*, 2020, **57**, 177–183.

133 Y. I. Avila, M. Chandler, E. Cedrone, H. S. Newton, M. Richardson, J. Xu, J. D. Clogston, N. J. Liptrott, K. A. Afonin and M. A. Dobrovolskaia, *Molecules*, 2021, **26**, 652.

134 A. Harada, N. Sekido, T. Akahoshi, T. Wada, N. Mukaida and K. Matsushima, *J. Leukoc. Biol.*, 1994, **56**, 559–564.

135 M. L. Bender, *Chem. Rev.*, 1960, **60**, 53–113.

136 K. F. Smart, R. B. M. Aggio, J. R. Van Houtte and S. G. Villas-Bôas, *Nat. Protoc.*, 2010, **5**, 1709–1729.

137 M. M. Cooper and M. W. Klymkowsky, Alcohols and an introduction to thiols, amines, ethers and sulfides, https://chem.libretexts.org/Bookshelves/Organic_Chemistry/OCLUE%3A_Organic_Chemistry_Life_the_Universe_and_Everything_(Copper_and_Klymkowsky)/06%3A_Alcohols_and_an_introduction_to_thiols_amines_ethers_and_sulfides, (accessed 20 February 2023).

138 J. Q. Zhang, J. Liu, X. L. Li and B. R. Jasti, *Drug Deliv.*, 2007, **14**, 381–387.

139 S. Wada, S. Kudo and H. Takiyama, *J. Cryst. Growth*, 2016, **435**, 37–41.

140 G. R. Fulmer, A. J. M. Miller, N. H. Sherden, H. E. Gottlieb, A. Nudelman, B. M. Stoltz, J. E. Bercaw and K. I. Goldberg, *Organometallics*, 2010, **29**, 2176–2179.

141 Imwitor 900 K, https://www.ioioleo.de/produkte/pharma/imwitor-900-k/.

142 P. Stott, *J. Control. Release*, 1998, **50**, 297–308.

143 A. Tatke, N. Dudhipala, K. Janga, S. Balguri, B. Avula, M. Jablonski and S. Majumdar, *Nanomaterials*, 2018, **9**, 33.

144 B. Siekmann and K. Westesen, *Colloids Surfaces B Biointerfaces*, 1994, **3**, 159–175.

145 I. Arduino, N. Depalo, F. Re, R. Dal Magro, A. Panniello, N. Margiotta, E. Fanizza, A. Lopalco, V. Laquintana, A. Cutrignelli, A. A. Lopedota, M. Franco and N. Denora, *Int. J. Pharm.*, 2020, **583**, 119351.

146 X. Cheng and R. J. Lee, *Adv. Drug Deliv. Rev.*, 2016, **99**, 129–137.

147 K. Ishihara and Y. Inoue, 2010, pp. 1–9.

148 S. Y. K. Fong, M. Brandl and A. Bauer-Brandl, *Eur. J. Pharm. Sci.*, 2015, **80**, 89–110.

149 C. Hogarth, K. Arnold, A. McLauchlin, S. P. Rannard, M. Siccardi and T. O. McDonald, *J. Mater. Chem. B*, 2021, **9**, 9874–9884.

150 P. Hansrani, S. Davis and M. Groves, *PDA J. Pharm. Sci. Technol.*, 1983, **37**, 145–150.

151 K. Hippalgaonkar, S. Majumdar and V. Kansara, *AAPS PharmSciTech*, 2010, **11**, 1526–1540.

152 H. Bunjes and M. H. J. Koch, *J. Control. Release*, 2005, **107**, 229–243.

153 Adaptive Correlation: Better insight to the presence of aggregates, https://www.malvernpanalytical.com/en/learn/knowledge-center/application-notes/AN180518AdaptiveCorrelationAggregateInsight.

154 J. J. Hobson, A. C. Savage, A. B. Dwyer, C. Unsworth, J. Massam, U. Arshad, H. Pertinez, H. Box, L. Tatham, R. K. R. Rajoli, M. Neary, J. Sharp, A. Valentijn, C. David, P. Curley, N. J. Liptrott, T. O. McDonald, A. Owen and S. P. Rannard, *Nanoscale*, 2021, **13**, 6410–6416.

155 A. Haque, *Der Pharma Chem.*, 2018, **10**, 108–111.

156 Lamivudine, https://pubchem.ncbi.nlm.nih.gov/compound/lamivudine#section=Melting-Point.

157 K. Ahern, I. Rajagopal and T. Tan, *Control of Enzymatic Activity*, 2018.

158 H. Yan and J. J. Harding, *Biochim. Biophys. Acta - Mol. Basis Dis.*, 1999, **1454**, 183–190.

159 M. Lima and J. W. Baynes, in *Encyclopedia of Biological Chemistry*, Elsevier, 2013, pp. 405–411.

160 R. Tong, L. Tang, L. Ma, C. Tu, R. Baumgartner and J. Cheng, *Chem. Soc. Rev.*, 2014, **43**, 6982–7012.

161 K. HASHIZAKI, C. ITOH, H. SAKAI, S. YOKOYAMA, H. TAGUCHI, Y. SAITO, N. OGAWA and M. ABE, *J. Japan Oil Chem. Soc.*, 1999, **48**, 871-876,928.

162 J. Maillard, K. Klehs, C. Rumble, E. Vauthey, M. Heilemann and A. Fürstenberg, *Chem. Sci.*, 2021, **12**, 1352–1362.

163 CleanCap™ Cyanine 5 EGFP mRNA(5moU), https://www.trilinkbiotech.com/media/productattach/l/7/l7701_insert.pdf.